FLOODING DYNAMICS AND NUTRIENT RETENTION IN THE MIDDLE EBRO FLOODPLAIN: EXPERIMENTAL ASSESSMENT AND NUMERICAL MODELING

Dinámica de flujo y retención de nitrientes en la llanura de inundación del tramo medio del Ebro: análisis experimental y simulación numérica

Author: María González Sanchis

Supervised by:

Antonio D. del Campo García

Francisco A. Comín

Javier Murillo

Jan Vermaat

A thesis submitted for the degree of

Doctor, PhD.

Marzo, 2012

Abstract

0.1 English version

The present work highlights the numerical simulation as a tool capable of reproducing and predict the main processes that produces and maintains the floodplain ecosystems. To that end, floodplain flow dynamics, geomorphic activity, sediment deposition and nutrient uptake are evaluated through field experimentation. Then, the experimental data are included in a numerical model to perform a complete simulation tool that predict flow dynamics, geomorphic activity, sediment deposition, river nutrient contribution and nutrient uptake. A 2-km river segment representative of the meandering Middle Ebro (NE Spain) reach is selected for the study.

The first task is to find the best representation of the floodplain hydraulics. We select a two-dimensional (2D) finite volume numerical model based on the 2D transient shallow water equations as the best option to perform the hydrodynamic simulation. Then, the importance of the correct characterization of the

roughness coefficient and the topography is emphasized in the study. The former is estimated from a previous classification of structurally homogeneous habitats and the latter is defined by merging Digital Terrain Model data with a hydraulic river bed elevation reconstruction algorithm. The calibration of the full model resulting from the roughness, bed river and flow simulation models is based on field measurements of flooded area for two steady discharges of 50 and 500 m^3/s. The validation is performed by comparing the numerical results with the water levels measured during five flooding events at certain times, with the flooded area and with time series of continuous point measurements of water-depth during different situations along the year 2007. The validation results of the flooded area and water level were 79 ± 13 % and 0.27 ± 0.05 m, respectively.

Since the model provide accurate predictions of the floodplain flooding, for both, low and high flow discharges, the simulation results are used to analyze the current floodplain flooding dynamics and its geomorphic potential. As a result, we obtain that although the current flow regime appears to be enough to induce the floodplain river nutrient contribution, it does not produce enough morphological activity to maintain the shifting mosaic of habitats (SMH) characteristic of the floodplain ecosystems. On the basis of this analysis, five possible restoration scenarios, based on the terrain or flow modification, are simulated. The results enhance the role of the constructed defenses in the mor-

phological activity decreasing.

A predictive nutrient uptake model is included into the 2D hydraulic model. For that purpose, retention of dissolved phosphorus and nitrogen is examined in several controlled experiments in an irrigation canal, located within the study site and whose flow comes from the Ebro river, and in a laboratory channel. The laboratory channel is used to estimate the sediment nutrient uptake capacity, whilst the irrigation canal is used to estimate the sediment and water column nutrient uptake capacity. Retention efficiency is measured using nutrient short-term nutrient and tracer injections to estimate nutrient uptake coefficient (k) during the irrigation period. Hydraulic tracer (Br^-) and soluble reactive phosphorus (SRP) were co-injected into both canals. Nitrogen uptake is measured using the ambient concentration. The results show an SRP load reduction of 20.7 $\pm$ 2.8 % of the net mass balance by means of the irrigation channel ecosystem, while the nitrogen concentration remained nearly unaltered. Hence, only the SRP is considered in the nutrient uptake formulation.

The new SRP uptake formulation is performed using the experimental data. First, main nutrient uptake agents are determined by means of an statistical analysis of the nutrient uptake coefficient and the physical, chemical and biological irrigation canal and laboratory channel characteristics. As a result, the sorption appears to be the main SRP uptake process, for both the sediment and the water column. Then, a non linear regression between the

main SRP uptake agents and the uptake coefficient is performed obtaining an SRP uptake function. The equation is included into the 2D hydraulic model as a decay term and validated in both the irrigation canal and the laboratory channel. The comparison between measured and simulated data provided always a significant linear regression ($p \leq 0.05$) whose $r^2 \geq 0.83$ in 19 out of 20 experiments, where 3 of them were carried out using a different spatial-temporal scale. Finally, the new formulation is validated in the selected river reach by means of three new experimentations. The model predictions show a good accuracy, where the linear regressions between measured and calculated SRP concentration of the three experiments were significant ($r^2 \geq 0.62$; $p \leq 0.05$).

The particulate solute transport and decay (sedimentation model) is also included into the hydraulic model, and is validated using field data collected during 2 real flooding events. The comparison between calculated and measured sediment deposition shows a significant ($p \leq 0.05$) linear regression, whose $r^2 = 0.97$ with a slope not significantly different from the unit ($p \leq 0.05$).

The complete model that includes the erosive potential, the solute transport and SRP uptake is used to simulate and analyze floodplain sediment deposition, river nutrient contribution and SRP uptake. According to this analysis, the main SRP uptake process appears to be the sediment sorption. The analysis also reveals a disequilibrium between erosion and sedimentation, where

sediment deposition prevails over erosive processes. Finally, simulation results suggest the presence of a lateral gradient of hydrological connectivity that decreases as distance to the river increases and control the floodplain river matter contribution. According to this gradient, remote floodplain zones would receive a very low or null suspended and dissolved nutrients, whilst the adjacent riparian areas would receive the highest concentrations. Hence, this lateral gradient could cause a lack of nutrient plant availability at the remote riparian forest.
Finally, the complete model was used to propose and simulate floodplain restoration scenarios based on terrain modification.

0.2 Versión en castellano

El presente trabajo destaca la simulación numérica como herramienta capaz de reproducir y predecir los principales procesos que producen y mantienen los ecosistemas de llanuras de inundación. Para ello, la dinámica del flujo, la actividad geomorfológica, la sedimentación y la captura de nutrientes de la llanura de inundación, son evaluadas experimentalmente. Seguidamente, los datos experimentales son incluidos en un modelo numérico para desarrollar una herramienta de simulación completa y capaz de predecir la dinámica del flujo, la actividad geomorfológica, la sedimentación, el aporte de nutrientes del río a la llanura de inundación así como la captación de los mismos. Para desarrollar

el estudio, se ha seleccionado un segmento de 2 Km del río Ebro (NE España), representativo de su tramo medio meandriforme.
Para representar correctamente la hidráulica de la llanura de inundación, se ha seleccionado un modelo nu- mérico bidimensional (2D), basado en las ecuaciones 2D de las aguas poco profundas y calculado a partir del método de los volúmenes finitos.
A continuación, se pone de manifiesto la importancia de una correcta caracterización del rozamiento y la topografía del terreno. El rozamiento ha sido caracterizado experimentalmente a través de la clasificación estructural de los distintos hábitats de la llanura de inundación. La topografía del terreno se define a través de un Modelo Digital del Terreno, cuyo río ha sido reconstruido mediante un algoritmo desarrollado en el presente estudio.
La calibración del modelo completo resultante del rozamiento, la topografía y el modelo numérico del flujo, se basa en medidas experimentales realizadas en la llanura de inundación bajo dos caudales estacionarios de 50 y 500 m^3/s. La validación del modelo se llevó a cabo comparando los resultados numéricos con las medidas experimentales de nivel de agua y extensión del área inundada realizadas en la llanura de inundación durante los cinco eventos de riada ocurridos en el año 2007. Dicha validación dio como resultado un ajuste medio del área inundada y del nivel del agua de 79 ± 13 % y 0.27 ± 0.05 m, respectivamente.
Dada la capacidad predictiva del modelo tanto para caudales elevados como bajos, las simulaciones fueron utilizadas para analizar

la dinámica actual de inundación de la llanura así como su actividad geomorfológica. Como resultado, se obtuvo que a pesar de que el presente régimen de caudales parece suficiente para inundar completamente la llanura de inundación y proveerla de nutrientes, no resulta suficiente para generar una actividad geomorfológica tal que mantenga el mosaico cambiante de hábitats característico de los ecosistemas de llanura de inundación. En base a este análisis, se proponen, simulan y analizan cinco posibles escenarios de restauración basados en la modificación del terreno o de la dinámica de caudales. Los resultados del análisis señalan a las defensas construidas del río como máximos responsables de la carente actividad geomorfológica actual.

Además del flujo y la capacidad erosiva, se ha incluido en el modelo 2D de simulación, un modelo predictivo de captura de nutrientes. Para ello, se ha examinado la retención de fósforo inorgánico y nitrógeno disueltos mediante una serie de experimentos controlados en una acequia de riego, situada en el área de estudio y cuyo flujo procede del río Ebro, y en un canal de laboratorio. Dicho canal se utilizó para estimar la retención de nutrientes por parte del sedimento, mientras que en la acequia de riego se evaluó la captura de nutrientes como resultado de la acción conjunta de la columna de agua y el sedimento. En ambos casos se realizaron una serie de experimentos basados en la inyección controlada de fósforo y un trazador (Br^-) para estimar el coeficiente de retención de nutrientes k. Debido a la elevada

concentración de nitrógeno en la acequia de riego, su retención fue evaluada utilizando la concentración ambiente del mismo. Los resultados mostraron una capacidad de reducción de fósforo por parte de la columna de agua y del sedimento de 20.7 ± 2.8 %. Por el contrario, el sistema presentó una capacidad nula para retener nitrógeno. Por tanto, sólo el fósforo inorgánico disuelto será considerado para en el desarrollo del modelo de retención de nutrientes.

La nueva formulación que describe la retención de nutrientes se ha desarrollado mediante la utilización de los datos experimentales. En primer lugar, se identifican los principales agentes relacionados con la captura de fósforo mediante el análisis estadístico del coeficiente de captura y las características físicas, químicas y biológicas del sistema (el canal de riego y el de laboratorio). Como resultado se obtuvo que el proceso responsable de la mayor parte de la retención del fósforo es la adsorción, tanto en el sedimento como en la columna de agua. A continuación, mediante una regresión no lineal entre el coeficiente de captura y los parámetros físicos, químicos y biológicos implicados en la retención de fósforo, se obtiene la ecuación que describe el proceso de captura de fósforo. Dicha ecuación se introduce en el modelo hidráulico 2D como término de decaimiento del fósforo, y se valida tanto en el canal de laboratorio como en la acequia. La comparación entre las predicciones del modelo y los datos experimentales dio como resultado regresiones lineales

significativas ($p \leq 0.05$), cuyas $r^2 \geq 0.8$ en 19 de los 20 experimentos.

El modelo de transporte y sedimentación de solutos particulados se incluyó también en el modelo hidráulico 2D y se validó en la llanura de inundación utilizando los datos experimentales recogidos durante dos eventos de riada. La comparación mediante lo calculado por el modelo y lo observado en campo dio como resultado una regresión lineal significativa ($p \leq 0.05$) con una r^2 de 0.97.

El modelo de simulación complete que incluye potencial erosivo, transporte de solutos y retención de fósforo inorgánico disuelto se utilizó para simular y analizar dichos procesos en la llanura de inundación. Según lo obtenido en dicho análisis, la adsorción del fósforo a los sólidos en suspensión y su posterior sedimentación parece ser el mayor responsable de la retención de fósforo en la llanura de inundación. El análisis también revela la existencia de cierto desequilibrio entre los procesos de erosión y sedimentación a favor de este último. Finalmente, las simulaciones sugieren la presencia de un gradiente lateral de conectividad que decrece con la distancia al río y gobierna el aporte de nutrientes a la llanura de inundación. Según este gradiente, las zonas más alejadas del río reciben una cantidad muy baja o incluso nula de sólidos disueltos y particulados, mientras que las zonas más cercanas reciben las concentraciones más elevadas. Por tanto, dicho gradiente lateral podría estar afectando negativamente a la

vegetación riparia de las zonas más remotas de la llanura de inundación.
Finalmente, el modelo completo ha sido utilizado para proponer, simular y analizar dos alternativas de restauración de la llanura de inundación basadas en la modificación del terreno.

0.3 Versió en Valencià

El present treball destaca la simulació numèrica com a ferramenta capaç de reproduir i predir els principals processos que generen i mantenen els ecosistemes de les planes d'inundació. Per això, s'avaluen experimentalment la dinàmica del flux, l'activitat geomorfològica, la sedimentació i la captació de nutrients de la planícia de inundació. A continuació, les dades experimentals són incloses en un model numèric per tal de desenvolupar una ferramenta de simulació completa i capaç de predir la dinàmica del flux, la activitat geomorfològica, la sedimentació, la capacitat de retenció dels nutrients i la contribució d'aquests a la plana d'inundació. Per desenvolupar l'estudi, s'ha seleccionat un segment de 2 quilòmetres del riu Ebro (NE Espanya), representatiu del seu tram mitjà meandritzant.
Per representar correctament la hidràulica de la plana d'inundació, s'ha seleccionat un model numèric bidimensional (2D), basat en les equacions 2D d'aigües poc profundes i calculat a partir del mètode dels volums finits. A continuació, es posa de manifest

la importància d'una correcta caracterització de la fricció i la topografia del terreny. La fricció ha estat caracteritzada experimentalment mitjançant la classificació estructural dels diferents hàbitats de la plana d'inundació. La topografia del terreny es defineix mitjançant d'un Model Digital del Terreny, on el riu ha estat reconstrut utilitzant un algoritme desenvolupat al present estudi. La calibració del model complet resultant de la fricció, la topografia i el model numèric del flux, es basa en mesures experimentals realitzades en la plana d'inundació sota els cabals estacionaris de 50 i 500 m^3/s. La validació del model es va dur a terme comparant els resultats numèrics en les mesures experimentals del nivell de l'aigua i la extensió de l'àrea inundada realitzades en la plana d'inundació durant els cinc esdeveniments de riuada de l'any 2007. La validació va donar com a resultat un ajust mitjà de l'àrea inundada i del nivell d'aigua de 79 ± 13 % y 0.27 ± 0.05 m, respectivament.

En la capacitat predictiva del model tant per cabals elevats com baixos, les simulacions foren utilitzades per analitzar la dinàmica actual d'inundació de la planícia així com la seua activitat geomorfològica. Els resultats mostren que a pesar de que el present règim de cabals sembla suficient per inundar completament la plana d'inundació i proveir-la de nutrients, resulta incapaç de generar una activitat geomorfològica tal que mantinga el mosaic canviant d'hàbitats característic dels ecosistemes de plana d'inundació. En base a aquest anàlisi, es proposen, simulen

i analitzen cinc possibles escenaris de restauració basats en la modificació del terreny o de la dinàmica de cabals. Els resultats de l'anàlisi assenyalen les defenses construdes com els màxims responsables de la manca d'activitat geomorfològica actual.

A més del flux i la capacitat erosiva, s'ha inclòs en el model 2D hidràulic de simulació un model predictiu de captació de nutrients. Per a tal objectiu, s'ha examinat la retenció de fòsfor inorgànic i nitrogen dissolts mitjançant una sèrie d'experiments controlats en una sèquia de regadiu, situada a l'àrea d'estudi i alimentada per aigua de l'Ebre, i a un canal de laboratori. Aquest últim es va utilitzar per estimar la retenció de nutrients per part del sediment, mentre que a la sèquia es va avaluar la retenció de nutrients com a resultat de l'acció conjunta de la columna d'aigua i el sediment. En ambdós casos es realitzaren una sèrie d'experiments basats en la injecció controlada de fòsfor i un traçador (Br^-) per estimar el coeficient de retenció de nutrients, k. Degut a l'elevada concentració de nitrogen a la sèquia, la seua captació va a ser avaluada utilitzant la seua concentració ambient. Els resultats mostren una capacitat de retenció de fòsfor per part de la columna d'aigua i del sediment de 20.7 ± 2.8 %. Pel contrari, el sistema va presentar una capacitat nulla de retenció de nitrogen. Per aquesta raó, sols el fòsfor dissolt serà considerat al desenvolupament del model de retenció de nutrients.

La nova formulació que descriu la retenció de nutrients es va desenvolupar mitjançant la utilització de les dades experimentals.

En primer lloc, es van identificar els principals agents relacionats amb la captació de fòsfor mitjançant l'anàlisi estadístic del coeficient de captació i les característiques físiques, químiques i biològiques del sistema (la sèquia i el canal de laboratori). Els resultats mostren que el procés responsable de la major part de la retenció del fòsfor és l'adsorció, tant al sediment com a la columna d'aigua. A continuació, mitjançant una regressió lineal entre el coeficient de captació i els paràmetres físics, químics i biològics implicats en la retenció de fòsfor, es va obtenir una equació que descriu el procés de captació de fòsfor. La equació s'introdueix en el model hidràulic 2D com a terme de decament del fòsfor, i es valida tant al canal de laboratori com a la sèquia. La comparació entre les prediccions del model i les dades experimentals donà com a resultat regressions lineals significatives ($p \leq 0.05$) amb $r^2 \geq 0.8$ a 19 dels 20 experiments.

El model de transport i sedimentació de soluts particulats també va ser inclòs al model hidràulic 2D i es va validar a la planícia de inundació utilitzant les dades experimentals arreplegades durant dos esdeveniments de riuada. La comparació dels càlculs del model i les observacions de camp donà com a resultat una regressió lineal significativa ($p \leq 0.05$) amb una r^2 de 0.97.

El model de simulació complet que inclou potencial erosiu, transport de soluts i retenció de fòsfor inorgànic dissolt va ser utilitzat per simular i analitzar aquestos processos a la plana d'inundació. Segons aquest anàlisi, la adsorció del fòsfor als sòlids en sus-

pensió i la seua posterior sedimentació pareix ser el major responsable de la retenció de fòsfor a la plana d'inundació. L'anàlisi també revela l'existència de cert desequilibri entre els processos d'erosió i sedimentació en favor d'aquest últim. Finalment, les simulacions suggereixen la presència d'un gradient lateral de connectivitat que decreix amb la distància al riu i governa la contribució de nutrients a la planícia de inundació. Segons aquest gradient, les zones més allunyades del riu reben una quantitat molt baixa o fins i tot nulla de sòlids dissolts i particulats, mentre que les zones més properes reben les concentracions més elevades. Per tant, el gradient lateral podria estar afectant negativament a la vegetació ripària de les zones més remotes de la plana d'inundació.

Finalment, el model complet ha estat utilitzat per proposar, simular i analitzar dos alternatives de restauració de la plana d'inundació basades en la modificació del terreny.

A mis padres y a Pau

Acknowledgements

Quisiera empezar dando las gracias de forma muy especial a dos de las personas que han hecho posible esta tesis, Pilar y Javier. Sin duda alguna, sin su apoyo y sobretodo sin su ayuda, ésto no habría sido posible. Gracias a vosotros no sólo he terminado la tesis, sino que lo he hecho aprendiendo y disfrutando más de lo que me hubiera imaginado.

También quiero darle las gracias a Antonio del Campo por darme la oportunidad de presentar la tesis en Valencia y por colaborar en todo aquello que ha podido y más, y además siempre con una sonrisa. Igualmente, quiero darle las gracias a Paco Comín, por la oportunidad de realizar la tesis y tratar de dotarme de los medios para ello.

I would like to thank Jan Vermaat for the incalculable contribution to this thesis, his teaching, his enormous patience, all the corrections he had to make and his kind welcome when I was in Amsteradam. In the same way, I would also like to thank the

IVM institute for bringing me a very kind stay in Amsterdam. I would specially like to thank Martin, Mairon, Eric, Eszter, Ángel and of course Willem (little brother), who became a good friend after my stay there.

Thanks to Tyris Films company (www.tyrisfilms.com) for the design of the cover.

Quisiera darle las gracias también a Francesc Sabater por resolverme tantas y tantas dudas cuando comenzaba el capítulo de los nutrientes y dedicarme el poco tiempo libre que tenía.

Quiero agradecer a Anna García Ortolà el haberme introducido en el mundo de la investigación y haberme animado y ayudado a que siguiera mi camino. Igualmente, quiero agradecer a Eva, Javi, Fran y Neus aquellos comienzos en la investigación. A Ester, no sólo los comienzos, sino todo el proceso, y por supuesto todas las veces que me has acogido en tu casa.

Me gustaría continuar por la gente del CPS que en mayor o menor medida han contribuido en esta tesis. Quisiera dar las gracias a Borja Latorre por su colaboración durante los comienzos de la tesis, durante los experimentos del canal y sobretodo por el desarrollo del algortimo de reconstrucción del río, creo que

sin eso no los resultados de la tesis no habrían sido ni la mitad de buenos. También quiero dar las gracias a Daniel Caviedes, por su paciencia, que es mucha, y las inumerables mallas y programas conversores que me ha facilitado. A Cuca, que me ha dejado siempre invadir su despacho. A Chuan, que aunque aquellos experimentos con la fluoresceína no fueron a buen puerto, se agradece el interés y sobretodo la ayuda. A Pedro Martín, por ayudarme con los experimentos del canal.

A la gente del IPE por supuesto también le quiero dar las gracias. A Merce, no se por donde empezar, si por los inumerbles cromas que me has pasado, por las veces que te has venido conmigo de campo, por todas las veces que me has animado con la tesis, por haberme ayudado a planificar los malditos experimentos de la acequia, y si me dejo algo lo siento, pero ya sabes que soy un poco despistada. A Alberto, también podría estar largo y tendido contigo. Gracias por todos los análisis que has hecho, por prepararme siempre los reactivos del fósforo, en definitiva por trabajar tan bien en el laboratorio. Aunque la verdad, una de las cosas que más agradezco de ti es que siempre me has hecho reir por muy agobiada de trabajo que estuviera. Y por supuesto, por todas esas noches en el Dumbo. A Antonio, que tamibién era especialista en hacerme reir, por todos los aperos que me ha hecho para la tesis y por supuesto, por arreglarme la espalda para que pudiera seguir trabajndo. A MPaz quiero darle las gra-

cias también de forma muy especial, no sólo por su inestimable ayuda con el GIS, sino por su apoyo, porfesional y personal y por ser como es. A Benito, que aunque estuviéramos en grupos diferentes, ha sido una parte muy importante de mi vida en el IPE, y que más que un compañero es un amigo. A Belinda, por su ayuda en los comienzos de la tesis y compartir conmigo esa afición de comer galletas en e campo. A los ayudantes del instituto Corona de Aragón, Irantzu y Samuel por su ayuda en el laboratorio. También quiero darle las gracias a Mattia y a Fabián que son parte del grupo de investigación. A Ana Constante, por sus ánimos, por preocuparse tanto y por su amistad. Por último, le doy las gracias a MariaLuisa por su ánimo, su interés y su tesón.

Quiero darle las gracias a una persona muy especial que de una forma u otra ha contribuido enormemente en esta tesis, Antonio el pastor de la reserva. Gracias no sólo por tu ayuda física, sino por todos los ratos que hemos pasado en el campo y todo lo que me has enseñado a cerca del mismo, que es mucho. También le doy las gracias a los forestales de la Reserva Natural, por ayudarme siempre que lo he necesitado.

Agradezco también a mis compañeras/os de piso de Zaragoza, que me amenizaron la estancia allí. Quería agradecer muy especialmente a Rebeca por estar conmigo desde el principio, tra-

garse todos mis cabreos y estreses del trabajo y por ser una amiga durante mi estancia allí.

Quisera continuar por personas que empezaron siendo tan sólo compañeros de trabajo y han acabando siendo muy buenos amigos. A Noemí, tendría que escribir una sección sólo para ti. Gracias por tu amistad, por tu forma de ver las cosas y sobretodo de compartirlas. Has sido una parte fundamental para mi en el IPE, y afortunadamente también lo eres fuera de él. A Leticia, que has sido un apoyo increíble en esta última etapa de mi tesis, y no sólo porque me des cobijo, que también, sino porque eres una de las mejores amigas que se pueda tener. A álvaro, que no se ni como darte las gracias. Has sido super importante en mi tesis, profesional y personalmente. Gracias por tu fuerza, tu buen humor, por compartir tantas cosas conmigo, por tu ”cabeza circular”, por los días inolvidables de campo y psicoanálisis y por mantener el contacto después de tanto tiempo. A Edu, que tampoco se ni por donde empezar. Gracias por todos esos días en el zulito, sin duda alguna sin ti no hubiera sido lo mismo, Gracias por esa complicidad, por esos interminables días de campo bajo el sol, la lluvia, la niebla o lo que tocara. Por entenderme tan bien, por tratar siempre de ayudarme, por tu profesionalidad, aunque no te lo creas, por tu fuerza, y en definitiva por ser tú.

Me gustaría continuar por mis amigos, personas que de una forma u otra siempre han estado ahí animándome. A Raquel, mi mejor amiga, por animarme y acompañarme desde hace tantos y tantos años. A Rodrigo, que siempre me hace reir cuando más lo necesito, por su forma de ver la vida, su ánimo y sobretodo por su amistad. A Merche, que aunque desde la distancia, siempre has estado ahí, y tu amistad siempre ha sido un referente para mi. A Jose, que además de siempre estar dispuesto a echar una cerveza en el mejor momento, es un buen amigo.

Quisiera seguir por mi familia, la gente que de verdad ha hecho posible que yo ha llegado hasta aquí. Gracias a mi padre y a mi madre, por ser siempre un referente en mi vida, por apoyarme siempre, animarme, ”centrarme”, y en definitiva, por ser como sois. Gracias a mi hermano, por animarme, en los buenos y en los malos momentos y por ser un referente para mi en muchas cosas. Gracias a Yola, por agunatarme y apoyarme siempre. Gracias a Teo, que aunque aún no la sabes, eres de las personas más importantes en mi vida. Gracias a mis primos Pablo y Jesús, por ser vosotros siempre. Gracias a Carles, que en esta última etapa ha sido una ayuda inestimable.

Por último, quisiera darle las gracias a la persona que más ha sufrido esta tesis, Pau. Has sido el mayor apoyo que haya podido tener. Gracias por aguantar todo lo que has aguantado,

por animarme incluso sin ganas, por entenderme, por cuidarme, por sonreir siempre, por interesarte y por ayudarme en todo momento. Por ser tú y estar ahí siempre.

Contents

CONTENTS

List of Figures

LIST OF FIGURES

LIST OF FIGURES

LIST OF FIGURES

List of Tables

LIST OF TABLES

LIST OF TABLES

LIST OF TABLES

1

Introduction

1.1 Floodplain ecosystems

Floodplains are ecotones between upland and river-channel environments that alternate between aquatic and terrestrial states (Junk et al. (102)). The dynamic interaction between water and land, generated by recurring flooding, is the main process that produces and maintains these ecosystems (Bayley (14)). As a result, a diverse shifting mosaic of habitat (SHM) patches is generated across the riverine landscape, where many species can co-exist (Hauer and Lorang (71)). This interaction is known as hydrological connectivity, and constitutes the driving force that produces the lateral interchange of particulate and dissolved matter, both via surface flow (the flood pulse concept of Junk et al. (102)) and via groundwater pathways (Heiler et al. (73), Ward and Standford (212), Galat et al. (59), Ward et al. (213)) (see Figure 1.1).

Hydrological connectivity between the river and the floodplain provides the opportunity for the floodplain to function as a natural sink for sediment

and nutrients, emanating from the headwaters and lateral sources such as agricultural crops, and urban and industrial effluents (Burt et al. (31)). Hence, the floodplain receives directly from the main channel all classes of nutrients, and its basic nutrient status would be expected to correspond to that of the river (Junk et al. (102)). However, ecotones are characterized by their own set of ecological processes and interactions (Odum (147)), and therefore, floodplains tend to establish their own cycles (Junk et al. (102)). For instance, gases such as CO_2, O_2, H_2S, CH_4 and N_2 are produced and/or consumed in the floodplain, within systems with slow, regular flood pulses, independently of processes in the main channel (Junk et al. (102)). Particulate inorganic matter increases its ecosystem relevance once it reaches the floodplain and becomes a basic part of the nutrient pool, available to primary producers in the dry phase and during part of the wet phase (Junk et al. (102)). Dissolved nutrient content is also affected by the floodplain biotic and abiotic processes (Junk et al. (102)), which tend to reduce the floodplain nutrient concentration.

The river nutrient contribution into the floodplain constitutes an elemental process for the floodplain production and maintenance. Essential nutrients, such as nitrogen (N) or phosphorus (P), are often floodplain productivity limiters, and needs the river inflowing to replenish their concentration (Junk et al. (102)). However, an excess of river contribution of N and/or P might produce the eutrophication of the system, and the consequent water quality decreasing. In the same way, a lack of N and/or P might produce an impoverishment of the freshwater ecosystem. Hence, the concentration and equilibrium between both compounds determines the floodplain ecosystem status.

The processes that undergoes the transformation and/or uptake of N and P in the floodplain are very different. The P cycle comprises the dissolved and particulate forms, its major source is the sedimentation (Mitsch and Dorge (131), Johnston (101); Vought et al. (206)) and the sorption and precipitation are considered the most important longterm P sequestration mechanisms (Richardson (171); Richardson and Marshall (172); Reddy et al. (166)). In contrast, the N cycle comprises three forms: dissolved, particulate and gas, and its main source varies among the floodplains. Some authors found the sedimentation as the major nitrogen contribution (Olde Venterink et al. (150)), whilst other authors pointed out the atmospheric deposition and nitrification as the main N sources (Koerselmanb and Verhoeven (109); Johnston (101); Vought et al. (206); Olde Venterink et al. (148)). Three processes contribute to N retention: denitrification, sedimentation and uptake by aquatic plants. The relative importance of each mechanism depends on the floodplain ecosystems characteristics (Saunders and Kalff (179)).

Sedimentation is therefore an essential process for both pollutant trapping and floodplain nutrient contribution. During the last decade, attention has focused on the fluxes of suspended sediment and particulate P through freshwater drainage systems because of severe eutrophication effects in rivers, lakes, reservoirs and coastal waters observed throughout the world (e.g. Meybeck et al. (126), Carignan and Vaithiyanathan (40), Bowes and House (23), Olde Venterink et al. (149), Braskerud et al. (26)). Several studies based on field measurements confirm the largely influence of the sedimentation process

on P uptake (Johnston (101), Alexander et al. (4), Bowes and House (23), Olde Venterink et al. (149)). Predictions of P retention in riparian buffers are nowadays extremely challenging because of the complex interactions and feedback between hydrology and biogeochemical transformations of P (Martin and Reddy (121); Cirmo and McDonnell (49); Hattermann et al. (70)), and so is its numerical modeling, that includes transport and transformation of both sediment and P (Carignan and Vaithiyanathan (41)).

1.2 Floodplain benefits and restoration need

Floodplains are among the biologically most productive and diverse ecosystems on earth (K. and Standford (103)). In the last few decades, the ecological services and goods that these ecosystems provide have been widely recognized, and even their value has been economically estimated. The major services of floodplains include disturbance regulation (37% of their total value), water supply (39%) and waste treatment (9%) (K. and Standford (103)), although these areas also are highly valued for their transportation potential, food and fiber production, recreation, and beauty. The estimated worldwide value of the services provided by flood plains is US 3920E09 yr^{-1}, assuming that the total floodplain area is about $2E06\ Km^2$ and area-based value is US 19580 ha/yr (K. and Standford (103)).

In spite of their values, floodplains are among the most threatened ecosystems in the world (K. and Standford (103)). Man induced alterations through impoundments, river regulation and channelization represent the major threat

to river systems worldwide. These impacts affect important riverine hydromorphological processes (fluvial dynamics), which define the dynamic equilibrium of habitat distribution with their characteristic biota (Giller (62), Nilsson et al. (145), Reckendorfer et al. (165), Schiemer et al. (180)). In many riverine systems, hydrological connectivity between the river and its floodplain is restricted to groundwater pathways, and geomorphological dynamics are mostly absent (Marchand (118); Heiler et al. (72)). As a result, river restoration has become a global issue in terms of geomorphology, hydrology and ecology, and river engineers are seeking the cooperation of these sciences to improve degraded waterways within small to large scale river restoration projects (Palmer et al. (154)).

Most river restoration efforts are almost exclusively based on empirical experience (Richards and Hughes. (170)), where the relationship between effort and results is not always satisfactory. Most of these empirical studies show a difficult application in other systems or even at other spatial-temporal scales within the same system. It is widely recognized that empirical data are necessary to understand the past, present and future of the riparian processes, but it is also true that considering the different spatial-temporal scales of the operating processes is fundamental in riparian system restoration (Ward et al. (215)). Including all spatial-temporal scales in the empirical approach requires a temporal and economic effort that is not always possible to assume. Therefore, numerical simulation can be a useful tool, capable of considering diverse spatial-temporal scales but without excluding the need of some empirical experience. Using numerical simulation it is possible to reproduce and

predict the dynamic interaction between river and its floodplain, and therefore, fundamental riparian processes such as solute transport, nutrient uptake and hydromorphological dynamics. Numerical simulation is commonly used as a predictive tool. Indeed, it can be an efficient restoration tool, capable of represent and predict the results of different riparian restoration alternatives before to carry them out. Furthermore, the accurate reproduction of the floodplain-river dynamic interaction, makes the numerical simulation a useful tool for a better understanding of the different spatial-temporal riparian processes.

At the same time, numerical simulation progress needs the empirical experience. The use of numerical simulation in real cases, makes possible the validation of the models, but it also stimulates the implementation of new functions as a response of the needs of a particular experience. Therefore, the use of numerical simulation for riparian restoration purposes favor the improvement of both disciplines.

1.2.1 The floodplain middle Ebro river

The middle Ebro river does not constitute an exception in the floodplain degradation problematic. The Ebro river is the largest Mediterranean river of the Iberian Peninsula, and therefore, it is a greatly regulated river. The alterations of river flows and floodplains have disrupted the intensity, frequency, and timing of the natural disturbance regime responsible for maintaining the ecological integrity of these ecosystems. During the last century, the flow

regime has been greatly disrupted. Irrigation of lowland areas and abandonment of farms-lands in upland areas during 20's century (García-Ruíz et al. (60), Ibanez et al. (92), Beguería et al. (18), Batalla et al. (9), Beguería et al. (17), Lopez-Moreno et al. (113), Vericat and Batalla (205)), construction of dams from 1913 to 1975 for irrigation purposes, and the agricultural production that since 1980's has been largely driven by an emphasis on the cultivation of water-hungry crops (Frutos et al. (58)), has resulted in a dramatically change of both hydrology and sediment transport and the occupation of river margins and massive construction for flood protection (Pinilla (160)).

Several studies have been carried out within the study reach reporting the current floodplain anthropic degradation. Regato (168) reported that natural vegetation had been strongly modified by anthropic alterations, and this was later confirmed by Castro et al. (45). Ollero (151) highlighted the morphological dynamics decreasing as a result of river regulation and protection structures. Cabezas et al. (34) reported a strong morphological stability of the floodplain that leads to a lack of landscape diversity. Cabezas et al. (36) measured biodiversity within the study site and reported the presence of an homogeneous river scape dominated by wetlands at mature successional stages as a result of the hydrological connectivity decrease. Cabezas and Comín. (33) pointed out that human occupation of the Ebro river region has lead to smaller accumulations of soil organic carbon and soil organic matter during the intervals between floods. González et al. (63) found successional and hydrological gradients within the floodplain, where the main successional activity is near the main river channel. These studies resulted in an important

scientific and ecological contribution that highlighted the need of a floodplain restoration strategy focused on restoring the hydromorphological dynamics. However, since all of them are exclusively based on field measurements, numerical simulation might be a necessary tool for an efficient selection of the best restoration alternative.

1.3 The hydraulic model

In the present work, the hydrodynamics of a floodplain are simulated, attending to the physical-chemical processes within the main river channel as well as within the floodplain. Therefore, it is crucial to choose a suitable simulation model capable of reproducing properly the hydraulics of the problem. Simulating a stream, floodplain, coastal areas or urban zone may not require the same numerical model. Thus, each problem needs to choose the most efficient solution, and our focus of attention is the floodplain modeling.

Floodplains are extended flooding areas, subjected to recurring floods whereas the properly representation of the flood wave advance is of doubtless interest. Therefore, a model that takes into account the complexity of the water movement over the terrain surface becomes necessary. It is important to make sure that the model is able to handle properly the topographic complexity as it is one of the major factors governing the water flow dynamics. Secondary channels, depressions and general terrain irregularities play an important role in environmental flows, and it dismiss simplistic approximations

Most popular hydraulic models use the one-dimensional (1D) Saint-Venant equations, or also called 1D shallow water equations. They consider that flow is directed only in the longitudinal direction of the river, and do not consider transversal variations for the water depth and for velocity. Being useful in problems where the flow is confined between river banks, in cases where water overflows and leaves the main river bed, they render useless. This is approximation is specially inappropriate in meandering rivers.

Being the flow in rivers three-dimensional (3D), models that make use of the Navier-Stokes equations seems to be the best option to represent flood-plain hydrodynamics. 3D models produce accurate results at the cost of a high computational effort. In fact, simulation of flooding events becomes unapproachable in cases of extent areas. When evaluating real flows in rivers the cost of the non-simplified three-dimensional numerical methods can be avoided using two-dimensional (2D) depth integrated models, as water depths involved allow for such kind of approximation.

As water in rivers and estuaries are usually well-mixed and flows are pressure-driven, so the dissolved chemicals are generally distributed uniformly over a water column. Understanding that dissolved solute transport is determined by the characteristics of the fluid flow, the shallow water model has been accepted as the basis for the development of ambitious environmental or hydraulic models (Vreugdenhil (207) and Wu (219)).

Indeed, looking at the available literature in surface environmental flood

Table 1.1: Model comparison.

Comparison of some of the most used 2D hydraulic models to the used in this work, SFS2D.

Model	Flow equations	Method	Coupled solute transport	Discretization	Field Application/validation
TELEMAC-2D (Hervouet (76) and Hervouet (77))	Shallow water equations with turbulence closure	Finite difference	No	Structured-unstructured quadrangular-triangular mesh	Horritt and Bates (82): 84 % flooded area agreement using low resolution satellite imaginary data. The authors conclude that a substantially more validation is required.
RMA-2 (Roig (174) and King (104))	Shallow water equations with turbulence closure	Finite element	No	Structured-unstructured quadrangular-triangular mesh	Wagner (208): 0.1 m difference between measured and calculated water depth using 3 gauging stations. Two of them were also used as a boundary conditions.
MIKE-21 (Institute (93))	Shallow water equations with turbulence closure	Finite difference	No	Structured square or rectangular mesh	(Ahmad (2)) 0.1-0.3 m difference between measured and calculated water depth in the gauging stations used as boundary conditions.
HYDRO2DE (Beffa and Connell (16))	Shallow water equations with turbulent diffusion	Finite volume	No	Structured-unstructured triangular mesh	Connell et al. (51): $\pm$0.26 m Standard error in water depth using resident-supplied information and photographs.
SFS2D (Murillo et al. (136) and Murillo et al. (138))	Shallow water equations with turbulent diffusion	Finite volume	Yes	Structured-unstructured triangular mesh	Validation in Chapter 1: 79% flooded area agreement using a differential GPS data.
IBER (CEDEX (47))	Shallow water equations with turbulent diffusion	Finite volume	No	Structured-unstructured triangular-quadrilateral mesh	

simulations, most studies use depth-averaged 2D models (Bates et al. (13), Somes et al. (187), Horritt (81), Beffa and Connell (16), Cobby et al. (50), Bates et al. (12).). Table 1.1 shows the comparison of the main properties of some of the most used 2D hydraulic models.

Some of the 2D models applied in floodplains are based on simplified models, neglecting the inertial terms and assuming important simplifications of the hydrodynamical effects. They are usefully if the emphasis is put in flooding impact in terms of flood extent, flood depth and flood duration, and provide information with a low computational cost (Hervouet (76) and Hervouet (77), Roig (174) and King (104), Horritt (81), Cobby et al. (50)).

In terms of the physical-chemical floodplain processes such as nutrient transport, simplification of the equations reduces significantly the accuracy of the results, as the responsible terms involved in transport are omitted or excessively simplified. On the contrary, using the full shallow water equation models (Murillo et al. (138)) instead of the simplified models, reliable information of the flow velocity can be provided, and it is of paramount importance when dealing with transport of dissolved chemical species.

Also, although numerical modeling of free surface flows with chemical transport over complex bed in realistic situations involves transient flow and movable flow boundaries, the conventional methods for performing environmental simulations in rivers uncouple the hydrodynamics and the transport of chemical agents. Ignoring unsteady hydrodynamical effects means that only

a quasi-steady process over very slowly varying bed level can be reasonably modeled, so that, the correct simulation of solute transport in rapidly varying flows containing shocks or discontinuities remain excluded. When solving real problems one is likely to encounter all sorts of situations, with a high probability that naive methods will compromise the quality and reliability of the solution.

In this context, we propose the use the SFS2D (Shallow Flow Simulation in 2D) numerical model developed by Murillo et al. (136) and Murillo et al. (138), which solves the full shallow water equation models and couples the hydrodynamic part and the solute transport. The numerical discretization is based on a finite volume method that used an augmented Roe's approximate Riemann solver. Detailed information of the numerical model is showed in Chapter 3.2.

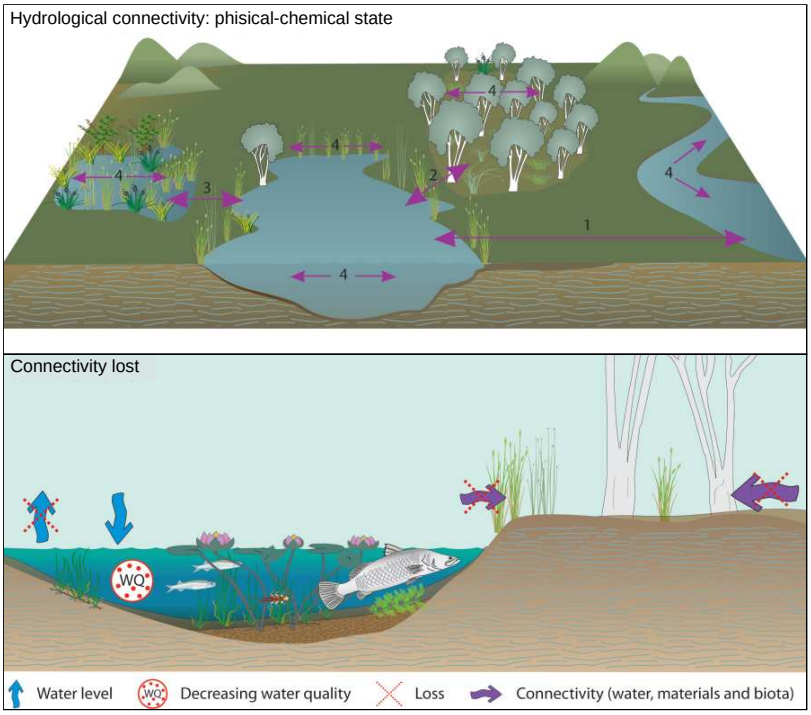

Figure 1.1: Floodplain hydrological connectivity.
Up: floodplain hydrological connectivity via surface flow. (1) Lateral floodplain-river connectivity, (2) tree swamp, (3) non-floodplain grass-sedge-herb swamp and (4) longitudinal connectivity and within system. Down: Loss of hydrological connectivity. Figure from Queensland Government, Australia.

1. INTRODUCTION

2

Aims of the project

Considering the relevance of the floodplain ecosystems and the hydrological connectivity as the main process that produces and maintain those ecosystems, we pretend to enhance the need of the restoration and preservation of its natural hydrodynamics. Hence, the focus is on floodplain hydrological connectivity, sedimentation, hydromorphological and nutrient dynamics. Taking into account the need of an efficient tool capable of understand and predict this hydrodynamics, the development of a simulation tool that includes those processes is a major part of the present work.

2.1 Final aim

Our ultimate goal is to analyze the hydrological and the physical-chemical processes that produce and maintain the floodplain ecosystem by means of the numerical simulation. We aim to establish the numerical simulation as

a predictive tool suitable for the management and restoration of the riparian ecosystems.

2.2 Preliminary aims

The main goal has been specified in nine specific objectives that cover both numerical and experimental floodplain analysis, in an attempt to develop, validate and apply a simulation tool that integrates flow dynamics, sediment transport and nutrient uptake. These objectives are described below:

1. Validate a complete 2D shallow water model in finite volumes.
2. Include a simple hydromorphological dynamics representation in the 2D shallow water model.
3. Development of an unsteady nutrient uptake model of predictive character and couple it to the 2D shallow water model.
4. Couple sediment transport to the 2D shallow water model.
5. Validate the complete simulation model in a real riparian system using experimental field data.
6. Analyze the current floodplain hydrological connectivity.
7. Analyze the influence of the current flow regime and the constructed river defenses in the floodplain geomorphic activity thorough the simulation tool.

8. Analyze the current sediment and dissolved phosphorus floodplain dynamics by means of the simulation tool.

9. Generate possible restoration scenarios through the simulation tool.

2.3 Study outline

Chapter 4 focuses on floodplain flooding dynamics (see fig. 2.1). A two-dimensional simulation model was validated using field data and GIS analysis. Then, we included a simple hydromorphological dynamics representation in the 2D shallow water model to analyze the current floodplain flooding dynamics and its geomorphological activity. Based on this current floodplain analysis, five possible hydromorphological restoration alternatives have been simulated and analyzed.

Chapter 4 has been accepted for publication in Journal of Hydraulic Engineering as: Gonzalez-Sanchis, M., Murillo, J., Latorre, B., Comin, F. and Garcia-Navarro, P. Transient two-dimensional simulation of real flood events in a mediterranean floodplain.

In Chapter 5, nutrient uptake capacity was examined by means of experimental and computational analysis (see fig. 2.1). Field experimentation was carried out in an irrigation canal within the study area, whose water discharge comes from the Ebro river. Solute transport, including both reactive and non reactive substances, was included in the two-dimensional simulation model. To determine the main factors related to the nutrient uptake, experimental

data were subjected to multivariate statistical analyses involving Principal Component Analysis (PCA). A nutrient uptake coefficient was estimated using different approaches: one-dimensional steady state, two-dimensional unsteady state and kinetic. A new nutrient uptake formulation was developed and included in the two-dimensional simulation model. Accuracy of the four nutrient uptake calculation methods was analyzed comparing experimental and calculated data thorough a linear regression analysis.

A summarized version of chapter 5 has been submitted to the journal Water Resources Research as: Gonzalez-Sanchis, M., Murillo, J., Vermaat, J., Comin, F. and Garcia-Navarro, P. Nutrient retention capacity of an agricultural drainage channel: developing a predictive model.

In Chapter 6, validation of the nutrient uptake and sediment transport model is performed by means of field experimentation in the Ebro river (see fig. 2.1). Then, floodplain solute dynamics, nutrient uptake and sedimentation pattern were analyzed using the complete two-dimensional simulation model. Finally, following the results of the floodplain analysis, two possible restoration scenarios have been simulated and analyzed.

Chapter 6 has been submitted to the journal Water Resources Research as: Gonzalez-Sanchis, M., Murillo, J., Cabezas, A. Vermaat, J., Comin, F. and Garcia-Navarro, P. Modeling nutrient and sediment dynamics in the middle Ebro river floodplain (NE Spain): a validation.

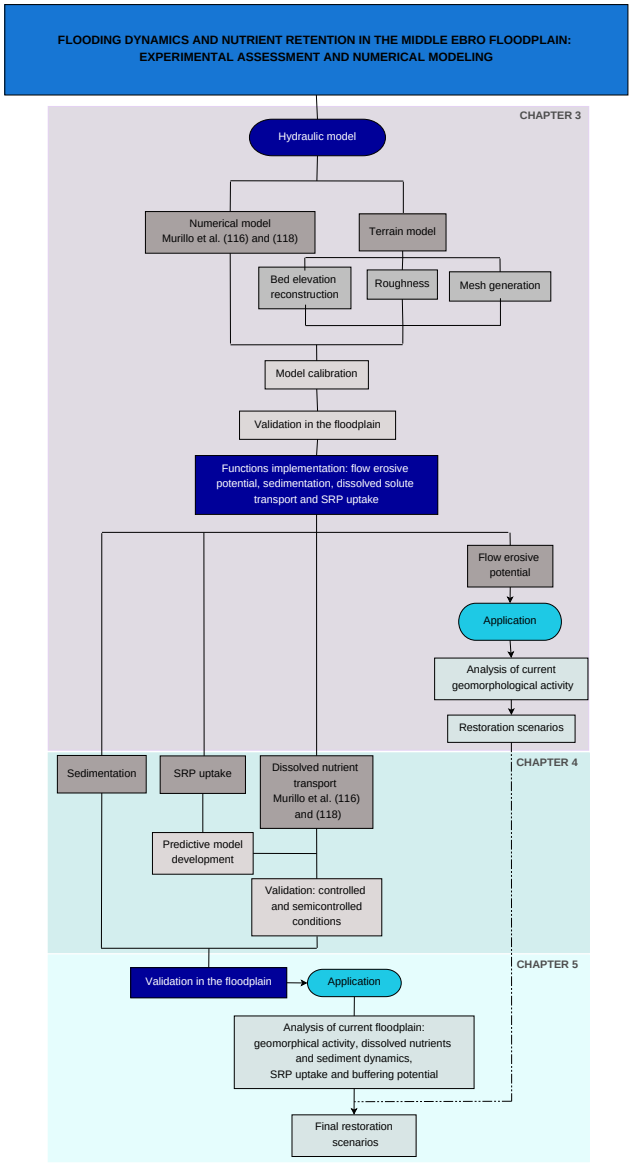

Figure 2.1: Study approach.
General study outlines. Main objectives are indicated and the chapter where they are accomplished.

2. AIMS OF THE PROJECT

3

GENERAL METHODOLOGY

3.1 Study Area

Three studies were carried out in a 2 Km river segment located along the middle Ebro basin, 12 Km downstream Zaragoza city (NE Spain). The reach of the Ebro river in the study area forms a meander (3.7 Km^2, river width: 110 m with one island and an oxbow lake) included in the Natural Reserve "Los Galachos de la Alfranca, Pastriz, la Cartuja y el Burgo de Ebro" (see Figure 4.1). The discharge, averaged over the years 1927 to 2010, within this reach is 230 m^3/s (Ebro River Basin Administration: www.chebro.es), and the surface elevation ranges from 175 m above sea level (a.s.l.) at the river channel to 185 m a.s.l. at the base of the old river terrace.

The Ebro is the largest Mediterranean river of the Iberian Peninsula, with a basin of 85 Km^2 and a channel length of 930 km. It has an annual discharge into the Mediterranean Sea of $1.8E07$ m^3/y, with a maximum in February, a minimum in August, and an asymmetry in the upward and downward curves

3. GENERAL METHODOLOGY

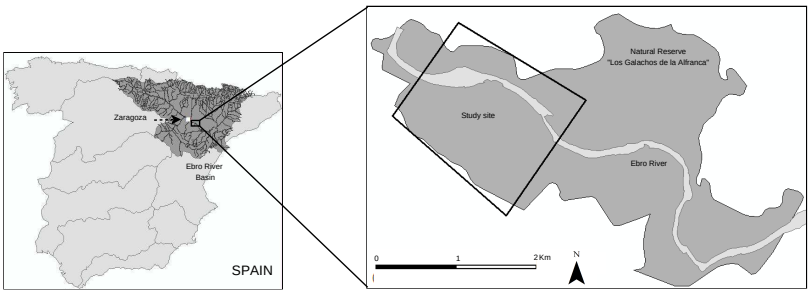

Figure 3.1: Location of the study area.
Black line represent the limit of the computational domain.

with a prolongation of the high water level in spring and the low water level in autumn (Ollero (153)). The water regime is regulated by the presence of 234 dams and reservoirs on the river basin, impounding 57% of the mean annual runoff (www.chebro.es), and whose main objective is irrigation purposes. Most (89.3%) of the water supply is dedicated to agriculture, whilst domestic and industrial activities ocupes 7.2 and 3.5 % respectively Bouza-Deano et al. (22). Hence, agricultural activities take up most of the Ebro catchment area (Pinilla (160)), and are directly related to the large number of lateral defenses constructed in the middle Ebro basin. As a result, the trend of middle Ebro river discharge has decreased, specially since the 1950s, and it causes a narrowing in the riparian corridor of the free meandering Ebro River over the last several decades (Ollero (153)) that reduces the natural floodplain forests to only 4.5% in the whole Middle Ebro (Ollero (152)). Furthermore, agricultural practices and the increasing of human activity during the last century decreases the water quality (Torrecilla et al. (198)).

3.1.1 Ecological aspects

The selected river segment is notably affected by embankment structures, where a 20% of its surface is occupied by crops and pasture. However, still some active morphological dynamics occurs, but this is restricted to the closest river floodplain (González et al. (63)). As a witness of the past hydrogeomorphic activity, the floodplain shows an oxbow lake and a paleochannel (see Figure 3.2), which still get superficially connected to the river during floodings, when sedimentation process prevail over erosion (Cabezas and Comín. (33)).

Steppic shrubby vegetation dominates the uplands adjacent to the floodplain. The riparian forest is composed of three softwood Salicaceae species: white poplar (*Populus alba*), European black poplar (*P. nigra*) and white willow (*Salix alba*), and five hardwood species: saltcedar (*Tamarix gallica*, *T. africana* and *T. canariensis*), narrow leaf ash (*Fraxinus angustifolia*) and field elm (*Ulmus minor*) (González et al. (63)). The flow regime creates a riparian forest gradient whereas the youngest vegetation is close to the main river channel, while the oldest is located in the upper floodplain terrace, further from the main river channel. Therefore, it is possible to find successional and hydrological gradients, where the main successional activity is near the main river channel (González et al. (63)).

The water quality is characterized by a high nitrogen concentration, high alkalinity, basic pH and low dissolved phosphorus content (see Table 3.1). The molar rate between total Nitrogen and Phosphorus (N:P 409:1) suggest

3. GENERAL METHODOLOGY

Figure 3.2: Natural and anthropic floodplain formations.
Numbers represents the different morphologic and anthropic formations, (1): crops and pasture fields, (2): young riparian forest, 3 is the old riparian forest, (4): paleochannel, (5): oxbow lake, (6): secondary channel and (7): constructed wetlands. White lines represent the lateral dikes built for flood protection. Dotted white lines denote the limits of the Natural Reserve "Los Galachos de la Alfranca, Pastriz, la Cartuja y el Burgo de Ebro". The black quadrant represent the limit of the computational domain. The aerial picture was taken in 2007.

that probably the phosphorus is a limiting nutrient for algal production (Zhen-Gang (221)).

Table 3.1: Water quality parameters at the study site.

Concentrations are expressed in mg/l, conductivity in $\mu S/cm$ and temperature in ^{0}C.

Water parameter	average±STD
Total Nitrogen	3.7±1.1
N-NO_3	2.4±1.5
N-NH_4	0.2±0.1
P-PO_4	0.04±0.01
Dissolved Oxygen	8.8±1.9
Alkalinity	239.9±106.0
pH	8.0±0.2
Conductivity	1156±466.6
Temperature	16.4±6.6

3.2 Two dimensional hydraulic model

A two-dimensional numerical model that includes dissolved and suspended solute transport, sedimentation and an estimation of the flow erosive potential was calibrated, validated and used to analyze and predict the floodplain morphological activity and flooding, dissolved nutrients and sediment dynamics. Furthermore, an SRP uptake model has been developed, calibrated, validated and coupled to the numerical model to represent the current SRP floodplain uptake as well as the total buffering capability.

3.2.1 Hydrodynamic simulation

A two-dimensional hydraulic simulation model, SFS2D, developed by Murillo et al. (136) and Murillo et al. (138) was used in the present work. Water flow under shallow conditions can be formulated by means of the depth averaged set of equations expressing water volume conservation and water momentum conservation. That system of partial differential equations will be formulated here in a conservative form as follows:

$$\frac{\partial \mathbf{U}}{\partial t} + \frac{\partial \mathbf{F}(\mathbf{U})}{\partial x} + \frac{\partial \mathbf{G}(\mathbf{U})}{\partial y} = \mathbf{S}(\mathbf{U}, x, y) \tag{3.1}$$

where

$$\mathbf{U} = (h,\ q_x,\ q_y)^T \tag{3.2}$$

are the conserved variables with h representing the water depth, $q_x = hu$ and $q_y = hv$, with (u,v) the depth averaged components of the velocity vector $\mathbf{u}$ along the (x,y) coordinates respectively. The fluxes of these variables are given by:

$$\mathbf{F} = \left(q_x,\ \frac{q_y^2}{h} + \frac{1}{2}gh^2,\ \frac{q_x q_y}{h}\right)^T, \qquad \mathbf{G} = \left(q_y,\ \frac{q_x q_y}{h},\ \frac{q_y^2}{h} + \frac{1}{2}gh^2\right)^T \tag{3.3}$$

where g is the acceleration of the gravity. The source terms of the system are the bed slope and the friction terms:

$$\mathbf{S} = \left(0,\ S_{ox} - \frac{\tau_{b,x}}{\rho_w},\ S_{oy} - \frac{\tau_{b,y}}{\rho_w}\right)^T \tag{3.4}$$

where the bed slopes of the bottom level z are:

$$S_{ox} = -gh\frac{\partial z}{\partial x}, \qquad S_{oy} = -gh\frac{\partial z}{\partial y} \tag{3.5}$$

The friction forces are expressed through the bottom shear stress $T_b = (\tau_{b,x}, \tau_{b,y})$, whose components can be written in terms of the Manning's roughness coefficient n:

$$\frac{\tau_{b,x}}{\rho_w} = ghS_{fx} \quad S_{fx} = \frac{n^2 u\sqrt{u^2+v^2}}{h^{4/3}}, \qquad \frac{\tau_{b,y}}{\rho_w} = ghS_{fy} \quad S_{fy} = \frac{n^2 v\sqrt{u^2+v^2}}{h^{4/3}} \tag{3.6}$$

System (3.8) is time dependent, non linear, and contains source terms. Under the hypothesis of dominant advection it can be classified and numerically dealt with as belonging to the family of hyperbolic systems. The mathematical properties of (3.8) include the existence of a Jacobian matrix, $\mathbf{J_n}$, of the flux normal to a direction given by the unit vector $\mathbf{n}$, $\mathbf{En}$, with $\mathbf{E} = \mathbf{F}n_x + \mathbf{G}n_y$, defined as:

$$\mathbf{J_n} = \frac{\partial \mathbf{En}}{\partial \mathbf{U}} = \frac{\partial \mathbf{F}}{\partial \mathbf{U}}n_x + \frac{\partial \mathbf{G}}{\partial \mathbf{U}}n_y \tag{3.7}$$

This Jacobian can be used to form the basis of the upwind numerical discretization that will be outlined in next section.

3.2.1.1 Dissolved solute transport

Solute transport and water flow under shallow conditions can be formulated by means of the depth averaged set of equations expressing conservation of

water volume, solute mass and flow momentum. The diffusion of the transported variables can be computed by inserting the formulation of the depth averaged κ-ε turbulence model (Rastogi and Rodi (164)), that are also modeled as transported scalars. Such a system of partial differential equations will be formulated here in coupled form for p general species as:

$$\frac{\partial \mathbf{U}}{\partial t} + \frac{\partial \mathbf{F}(\mathbf{U})}{\partial x} + \frac{\partial \mathbf{G}(\mathbf{U})}{\partial y} = \mathbf{S}(\mathbf{U}) + \mathbf{R}(\mathbf{U}) + \overrightarrow{\nabla}\mathbf{D}(\mathbf{U}) \tag{3.8}$$

where in matrix notation

$$\mathbf{U} = \begin{pmatrix} h & q_x & q_y & h\phi_1 & h\phi_2 & \dots & h\phi_p & h\kappa & h\varepsilon \end{pmatrix}^T \tag{3.9}$$

describes the conserved variables with h representing the water depth, q_x and q_y, with (u,v) the depth averaged components of the velocity vector **u** along the x and y coordinates respectively, ϕ_1,ϕ_2 ,...,ϕ_p representing the scalar depth-averaged concentration of the different quantities transported, κ the turbulent kinetic energy and ε the dissipation rate. The diffusion term **D** and the reaction term **R** are constructed using the $\kappa - \varepsilon$ model proposed by Rastogi and Rody (Rastogi and Rodi (164)). The fluxes of the conserved variables are given by:

$$\begin{aligned} \mathbf{F} &= \begin{pmatrix} q_x & \frac{q_y^2}{h} + \frac{1}{2}gh^2 & q_x q_y/h & q_x\phi_1 & q_x\phi_2 & \dots & q_x\phi_p & q_x h\kappa & q_x h\varepsilon \end{pmatrix}^T \\ \mathbf{G} &= \begin{pmatrix} q_y & q_x q_y/h & \frac{q_y^2}{h} + \frac{1}{2}gh^2 & q_y\phi_1 & q_y\phi_2 & \dots & q_y\phi_p & q_y h\kappa & q_y h\varepsilon \end{pmatrix}^T \end{aligned} \tag{3.10}$$

where g is the acceleration of gravity. The first source term **S** includes the

bed slope and friction in the momentum equations:

$$\mathbf{S} = \begin{pmatrix} 0 & gh(S_{ox} - S_{fx}) & gh(S_{oy} - S_{fy}) & 0 & 0 & \dots & 0 & 0 & 0 \end{pmatrix}^T \quad (3.11)$$

where the bed slopes of the bottom level z are

$$S_{ox} = -\frac{\partial z}{\partial x} \qquad S_{oy} = -\frac{\partial z}{\partial y} \quad (3.12)$$

and the friction losses are written in terms of the Manning's roughness coefficient n:

$$S_{fx} = n^2 u\sqrt{u^2+v^2}/h^{4/3} \qquad S_{fy} = n^2 v\sqrt{u^2+v^2}/h^{4/3} \quad (3.13)$$

3.2.1.2 Suspended solute transport and sedimentation

The suspended solute ϕ transport is calculated from:

$$\frac{\partial(h\phi)}{\partial t} + \frac{\partial(hu\phi)}{\partial x} + \frac{\partial(hv\phi)}{\partial y} = \frac{\partial}{\partial x}(hD_{xx}\frac{\partial \phi}{\partial x}) + \frac{\partial}{\partial y}(hD_{yy}\frac{\partial \phi}{\partial y}) + w_S(D-E) \quad (3.14)$$

where w_S is the particle settling velocity and D, E are the deposition and erosion rates respectively. w_S is calculated following Jimenez and Madsen (98) formulation.

3.2.1.3 Flow erosive potential estimation

To represent the floodplain geomorphological activity it is necessary to add a new term in the numerical scheme. As previously stated, the system of equations 3.8 assumes fixed bed. However, it is also possible to obtain information regarding the erosive capability of the flow. The bed erosion rate is directly related to the dimensionless bottom shear stress or Shields parameter (Wu (219)):

$$\theta = \frac{|\mathbf{T}_b|}{g(\rho_s - \rho_w)d_m} \tag{3.15}$$

where ρ_s and ρ_w are solid material and water densities, d_m is the bed particles median diameter (mm) and θ_c the critical Shields parameter, expressing the critical condition for incipient motion of sediment. The value of θ_c can solely be determined by fluid and sediment characteristics Cao and Meng (39) by means of the particle Reynolds number $Re = \sqrt{d_m^3(s-1)g}/\nu$, being ν the fluid kinematic viscosity.

The mathematical model does not account for morphodynamic changes of the bed, but it is possible to evaluate the following parameter:

$$r_\theta = \frac{\theta}{\theta_c} \tag{3.16}$$

and when $r_\theta > 1$ erosion is likely to occur.

3.2.2 Finite Volume Model

For the application of the finite volume scheme, (3.8) is integrated in a volume or grid cell Ω:

$$\frac{\partial}{\partial t}\int_{\Omega}\mathbf{U}d\Omega+\int_{\Omega}(\overrightarrow{\nabla}\mathbf{E})d\Omega=\int_{\Omega}\mathbf{S}d\Omega \tag{3.17}$$

Following previous work, it is assumed that the third integral can be re-formulated as in (**?**)

$$\int_{\Omega}\mathbf{S}d\Omega=\oint_{\partial\Omega}(\mathbf{Tn})dl \tag{3.18}$$

where $\mathbf{T}$ is a suitable numerical source matrix. This enables the following formulation

$$\frac{\partial}{\partial t}\int_{\Omega}\mathbf{U}d\Omega+\oint_{\partial\Omega}\mathbf{En}dl=\oint_{\partial\Omega}\mathbf{Tn}dl \tag{3.19}$$

When the domain is sub-divided in cells Ω_i ,using a mesh fixed in time, (3.19) can also be applied to each cell. Assuming first order in space approach equation (3.19) reduces to (Murillo et al. (138)):

$$\frac{(\mathbf{U}_i^{n+1}-\mathbf{U}_i^{n})}{\Delta t}A_i+\sum_{k=1}^{NE}(\delta\mathbf{E}-\mathbf{T})_k\mathbf{n}_k l_k=0 \tag{3.20}$$

where A_i is the cell area, $\delta\mathbf{E}=\mathbf{E}_j-\mathbf{E}_i$, with $\mathbf{E}_i$ and $\mathbf{E}_j$ the value of the function $\mathbf{E}$ at cell i and at cell j respectively, with j a neigbouring cell of i connected through the edge k, $\mathbf{n}_k=(n_x,n_y)$, is the outward unit normal vector to the cell edge k, l_k is the corresponding edge length, NE is the number of edges in the cell and $\mathbf{T}_k$ to be defined.

Due to the non-linear character of the flux **E**, the definition of an approximated Jacobian matrix, $\widetilde{\mathbf{J}}_{\mathbf{n},k}$, allows for a local linearization and is exploited here Roe (173). The problem is reduced to a 1D Riemann problem projected onto the direction **n** at each cell edge.

Following the unified discretization in (Burguete et al. (30)) with the discretization of the friction term based on Murillo et al. (138). Both bed slope and friction term can be split on the basis of eigenvectors in order to enforce the discrete equilibrium with the flux derivative terms, so (C-property) is ensured in steady cases with nil and not nil velocity (Murillo et al. (138) and Rosatti et al. (175)).

A careful discretization is specially required for the automatic treatment of wet/dry borders since it avoids unphysical results (Murillo et al. (138)). To allow the computation at the minimum computational cost a conservative flux redistribution presented in (Murillo et al. (138)) not affecting the accuracy of the results, has been used in this work. Also, a hybrid technique combining pointwise implicit and upwind explicit formulations for the friction source term presented in Murillo et al. (138), has been applied.

3.2.3 Hydrodynamic river bed reconstruction

In general Digital Terrain Models (DTM) developed in permanent rivers do not furnish any information of the region covered by the water, or at least, not with the same resolution as the rest of the terrain. However, when using 2D hydraulics models, it is necessary to provide the complete DTM, including

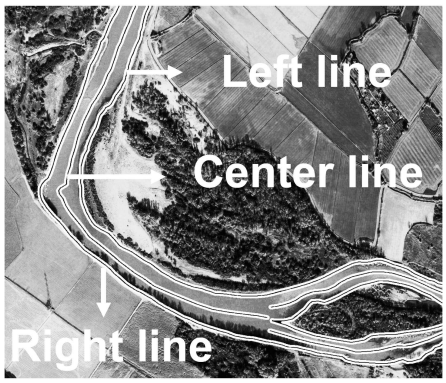

Figure 3.3: Example of auxiliar lines in the river reach.

the river bed elevation. Hence, an alternative method to interpolate and/or reconstruct the river bed elevation is necessary. The present work, propose a new method whose starting point is a gridded DTM of the area that includes the water surface level in the river at a given value of the river discharge. The information concerning the water surface elevation and the discharge is used to reconstruct the river bed. For that purpose, three auxiliar lines corresponding to the longitudinal axis and the left and right banks of the river are drawn (see Figure 3.3).

Several points along the axial or central line are chosen in order to assign them the water level elevation and to get an approximation of the water surface elevation derivative along the channel axis. The free surface level variations between adjacent points has a lower limit in the resolution of the terrain measurement technique used. Therefore, the computation of the surface elevation derivative at a point requires the use of information from other points located as far away as required by this limit. Furthermore, the com-

puted derivatives must be locally averaged in order to damp possible peak values and to produce realistic and smooth distributions. Only values of the derivative strictly greater than zero are allowable and a lower limit of 10^{-4} was selected in this study.

The river bed is reconstructed by following a path along all the P points in the original DTM file and applying a method that can be summarized as:

1. Every point P is identified as located inside or outside the river bed.

2. If point P is outside the river bed, the original bed elevation is kept and another point is considered.

3. If point P is in the river, the nearest point in the river axis P_C is sought. A straight line between P and P_C is drawn so that the intersection with the bank lines provides two new points P_R and P_L. See Figure 3.4 (left).

4. Points P_R and P_L define a cross section S in the river that contains point P and the top width of this cross section $2W$ is estimated as the distance between P_R and P_L. The value of the water surface level derivative along the river axis at point P_C, previously calculated, is assigned to the cross section as well as a value for the roughness coefficient.

5. A simplifying hypothesis concerning the cross section shape is made by assuming a symmetric triangular geometry. Then, with reference to Figure 3.4(right) the required depth ξ to convey the assumed water discharge Q across this section under uniform flow conditions is

estimated:

$$S_d = \frac{\partial(h+z)}{\partial l_r} = \frac{n^2 Q^2}{A^2 R_h^{4/3}} \tag{3.21}$$

where l_r is the coordinate direction that follows the channel axis defined by the central line containing point P_C and

$$A = W\xi \tag{3.22}$$

$$R_h = \frac{A}{2\sqrt{\xi^2 + W^2}} \tag{3.23}$$

From (3.23), the following non linear equation, $f()$, for the unknown ξ can be worked out in terms of n, Q and S_d:

$$f(\xi) = W^{10/3}\xi^{10/3} - \frac{n^2 Q^2 2^{4/3}(\xi^2 + W^2)^{2/3}}{S_d} = 0 \tag{3.24}$$

The roots of $f(\xi)$ are computed using the Newton-Raphson method, that requires the derivative

$$f'(\xi) = \frac{df}{d\xi} = \frac{10}{3}W^{10/3}\xi^{7/3} - \frac{4}{3}\frac{n^2 Q^2 2^{4/3}(\xi^2 + W^2)^{-1/3}\xi}{S_d} = 0 \tag{3.25}$$

Starting with an approximated value of, for instance, $\xi_0 = 0.5m$, the iterative procedure leads to the desired convergence in the solution that,

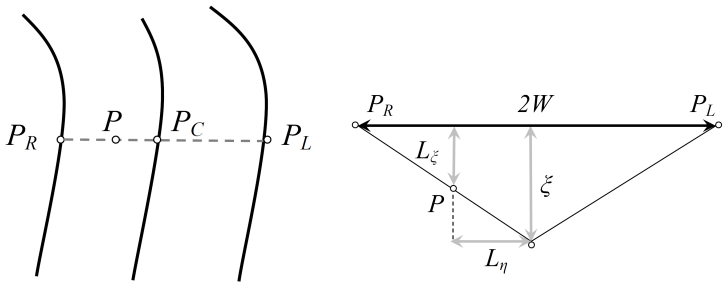

Figure 3.4: Example of auxiliar lines in the river reach.

in our case, was fixed in $10^{-3}m$.

$$\xi_{n+1} = \xi_n - \frac{f(\xi_n)}{f'(\xi_n)} \tag{3.26}$$

Being a quadratic convergence, the solution is obtained in no more than three or four iterations.

6. Once the cross sectional shape is determined, the water depth and therefore the bed level at point P can be calculated

$$L_\xi = \frac{\xi(W - L_\eta)}{W} \tag{3.27}$$

being L_η the distance between P and the midpoint of the line (P_L, P_R).

The application of these steps to all the points in the DTM provides an estimation of the full river bed reconstruction.

4

MODELING THE MIDDLE EBRO FLOODPLAIN FLOODING DYNAMICS AND ITS IMPLICATIONS FOR ECOLOGICAL RESTORATION

4.1 Introduction

Floodplains are domains situated between upland and river channel environments (Hauer and Lorang (71)) where aquatic and terrestrial systems coexist and are subject to recurrent flooding. The principal process that produces

and maintains river-floodplains is the dynamic interaction between water and land (Bayley (14)). The fluvial action of flooding creates a shifting mosaic of habitat (SHM) patches across the riverine landscape (Ward et al. (214)) and is a fundamental part of the hydrographical dynamics of riparian zones (Junk et al. (102), Standford (188)). Flooding, geomorphic change owing to cut and fill alluviation, and subsequent succession of the floodplain vegetation, continually transform the SHM establishing a transient equilibrium among new and old habitats (Hauer and Lorang (71)).

To interpret and predict the changes in river-floodplain interaction under different flow regime and/or management conditions, the numerical simulation of the overland water flow can be used as a tool to know the hydrological floodplain dynamics and to predict the hydrological behavior. When evaluating real flows in rivers, the cost of the non-simplified three-dimensional numerical methods can be avoided using depth integrated models, as water depths involved allow for such kind of approximation in most cases (Murillo et al. (138)). In river modeling, the use of the Shallow Water equations has been often justified (Vreugdenhil (207) and Wu (219)), where the flow can be assumed to be governed by the bottom friction and bed level irregularities maintaining the temporal transient character. This allows for an adequate representation of the surface flow processes that are a basic part of the mentioned hydraulic connectivity which is conditioned in part by the terrain topography Florsheim and Mount (56). When performing numerical simulations, this topography must be represented with enough fidelity to ensure accurate results, otherwise a different scenario will be simulated (Cook and Merwade (52)). In

this context, Digital Terrain Models (DTMs) provide exhaustive information of the floodplain, but the regions covered by water are a source of uncertainty (Hunter et al. (89)). Therefore, the decisions made to represent the river bed elevation may be of primary importance for some discharge values.

When the shallow water equations are solved in order to model the flow evolution in a river for floodplain inundation prediction or some other kind of eco-hydraulic simulation, the choice of the spatial model involves more than a change in the governing system of equations. A one-dimensional approach is led by boundary conditions at two points, the inlet and the outlet, and the computational domain is well defined between them. A two-dimensional approach involves a new difficulty: the computational domain is no longer fixed and well defined but can change as the flow evolves and is determined by a combined influence of the flow properties and the bed form.

Structured quadrilateral grids are generally preferred in hydraulic engineering practice since the connectivity between neighboring cells is trivial and there is no requirement for grid generation, in principle. These grids either fit perfectly or introduce undesirable corners in the borders of the wet computational domain. Triangular grids are useful mainly for their potential interest in adaptation to irregular boundaries but have not yet gained the same acceptance as quadrilateral grids for hydraulic applications. Therefore, not only most of the flow dynamics is considered in the mathematical formulation but it is also complemented with the best discrete representation of the relevant terrain information (Uchida et al. (201), Schubert et al. (181), Brown

et al. (27)).

In recent years, the development of robust and efficient explicit finite volume models of shallow water flow has been the matter of research in the computational hydraulics literature as the basis for the development of more ambitious environmental or hydraulic models. Bottom friction and bed level irregularities have been shown to influence not only flood waves behavior but also numerical methods performance drastically. A few efforts have been reported on the search for the best methods (Vazquez-Cendon (203), Hubbard and García-Navarro (86)) in presence of flow over irregular geometries (Zhou et al. (223), Audusse et al. (7), Murillo et al. (137)). When dealing with simulation problems that involve bed variations and transient flow over a dry bed, a correct numerical treatment becomes crucial. The best treatment of the wet/dry frontier in shallow water finite volume computation has been a matter of some activity (Akanbi and Katopodes (3), Bradford and Sanders (25), Murillo et al. (136)).

The present chapter is devoted to the application of a complete 2D shallow water model in finite volumes (see Chapter refGeneral Methodology) to the simulation of overland flow problems and to the validation of the numerical results with measured data with the aim of developing a tool capable of predicting the hydrodynamic floodplain behavior that could play a key role in the ecological restoration. For that purpose, first the area of study is described and the importance of the decisions concerning the use of the topographic data is emphasized. For that reason, the full model is defined as a

combination of the hydrodynamic flow simulation part, the roughness model and the topographic data representation. In order to gain confidence in the forecasts of mathematical models as a practical tool it is necessary to confront them with real life data. The necessary calibration phase is performed to decide the best roughness coefficients and the best topographic data representation. After that, the validation is performed by comparing the numerical results obtained from the complete model so defined with the water levels measured during other five flood events, with time series of continuous water-depth point measurements during different situations along the year and with flooded area measurements.

Once the model is validated, the simulations are used to evaluate the current floodplain geomorphic dynamics. Finally, different topographic scenarios, based on changes in the hydraulic river-floodplain connectivity, are generated in order to analyze their potentially beneficial effect in the floodplain geomorphic dynamics.

4.2 Objectives

Present chapter develops a tool to predict floodplain hydrodynamics that can be used as an ecological restoration tool. In this way, the specific objectives of the present work are:

1. Find an efficient representation of the roughness and terrain topography, including the main channel bed.

2. Validate a complete 2D shallow water model in finite volumes.

3. Analyze the current floodplain hydromorphological activity through the simulation model.

4. Analyze the influence of the current flow regime and the constructed river defenses in the floodplain geomorphic activity.

5. Propose and simulate possible geomorphological restoration scenarios.

4.3 Description of the study area

The study was carried out in a reach of the middle Ebro River, 12 Km downstream Zaragoza city. The reach was 2 Km long with an island and an oxbow lake (see Figure 4.1) and is included in the Natural Reserve ”Los Galachos de la Alfranca, Pastriz, la Cartuja y el Burgo de Ebro”. The discharge, averaged over the years 1927 to 2010, within this reach is 230 m^3/s (Ebro River Basin Administration: www.chebro.es), and the surface elevation ranges from 175 m above sea level (a.s.l.) at the river channel to 185 m a.s.l. at the base of the old river terrace.

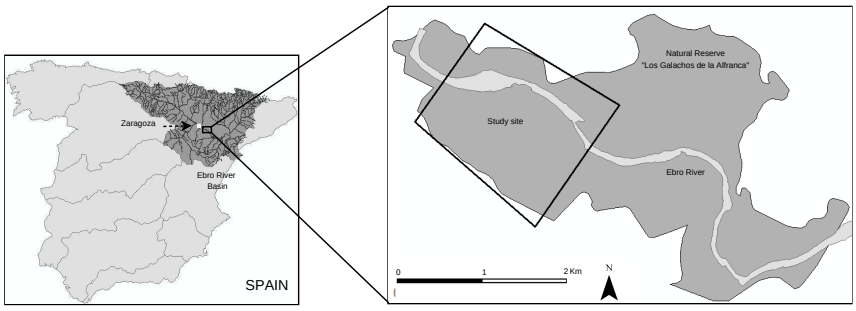

Figure 4.1: Location of the study area.
Black line represent the limit of the computational domain.

The flooded area by the 19 *yr* return period flood (3000 m^3/s, 1927 – 2010) is 3.7 Km^2, whilst only about 30 % of the area is flooded by a river discharge of 1000 m^3/s (0.37 *yr* return period, 1927 – 2003), and only 10 % is flooded by a river discharge of 600 m^3/s (0.14 *yr* return period, 1927 – 2003). The oxbow lake is connected with the river when the discharge reaches 1000 m^3/s, and this occurs 1-3 times per year.

4.3.1 Roughness

Floodplain roughness has been characterized in situ, dividing the floodplain in a set of habitats of homogeneous structure using differential GPS Topcon® (0.03 *m* accuracy). The Manning roughness coefficient has been assigned to each habitat according to the recommendations found in the specialized bibliography as detailed in table 4.1. Figure 4.2 shows the roughness map used in the simulations.

Table 4.1: Manning coefficients.

Roughness coefficients used in the floodplain.

Description	Manning's n	Reference
Main channel	0.035	Acrement and Schenides (1)
Urban	0.05	Sande van Der et al. (177)
Crops	0.035	Palmeri et al. (155)
Permanent water	0.024	Palmeri et al. (155)
Pine forest	0.124	Poole et al. (161)
Unsurfaced road	0.027	Chow (48)
Grassland	0.033	Palmeri et al. (155)
Poplar plantation	0.05	Martin Vide (122)
Gravel	0.028	Acrement and Schenides (1)
Cottonwood or willow dominant $5-10yr$ with gravel soil	0.1	Acrement and Schenides (1)
Cottonwood or willow dominant $10-15yr$ with sand soil	0.04	Acrement and Schenides (1)
Cottonwood or willow dominant, $<2m$ tall and $<5cm$ in diameter at base	0.13	Poole et al. (161)
Reed	0.13	Rhee et al. (169)
High grassland and disperseed willow $1-5yr$	0.124	Acrement and Schenides (1)
Mature forest with blackberry undergrowth	0.12	Poole et al. (161)
Old secondary channel	0.13	Poole et al. (161)
Dispersed cottonwood and Tamarix $15-20yr$ with gravel soil	0.036	Bedient and Huber (15)
Scarp	0.023	Chow (48)

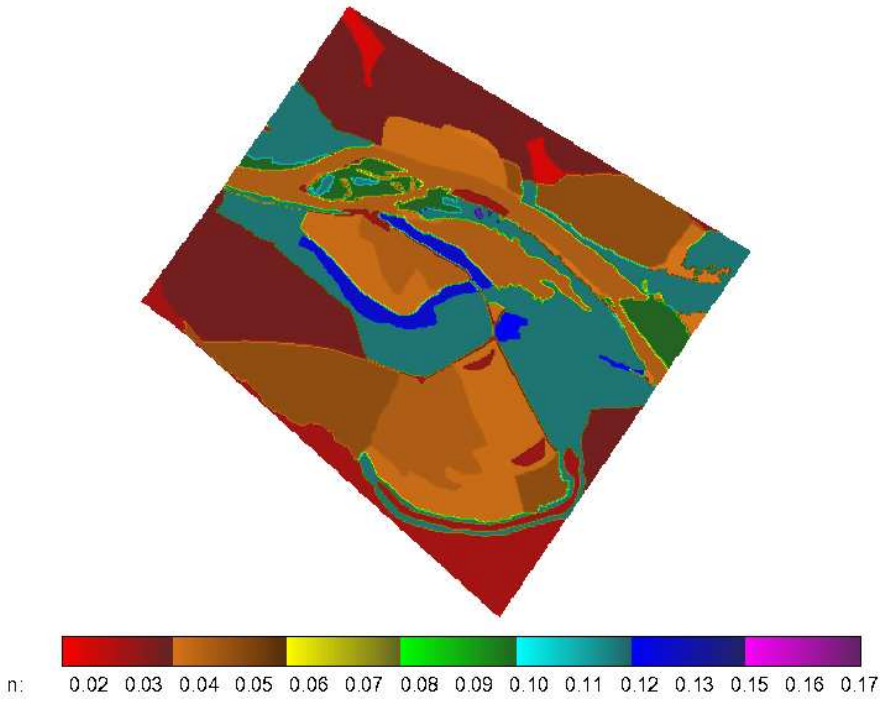

Figure 4.2: Roughness map.
Roughness coefficient, *n*, in the area of study.

4.3.2 Discharge

As this is a natural reserve it is not possible to build a proper gauging station in the domain of interest. The best approximation to estimate the time evolution of the inlet discharge into our area of study is given by a gauging station belonging to the Ebro River Authority located approximately 12 *km* upstream the reserve, therefore, data from this station have been used.

4. MODELING THE MIDDLE EBRO FLOODPLAIN FLOODING DYNAMICS AND ITS IMPLICATIONS FOR ECOLOGICAL RESTORATION

In order to relate discharge with water depth at the outlet section and therefore be able to provide a downstream boundary condition to the model, the natural narrowing of the river, leading to an acceleration of the flow in this region, was used. This was useful to define a discharge/stage rating curve by means of observed field data (using differential GPS Topcon®), so that pairs of values of water discharge and water level were supplied. For values of discharge greater than 2250 m^3/s it was not possible to collect field data, so the gauging curve has been completed by extrapolation. On the other hand, the computational grid is divided into internal cells and boundary cells. The boundary cells are also labeled as inlet and outlet. When performing simulations of the river flow, the outlet boundary cells are forced to meet two conditions simultaneously: they must share a single value of surface water level (the water depth varying according to bed level variations) and the sum of the individual discharges must correspond to the total discharge in the gauging curve. The final $Q(h)$ curve used as outlet boundary condition is displayed in Figure 4.3.

As shown in Figure 4.3, the outlet flow curve has a sigmoid form. The first part, from 0 to 1000 m^3/s, represents the water depth rising within the main channel, that corresponds to a linear adjustment. The value, 1000 m^3/s corresponds to the threshold where the river burst its banks (observed data), and it represents an inflexion point within the gauging curve. From 1000 to 2000 m^3/s the relation between the river discharge and the water level depends on the floodplain topography, which induces an irregular shape.

As figure 4.3 shows, the outlet curve has a sigmoid form. The first part of

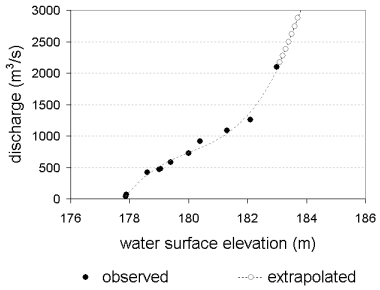

Figure 4.3: Gauging curve used in the outflow section.

the curve, from 0 to 1000 m^3/s, represents the water depth rising within the main channel, whose representation corresponds to a linear adjustment. The value, 1000 m^3/s corresponds to the threshold where the river burst its banks (observed data), and it represents an inflexion point within the gauging curve. From 1000 to 2000 m^3/s the relation between the river discharge and the water level depends on the floodplain topography, which induces an irregular shape.

4.3.3 Topography

The Digital Terrain Model (DTM) used in this work was provided by the Ebro River Basin Administration (www.chebro.es) as a support to the research project. It had been obtained using the Laser Induced Direction and Ranging (LIDAR) data, by means of a single pulse scanning sensor, with 0.15 *m* vertical accuracy and 1 *m* horizontal resolution. Scanning LIDAR sensors produce distributed high quality topographic data that provides a good terrain information to integrate with two-dimensional numerical hydraulic models

(Marks and Bates (119)).

However, since triangular grids are the best discrete representation of the relevant terrain information (Uchida et al. (201), Schubert et al. (181), Brown et al. (27)), we discretized the DTM into a triangular structured grid. The triangular computational cells were created from the 5m side gridded DTM by drawing the main diagonals. As a result, a triangular mesh with 214880 cells was developed (see Figure 4.4).

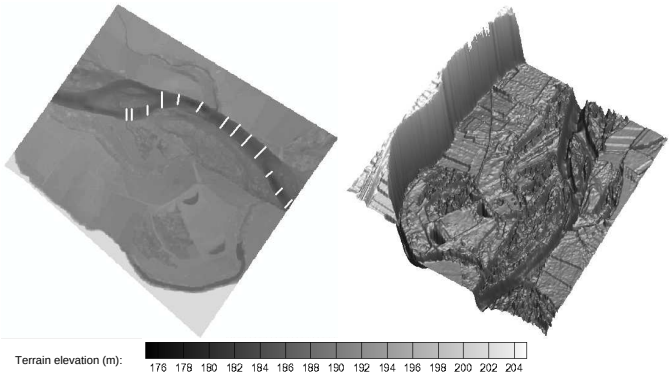

Figure 4.4: Digital Terrain Model using triangular mesh.
Left: 2D DTM view. White lines represents the measured river cross sections at the study area. Right: 3D DTM view.

4.3.3.1 Main channel characterization

The DTM supplies good quality information about all the surface not covered by water, but does not furnish any information of the region covered by the water. The main channel shape was characterized with an in-situ bathymetry

within the 2 *Km* study reach length, where 13 cross sections were measured using a portable depth sounder with the help of the Army Corps of Sappers (see Figure 4.4 left).

A first bed elevation map of the full domain was thereafter produced by interpolating these measured values with the DTM data using ArcGis software (resample tool), by transforming the network from 1 *m* resolution to 5 *m*. Most floodplain flooding studies use DTM with $10-100$ *m* resolution (Horrit and Bates (80), Connell et al. (51), Bates and De Roo (11), Marks and Bates (119)), but in our case, with these resolutions many of the terrain details are lost, and therefore, the floodplain hydraulic behavior is represented too superficially to comply with the objectives of this paper. This river bed reconstruction will be called *RB*1 from now on. The interpolation methods based on statistical treatment of the overall information provided incorrect results when reconstructing the river bed as will be seen later. For this reason, another interpolation method intended to produce a better representation of the river bed from the available data was developed and is outlined in Chapter 3.2.3. This second terrain model will be called *RB*2 from now on. A comparison of river bed sections using the three terrain models (LIDAR data, *RB*1 and *RB*2) is shown in figure 4.5.

4.4 Full simulation model

The full model presented in this work combines the hydrodynamic simulation and the topographic data submodels. The hydrodynamic simulation is shown

in Chapter 3.2.

The topographic submodel includes the terrain representation and the roughness characterization. Both variables are fundamental in a simulation model, where its incorrect representation produces unrealistic simulation results. In that sense, we developed a triangular structured mesh using the LIDAR data and the bed channel reconstruction, which is shown in 4.3.3. The roughness representation is shown in 4.3.1.

Application of the full model requires two steps: calibration and validation. Calibration establish the sensitivity of the hydrodynamic simulation submodel to the topographic data representation. Validation refers to the accuracy evaluation of the complete model through comparison of simulated and available field information.

4.5 Model calibration

The calibration step is an important point that states the sensitivity of the hydrodynamic simulation submodel to the topographic data representation. At the present work the sensitivity was stated on the basis of a steady state discharge.

Although some authors agree that river bathymetry is a key part of a field survey, it is also true that a high number of measured cross section data is not always available, and sometimes is absolutely missing in a LIDAR dataset

(Cook and Merwade (52)). Our results were highly sensitive to the precise definition of the full river channel shape required by the 2D model and this is the point we want to emphasize.

For calibration purposes, the hydrodynamic model was used to simulate two steady flows in the river reach. All the calculations in this work were performed over triangular grids in order to better fit the terrain irregularities.

To check the validity of the river bed reconstruction, a steady state solution for a constant discharge equal to 50 m^3/s, low regime, was computed using the described shallow water model and run to convergence. The quality of the reconstruction can be evaluated by comparing the numerical results for the water level surface with the information provided by the original DTM of the area (Figure 4.7). Figure 4.7 (upper) shows the water level surface computed over the $RB1$ bed elevation model and it shows unrealistic dry areas and overflooded regions when compared to the LIDAR information of the water surface at that discharge (Figure 4.7 lower). Comparison between measured and predicted flooded area has been estimated according to Bates and De Roo (11) criteria, where the accuracy of the calculated flood extent versus the observed is defined on:

$$Fit_A(\%) = 100\frac{(A_o \bigcap A_c)}{(A_o + A_c) - (A_o \bigcap A_c)} \tag{4.1}$$

where A_o corresponds to observed flooded area, A_c corresponds to calculated flooded area and $A_o \bigcap A_c$ is the intersection between observed and calculated flooded areas.

Following this criterion, *RB*1 shows an agreement between observed and calculated flooded area of Fit_A = 85.4%, while the agreement for *RB*2 is Fit_A = 98.3%. Therefore, if the bed elevation provided by *RB*2 is used, the predicted water surface in the river is more accurate. Figure 4.7 (lower) shows the agreement between measured and computed data.

The second set of simulations at discharge of 500 m^3/s flowing at steady state, was performed to assess the quality of the predicted river bed elevation. The extension of the flooded area was also measured using the differential GPS. When using the *RB*1 bed elevation, the computed floodplain was excessively flooded and many habitats were erroneously connected to the river. This is shown in Figure 4.8 (upper) where the calculated flooded area has been plotted together with a dashed line representation of the measured flooded area. The flooded area obtained using the *RB*2 interpolation technique is shown in Figure 4.8 (lower) and it can be seen that both computed and measured (dashed zone) flooded areas match rather better.

The sensitivity of the numerical results to the choice of roughness coefficients was low for a given topographic data submodel and a given computational mesh. Variation of the Manning's roughness coefficients shown in Table 4.1 with $\pm$ 40 % led to negligible differences in the flooded area extent (data non shown).

4.6 Validation of the complete model

The calibration step was useful to decide that RB2 was the best topographic data submodel. The rest of the computations were carried out to validate the full model with no more changes than the inlet discharge corresponding to the individual flooding events. This process is based on the comparison of the computed results and the available field information, where several field data such as flooded area, water depth and flow velocity are required. The agreement between the measured and predicted flooded area has been estimated using equation 4.1.

4.6.1 Experimental techniques and field measurements

The collection of field data for validation proposes was carried out during 2007, registering the five flooding events occurred within this year. The data collection covered a wide range of discharges from 400 to 2250 m^3/s, with a return period of: 0-7 *yr* (estimated within 1980-2010), and was focused on water depth and flood inundation extent. Water velocity was not registered because of, as Bates et al. (10) pointed out, the collection of a full representation of the variability of flow velocities during flood events, especially in an extensive floodplain, is very difficult.

4.6.1.1 Flood inundation extent

The shoreline of the maximum flooded area was measured in situ in every flooding event using differential GPS Topcon® (0.03 *m* accuracy). Points were manually recorded every $5 - 20$ *m* within the limit between the dry and

wet area. Point recording was $1-3$ *hr* long, whereas the maximum inlet discharge variation was 5.2 m^3/s. Inland dry areas were also recorded using the same methodology, except for the highest river discharge, 2250 m^3/s, where it was not possible to enter in the floodplain, and it was observed from the old river terrace.

4.6.1.2 Water depth

Water level was registered both manually and automatically during 2007, where the measuring locations will be referred to as locations L1, L2, L3, L4, L5 and L6. L1 to L5 are located in a secondary channel close to the main river channel that is hydrologically connected with the river in ordinary flooding events. L6 is located in the oxbow lake, and is the farthest probe from the river (see Figure 4.9).

Water level was registered manually at probes L2, L3, L4 and L5 using a ranging rod during the five flooding events, as soon as it was possible to enter the secondary channel. 1-3 daily water level measurements were registered at each probe during the whole flooding event, whose took from 2 to 4 days each one.

At probes L1 and L6 Water level was recorded continuously every 30 minutes using water depth and temperature sensors (Diver®, 0.5 *cm* accuracy) with a barometric correction, during 2007. The agreement between measured and predicted water level is estimated as follows:

$$Fit_D = \frac{1}{N}\sum_{i=1}^{N}|(D_p - D_o)_i| \tag{4.2}$$

where D_p is the predicted water level, D_o is the observed water level and N is the number of observations.

Five simulations, corresponding to the five real events (see Section 4.6.1.1), that will be referred to as hydrographs I, II, III, IV, and V were performed (see Figure 4.10). Every event was simulated starting from the previously computed steady state of the river, that correspond with the initial discharge of each flood event, and was compared to the field measurements. The computational cost was 60, 64, 64, 68 and 73 *hr* for hydrographs I, II, III, IV and V respectively. Computed and measured data comparisons are stated bellow.

4.7 Validation results

Hydrograph I (Figure 4.11) is representative of an ordinary flooding event of peak discharge 420 m^3/s in 50 *hr*. Figure 4.11 shows four snapshots of the numerically predicted flooded area at times $t = 0h$, $t = 15h$, $t = 30h$ and $t = 45h$. At the initial time all the probes are dry. As the flood progresses, a back flow appears submerging L1. Figure 4.12 displays the comparison of predicted and measured flooded area at maximum discharge. The agreement between measured and predicted flooded area Fit_A is 78%. Once the peak discharge passes, the level decreases retaining water in the area surrounding L1. Figure 4.13 shows the comparison of the numerical predictions and the field measurements of the water surface level at probe L1, where the average of the difference between measured and predicted water level is $0.19 \pm$ with an Standard Deviation of ± 0.20 *m* using equation 4.2. In agreement with the field observations, the numerical simulation predicted no flooding in lo-

cations L2, L3 and L5. The simulation predicts that location L6 in the oxbow lake is not affected by this flooding, in agreement with field observations.

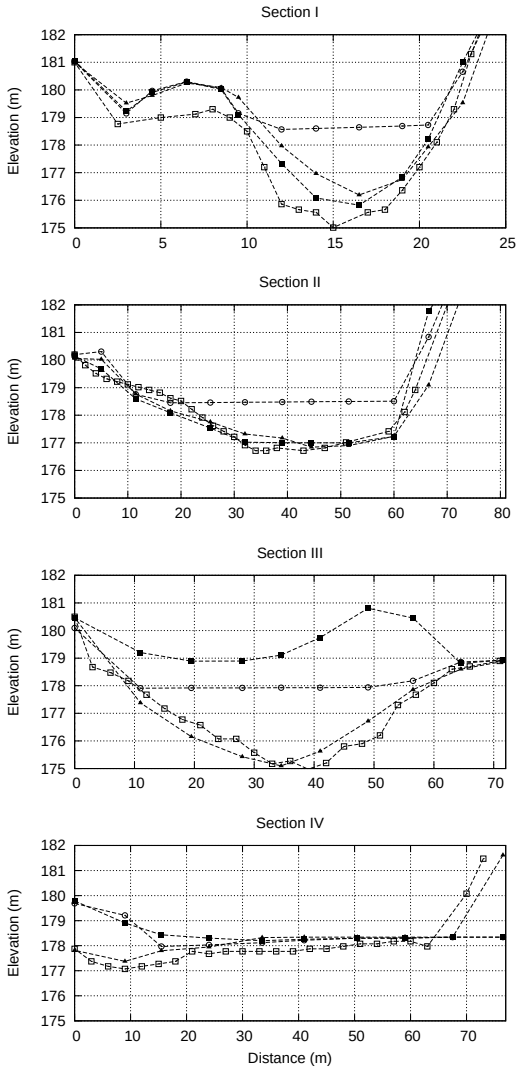

Figure 4.5: River bed sections.
Comparison of four river bed sections using LIDAR data (circle), *RB*1 reconstruction (square) and *RB*2 reconstruction (triangle).

4. MODELING THE MIDDLE EBRO FLOODPLAIN FLOODING DYNAMICS AND ITS IMPLICATIONS FOR ECOLOGICAL RESTORATION

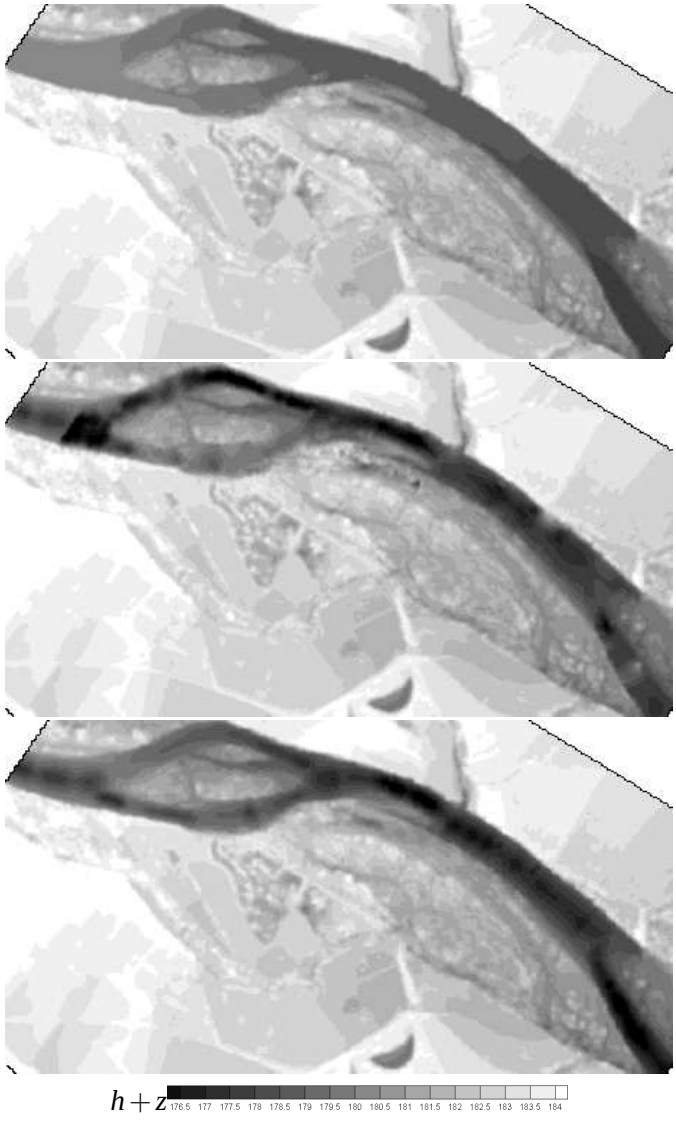

Figure 4.6: River bed reconstruction
Upper, original elevation as taken from the DTM. Middle, *RB*1. Lower, *RB*2.

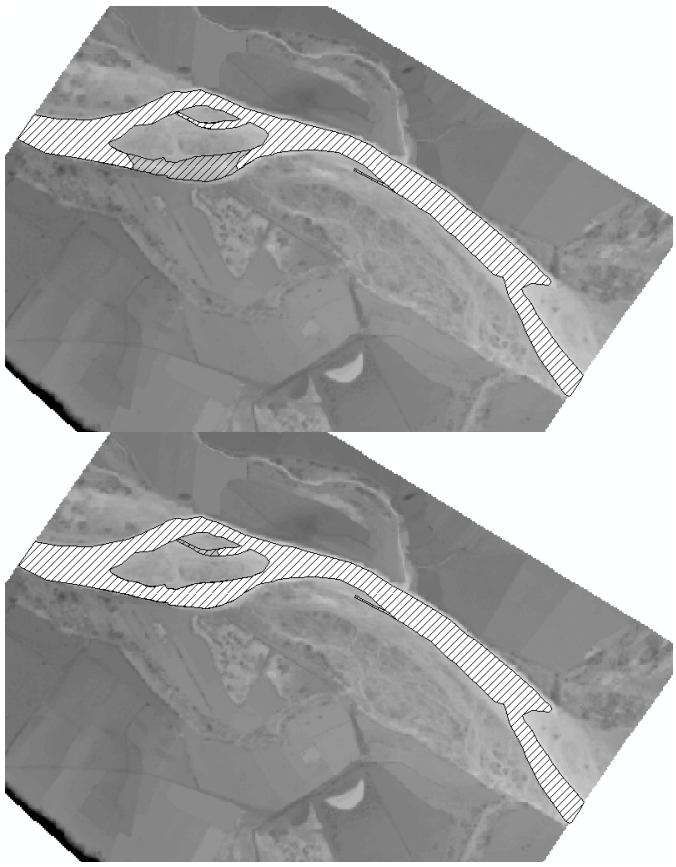

Figure 4.7: Computed and measured flooded area at $Q = 50m^3/s$.
Comparison of computed (white) and measured (hatch) flooded areas at $Q = 50m^3/s$. Upper, computed using the *RB*1 river bed reconstruction. Lower, computed using the *RB*2 reconstruction.

4. MODELING THE MIDDLE EBRO FLOODPLAIN FLOODING DYNAMICS AND ITS IMPLICATIONS FOR ECOLOGICAL RESTORATION

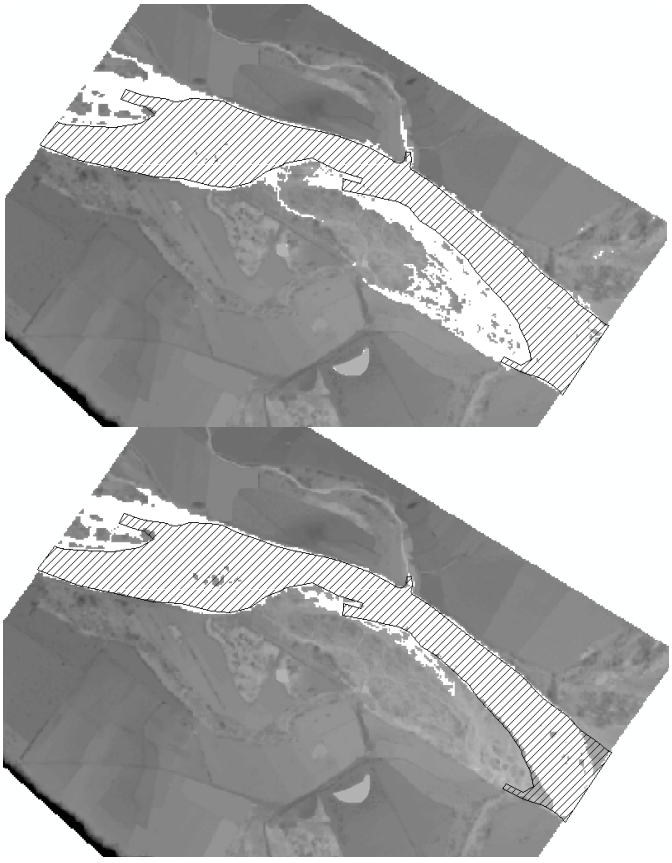

Figure 4.8: Computed and measured flooded area at $Q = 500m^3/s$.
Comparison of computed (white) and measured (hatch) flooded areas at $Q = 500m^3/s$. Upper, computed using the $RB1$ river bed reconstruction. Lower, computed using the $RB2$ reconstruction.

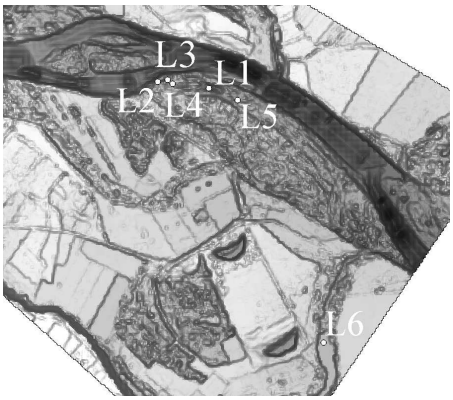

Figure 4.9: Probes location.

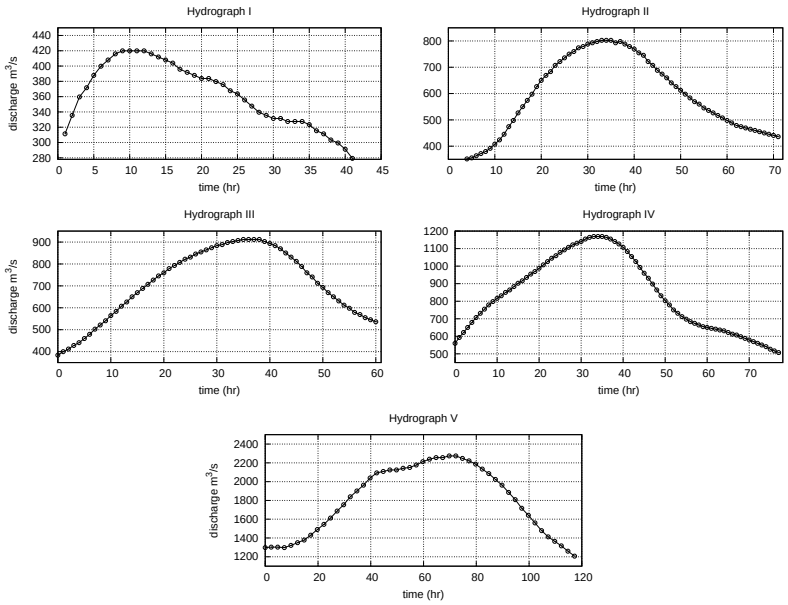

Figure 4.10: Hydrographs of the simulated flooding events.

4. MODELING THE MIDDLE EBRO FLOODPLAIN FLOODING DYNAMICS AND ITS IMPLICATIONS FOR ECOLOGICAL RESTORATION

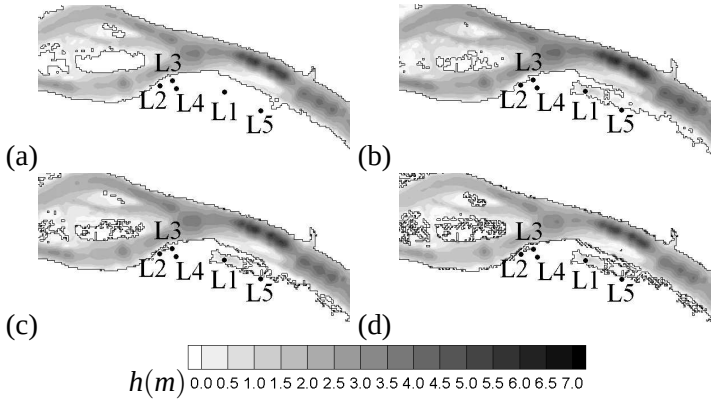

Figure 4.11: Flooding area temporal evolution for hydrograph I. Inundation area at (a) $t = 0h$, (b) $t = 15h$, (c) $t = 30h$ and (d) $t = 45h$ for hydrograph I.

Hydrograph II is also representative of an ordinary flooding event (see Figure 4.10). Figure 4.14 shows four snapshots of the predicted flooded area at times $t = 0$, $t = 20h$, $t = 40h$ and $t = 70h$. In the initial time, locations L1 to L5 are dry and, as time evolves, the five locations get flooded. Figure 4.12 displays the comparison of predicted and measured flooded area at maximum discharge. The agreement between both areas in this case is Fit_A = 76%. Once the peak discharge passes, the level decreases again leaving water stored in the areas surrounding L2, L3 and L4, whilst L1 and L5 remain hydraulically connected with the river channel. Figure 4.15 shows the comparison of the computed and measured water surface levels at the five probes. A good agreement between the numerical predictions and the field measurements, particularly for locations L2, L3 and L4, can be observed. The largest errors are produced in the initial and final times, being the average of the difference between measured and predicted water level 0.49 ± 0.14 m. This desagreement could be due to the interactions of the surface water-groundwater, which is relevant at these stages of the flooding, and they have not been considered in the mathematical modelling of the present work. Otherwise, excluding the initial and final stages of the flooding event, the average of the difference between measured and predicted water level is 0.23 ± 0.04 m. This lack of information also affects the first stages of numerical evolution of locations L1 and L5 as displayed in 4.13. As these two probes continue to be connected with the river flow during the recession part of the hydrograph, the water elevation surface predicted is more accurate at that stage (0.16 ± 0.34 m). The simulation predicts that location L6, in the oxbow lake, is still not affected by the flooding, according to field observations.

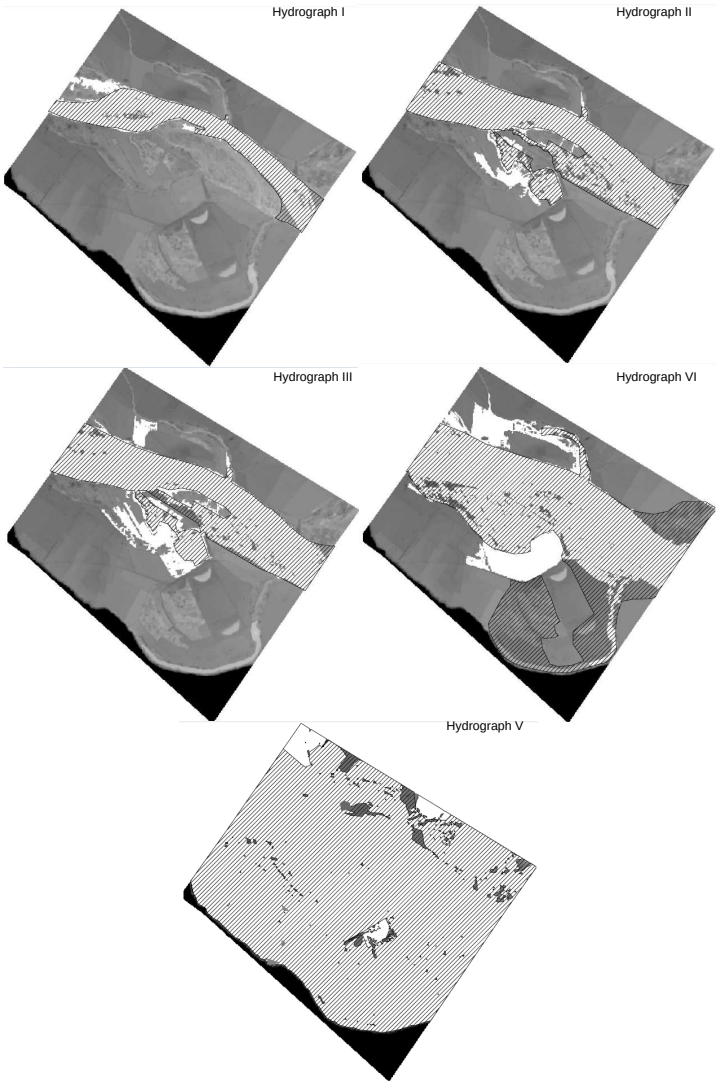

Figure 4.12: Flooded area at peak discharge of hydrographs I, II, III, IV and V. Computed (white) and measured (hatch) flooded area.

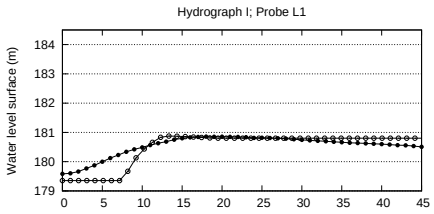

Figure 4.13: Water surface elevation at probe 1 and hydrograph I.
Computed (white circles) and measured (black circles) water elevation at probe 1 and hydrograph I.

4. MODELING THE MIDDLE EBRO FLOODPLAIN FLOODING DYNAMICS AND ITS IMPLICATIONS FOR ECOLOGICAL RESTORATION

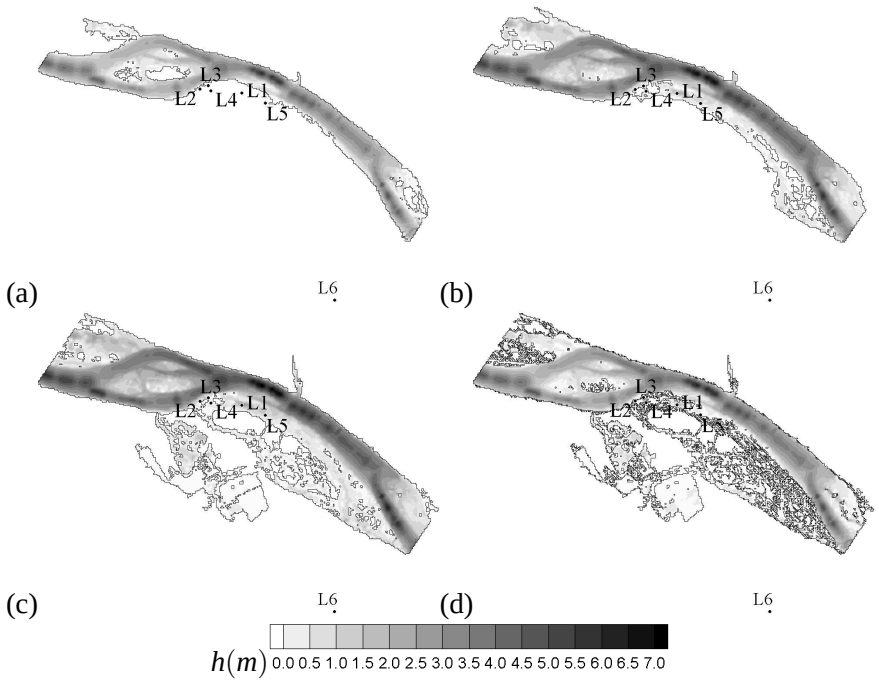

Figure 4.14: Flooded area temporal evolution for hydrograph II. Inundation area at (a) $t = 0h$, (b) $t = 20h$, (c) $t = 40h$ and (d) $t = 70h$ for hydrograph II.

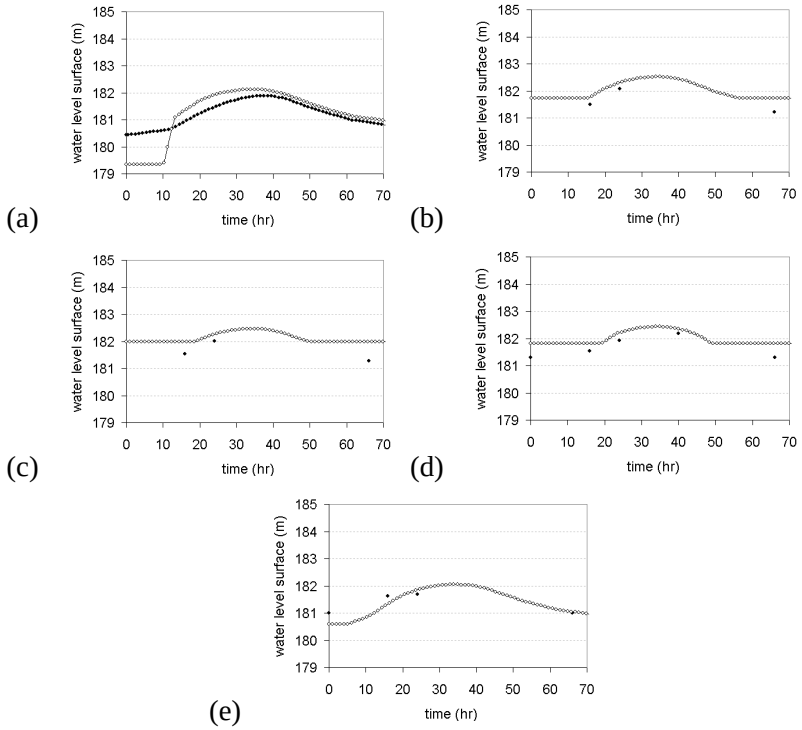

Figure 4.15: Probes water surface level under hydrograph II.
Comparison of measured (black circles) and simulated (white circles) water level at probes (a) L1, (b) L2, (c) L3, (d) L4 and (e) L5, during hydrograph II.

Hydrograph III is an ordinary flooding event (see Figure 4.10), whose peak discharge is only about 100 m^3s bigger than the peak discharge of hydrograph II, but enough to increase the hydrological connectivity between the river and the floodplain. Figure 4.16 shows the flooded area at $t = 40h$ and at $t = 60h$, and how only locations L1 and L5 in the artificial secondary chan-

nel remain connected with the river. The comparison among field data and predicted values for the water level elevation at the five L1 to L5 probes is shown in Figure 4.17 showing a good agreement in general ($0.36 \pm 0.03\ m$). Figure 4.12 (III) displays the comparison of predicted and measured flooded area at maximum discharge, where the agreement Fit_A is 74%. The simulation predicts also in this case that location L6 in the old meandering channel is not affected by the flooding, according to field observations.

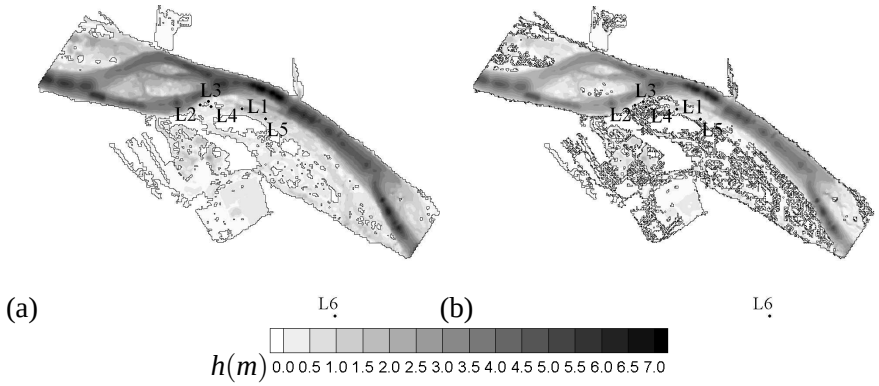

Figure 4.16: Flooding area temporal evolution for hydrograph III. Inundation area at (a) $t = 40h$ and (d) $t = 60h$ for hydrograph III.

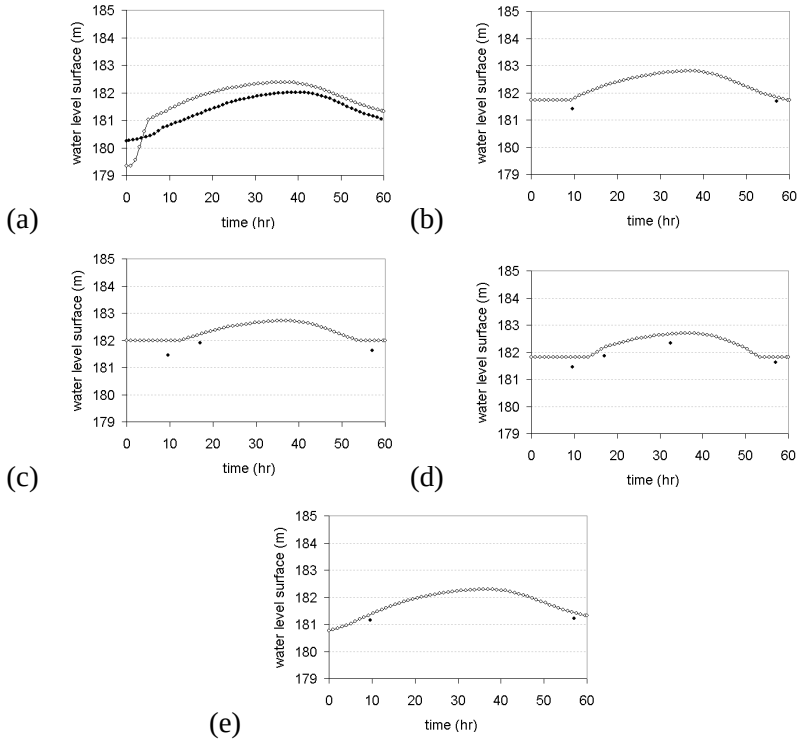

Figure 4.17: Probes surface water level for hydrograph III
Comparison of measured (black circles) and simulated (white circles) water level at probes (a) L1, (b) L2, (c) L3, (d) L4 and (e) L5, during hydrograph III.

Hydrograph IV at Figure 4.10 is a case of great interest to validate the accuracy of the full model as in this case the old river oxbow must be hydrologically connected to the river by means of the surface flow for a certain period of time. It corresponds to a peak discharge of 1169 m^3/s in 70 hr. Figure 4.18 shows the evolution of the computed inundation area by means

of six contour plots at times $t = 20h$, $t = 30h$, $t = 35h$ and $t = 70h$, and how the oxbow lake becomes connected at a certain time through a secondary channel. Due to the magnitude of the flooding wave, only information regarding water surface elevations at locations L1 and L6 was recorded. Figure 4.19 shows the comparison of the time evolution of the water level surface measured and computed at those locations showing a good accordance. Location L1 is flooded all along the entire simulation and the difference between measured and predicted water level is 0.29 ± 0.08 m using (4.2). The time dependent hydraulic connectivity between the oxbow lake ant the river is well reproduced by the model as reflected by the results at L6. Figure 4.12 (IV) displays the comparison of predicted and measured flooded area at maximum discharge, where the agreement Fit_A is 66 %.

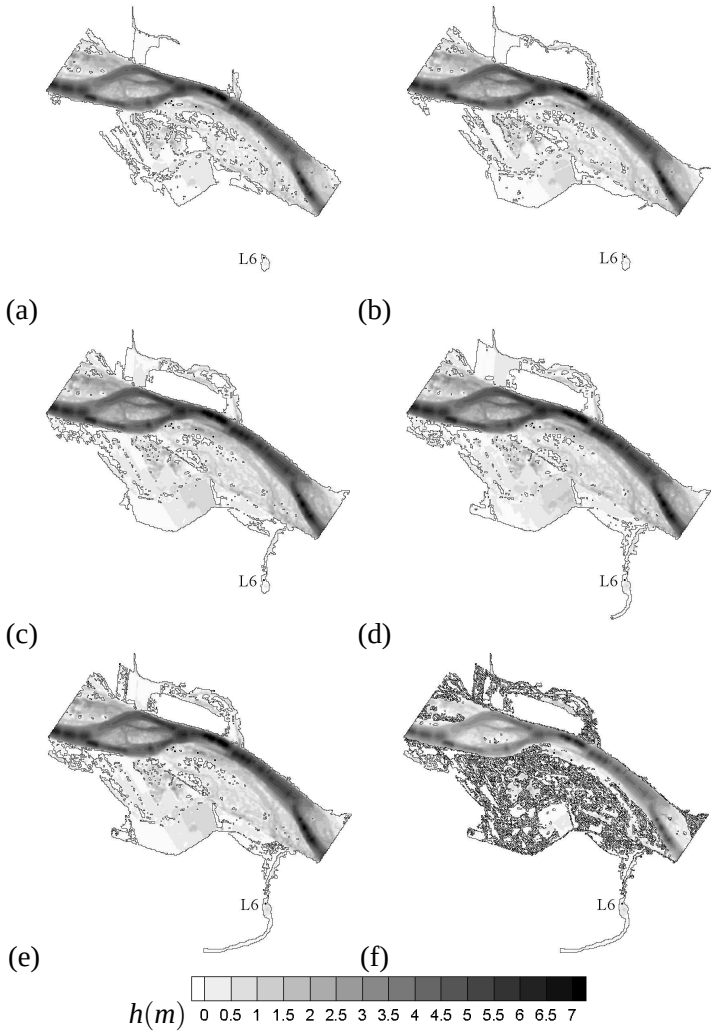

Figure 4.18: Flooded area temporal evolution for hydrograph IV. Inundation area at (a) $t = 20h$, (b) $t = 25h$, (c) $t = 30h$, (d) $t = 35h$, (3) $t = 40h$ and (f) $t = 70h$ for hydrograph IV.

(a) 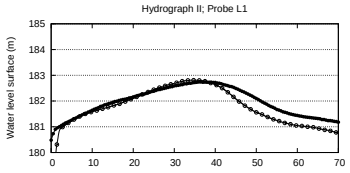

(b) 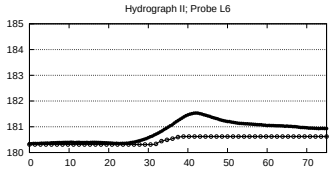

Figure 4.19: Probes water surface elevation for hydrograph IV. Comparison of measured (black circles) and simulated (white circles) time evolution of water surface elevation at probes (a) L1 and (b) L6, with hydrograph IV.

Hydrograph V (Figure 4.10) is a high flooding event of 2250 m^3/s in 120 *hr* that corresponds to a case of extensive inundation and the old river oxbow also hydrologically connected to the river by means of the surface flow for a long period of time. Figure 4.12 (V) is a comparison of the extent of the computed flooded area with the observed flooded area, in dashed lines, at $t = 60h$ where the agreement between the observed and predicted flooded area Fit_A is 92 % using (4.1). Figure 4.20 shows the comparison of the time evolution of the water level surface measured and computed at locations L1 and L6 showing a good accordance (0.29 ± 0.12 *m* using (4.2)). The time dependent hydraulic connectivity between the oxbow lake and the river is well reproduced by the model as reflected by the results at L6.

4.8 Discussion

The predicted flood extension is in good agreement with the observed flood extension in all cases (Fit_A average of $79 \pm 13\%$). An accurate prediction of

(a) 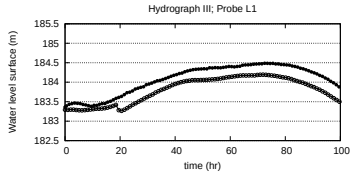

(b) 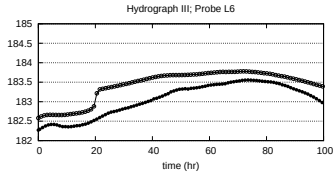

Figure 4.20: Probes water surface elevation for hydrograph V.
Comparison of the measured (black circles) and simulated (white circles) time evolution of the water surface elevation for probes (a) L1 and (b) L5, with hydrograph V.

flood inundation extent is a good test of model capabilities and is of a significant practical interest Bates et al. (10). The flood extension provides, in some way, the superficial hydrological connectivity between the river and the floodplain. As mentioned in the introduction, the hydrological connectivity is essential to the riparian ecosystems maintenance, and with this results, new flow regime scenarios can be drawn in order to improve the floodplain functions.

Given that the hydraulic behavior of the floodplain can condition the floodplain functions, the detailed information of the flow characteristics over the irregular floodplain is of maximum interest. This information is one of the present model results and has been validated by paying attention to the local water level measurements. In this way, although the simulated water levels were in agreement with the measured data in general, some errors were found at the initial and final stages of most flood events at the L5 location. However, as Cabezas et al. (36) pointed out in a previous study, this location is

a groundwater discharge zone, so this disagreement between the simulated and measured data could be due to the surface water-groundwater interaction that is not considered in the present hydrodynamic model. At floodplains, there are zones of groundwater recharge or discharge, and there exists a close relationship between the water table and the topography Zhou et al. (222). The L5 location is one of the lowest points of the riparian forest and, given that a flood event is the result of the joint action of surface and groundwater flows, this point is wet with exfiltered water since the beginning of the flood events season. However, when this location is connected to the river by surface pathways, surface and groundwater flows mix and, above certain river discharge, the surface flow is dominant. As the surface-groundwater flow interaction has not been considered in the present mathematical modeling, the initial state where the L5 location has an exfiltration water is not included in the simulation. Therefore, there is an initial disagreement at the beginning of every simulated flood event that can be noticed in the water level values and the water level time evolution. The groundwater exfiltration phenomenon at the L5 location can be detected using continuously water temperature measurements. The exfiltered water at the beginning of the flood event remains stagnant so that its temperature depends on the ambient temperature variations as well as on the water exfiltration temperature. When exfiltered and surface water are connected, water temperature depends also on that of the new entering flow. Above certain river discharge, when the surface flow predominates, a sudden temperature change is observed, being the new temperature better explained by that of the river surface flow. Figure 4.21 shows the temperature an water level measurements at each simulated flood event at L5.

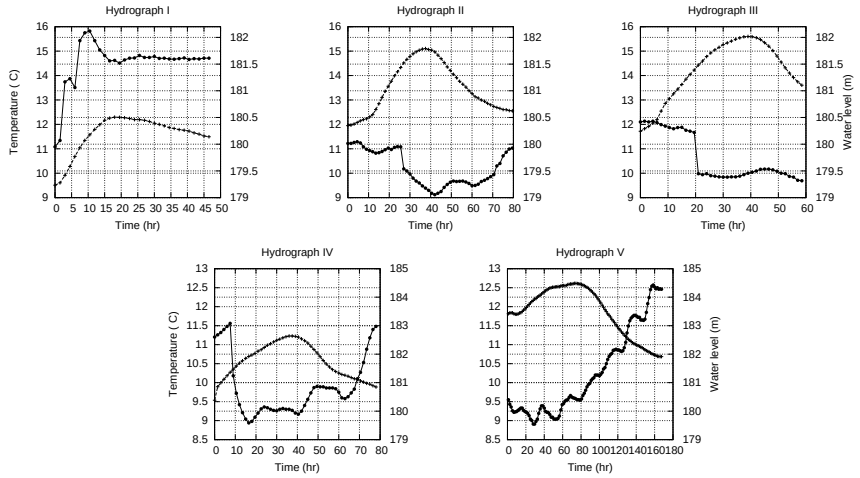

Figure 4.21: Measured water level and temperature.
Temperature (circle) and water level (cross) time evolution at probe L5 for each flooding event.

At the hydrographs II and III, the temperature change was abrupt. This change was produced with very similar river discharge (751 m^3/s in the hydrograph II and 760 m^3/s in the hydrograph III), and at the same measured water level (181.4 m.). It suggest the surface flow predominance over the total water volume occurs when the river discharge is about 750 m^3/s and 181,4 m. water level.

In contrast, at the hydrograph I, the temperature change was not so sudden. The L5 location was flooded with bakflow, and providing that this flooding rate is slowly, the temperature change should be more gradual. In addition, as we mention above, the surface discharge predominance should occur

when the river discharge is about 750 m^3/s and the water level 181,4 m., and either of them occurs in this flood event. Therefore, the surface flow did not predominate over the total water volume, and it could cause the diffuse temperature change.

At the hydrograph IV, the temperature change was sudden, and in agreement with the hydrographs II and III, it occurs when the river discharge was 760 m^3/s and the water level 181.4 m. In this flood event, the river discharge overcomes very soon (at 10 hr.) the 760 m^3/s, therefore, the initial disagreement is lower than at the previous hydrographs.

At the hydrograph V any sudden or gradual temperature change was observed. This could be due to the surface flow predominance over the total water volume, because of the river discharge and the water level were always above 1150 m^3/s and 181.9 m., respectively. Therefore, the water temperature at the L5 location should be the river surface flow temperature, and no initial disagreement should be observed at the simulated and measured results.

4.9 Ecological application of the full model

On the basis of the observed and calculated results, we can affirm that the full model is a suitable tool to predict the hydraulic connectivity between river and floodplain. In this way, the model becomes a useful tool in ecohydrology, where the hydrologic/hydraulic mechanisms that underlie important ecological processes such as nutrient transport or sedimentation patterns need

to be interpreted and predicted.

In the same way, a fundamental process such as the geomorphic activity can also be represented and predicted. Hydromorphological processes define the dynamic equilibrium of habitat distribution with their characteristic biota (Schiemer et al. (180)), and are critical in the production and maintenance of the floodplain ecosystem (Bayley (14)). Hence, the full model, including the flow erosive potential estimation (see Chapter 3.2.1.3) has been used to evaluate current floodplain geomorphic dynamics and to propose different scenarios that might induce geomorphological activity.

4.9.1 Analysis of current floodplain hydromorphological dynamics

The geomorphological processes that we refer to in the present work are mainly bank erosion and sediment deposition (see Chapter), which at the reach scale are seen as lateral movements of the channel across a floodplain. This movement is usually based on the equilibrium between concave bank erosion and the convex bank sedimentation. Point bar features tend to be built along convex banks, whilst concave banks are eroded into higher floodplain and bench features. As a result, concave banks tend to be bordered by higher riparian margins that are less frequently flooded than convex banks (Steiger and Gurnell (190)).

However, the selected river segment is notably affected by embankment structures, where limited morphodynamic activity has been observed since

the last half of the twentieth century (Ollero (152), Cabezas et al. (34), Cabezas et al. (37)). Indeed, cut-avulsion phenomenon is almost restricted to the river adjacent floodplain González et al. (63), whilst in the rest of the floodplain sedimentation prevails over erosion (Cabezas et al. (37)). Hence, our focus is on erosive processes.

Table 4.2: Flooded and eroded area.

Flooded and potentially eroding area at the current scene, under six different peak discharge. The recurrence period (T) has been estimated within the years 1927-2010.

Q	T	Flooded area		Eroded area	
m^3/s	$yr.$	m^2	%	m^2	%
400	< 0.1	277800	11	0.31	0.00
800	0.21	522400	21	0.83	0.00
900	0.25	627850	25	0.00	0.00
1169	0.40	965350	38	0.00	0.01
2250	3.4	2355700	94	854	0.03
3000	18.7	2476350	99	12983	1

In order to study the current geomorphological floodplain dynamics, the erosive potential of six ordinary and extraordinary flooding events has been analyzed. According to the results, the study area is almost completely flooded with a return period of 3.4 yr, where almost 30 % of the study area is flooded every year (see Table 4.2 and Fig. 4.22). The frequently flooded area is adjacent to the main channel, and mainly corresponds to riparian forest.

Simulation results also show a lack of hydromorphological activity, where the highest erosive potential is only capable of eroding 1 % (12983 m^2) of the study area (see Table 4.2). Moreover, this erosive phenomenon corresponds

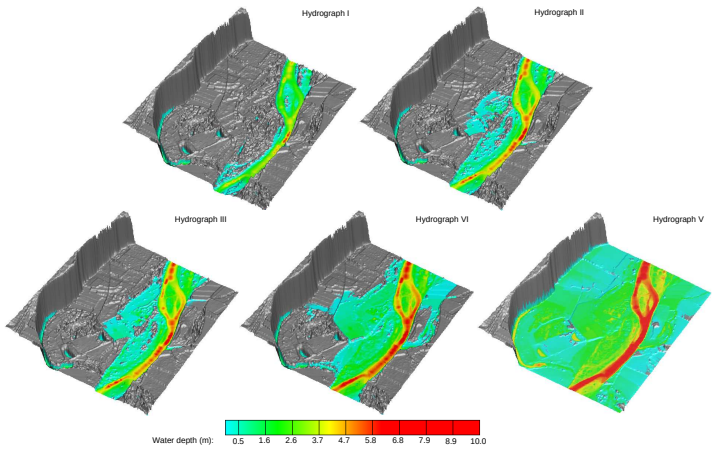

Figure 4.22: Flooded area under the peak discharge of each hydrograph. Water depth the current situation under 400 (I), 800 (II), 900 (III) and 1169 (IV) and 225 m^3/s (V) river discharge.

to an extraordinary flooding event, with 18.7 *yr* recurrence period and 3000 m^3/s of river discharge, where its major erosive potential is restricted to river defenses and urban and agricultural constructions (see Figure 4.23). In agreement with these results, we can affirm that after a 2250 m^3/s river discharge flooding event, the only significant geomorphological change that we found in the study area was a gravel bar deposition that destroyed the artificial secondary channel (Gonzalez-Sanchis et al. (65)) (see Figure 4.24).

The current lack of hydromorphological activity of the middle Ebro river floodplain has previously been pointed at many studies (i.e. Ollero (151), Ollero (152), Cabezas et al. (34), Cabezas et al. (37), González et al. (63), Ollero (153), Magdaleno and Fernandez-Yuste (116)), where some of them

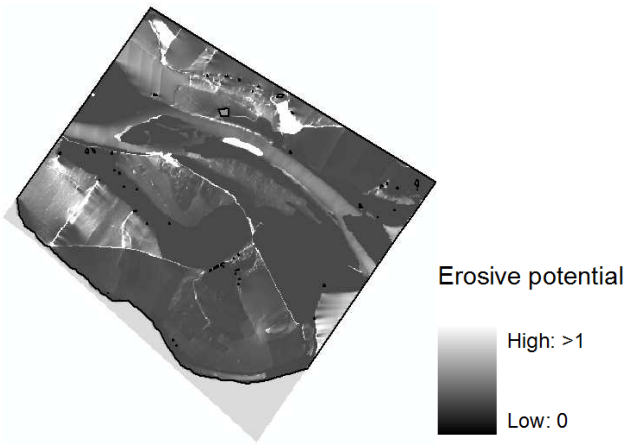

Figure 4.23: Eroded area under 3000 m^3/s river discharge.
Erosive potential under 3000 m^3/s river discharge at the current situation.

has been developed in the same study area (Ollero (151), Cabezas et al. (34), Cabezas et al. (37) and González et al. (63)). In that sense, González et al. (63) confirm that maintenance of current hydrogeomorphological patterns will not produce disappearance of most of the existing forests but will keep aging them, and new pioneer forests will be confined to smaller and more dynamic areas (usually close to the main channel or in-channel areas). Ollero (152) stated that the Ebro river, at the 'Natural Reserve Los Galachos', has lost its geomorphic dynamics, and therefore, no more oxbow lakes will be provided. An aerial photograph of the same study area can be observed in Cabezas et al. (34) and Cabezas et al. (37), where the authors pointed the presence of limited morphodynamic activity since the last half of the twentieth century.

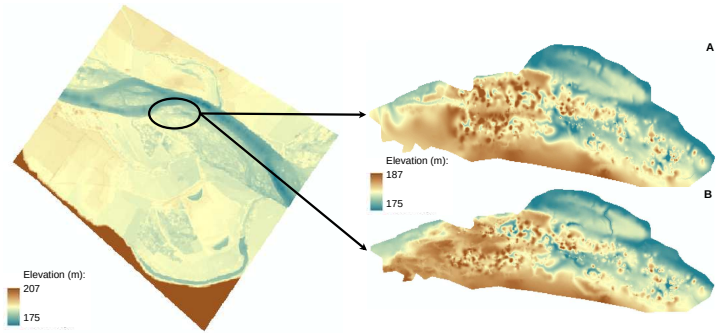

Figure 4.24: Gravel deposition.
Comparison of the constructed secondary channel before (**A**) and after (**B**) a flooding event of 2250 m^3/s peak discharge. Circle shows the gravel deposition area.

When the current flow regime has a very limited erosive potential, the recovering of an actively shifting mosaic of habitats (SMH) would require hydrologic restoration measures.

The lack of a significant hydromorphological activity could be due to the current flow regime, the constructed river defenses or a combination of both. River flow regulation has decreased the number of peak discharges and the duration of flooding events (Cabezas et al. (34) and Magdaleno and Fernandez-Yuste (116)), while river defenses have decreased the floodplain eroding capability and the hydraulic connectivity between the river and the floodplain (Ollero (152) and González et al. (63)). Hence, a restoration of floodplain hydrogeomorphology needs a change in the river basin management (Ollero (152), González et al. (63), Cabezas et al. (35)), where flow

regime as well as river defense construction policy should be reconsidered. Floodplain restoration purposes also have to consider the social-economic situation, which is actually devoted to agriculture, pasture, and recreational use. In this context, we propose the numerical simulation as a useful tool capable of predict the result of the possibles restoration alternatives, and choose the most efficient solution. In the present chapter, four possible restoration alternatives based on terrain modification and/or the discharge increase are proposed:

1. Discharge increase.
2. Initial river defense height reduction.
3. River island elimination.
4. Height reduction of the river defense and its adjacent crops.

The alternatives based on terrain modification (2, 3 and 4) have been analyzed by means of the simulation of the erosive potential of the highest flooding events (1169, 2250 and 3000 m^3/s).

4.9.2 Scenario 1: river discharge increasing

Discharge can be increased by means of two alternatives: increasing the water discharge of one flooding event, producing a huge flooding event, or just increasing the frequency of certain flooding events.

In order to test the first alternative, we simulated three peaks discharge of 4000, 5000 and 6000 m^3/s, respectively, whose recurrence period are higher

than 250 *yr.* (see Table 4.3). Simulation results showed that in spite of the high river discharge considered, the possible eroded area does not significantly increase from the one provided by the flooding event of 3000 m^3/s river discharge. Therefore, this alternative produce non satisfactory results, which in addition, has a high economic and social cost because the Spanish water policy management.

Table 4.3: Scenario 1.

Flooded and eroded area at the scene 1 and under three different peak discharge.

Q	Flooded area		Eroded area	
m^3/s	m^2	%	m^2	%
4000	2494575	99	27176.7	1.1
5000	2494575	99	31541.7	1.3
6000	2494575	99	34835.2	1.4

Usual river flooding events, such us the ones simulated in Section 4.9.1, does not produce significant hydromorphological dynamism (see table 4.2. However, reducing its recurrence period without a discharge increase, can be an alternative to restore the floodplain hydromorphological activity. In this way, if for instance, natural flooding events with a peak discharge of 2250 m^3/s occurs every 1 or 2 years instead of the current 3.4 yr, there could be a significant increase of the eroding area. Nevertheless, considering that most of this erosive potential is restricted to the dikes, it is necessary not to restore these dykes after the flooding events.

This second alternative is also difficult to apply because of the Spanish water policy management, where a conflict between ecology and agriculture

and risk management, can be produced. On the other hand, providing that the eroding area increase is slow and can take years to restore the morphological dynamism, the efficiency of the alternative is not satisfactory, although it might restore the hydraulic connectivity between the river and the floodplain in the end.

4.9.3 Scenario 2: 1 *m* dike reduction

The study area has a river defense to protect the agricultural fields from flooding events. The crops are located adjacent to the river bed inside the floodplain (Ollero (152)), and the river defense extends to riparian forest. In order to combine floodplain restoration and risk management, we propose to reduce the height of the river defense top 1 *m*, corresponding to riparian forest defense (see Figure 4.26). This strategy is proposed to enhance the flooded area and erosive potential of the flow, but without damaging agricultural fields.

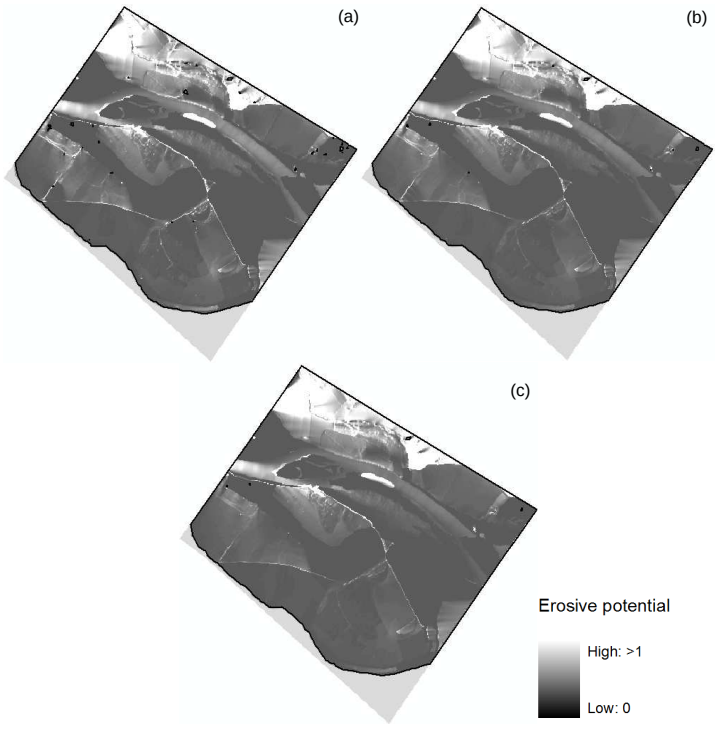

Figure 4.25: Erosive potential under scenario 1.
Erosive potential under 4000 m^3/s river discharge (a), 5000 m^3/s (b), 6000 m^3/s (c).

4. MODELING THE MIDDLE EBRO FLOODPLAIN FLOODING DYNAMICS AND ITS IMPLICATIONS FOR ECOLOGICAL RESTORATION

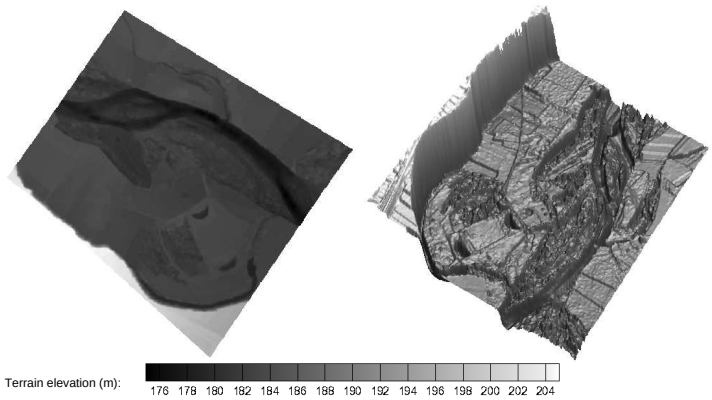

Figure 4.26: Digital Terrain Model of the Scenario 2.
Left: 2D DTM view. Right: 3D DTM view.

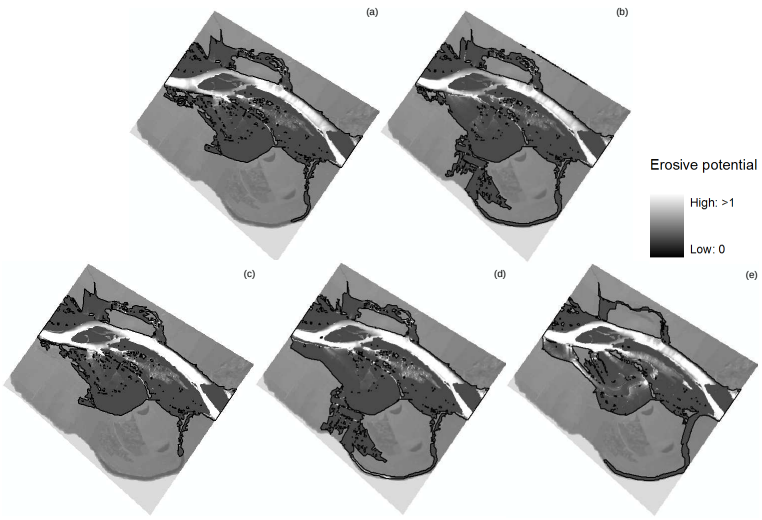

Figure 4.27: Erosive potential under 1169 m^3/s river discharge.
Erosive potential under 1169 m^3/s river discharge at the current situation (a), scenario 2 (b), scenario 3 (c), scenario 4 (d) and scenario 5 (e).

According to the simulation results, this scenario increases a 4 % the flooded area (Table 4.4). At the same time, the new flooded area does not include the crops, where the erosive potential is the same as at the one at the initial situation. The increase of the flooded area also improves the floodplain-river hydrological connectivity, where the oxbow lake and paleochannel are connected to the river surface pathway under lower discharge values than at the initial situation (Figure 4.28). In contrast, the results show only a slight erosive potential increase. The erosive potential is restricted mainly to urban constructions and near river areas. Although the eroded area and hydrological connectivity would increase compared to the current situation, they are

not large enough to restore floodplain hydrogeomorphologic dynamics, but can only recover hydrological connectivity and some of the geomorphological activity.

Table 4.4: Scenario 2.

Flooded and eroded area at the scene 2 and under three different peak discharge.

Q	Flooded area		Eroded area	
m^3/s	m^2	%	m^2	%
1169	1083550	43	108	0.01
2250	2436175	97	6487	0.26
3000	2494575	99	47	0.00

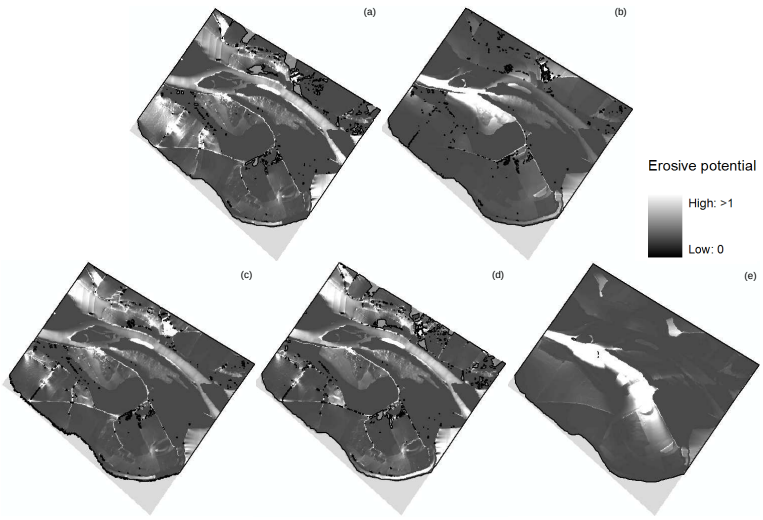

Figure 4.28: Erosive potential under 2250 m^3/s river discharge
Erosive potential under 2250 m^3/s river discharge at the current situation (a), scenario 2 (b), scenario 3 (c), scenario 4 (d) and scenario (5).

4.9.4 Scenario 3: island removing

Removing the island could be another strategy that combines floodplain hydogeomorphological activity and risk management, where the flood erosive potential can be increased, but without increasing flooded area. This strategy could be easily carried out using heavy machinery during the summer dry period. However, to study its efficiency through the simulation tool, the island has been removed from the DTM and replaced by a river bed reconstruction (see Figure 4.29).

According to the simulation results, this strategy does not increase the

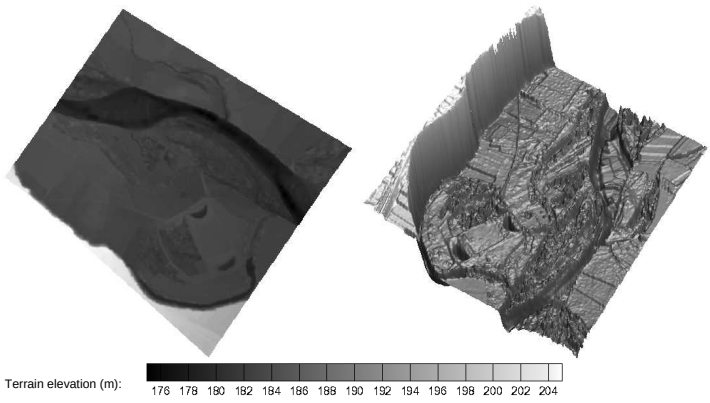

Figure 4.29: Digital Terrain Model of the Scenario 3.
Left: 2D DTM view. Right: 3D DTM view.

flooded area, but only the erosive potential (Table 4.5). Hydrological connectivity between river and floodplain remains the same as in the initial situation but, in contrast, flow energy increases and makes possible the morphological changes. These changes are located mainly at adjacent river areas, being very difficult to find geomorphological activity at the rest of the riparian forest (Figures 4.28 and 4.27 (d)). The erosive potential increase is bigger than in the previous scenario, but is still not enough to restore floodplain hydrogeomorphologic dynamics, where a more drastic change in the floodplain is needed.

Table 4.5: Scenario 3.

Flooded and eroded area at the scenario 3 and under three different peak discharge.

Q	Flooded area		Eroded area	
m^3/s	m^2	%	m^2	%
1169	955500	38	259.1	0.01
2250	2435575	97	8342	0.33
3000	2496550	99	1132.7	0.05

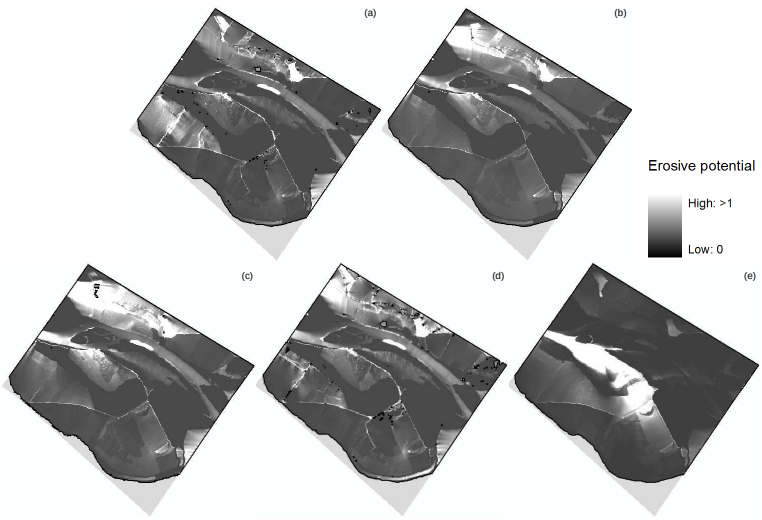

Figure 4.30: Erosive potential under 3000 m^3/s river discharge.
Erosive potential under 3000 m^3/s river discharge at the current situation (a), scenario 2 (b), scenario 3 (c), scenario 4 (d) and scenario (5).

4.9.5 Scenario 4: 2 *m* dike reduction

Reduction of the initial river defense height seems not enough to enhance flow erosive potential. Since the land adjacent to this river defense is an abandoned crop, we propose to reduce 2 *m* height of the river defense and abandoned crop in order to increase floodplain hydraulic connectivity and hydogeomorphological dynamics, but without affecting the agricultural fields (see Figure 4.31).

This strategy increases flow erosive potential more than the previous scenarios (Table 4.6). Although the erosive potential is restricted again mainly to urban constructions and river adjacent areas, some of the riparian forest zone

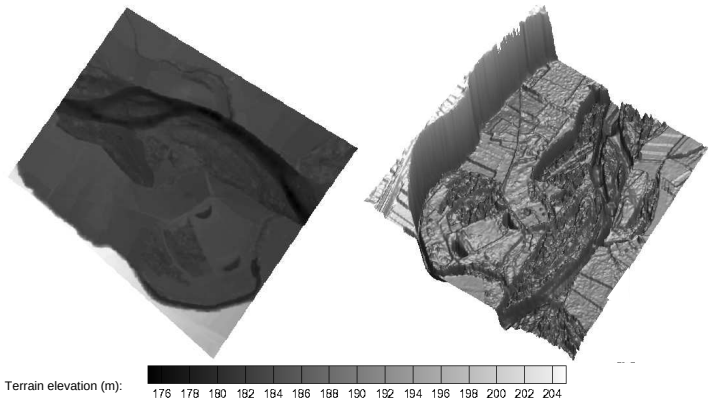

Figure 4.31: Digital Terrain Model of the Scenario 4.
Left: 2D DTM view. Right: 3D DTM view.

is affected by this flow energy. This scenario does not produce a sudden hydromorphological dynamic restoration, but since some of the riparian forest is affected, a progressive hydromorphological dynamic recovering could be expected. Hence, this scenario would be able to restore some of the hydrogeomorphological floodplain activity but affecting part of the urban construction located inside of the Natural Reserve.

Table 4.6: Scenario 4.

Flooded and eroded area at the scenario 4 and under three different peak discharge.

Q	Flooded area		Eroded area	
m^3/s	m^2	%	m^2	%
1169	1114600	44	1116	0.04
2250	2364975	97	6419	0.30
3000	2489375	99	20470	0.82

4.9.6 Scenario 5: hydrological connectivity increasing

Increasing the surface hydraulic connectivity of the paleochannel, the secondary channel and the oxbow lake, reproduces in some way the floodplain structure corresponding to the one previous to the regulation of the Ebro river (see Figure 4.32). Hence, this scenario should increase the hydromorphological activity at these areas.

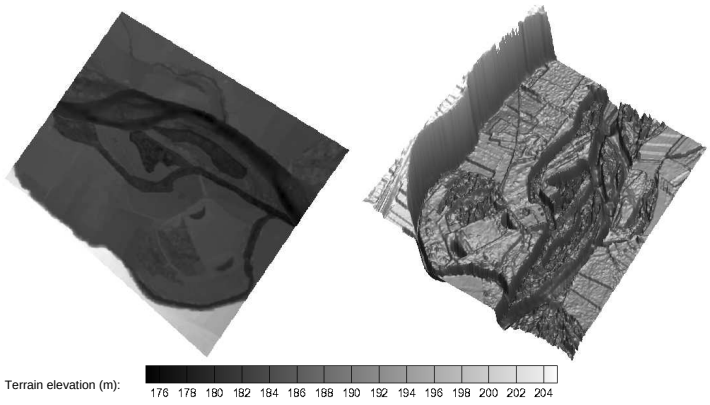

Figure 4.32: Digital Terrain Model of the Scenario 5.
Left: 2D DTM view. Right: 3D DTM view.

As expected, simulation result shows an increasing erosive potential compared to Scenarios 2 and 3 (see Table 4.7). Moreover, the erosive potential increasing does not affect urban area nor agricultural fields, but it is mainly restricted to the natural floodplain habitats. Although the total eroded area does not rise 1% of the floodplain, this restoration strategy is capable of inducing morphological activity at the paleochannel as well as at the riparian forest under an ordinary flooding event (see Figure 4.27 (e)). The potentially

eroded area increases with the river discharge, and affects remote floodplain habitats such as one of the constructed wetlands.

Table 4.7: Scenario 5.

Flooded and eroded area at the scenario 5 and under three different peak discharge.

Q	Flooded area		Eroded area	
m^3/s	m^2	%	m^2	%
1169	934843	37	4082	0.16
2250	2499535	99	6839	0.30
3000	2499940	99	21198	0.84

According to the present results, Scenario 5 is the best strategy to restore the floodplain hydromorphological activity without affecting urban nor agricultural zones. Moreover, since this strategy induces hydromorphological activity from ordinary flooding events, the floodplain restoration process becomes faster and does not need a new flow policy management.

4.10 Conclusions

A river flow simulation model has been presented and its performance as a predictive tool has been analyzed. The model is based on a finite volume hydraulic model of the surface water flow, a roughness model and a topographic model from the available DTM. The method provides information of the time and space variation of the water depth, the depth-averaged velocities and the friction bottom stress, indicative of the erosive capacity of the flow. The calibration of the model has been based on available field information on water

level elevations for two discharges. The calibration phase has revealed the extreme sensitivity of the hydraulic model to the river bed shape. As standard LIDAR techniques do not supply information on the part of the river covered by water, this can be considered an important issue. The interpolation methods based on statistical treatment of the overall information, such as the GIS tools, provide incorrect results when reconstructing the river bed and are therefore unable to recover with accuracy the measured field data. In consequence, the numerical results for flood modeling based on the GIS model reconstruction alone are inaccurate. In this work, a simple procedure to recover the river bed shape from both geometric and hydraulic information has been proposed leading to a correct model performance in almost all the measured situations.

A systematic discrepancy still remains during the rising limb of the flood at one of the measured probes. The explanation for this discrepancy comes from the groundwater-surface flow interaction, at that particular location, that is not considered in our model. The field observations concerning water temperature indicate important mixing of water from different sources near that point. The extension of the model to include this flow interaction is part of the immediate future work but is outside the scope of the present work.

In the validation shown here, the full model has demonstrated to be an excellent tool to predict the hydrological connectivity between river and floodplain, provided that the correct topographical information is supplied. At the same time, the model supplies detailed information on the flow characteristics

over the irregular floodplain. These flow characteristics determine important ecological properties such as the particulate organic matter contribution, the dissolved oxygen content or the type of macroinvertebrate at certain habitat.

The floodplain analysis highlight its limited erosive potential under the current topography and flow regime. The restoration scenario based on increasing the water discharge indicates that probably, the lack of geomorphic activity is actually influenced more by the constructed river defenses and the floodplain land use than the Ebro river basin discharge regulation. In this way, the best restoration alternative appears to be recovering the past floodplain structure.

4. MODELING THE MIDDLE EBRO FLOODPLAIN FLOODING DYNAMICS AND ITS IMPLICATIONS FOR ECOLOGICAL RESTORATION

5

NUTRIENT RETENTION CAPACITY OF AN AGRICULTURAL DRAINAGE CHANNEL: DEVELOPING A PREDICTIVE MODEL

5.1 Introduction

Nutrient loads to water became a great concern in the industrialized Western countries as their concentration increased exponentially since the sixties, mainly due to the increased use of mineral fertilizers and phosphorus com-

pounds in detergents (Baker (8)). The impact of human activity on surface stream habitats has been extensively studied throughout the world (Hynes (91), Johnson et al. (100), Townsend et al. (199), Parker et al. (156)), forming the basis for many stream restoration efforts (Standford et al. (189), Wissmar and Beschta (217)). Indeed, the European Union has approved specific directives relative to Nitrates and Phosphorus in an attempt to control the problem with medium and long-term perspectives (Directives: 91/271/EEC, 91/676/EEC and 2000/60/EC). As a consequence, over recent decades, particularly point sources of water pollution have been reduced. However, non-point sources such as agriculture, are still substantial, agriculture being considered one of the main nutrient sources worldwide (Baker (8)).

Streams in relatively undisturbed ecosystems differ substantially from those found in agricultural regions, where a high nutrient concentration and reduced riparian vegetation increases primary production (Melody et al. (125)). Indeed, nutrient concentrations in catchments with high agricultural activity can be orders of magnitude higher than in undisturbed catchments (Melody et al. (125)), which contributes to the eutrophication of aquatic systems (Carpenter et al. (42)).

A large number of studies has identified water courses as important systems for nutrient uptake (Meyer (127); Klotz (107); Richardson (171)). The retention of nutrients is due to both, biotic and abiotic mechanisms (Reddy et al. (167)). In agricultural landscapes, the drainage and irrigation network could also be considered as a nutrient removal system. In irrigated agricul-

ture, the channel networks are designed and managed to optimize water delivery and drainage from the crops (Santos (178)), and this drainage water is often discharged into existing streams or rivers. Hence, part of the agricultural nutrient load is located in the channel networks. Drainage channels often carry residual nutrients, pesticides and suspended solids, altering the water quality of the receiving stream (Terrado et al. (195), Castaneda and Bhuiyan (44), Causape et al. (46)), which may affect in-stream biota and create a concern for river management. Possibly, part of the load is retained in the drainage channels themselves, and the retention capacity could be comparable to that of first order streams because of morphological similarities. Irrigation channel, thus, can be understood as rivers or streams, where the same uptake models can be applied.

The linkage between solute reactions and transformations and downstream transport with the stream has been incorporated in several models (Bencala and Walters (20), Newbold et al. (141), Kuwabara and Helliker (111)). The most widely used are the one-dimensional (1D) models that assume steady state and uniform cross-sectional parameters (Mulholland et al. (135), Martí and Sabater (120), Haggard et al. (68), Melody et al. (125), Hoellein et al. (79)). However, these models have two disadvantages. On the one hand, adopting the simplification is not always adequate to represent a real river or stream (Workshop (218)). On the other hand, their application needs the outlet and inlet nutrient data, which are not always available. Therefore, another formulation that represents more realistically the river and whose application does not need the inlet and outlet nutrient data is required.

In this context, the present paper proposes two main objectives. The first one pretends to evaluate the irrigation infrastructure nutrient uptake potential through a set of 20 nutrient addition experiments in a selected irrigation canal. The second evaluates the steady-state one-dimensional calculation method for nutrient uptake and proposes to overcome its two disadvantages by means of an alternative model supplied with new nutrient uptake formulation based on the nutrient addition experiments. At each time step the system is under steady state conditions, but flow conditions could vary among them. Therefore, it makes possible to consider flow velocity and water depth variation. The second disadvantage is solved by formulating the nutrient uptake as a function of the most uptake influential parameters, where the function does not need the outlet nutrient data, and can vary in time and space according to the selected uptake parameters.

5.1.1 Nutrient cycling

Nitrogen and phosphorus are widely recognized for their importance in agricultural and forest production as well as for their roles as limiting nutrients in the eutrophication of lakes, streams, estuaries, and near coastal oceans (Binkley et al. (21)). The directly available forms in aquatic systems are mainly inorganic, although some algae are able to use organic forms of these nutrients (Darley (53)). Its dissolved inorganic forms are ammonium (NH_4), nitrite (NO_2), nitrate (NO_3), and orthophosphate (PO_4). Both nutrients have a different metabolic cycle, where the greatest difference lies in the interference of micro-organisms in the cycle, opening up N_2 fixation and denitrification as

pathways to and from the atmosphere that are not available for *P*.

Major processes affecting nutrient concentration of cycling are:

1. Algal uptake
2. Hydrolysis converting particulate organic nutrients into dissolved organic form
3. Mineralization and decomposition of dissolved organic nutrients
4. Chemical transformation of nutrients
5. Sediment sorption and desorption
6. Settling of particulate matters
7. Nutrient fluxes from sediment bed
8. External nutrient loading

Phosphorus is often considered the limiting nutrient in many freshwater systems (Reddy et al. (167)). It is typically present in both inorganic and organic forms. Total phosphorus consists of phosphorus in particulate and dissolved forms, and it can be classified as: dissolved organic and inorganic phosphorus (P) and particulate organic and inorganic P.

Dissolved and particulate organic P generally are the main components of total phosphorus. Dissolved inorganic P is considered bioavailable, where organic and particulate P forms generally must undergo transformations to

inorganic forms before they are considered bioavailable (Reddy et al. (167)). PO_4 reacts with many cations, such as iron and calcium, and readily sorbs to suspended solids in the water column, but the phosphorus cycle is a function of a number of biotic and abiotic processes (Reddy et al. (167)). Biotic processes include assimilation by vegetation, plankton and periphyton. Abiotic processes include sedimentation, adsorption by sediments/soils, precipitation, and exchange processes between soil/sediment and the overlying water column. Organic forms of phosphorus are generated by the death of algae and then are mineralizated to phosphate. Particulate phosphate sorbs to sediments and settles to the sediment bed. Dissolved phosphate is sorbed to particulate matter, taken up by algae, plants and bacteria into the food chain, and eventually returned to the water as organic phosphorus. Therefore, the processes that affect phosphorus concentrations are sorption and desorption of phosphate to suspended and sedimented particles, algal metabolism and algal predation and mineralization and hydrolysis.

Nitrogen is a major component of proteins and is used by animals and plants to synthesize protein, and its cycle comprises several forms in the water column, in the air and in the sediment bed. In this way, nitrogen can enter the ecosystem in several chemical forms:

1. Dissolved and particulate organic nitrogen

2. Inorganic nitrogen, both in detritus and live organisms: as a gas N_2, nitrate NO_3, nitrite NO_2 and ammonia NH_3.

The major components of the nitrogen cycle are organic nitrogen, ammonia and nitrate. Organic nitrogen is one of the primary forms of the external nitrogen loadings, undergoes bacterial decomposition and is mineralized to ammonia. Ammonia is often the major form of nitrogen used for algal growth. Algae will use NO_2 + NO_3 for growth as the ammonium concentration becomes depleted.

The present chapter presents an analysis of the irrigation canal phosphorus and nitrogen uptake potential. Then, the steady-state one-dimensional calculation method for nutrient uptake is evaluated, and finally, an alternative formulation to estimate the nutrient uptake is presented.

5.2 Objectives

Our main hypothesis is that a drainage channel system composed of vegetation, sediment, micro-organisms and periphyton, works as a nutrient sink, whose damping capacity can be modulated by channel operation and maintenance. The specific objectives of the present work are:

1. Quantification of the dissolved phosphorus and nitrogen uptake capacity of a Mediterranean drainage channel system.

2. Identification of the parameters most influential in dissolved phosphorus and nitrogen uptake.

3. Validation of the steady flow one-dimensional reactive transport model.

4. Development of a new unsteady nutrient uptake model of predictive character where the outlet nutrient data are not necessary.

5. Validation of the proposed nutrient uptake model in a different spatial-temporal scale.

A scheme of the chapter is presented below (see Table 5.1 and fig. 5.1) indicating the corresponding method, model and section for each objective.

Table 5.1: Objectives.

Breakdown of approach applied in each objective, experiments (Exp.) used and the section where is reached each objective.

Objective	Method	Model	Exp.	Section
1	Field experimentation: nutrient addition at the irrigation canal	Mass balance	1-12	5.5
2	Field and laboratory nutrient addition experimentation; differentiation between sediment (laboratory) and water column (field) uptake	Principal Component Analysis of both sediment and water column experimentation	1-12 and 16-20	5.5
3	Comparison between measured and simulated water column and sediment uptake	1D steady flow reactive transport model and 2D unsteady flow reactive transport model	1-12 and 16-20	5.6
4	Non-linear regression of water column and sediment data	2D Unsteady simulation model with the new uptake term	1-12 and 16-20	5.7
5	Field nutrient addition experiment under a higher spatial-temporal scale	2D unsteady simulation model with the new uptake term	13-15	5.8

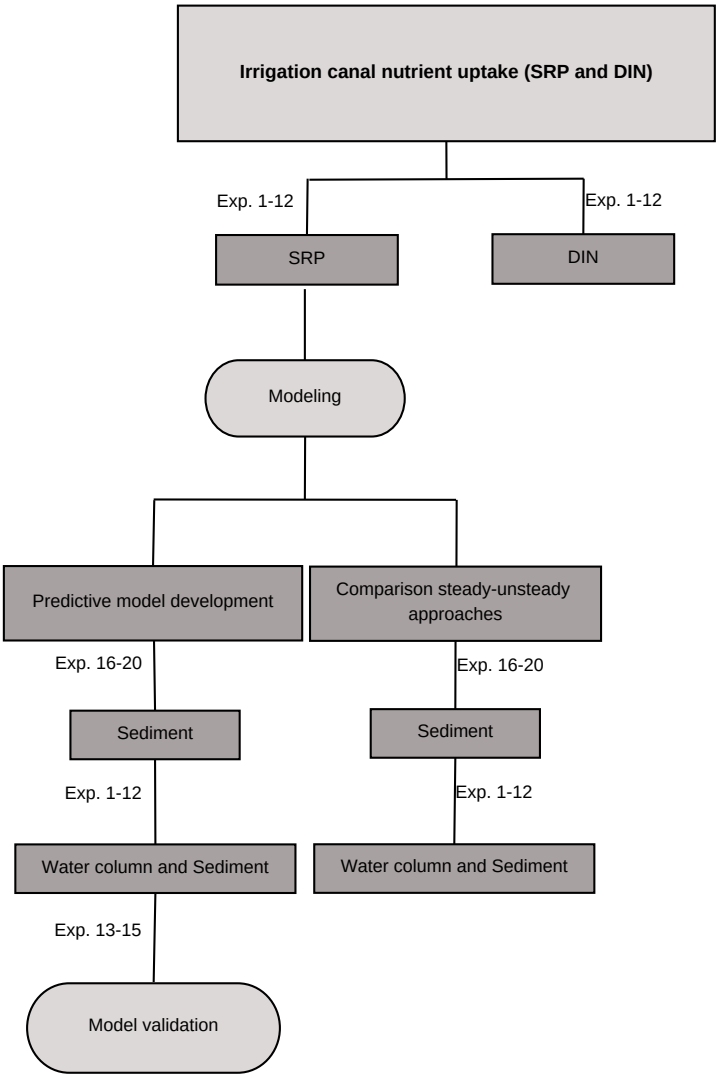

Figure 5.1: Scheme of Chapter 5.
Scheme of the main raised points and the used experiments (Exp.) in the present chapter

5.3 Study area

The study area is located along the floodplain middle Ebro river in Northeast Spain (fig. 5.2). It has a Mediterranean climate, with marked seasonal variation where the mean annual precipitation is 318 *mm* and the mean annual temperature is 15^oC. Most of the floodplain is covered with farming land, and major crops are corn, alfalfa and poplar plantation. Organic and inorganic fertilizers are applied in the catchment. Torrecilla et al. (198) estimated a contribution by agricultural drainage to the Ebro load of 113.2 and 0.4 $Kg/(dayKm)$ of NO_3-N and PO_4-P respectively.

The irrigation channel chosen is situated in the floodplain 12 *Km* downstream of Zaragoza city and is included in the Natural Reserve "Los Galachos de la Alfranca" ($41^o36^{'}$ N; $2^o55^{'}$ W). The irrigation network is variable in geometry and construction materials. Most channels have a concrete rectangular cross section, where some semicircular stretches are made of earth. The study reach is a section of irrigation a canal, within 2 *Km* of the discharge point into the Ebro river. Since it is one of the ends of the local irrigation network, the canal also receives some of the irrigation drainages.

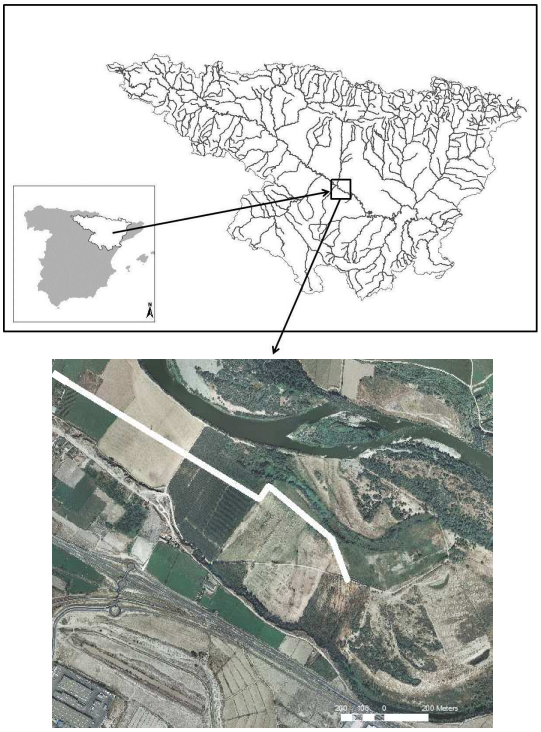

Figure 5.2: Location of the study site.
Upper: location. Lower: White line indicates the irrigation channel.

The canal is flooded by the Ebro river with a recurrence period of 0.4 *yr*, so that some material (seeds, sediment, organic matter, etc.) is deposited in the channel quite frequently. The reach has natural vegetation and sediment which are never removed (fig. 5.9). The channel flows full of water most of the year except in February, when it is left dry because of the upstream irrigation network cleaning.

The canal reach is 1.1 *m* wide, 1.5 *m* deep, 0.001 % slope and its longitude ranged between 57 and 300 *m*, depending on the experimentation. The bed topography was characterized by a digital terrain model (DTM) with 0.25 *m* resolution and 0.03 *m* accuracy, using a differential GPS (Topcon®). Bed channel roughness was characterized after dividing the channel in a set of habitats of homogeneous structure. The roughness coefficient was assigned to each habitat according to the recommendations found in the specialized bibliography (Palmeri et al. (155), Acrement and Schenides (1)).

5.4 Methods

The nutrient uptake potential of the irrigation canal was evaluated by means of 12 short-term nutrient addition experiments (experiments 1-12). In order to differentiate between sediment and water column uptake, 4 nutrient addition experiments were performed in a laboratory channel using fresh sediment from the irrigation canal (experiments 16-20). At the same time, 5 sediment incubations were carried out.

Once the irrigation canal nutrient retention efficiency was evaluated, the phosphorus was selected as the nutrient to be modeled. The steady-sate 1D and unsteady-state 2D reactive transport models were compared. Then, a new alternative phosphorus uptake model was developed and validated. The models comparison and the new formulation validation were carried out by means of a linear regression between measured and calculated phosphorus

uptake for each model using SPSS® 14.0 software. For the validation purposes, 3 new nutrient addition experiments were carried out at the irrigation canal using a higher spatial-temporal scale (experiments 13-15).

5.4.1 Experimental techniques

5.4.1.1 Experimental set 1: short length irrigation canal, experiments 1-12

A set of 12 short-term (60-80 min) nutrient additions to the irrigation canal under semi-controlled conditions were carried out in the irrigation period (March-August, October-December) on 2008-2009. Only dissolved inorganic phosphorus was added because the agricultural drainage water was known to have a high Dissolved Inorganic Nitrogen (DIN) concentration. Bromide (Br^-) was used as a conservative tracer.

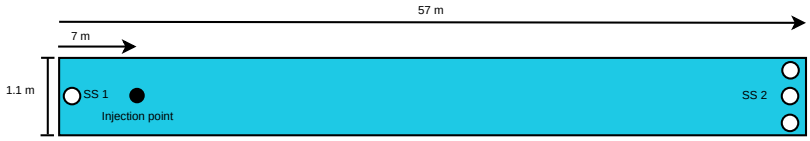

Figure 5.3: Irrigation canal scheme.
White dots represents the Sampling Stations: SS 1 and SS 2.

Two sampling stations located at $-7m$ and $+50m$ of the injection point were defined. At the second section ($50m$), three sampling points along the cross section were used, whilst only one sampling part was used at the first section ($-7m$) (see Figure 5.3). After collecting three background samples of channel solute concentration, a solution of KH_2PO_4 and conservative tracer

(*KBr*) was pumped steadily into the channel using a peristaltic pump (see Figure 5.4). Water samples were taken every 5 minutes for 60-80 min at both sampling sections using acid-washed PP bottle (100*ml*). Conductivity (WTW® Multiline P4) was registered every 2.5 min from the injection starting time until conductivity returned to near-background levels after the injection ended (see Figure 5.4).

Figure 5.4: Irrigation canal experimentation: 1-12.
Left: deposit of the SRP and tracer injected at the inlet of the domain. Right: conductivity measurement at the outlet of the domain.

5.4.1.2 Sediment experiments

In order to verify the potential sediment uptake capacity, the irrigation canal sediment was isolated to perform two different laboratory experiments: sediment incubations and laboratory channel nutrient addition experiment under controlled conditions.

- Experimental set 3: Sediment incubations

Five sediment incubations were developed where undisturbed sediment cores (6 *cm*) were taken at three locations in the channel reach using transparent PVC tubes (diameter = 0.46 *cm*). The sediment phosphorus uptake (SPU) capacity was determined by incubation of sediment in a 0, 0.5, 1, 1.5 and 2 ppm of PO_4-P solution at ambient temperature (20^o C). After 24 h shaking, the supernatant was filtered, analyzed (Murphy and Riley (139)) and the results were expressed as mass (g) of phosphorus uptake per unit mass (μg) of dry sediment. The equilibrium phosphorus concentration (EPC_o) was determined incubating an amount of sediment in five different solutions of PO_4-P (0, 0.1, 0.25, 0.35 and 0.50 mg/l) during 24 hour whilst being gently shaken (House and Denison (83)). Simple linear regression of P sorbed ($mg\ P_{sorbed}\ kg^{-1}$ dry sediment) against final Soluble Reactive Phosphorus (SRP) concentration (SRP_{final}, mg/l) in the solution was used to estimate sediment EPC_o, where the x intercept represents the point of negligible P adsorption or release from sediments to the aqueous solution. The slope (K_{slope}) of this line was used as a measure of sediment adsorption capacity, where greater K_{slope} values would indicate a stronger ability to adsorb P from the aqueous solution (Froelich (57)).

- Experimental set 4: Sediment laboratory channel experiments; experiments 16-20

  We used a laboratory channel to perform five nutrient addition experiments using the irrigation canal sediment as a substrate. The laboratory channel is 5 *m* length, 0.24 *m* width and 0 slope, and fed with controlled tap water discharge (see Figure 5.5 and 5.6). Velocity and water

depth were manipulated in order to reproduce the irrigation canal water parameters. Both parameters where manipulated in the laboratory channel until the Froude Number was within the same magnitude of order as the obtained at the irrigation canal.

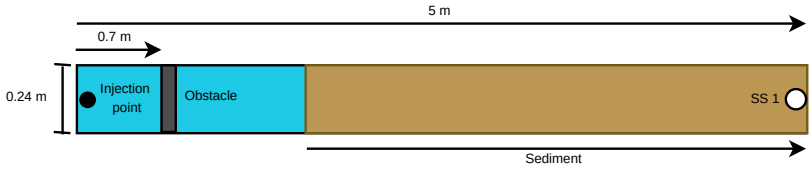

Figure 5.5: Laboratory canal scheme.
White dot represents the Sampling Station SS 1. Black dot represents the injection point.

$0.027 - 0.033\ m^3$ of sediment were removed from the irrigation canal and replaced at the laboratory channel, where $2.02 - 2.73\ m$ of the channel were covered with sediment, depending on sediment availability. Then, 5 short term additions (30-60 min) of phosphate and a conservative tracer (Br^-) were carried out with different phosphorus concentrations. A solution of KH_2PO_4 and conservative tracer (KBr) was pumped steadily using a peristaltic pump. The mixing across the channel length and depth was produced with an obstacle at $0.7m$ from the injection point, before the sediment (see Figure 5.5 and 5.6). At each nutrient addition the sediment was renewed so as not to condition the nutrient uptake with the previous addition. Water samples were taken at the end of the canal every 2-5 minutes using acid-washed PP bottles ($100\ ml$). Conductivity was registered at the same point every single

minute from the injection starting time until conductivity returned to near-background levels after injection ended.

Figure 5.6: Laboratory canal experimentation: 16-20.
Left: Laboratory channel during one experiment. Right: obstacle placed upstream from the inlet of the domain.

5.4.1.3 Experimental set 2: large length irrigation canal; experiments 13-15

In order to validate the model at a different spatial-temporal scale, a set of 3 new nutrient addition experiments were carried out in the drainage canal. The experiments were performed using the same methodology as before, but with an increased spatial and temporal scale: $300m$ length and $2-4$ hr nutrient addition duration. Two sampling stations were established at $-7m$ (upstream)

and 300*m* (downstream) of the injection point. A solution of KH_2PO_4 and conservative tracer (KBr) was pumped steadily into the channel using a peristaltic pump. Water samples were simultaneously taken every $20-30$ minutes for $2-4$ hr at both sampling sections using automatic samplers (Sigma® SD900) and acid-washed (HCl 50 %) PP bottles (1 *l*) (see Figure 5.7). Conductivity (WTW® Multiline P4) was registered every $5-10$ min from the injection starting time until conductivity returned to near-background levels after the injection ended. Temperature and pH were measured in situ using a WTW® Multiline P4 probe. Water velocity was measured at the upstream sampling point using a current meter (Hydrobios®), and the measure was verified with conductivity data at the outlet sampling station.

Figure 5.7: Irrigation canal experimentation: 13-15.
Left: automatic sampler. Right: irrigation canal.

5.4.1.4 Sample analysis

All the samples, both from the field and the laboratory experimental campaigns, were transported to the chemical laboratory in dark cool-boxes and filtered with nitrocellulose filters (Millipore, 0.45μm-pore size). Soluble reactive phosphorus (SRP), total dissolved nitrogen (TDN) and alkalinity were analyzed within 24 h. The remaining samples were preserved frozen before analysis of nitrate (NO_3) and bromide (Br^-). SRP was analyzed using Murphy and Riley (139) molybdenum blue colorimetric method. TDN was analyzed by catalytic combustion at high temperature (850^{o}C) using a Multi-N/C 3100 analyzer (AnalytikKjena®). Nitrate and bromide were analyzed using ionic chromatograph (Metrhom 861 Advanced compact IC) fitted with 100μl sampling loop.

Background samples from experiments 1-12 and all samples for experiments 13-15 were used to quantify alkalinity, suspended and dissolved solids. Alkalinity of unfiltered water was estimated within 4 h of collection by a potentiometric automatic titration with H_2SO_4 0.04 N (APHA (5)). Total Suspended Solids (TSS) was determined by filtering samples through pre-combusted (450^o C, 2 h) 0.45 μm-pore size Whatman® GF/F glass-fiber filters, followed by drying filters at 60^o C until a constant weight was reached. This filter was used then to determine the Suspended Particulate Inorganic Matter (SPIM) by means of combustion (450^o C, 4 h) followed by weighing. Suspended Organic Matter (SPOM) was calculated as the difference between TSS and SPIM. Total Dissolved Solids (TDS) were determined by weighing the residue after evaporating 25 ml of filtered water at 100^{o}C (APHA (5)).

Suspended Chlorophyll (a, b, c and d) was determined by filtering samples through 0.45 μm-pore size Whatman® GF/F glass-fiber filters, followed by 23 h of filter extraction in acetone 90 %, adsorption measurements in a spectrophotometer equiped with a 1 cm quartz cuvette and using the mixed phytoplankton extinction coefficients (Jeffrey and Humphrey (97)).

To quantify covariance of nutrient uptake with the stream and water quality characteristics, a Principal Component Analysis (PCA) based on the Ward algorithm (SPSS® 14.0 package) was carried out.

5.4.2 Computational analysis: nutrient uptake estimation models

Several modeling approaches have proved to be useful in predicting nutrient uptake in streams. This section describes the following: Steady one-dimensional reactive transport model, transient storage, kinetic nutrient uptake and unsteady two-dimensional reactive transport model. Finally, the methodology to generate the new predictive phosphorus uptake model is described.

5.4.2.1 Steady one-dimensional reactive transport model

The model is based on the solute mass conservation equation that represents the cross sectional averaged solute concentration dynamics as governed by one-dimensional (1D) advection and dispersion in uniform channels with

constant discharge:

$$\frac{\partial AC}{\partial t} = -\frac{\partial uC}{\partial x} + \frac{\partial}{\partial x}[AD\frac{\partial C}{\partial x}] \tag{5.1}$$

where C is solute concentration, t is time, x is distance, A is the cross sectional area, u is water velocity and D is a dispersion coefficient.

For non-conservative solutes, equation (5.1) must be modified by adding terms to simulate solute decay or uptake:

$$\frac{\partial C}{\partial t} = -\frac{Q}{A}\frac{\partial C}{\partial x} + \frac{1}{A}\frac{\partial}{\partial x}[AD\frac{\partial C}{\partial x}] - kAC \tag{5.2}$$

where k (T^{-1}) is the first order uptake coefficient and Q is the discharge. To compartmentalize the nutrient uptake in benthic uptake, sediment uptake, periphyton uptake, etc. additional first order terms k_xC can be added with k_x standing for the x individual nutrient uptake complexes.

It is widely admitted that the assumption of steady uniform flow is valid, and instead of (5.2) the concentration dynamics is formulated as:

$$\frac{\partial C}{\partial t} = -u\frac{\partial C}{\partial x} - \frac{kC}{A} \tag{5.3}$$

Then, the global nutrient uptake coefficient k is usually calculated by means of a simplification of (eq. 5.2) that consists of considering constant discharge, uniform velocity and cross sectional area and uniform distribution of concentration in the whole domain. In those conditions, it is possible to

write:

$$C = C_0 e^{-k\frac{x-x_o}{u}} \quad \Rightarrow \quad ln(\frac{C}{C_0}) = -k\frac{x-x_o}{u} \tag{5.4}$$

This formulation requires the inlet and outlet nutrient concentration to calculate the nutrient uptake coefficient k. This could an inconvenient when one or both data are not available.

Using the uptake coefficient k, it is possible to calculate another uptake metrics such as: uptake length, transfer coefficient and uptake rate (Workshop (218)).

The uptake length is then obtained according to the cross sectional water velocity:

$$S_w = \frac{u}{k} \tag{5.5}$$

It is a characteristic length related to the 1D distance traveled by the solute in dissolved form (Workshop (218)). It is possible to define also the turnover length, which is the sum of distances traveled in particulate form (Workshop (218)).

The transfer coefficient V_f represents the nutrient uptake normalized by the concentration in the water column (Workshop (218)):

$$V_f = \frac{uh}{S_w} \tag{5.6}$$

where h is the water depth.

Finally, the uptake rate ($U(mg/m^2s)$) is the total flux of nutrient from the water column to the stream bottom, and it refers only to gross uptake rather than retention.

$$U = \frac{Q(C_i - C_o)}{S_w W} \tag{5.7}$$

where $C_i(mg/\mathrm{l})$ is the input nutrient concentration, $C_o(mg/l)$ is the output nutrient concentration, and W is the canal width (m).

The model assumes that nutrient concentrations are at steady state, and discharge and cross sectional area do not vary over the reach, and that transport is controlled by advection only. Therefore, this simplification could be a problem in some systems, where the heterogeneity plays an important role in the nutrient uptake (Newbold et al. (142)).

5.4.2.2 Transient storage

The transient storage model is based in the above mentioned steady one-dimensional reactive transport model. Solutes can be temporally retained in zones of nearly still water. The eventual movement of this water may return the solutes back to the stream. This phenomenon is known as Transient Storage (Bencala and Walters (20), Bencala (19)) and it can be included in the nutrient uptake formulation. The most widely used version of the transient

storage model adds an additional term to equation 5.2 (OConnor et al. (146)) as follows:

$$\frac{\partial C}{\partial t} = -\frac{Q}{A}\frac{\partial C}{\partial x} + \frac{1}{A}\frac{\partial}{\partial x}[AD\frac{\partial C}{\partial x}] + \alpha(C_s - C) - kC \tag{5.8}$$

$$\frac{\partial C_s}{\partial t} = \alpha\frac{A}{As}(C - C_s) - k_s C_s \tag{5.9}$$

where α is the storage zone exchange coefficient; C_s is the solute concentration in the storage zone; A_s is the cross sectional area of the storage zone and k_s is the first-order reaction coefficient in the storage zone. Storage parameters can be estimated using a variety of techniques, from physical measurements to empirical relationships.

Transient storage refers to the temporary retention of solutes and its subsequent returning to the stream. Presence of pools and riffles or some obstacle such as emergent vegetation, generates water recirculation phenomenon or transient storage. Provided that the model assumes steady state and uniform velocity and cross sectional area, an additional coefficient is needed to cover transient storage, because exclusion of transient storage underestimate nutrient uptake (OConnor et al. (146)). However, a transient flow model with a non uniform velocity cross sectional area, may not need an special transient storage coefficient, because recirculating zones are defined through flow velocity and area.

5.4.2.3 Kinetic nutrient uptake

The uptake rate formulated in eq. (5.7) is a linear function of nutrient concentration C. Some systems display under non-linear uptake rates, where another formulation is needed. In this context, the commonest formulation is Michaelis-Menten function (Workshop (218)), also referred as Monod formulation (Monod (132)). This function was developed for enzyme kinetics, but it has been used to describe the rate of nutrient uptake by natural streambed communities (e.g. Bowie et al. (24), Mcintire and Colby (124), Mulholland et al. (133), Payn et al. (158)), and others saturating processes:

$$U = \frac{U_{max} C}{K_s + C} \tag{5.10}$$

where U represents the uptake flux of a nutrient or organic solute (mass per unit stream bed area per unit time), U_{max} is the maximum uptake flux that would occur under high (saturating) water-column nutrient concentration (C) and K_s is the half-saturation concentration, i.e., the concentration at which:

$$U = \frac{U_{max}}{2} \tag{5.11}$$

This approach provides a saturation curve (Figure 5.8) that represents the usual system behavior: lower nutrient concentrations cause a linear uptake increases, while high concentrations, lead to saturation.

Another common formulation is the Elovich equation, which is frequently used to interpret the kinetic data for phosphate exchange in mixed systems

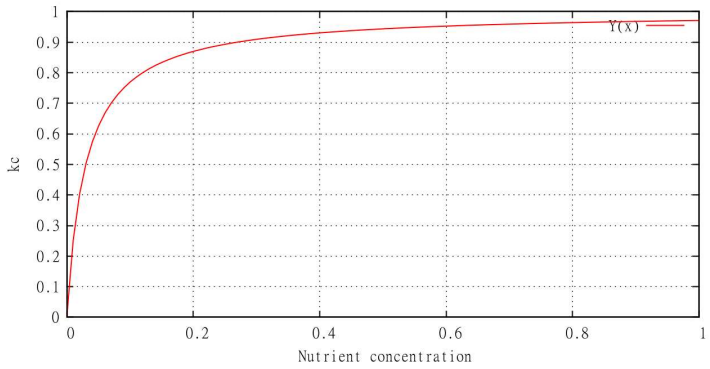

Figure 5.8: Schematic representation of the Michaelis-Menten formulation.

(e.g. sediment water phases):

$$\frac{dU_{NET}}{dt} = aexp(-bU_{NET}) \tag{5.12}$$

so that $\frac{dU_{NET}(0)}{dt} = a$. With the condition that $n = 0$ at $t = 0$, this integrates:

$$U_{NET}(t) = [\frac{1}{b}]ln[1+abt] \tag{5.13}$$

where U_NET is the net uptake (mg/m^2), t is time (min), a is the initial uptake rate (mg/m^2min) and b the rate constant (m^2/mg).

Both formulations provides two coefficients that describes the system uptake capacity, and those coefficients need experimental calibration. Therefore, if we change the aquatic system or some of the water quality conditions,

the coefficients must be different, being necessary more experimental data to recalculate again the coefficients. This is one of the major inconvenient of this kind of formulation, where predictive capacity is reduced to an aquatic system with an specific water quality parameters. To avoid this lack of predictive potential, we tried to find an equation where the coefficients are described in terms of sediment and water parameters, making possible its application in other systems.

On the other hand, kinetic or non-linear nutrient uptake formulation solves the nutrient uptake estimation, but not the stream flow dynamics. A complete stream nutrient uptake model needs the nutrient decay expression as well as a flow dynamics representation, where a steady or unsteady flow model can be used.

5.4.2.4 Unsteady two-dimensional simulation model

The 2D unsteady simulation model SFS2D developed by Murillo et al. (136) and Murillo et al. (138) was used to evaluate the 1D steady model accuracy and to estimate the 2D unsteady uptake coefficient. The 2D simulation model is showed in 3.2.

The 1D steady model evaluation was developed including its uptake coefficient obtained from equation 5.3 in the 2D unsteady simulation model in equation (3.8) as a reaction term in ($\mathbf{R}(\mathbf{U})$). For a general solute ϕ_p the

reaction term is

$$R_p = -h\phi_p \tag{5.14}$$

where is the steady-state nutrient uptake coefficient.

The unsteady uptake coefficient has been obtained by a trial and error procedure using the steady-state uptake coefficient as a starting point.

The suspended solute transport is calculated as expressed in Chapter 3.2.1.2

5.4.2.5 Predictive SRP uptake formulation

A new SRP uptake formulation for both, sediment and water column SRP uptake, is developed considering the system under quasi steady state flow conditions instead of stationary. The SRP uptake coefficient of experiments 16-20 (sediment) and 1-12 (water column and sediment) was calculated, for every time step, using equation (5.4). Then, non-linear regressions between the calculated SRP uptake coefficients and the most influential SRP uptake parameters were performed for both the sediment and the water column using SPSS® 14.0 software. The resulting equations were considered as the new SRP uptake formulation.

Both formulations were validated using experiments 16-20 (sediment) and 1-12 (sediment and water column). Since there were no experiments developed without sediment, the water column formulation was validated with

the sediment formulation using experiments 1-12. For the validation, the sediment and the water column SRP uptake formulations were included in the 2D unsteady simulation model in equation (3.8) as a decay terms ($\mathbf{R}(\mathbf{U})$). Then, experiments 16-20 and 1-12 were simulated, and a linear regression between measured and calculated outlet SRP concentration was performed to analyze its accuracy.

Finally, to validate the model on a different spatial and temporal scale, experiments 13-15 were simulated using the new formulation. A linear regression between measured and calculated outlet SRP concentration analyzes the accuracy of the new model.

5.5 Nutrient retention in the drainage canal

5.5.1 Physical, chemical, and biological canal parameters

The channel bed was irregularly covered by a 0 to 5 *cm* deep layer of sediment and vegetation (mainly *Rumex sp.* and *Poa sp.*; fig. 5.9). Sediment composition was dominated by silt. During our observations, the discharge ranged between $19-94\ l\ s^{-1}$ and velocity varied from $0.06\ m\ s^{-1}$ to $0.3\ m\ s^{-1}$ (Table 5.2).

Table 5.2: Physical and chemical characteristics of the experimental irrigation canal.

Concentration variables (arithmetic mean $\pm$ SD) are expressed in mg/l except SRP and Chl-a, which are in $\mu g/l$. Nomenclature: Temp: Temperature, Ca^{+}: Calcium, DIN: Dissolved Inorganic Nitrogen, TDN: Total dissolved Nitrogen, SRP: Soluble Reactive Phosphorus, SPOM: Suspended Particulate Organic Matter, SPIM: Suspended Particulate Inorganic Matter, TSS: Total Suspended Solids and TDS: Total Dissolved Solids.

Variable	Spring	Summer	Autumn	Winter
Discharge(m^3/s)	0.09 ± 0.02	0.06 ± 0.02	0.05 ± 0.01	0.05 ± 0.02
Temp.(^oC)	18.23 ± 3.61	18.33 ± 3.93	11.95 ± 4.95	6.44 ± 0.99
pH	8.33 ± 0.09	8.43 ± 0.05	8.35 ± 0.05	8.38 ± 0.07
Ca^{+}	93.6 ± 7.2	83.7 ± 6.1	113.1 ± 4.8	97.3 ± 19.5
DIN	1.50 ± 0.03	2.05 ± 0.48	2.58 ± 0.81	2.35 ± 0.27
TDN	2.16 ± 0.01	3.35 ± 0.24	2.85 ± 0.75	2.76 ± 0.20
SRP	0.01 ± 0.01	0.02 ± 0.01	0.03 ± 0.01	0.03 ± 0.01
Chl-a	12.00 ± 1.00	14 ± 6	4 ± 1	3 ± 1
SPOM	8.48 ± 1.11	10.45 ± 3.54	8.33 ± 1.00	7.60 ± 2.08
SPIM	25.93 ± 2.29	41.50 ± 13.88	76.33 ± 33.00	29.92 ± 18.00
TSS	34.41 ± 2.90	51.95 ± 15.32	84.67 ± 34.00	37.52 ± 16.02
TDS	500.00 ± 37.67	717.33 ± 174.12	564.00 ± 4.00	560.00 ± 68.20

At base flow, $N-NO_3$ concentrations were high ($1.78-3.13\ mg\ l^{-1}$), representing more than 70 % of TDN, and practically 100 % of DIN. Indeed, we found no significant differences among the $N-NO_3$ and DIN concentrations (t test, $P>0.05$). Hence, to avoid collinearity problems, we have only included the DIN uptake metrics.

Ambient SRP concentrations ranged from 1 to 46 $\mu g\ l^{-1}$, and the mean molar DIN:SRP ratio was 206 : 1. Ambient nutrient concentrations were

higher than in most of the reported studies on streams (Hoellein et al. (79), Melody et al. (125), Newbold et al. (142), Mulholland (134), Martí and Sabater (120), House et al. (84)), but nutrient concentration in streams with high agricultural activity can be orders of magnitude higher than in undisturbed systems (Melody et al. (125)).

Figure 5.9: Irrigation canal used for the field experiments.
Left: detailed view of the vegetation. Right: view of channel reach dimensions: width: 1.1 m, height: 1.5 m, length: $57-300$ m.

5.5.2 Net retention of Soluble Reactive Phosphorus; experiments 1-12

The net mass balance of each experiment reveals an average decrease in SRP concentration over the length of the study reach of 16.0 ± 3.5 % of the net mass balance, corresponding to 0.70 ± 0.10 $mg\ m^{-2}\ h^{-1}$. Several factors may have affected this retention, and their covariance pattern was explored in a PCA (fig. 5.10). The three first principal components together accounted for 73% of the total variability. Variance among and within variables was

considerable, and most variables correlated significantly with one principal component (10 out of 16 with p¡0.01; Table 5.3), (fig. 5.10). The first principal component (PC1, explaining 31 % of variance) appearst to correspond to suspended solids (SPOM, TSS and SPIM), pH and SRP retention, suggesting a relation between TSS, pH and SRP uptake.

Table 5.3: Irrigation canal PCA for experiments 1-12.

Correlation of measured channel variables and nutrient mass balance estimates with the first three components of a PCA analysis (73 % explained variance). A correlation is considered significant if $p \leq 0.01$ ($r > 0.71$) and printed bold. Correlations significant at $p \leq 0.05$ ($r > 0.59$) are in italics.

Variable	PC1(31 %)	PC2(26 %)	PC3(17 %)
Velocity	0.38	-0.54	-0.56
Discharge	0.13	**-0.84**	0.05
pH	**0.82**	-0.03	-0.14
Temp.	0.25	-0.68	0.46
TSS	**0.85**	-0.05	-0.26
SPOM	**0.87**	-0.18	-0.31
TDS	0.49	0.50	0.61
Alkalinity	0.03	**0.82**	0.17
Chl-a	0.60	-0.23	0.67
SRP added	-0.24	0.63	-0.22
SPIM	**0.79**	-0.01	-0.23
DIN	0.26	**0.74**	-0.20
DTN	0.44	**0.81**	0.04
Depth	0.27	-0.02	**0.93**
DIN consumed	0.51	0.00	0.11
SRP consumed	**0.81**	0.22	-0.18

The second principal component (PC2, 26 % of variance) relates to vari-

ation in alkalinity, TDN and DIN. At the same time, it was negatively correlated to discharge and water temperature. This negative correlation could be due to a dilution effect produced by the higher discharge that is maintained during the main irrigation period, the summer. The third principal component (PC3, 17 %), still explains a considerable proportion of the total variance, and it correlates to water depth (fig. 5.10).

The PCA results provides a differentiation among factors in SRP retention. It appears that TSS, SPOM, SPIM and pH could be the most positively influential variables, indicating an abiotic phosphorus uptake process taking place in the water column. Correlation between SRP retention and suspended solids suggests that probably the main SRP uptake process is phosphorus adsorption. This process states that in presence of oxygen, dissolved phosphates combine with suspended particles, and these particles settle to the sediment bed to be temporally removed from the phosphorus cycling process (Zhen-Gang (221)). The settling of suspended solids and adsorbed phosphorus can provide a significant transport mechanism of phosphorus from the water column to the bed (Zhen-Gang (221)).

The positive correlation with pH may imply that higher concentrations of suspended solids go together with increased alkalinity. Variability among experiments was very low (pH = 8.32 $\pm$ 0.08), and it should not cause any effect on phosphorus consumption. Therefore, TSS, SPOM, SPIM could be identified as the most influential SRP uptake parameters.

On the other hand, chlorophyll a (Chl-a) covaried positively with SRP

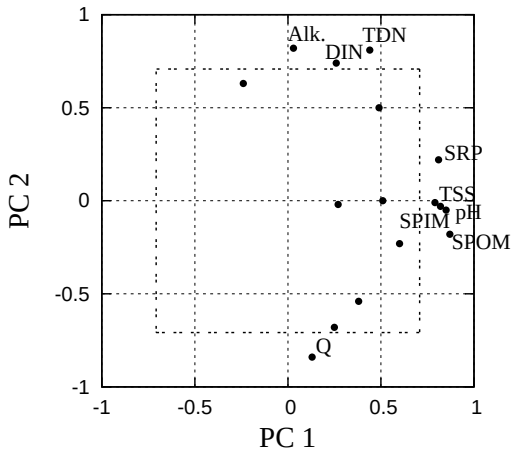

Figure 5.10: Irrigation canal PCA; experiments 1-12.
Correlation coefficients of measured variables and nutrient uptake with the first two principal components. The interior square indicates the area where the correlations are > 0.71.

uptake (p = 0.05) but also with PC3, suggesting an increase of the Chl-a concentration with water depth, that is during stagnation of the flow. This correlation also suggests the presence of algal phosphorus uptake in the water column. However, biotic phosphorus uptake takes more time than the abiotic processes, being the former on the order of days, and the latter on the order of minutes (Zhen-Gang (221)). Providing that the experiments were based on short term additions ($60 - 80$ min), it was no time enough to notice a significant biotic phosphorus consumption. Therefore, dominant SRP uptake process may be abiotic, and in this case it is addressed by adsorption process.

5.5.3 Net nitrogen retention; experiments 1-12

The net DIN mass balance showed an irregular behavior, suggesting DIN release from the channel in some of the experiments. The budget balance average was -0.31 ± 2.42 % and which did not differ significantly from 0 ($t = -0.19$; $p = 0.85$). Therefore, there was no DIN system uptake. At the same time, as the PCA analysis has revealed, this DIN budget balance did not covary with flow or any water quality parameter (Table 5.3). The DIN concentrations (1.78 to 3.13 mg/l of $N-NO_3$) may well suggest saturation similar to the observations of Haggard et al. (68) at a range of 0.52 to 2.65 mg/l of $N-NO_3$.

Under these results, we can affirm that there is no DIN uptake at the irrigation canal, hence, only the SRP will be considered in the sediment isolation experiments.

5.5.4 Sediment SRP uptake

5.5.4.1 Sediment incubation

Sediment incubations showed a high SRP uptake, with an estimated k_{slope} of 130 (l/kg); (fig. 5.11). This suggests that retention mainly occurs across the sediment-water surface, through benthic plant uptake, co-precipitation and sedimentation. However, the incubation methodology provides a full and prolonged contact between SRP and the whole sediment. This mixing generally does not occur in the canal system, where only a few millimeters

of the sediment column are in a permanent contact with the water column. Therefore, the sediment phosphorus uptake was probably overestimated.

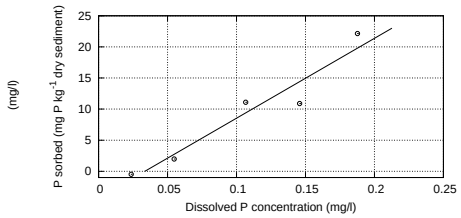

Figure 5.11: Relationship between the P sorbed and final SRP concentration. The sediment EPC_o value was obtained using the regression equation $y = 130.0x - 4.4$ (r^2 = 0.93), where the intercept represents the EPC_o. "○" represents the SRP concentration.

5.5.4.2 Laboratory channel experiments; experiments 16-20

Nutrient addition experiments always resulted in a positive net SRP mass balance ($21 \pm 3\ g/m^2 s$), indicating SRP retention in each experiment. This retention may be affected by several factors and their covariance pattern was explored in a PCA. All the measured parameters were included in the PCA, including the proportional relationship between sediment and water mass (sediment mass/water mass), which is labeled $RATE$ here. As sediment incubations showed, the proportion of the sediment in contact with water affects to SRP uptake potential.

PCA results showed that the three first principal components together accounted for 88% of the total variability, and all variables correlated signifi-

cantly with one of these three principal component (9 out of 9 with p$\leq$ 0.01; Table 5.4), (fig. 5.12). The first principal component (PC1, explaining 40 % of variance) corresponds to SRP retention, SRP inlet concentration, water temperature, Reynolds number and discharge, suggesting positive relationships among water temperature, SRP concentration, flow turbulence and SRP uptake.

Table 5.4: Laboratory channel PCA for experiments 16-20.

Correlation of measured channel variables and nutrient mass balance estimates with the first three components of a PCA analysis (88 % explained variance). A correlation is considered significant if $p \leq 0.01$ ($r > 0.71$) and printed bold. Correlations significant at $p \leq 0.05$ ($r > 0.59$) are in italics.

Variable	PC1(31 %)	PC2(26 %)	PC3(17 %)
SRP added	**0.79**	-0.25	-0.26
Time step	-0.28	0.46	-0.35
ΔSRP	**0.68**	-0.43	0.02
Temp.	**0.83**	0.02	-0.29
Discharge	**0.64**	0.37	0.59
Re	**0.61**	0.47	0.54
Sediment length	-0.30	**0.74**	-0.28
Chl-total	-0.43	0.04	0.85
RATIO	-0.41	**-0.78**	0.23

The second principal component (PC2, 29 % of variance) includes the variation in sediment lenght and the *RATE* parameter with a negative correlation. This pattern probably is a consequence of the experimental design, where the highest water depth corresponds to the shortest sediment layer.

The third principal component (PC3, 19 %), still explains a significant proportion of the total variance, and it corresponds to sediment chlorophyll concentration (fig. 5.10). Sediment chlorophyll content appears an important parameter in the total experiment variability, but it did not correlate with any other parameter, hence did not explain variation in uptake among experiments.

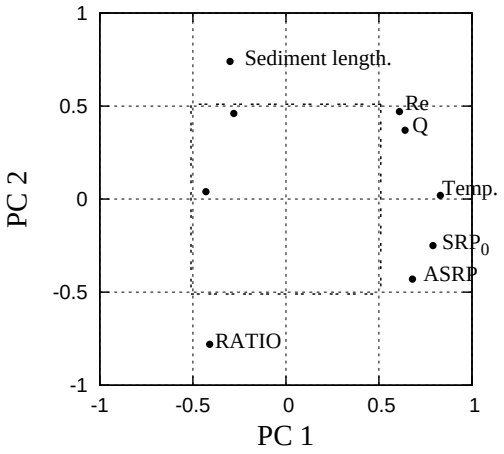

Figure 5.12: Laboratory channel PCA; experiments 16-20.
Correlation coefficients of measured variables and nutrient uptake with the first two principal components. The interior square indicates the area where the correlations are > 0.71.

The PCA results provides a differentiation among factors in SRP sediment retention, where SRP inlet concentration, water temperature and flow characteristics appear the most positively influential variables. These correlations suggest dominance of an SRP adsorption process in the total uptake. The role of sediment in regulating P concentrations of the porewater

and the overlying water column is well known (Johnson et al. (99), McCallister and Logan (123); Hill (78), Reddy et al. (167)). Meyer (127) reported abiotic sorption by stream sediments as primary regulators of P concentration in Bear Brook, New Hampshire. Moreover, the composition of sediment in our stream (silt predominance), enhances dissolved phosphorus adsorption (Froelich (57), House et al. (84) and Haggard et al. (67)). Phosphorus adsorption should also be influenced by sediment length and the $RATE$ parameter, and both parameters explain a great part of the total variability.

Abiotic phosphorus uptake is probably not the only phosphorus uptake process, biotic SPR uptake is probably occurring through the periphyton. Sediment chlorophyll content covaries with one of the main components (PC3), and it could be an indicator of biotic uptake.

5.6 Nutrient uptake estimation

5.6.1 Sediment SRP uptake: kinetic approach

Application of the experimental data to the Elovich equation (eq. (5.12)), did not provide a significant model curve fit. That suggest this model is not applicable for the current data set. In the same way, using our experimental data to fit Michaelis-Menten equation results in a non significant model. Both formulations describe a saturation curve, and to describe it properly through experimental data, it is necessary to provide data from at least three parts of the saturation curve. Our experimental data are probably representing only

the saturated part of the curve, preventing a satisfactory curve fit across the fully necessary range of concentrations.

5.6.2 Sediment uptake estimation: steady and unsteady approaches

Laboratory channel uptake coefficient estimations through first order reaction simplification (eq. (5.4)) supplied always positive values of uptake coefficients, indicating an SRP retention in each experiment. SRP uptake coefficients ranged from $1.70E-04$ to $3.46E-05$ s^{-1} (see Table 5.5).

Table 5.5: SRP uptake coefficients at the laboratory channel experiments using the steady and unsteady approaches.

Arithmetic mean ± SD.

Model	$k(s^{-1})$	S_w (m)	Vf $(m\ s^{-1})$	U $(mg\ m^{-2}\ s^{-1})$
Steady	6.6E-05±5.3E-05	912.1±454.2	6.07E-06±5.1E-065	1.8E-02±1.9E-02
Unsteady	4.7E-03±6.7E-03	385.5±466.1	6.76E-06±1.0E-05	1.8±3.4

The unsteady two-dimensional (2D) model was applied to simulate each laboratory channel experiment. To evaluate the accuracy of the numerical model, measured and calculated Br^- concentrations were compared with linear regressions (Table 5.6). All the experiments except number 19 showed an excellent agreement between measured and calculated bromide concentrations, with $R^2 \geq 0.91$, and slopes not significantly different from 1 (see Table 5.6 and Figure 5.13). However, the agreement in experiment 19 was lower than in the rest, where the slope and the intercept were significantly different from 1 and 0 respectively, which introduces a systematic error in the prediction of tracer concentration (Table 5.6). Most of the disagreement in experi-

ment 19 occurred at the beginning and at the end of the experiment. When the comparisons are limited to the period that bromide concentration remained more or less stable, the agreement improved: $R^2 = 0.74$; $slope = 0.96 \pm 0.11$ ($p \geq 0.5$); intercept = 0.69 ± 1.98 ($p \geq 0.5$). Since the experimental methodology assured the complete water mixing across channel length and depth, we speculate that the initial and final disagreement in experiment 19 is due to a transient storage effect, where bromide was temporally retained in sediment pores.

Table 5.6: Comparison of measured and calculated bromide concentrations in laboratory channel experiments (16-20).

Presented are r^2, the slope, the intercept, and p values of t-test comparing the slope with 1 and the intercept with zero. Slopes differ significantly from 1 at $p \leq 0.05$ and are printed in bold. Intercepts differ significantly at $p \leq 0.05$ and are printed in bold.

Experiment	df	r^2	Slope±SE	p_{slope}	Intercept±SE	$p_{intercept}$
16	19	0.91	1.00±0.07	1	-0.04±0.09	1
17	14	0.99	0.96±0.04	1	0.10±0.13	1
18	16	0.99	0.95±0.03	1	0.18±0.13	0.2
19	33	0.76	0.83±0.08	**0.02**	2.35±1.22	**0.05**
20	25	0.97	0.94±0.03	0.1	0.83±0.60	0.1

Once we were sure the unsteady 2D model correctly represented the dissolved solute transport, the outlet and inlet SRP concentrations were used to find the unsteady SRP uptake coefficient. In this way, the new k values found from the unsteady model simulations ranged from $1.4E-02$ to $2.60E-05\ s^{-1}$, which were not significantly different from the k steady val-

ues ($t = -1.27$; $p \geq 0.05$) (Table 5.9 and Figure 5.14).

The linear regression between measured and calculated SRP outlet concentration shows a significant correlation for both approaches ($p \leq 0.05$), where there were no significant differences in explained variance between the steady and unsteady approaches (compare R^2 values, Table 5.7). However, both approaches often led to systematic deviations from observed values. For both approaches, slopes differed significantly from 1 (steady-state 5 times, unsteady 3 times) and intercepts differed from 0 (3 times in both models). Still, slopes and intercepts were much more closer to 1 and 0 in the unsteady approach. Furthermore, experiment 19 appeared the most difficult to predict, which is in agreement with the bromide observations.

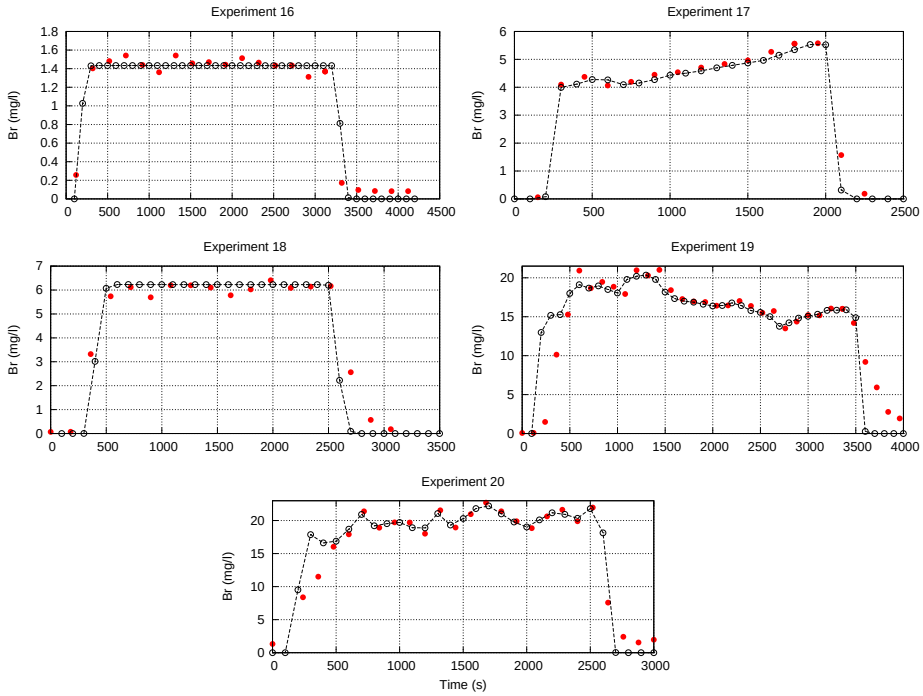

Figure 5.13: Laboratory channel passive tracer (16-20).

Comparison of the passive tracer concentration during the addition experiments as computed with the 2D unsteady model and measured at the outlet sampling point. Red dots Represents the measured tracer, black dots represents the computed tracer.

Table 5.7: Comparison of measured and calculated SRP concentrations in laboratory channel experiments (16-20).

Presented are r^2, the slope, the intercept (Int.), and p values of t-test comparing the slope with 1 and the intercept with zero. Slopes differ significantly from 1 at $p \leq 0.05$ and are printed in bold. Intercepts differ significantly from 1 at $p \leq 0.05$ and are printed in bold.

		Steady-state					**Unsteady-state**				
Exp.	**df**	R^2	**Slope**±**SE**	p	**Int.**±**SE**	p	$\mathbf{r}^2$	**Slope**±**SE**	p_{slope}	**Int.**±**SE**	$p_{intercept}$
16	19	0.99	0.90±0.02	≤**0.01**	0.00±0.01	0.5	0.98	0.90±0.02	0.5	0.04±0.01	0.5
17	14	0.71	0.75±0.12	**0.05**	0.11±0.05	**0.01**	0.71	0.79±0.13	0.1	0.11±0.05	**0.01**
18	16	0.89	0.81±0.07	**0.01**	0.11±0.03	0.5	0.89	0.81±0.07	**0.01**	0.11±0.03	0.5
19	33	0.91	0.36±0.02	≤**0.01**	0.10±0.04	≤**0.01**	0.90	0.89±0.05	**0.02**	0.12±0.04	≤**0.01**
20	25	0.95	0.84±0.04	≤**0.01**	0.22±0.07	≤**0.01**	0.95	0.89±0.04	**0.02**	0.20±0.08	≤**0.01**

Similarities among predictions of both approaches is probably due to the uniform cross sectional area experiment conditions. Experiments were carried out in a laboratory channel where, a uniform cross sectional area, one of the steady-state model assumptions, was provided quite well.

5.6.3 Irrigation canal SRP uptake estimation: steady and unsteady approaches

Estimated first order SRP uptake coefficients were always positive and significantly different from 0 ($t = 3.557$, $p = 0.004$), indicating an SRP retention in each experiment. Variation among experiments was higher than that derived from the mass balances, with a coefficient of variation (98%) twice as much as that of the mass balance calculations (52 %; fig. 5.15).

The unsteady two-dimensional model was applied to simulate each canal experiment. To evaluate the accuracy of the numerical simulations, measured and calculated Br^- concentrations, were compared with linear regressions (Table 5.8). These showed an excellent agreement between measured and calculated concentrations, with $R^2 \geq 0.93$, and the slopes were not significantly different from 1 (Table 5.8). Then, the outlet and inlet SRP concentrations were used to find the unsteady SRP uptake coefficient. In this way, the new k values found from the unsteady model simulations ranged from $2.5E-03$ to $2.6E-04$ s^{-1}, which are significantly ($t = 3.576$; $sig. = 0.004$) higher than those estimated from the steady-state model (Table 5.9). Both approaches differ by one order of magnitude, the unsteady uptake coefficients being higher.

Table 5.8: Comparison of measured and calculated bromide concentrations using the 2D unsteady model for experiments 1-12.

Presented are R^2, the slope, the intercept, and p values of t-test comparing the slope with 1 and the intercept with zero.

Exp.	df	R^2	Slope±SE	p_{slope}	Intercept±SE	$p_{intercept}$
1	10	0.98	0.99±0.03	1	-0.08±0.08	1
2	14	0.99	0.99±0.06	1	0.14±0.16	1
3	14	0.99	1.00±0.02	1	0.01±0.04	0.5
4	14	0.98	0.99±0.03	1	0.03±0.09	1
5	12	0.99	0.95±0.03	0.1	0.12±0.12	1
6	12	0.99	0.97±0.03	0.3	0.28±0.17	1
7	10	0.99	0.97±0.01	0.1	0.02±0.04	1
8	11	0.98	0.96±0.04	0.4	0.17±0.43	0.5
9	12	0.99	0.97±0.02	0.2	0.06±0.06	1
10	12	0.99	0.96±0.02	0.1	0.01±0.03	1
11	14	0.99	0.97±0.02	0.1	0.01±0.02	1
12	8	0.99	0.98±0.02	0.3	-0.02±0.03	1

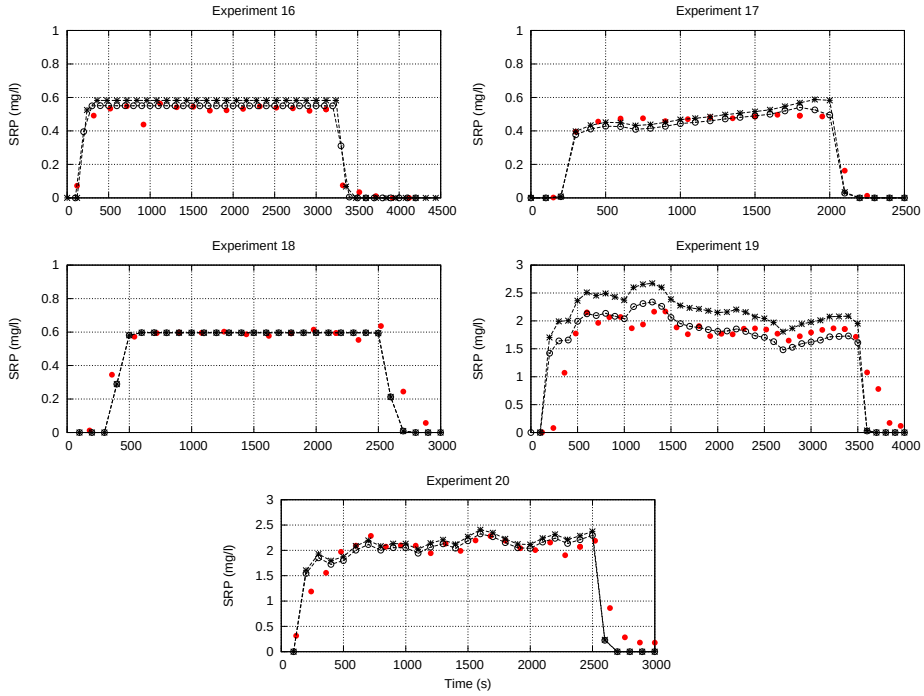

Figure 5.14: SRP time evolution at the laboratory channel experiments (16-20).

Comparison of the time evolution of the SRP concentration as estimated from the steady approach ("∗"), computed with the 2D unsteady (black dots) and measured (red dots) at the sampling point.

5. NUTRIENT RETENTION CAPACITY OF AN AGRICULTURAL DRAINAGE CHANNEL: DEVELOPING A PREDICTIVE MODEL

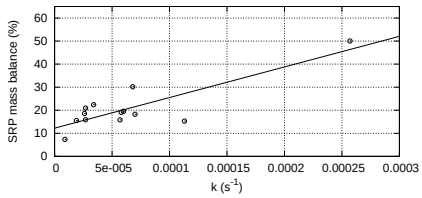

Figure 5.15: Mass balance and steady SRP uptake coefficient at the irrigation canal experiments (1-12).

Relationship (line) between the SRP net budget difference and the steady SRP uptake coefficient (k) (”○”). The linear regression has a r^2 = 0.70 and $p<0.00$.

As stated in Section 5.4.2.4, to evaluate the accuracy of both methods (steady and unsteady), the steady SRP uptake coefficient was introduced in the unsteady 2D model as a reaction term in equation 3.8. The comparison of both methods is shown in Table 5.10. Both calculation methods showed a good agreement between the calculated and the measured concentration. The linear regressions were always significant (p = 0.01) and there were no significant differences in explained variance between the steady and unsteady approaches (compare R^2 values, Table 5.10). In the same way, intercepts did not differ significantly from 0 in any of the steady and unsteady state calculations. However, the steady-state approach showed systematic discrepancies in three of the experiments, their regression slopes being significantly different from 1 (Table 5.10). This systematic error was found mainly in experiments where the flow varied with time. Hence, this disagreement could be due to the simplification in the solute mass conservation equation and probably to the assumption of a constant decay term (eq. (5.2)). In contrast, the regression slopes of the unsteady approach did never differ significantly from 1, suggesting a closer reproduction of the phosphorus dynamics in the channel. Hence, the assumption of a constant decay term, as in the steady approach, could introduce a disagreement between the measured and calculated concentrations (fig. 5.16, experiment 17).

Table 5.9: Irrigation canal nutrient uptake coefficients.

Nutrient uptake coefficients (arithmetic mean ± SD) at the irrigation canal using the steady and unsteady approaches.

Model	Nutrient	$k(s^{-1})$	S_w (m)	Vf $(m\ s^{-1})$	U $(m\ m^{-2}\ s^{-1})$
Steady	SRP	6.31E-05 ± 6.23E-05	5.04E+03 ± 5387.63	1.67E-05 ± 1.35E-05	2.28E-02 ± 0.028
Steady	DIN	2.00E-05 ± 6.08E-05	-1190.61 ± 85780.30	7.13E-06 ± 2.06E-05	0.036 ± 0.11
Steady	TDN	1.21E-05 ± 1.53E-05	16875.48 ± 52688.98	0.20E-05 ± 2.53E-06	3.37E-06 ± 0.01
Unsteady	SRP	6.70E-04 ± 1.72E-04	956.54 ± 615.99	2.32E-04 ± 5.97E-05	0.56 ± 0.28

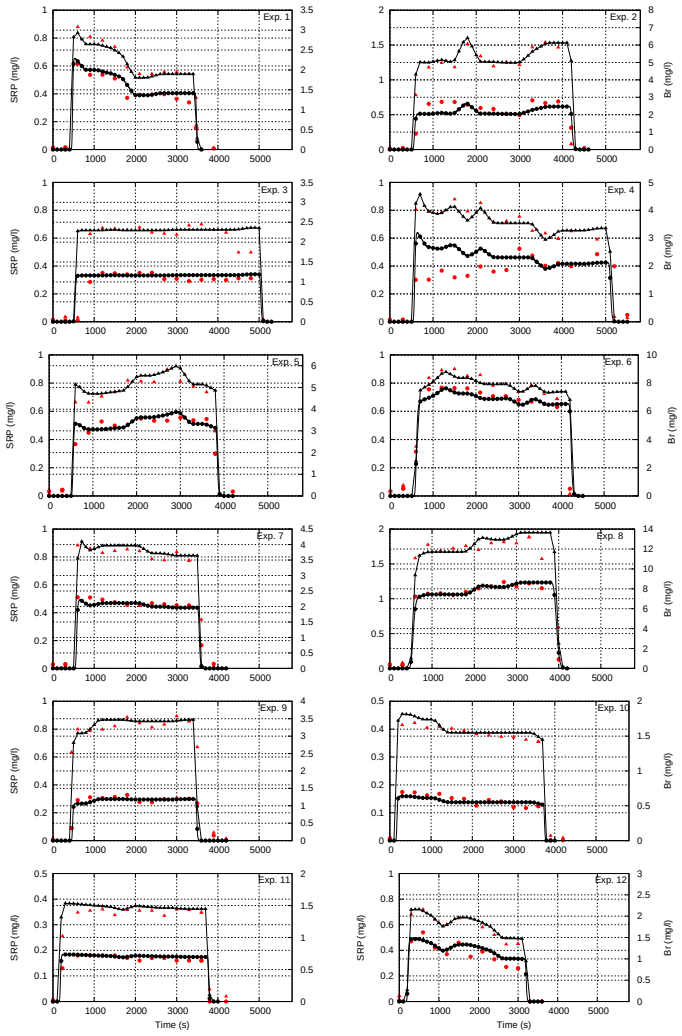

Figure 5.16: SRP and tracer concentration at the irrigation canal experiments (1-12).

Comparison of the measured (black) and calculated (red) Br^- (triangles) and SRP (dots) concentration at the second sampling section (average of the three measurement points) during the addition experiments using the 2D unsteady model.

5.6.4 Irrigation canal Nitrogen uptake estimation: steady and unsteady approaches

As in the mass balance calculations, the average DIN uptake coefficient (k_{DIN}) was not significant different from 0 (t=1.081; sig.0.298), and in some experiments it was negative, possibly as a result of DIN desorption.

The nitrogen uptake simulation did not reproduce the measured nitrogen uptake with the same accuracy as in the case of phosphorus (compare figs. 5.16 and 5.17). Linear regressions have been calculated between the observed and calculated nitrogen concentrations using both steady and unsteady approaches, and both of them were not significant (data not shown).
Therefore SRP will be the only nutrient to be considered in the predictive formulation.

5.7 Predictive SRP uptake formulation

As stated at the introduction, the steady approach (eq 5.3) has two disadvantages: the river uniform representation, where steady-state, uniform cross-sectional flow parameters are assumed, and the need of the outlet and inlet nutrient data to its application, where the kinetic approaches can also be included. To solve both problems, we propose an alternative formulation that considers quasi steady state flow conditions instead of stationary, and whose formulation is expressed as a function of the most uptake influential parameters. In the present section, a predictive dissolved phosphorus uptake model is developed, first for the sediment, and then for the whole drainage canal system.

Table 5.10: Comparison of measured and calculated SRP concentrations for experiments 1-12.

Presented are R^2, the slope, the intercept, and p values of t-test comparing the slope with 1 and the intercept with zero. Slopes differ significantly from 1 at $p \leq 0.05$ and are printed in bold.

		Steady-state					Unsteady-state				
Exp.	df	r^2	Slope±SE	$p-value$	Intercept±SE	$p-value$	r^2	Slope±SE	p_{slope}	Intercept±SE	$p-value$
1	14	0.87	1.36±0.04	**0.001**	0.00±0.04	0.3	0.95	1.01±0.02	1	-0.01±0.02	1
2	16	0.93	1.01±0.02	0.5	0.01±0.02	0.5	0.95	0.98±0.02	0.3	-0.01±0.03	1
3	16	0.97	1.14±0.33	1	0.00±0.01	0.3	0.96	1.00±0.04	1	-0.01±0.01	1
4	18	0.70	1.23±0.11	0.1	0.06±0.04	1	0.71	0.99±0.12	1	0.05±0.04	1
5	15	0.87	1.08±0.03	**0.01**	0.01±0.04	0.4	0.96	1.01±0.05	1	0.02±0.02	1
6	15	0.89	1.16±0.08	0.1	0.03±0.05	1	0.99	0.99±0.02	1	0.01±0.01	1
7	14	0.97	1.15±0.05	**0.01**	0.03±0.02	0.2	0.99	0.97±0.03	0.4	0.01±0.02	1
8	14	0.99	1.02±0.03	0.4	0.01±0.02	0.5	0.99	0.99±0.03	1	0.00±0.01	1
9	15	0.81	0.88±0.11	0.4	0.01±0.03	1	0.98	0.99±0.03	1	0.00±0.01	1
10	15	0.99	0.95±0.06	0.4	0.00±0.01	1	0.95	0.99±0.03	1	0.00±0.01	1
11	15	0.98	1.09±0.04	**0.05**	0.00±0.00	1	0.98	1.03±0.03	0.3	0.00±0.00	1
12	13	0.97	1.03±0.05	1	-0.01±0.02	1	0.97	1.03±0.05	1	-0.01±0.02	1

5.7.1 Predictive sediment SRP uptake formulation

Using the quasi steady state approach to estimate nutrient uptake coefficient supplies a positive general uptake coefficient ($0.009 \pm 0.001\ s^{-1}$). In agreement with the previous results, this positive coefficient suggest an SRP retention in each experiment. However, the partial uptake coefficients were not always positive, but in experiment five some of them were negative. This result may indicate a partial SRP desorption or a transient SRP storage.

To create the predictive SRP uptake equation we use the parameters provided by the sediment PCA analysis: SRP inlet concentration, water temperature, Reynolds number and water discharge. However, the rate of sediment mass to water mass in the column may also have some influence in nutrient uptake. A deep water column implies that not all the nutrients in the column can exchange with the sediment. On the contrary, in shallow waters, the contact between nutrient in the water column and sediment is more intense. A gradual increase in SRP retention with decreasing stream size can be explained by the ratio between water volume and benthic surface area, which also increases with stream size (Peterson et al. (159)). A small ratio signifies a high reactive surface area relative to the volume, promoting sorption and uptake of soluble nutrients by the benthic community (Peterson et al. (159)). As we intend to extrapolate the predictive sediment SRP uptake model to other systems, such as canal or natural river, it is necessary to include a factor that contemplates this proportion effect. This additional factor could be as

follows:

$$\frac{M_s}{M_w} = \frac{\rho_s(1-POROSITY)h_s}{\rho_w h_w} \tag{5.15}$$

where ρ_s and ρ_w are sediment and water density and h_s and h_w are sediment and water depth. Moreover, equation 5.15 also includes some of the sediment characteristics that may influence sediment phosphorus uptake capacity.

Hence, using M_s/M_w relationship, SRP inlet concentration, water temperature, Reynolds number and water discharge, we developed the following non-linear regression with the quasi steady state uptake coefficients:

$$k = \frac{C_1 C_{SRP}(1+\frac{1}{Re})T}{C_{SRP}+ln(T)ln(Re)}\frac{M_s}{M_w} \tag{5.16}$$

where C_1 is a constant value of 0.006, C_{SRP} is the inlet phosphorus concentration (g/m^3), Re is the Reynolds number and T the water temperature (^0C).

This equation (5.16) provides a saturation curve that depends on the water temperature, Reynolds number and the sediment-water proportion. Therefore, the SRP uptake coefficient is variable in time and space. These parameters also should have an influence on biotic uptake, but since we did not measure algae or bacteria growth during the nutrient addition experiments, these cannot be introduced in the formula with an explicit expression. Sediment presented a biofilm where the chlorophyll concentration was measured.

However, there was no direct relationship between this concentration and phosphorus uptake. Hence, although probably there was a biotic phosphorus uptake, the main uptake appears to be addressed by abiotic processes such as sediment adsorption. Therefore, the general sediment phosphorus uptake of our system can be expressed using equation (5.16).

5.7.2 Validation of the predictive SRP sediment uptake formulation

The new SRP uptake equation (5.16) was introduced in the unsteady 2D model in equation (3.8). Then, the accuracy of the new formulation was evaluated comparing linear regressions of measured and calculated SRP. Table 5.11 shows the comparison of measured and calculated phosphorus concentrations in successive experiments using equation (5.16).

Table 5.11: Comparison of measured and calculated SRP concentrations using the sediment SRP uptake formulation for experiments 16-20.

Presented are R^2, the slope, the intercept, and p values of t-test comparing the slope with 1 and the intercept with zero. Slopes differ significantly from 1 at $p \leq 0.05$ and are printed in bold. Intercepts differ significantly from 0 at $p \leq 0.05$ and are printed in bold.

Experiment	df	r^2	Slope±SE	p_{slope}	Intercept±SE	$p_{intercept}$
16	19	0.97	0.90±0.02	**≤0.05**	0.00±0.01	0.5
17	14	0.94	1.06±0.07	0.4	0.01±0.03	1
18	16	0.99	1.00±0.02	1	0.01±0.01	1
19	33	0.90	0.50±0.03	**≤0.05**	0.09±0.04	**≤0.05**
20	25	0.95	0.93±0.04	0.1	0.21±0.08	**≤0.05**

The new formulation (5.16) provided significant linear regressions in all the experiments ($R^2 \geq 0.90$; $p \leq 0.05$) (Table 5.11). However, systematic discrepancy differences were found in experiments 16 (slope), 19 (slope and intercept) and 20 (intercept). Major discrepancies were only present in experiments 20 (slope and intercept $p \leq 0.05$) and 5 (intercept p≤ 0.05).

The predictive capability of the three successive approaches can be evaluated from their explained variance and the slopes and intercepts of regressions of observed vs. predicted values. Explained variance was quite satisfactory for all the three models ($r^2 \geq 0.71$; eq. 5.16 $r^2 \geq 0.90$). Slopes however always differed significantly from unity for the steady-state model ($0.4 - 0.9$), twice for the unsteady model ($0.8 - 0.9$) and twice for the new predictive model ($0.5 - 1.1$). Intercepts were closest to zero for the new predictive model. We conclude that the steady-state model performed worst, where the other two were comparable. The new predictive model had difficulty in predicting experiment 19, but performed better, overall.

5.7.3 Water column SRP uptake formulation

The sediment predictive equation can be used to represent sediment SRP uptake, but we still need a formulation that represents SRP uptake in the water column. To do so, it is necessary to identify uptake agents in the water column. According to the PCA results (Section 5.5.2), *TSS*, *SPOM* and *SPIM* appeared the most influential variables. However, in order to generate the non-linear regressions, some changes were introduced in the original variables. On the one hand, *TSS* was replaced by *SPOM* and *SPIM*. Since *TSS* is the result of adding up *SPOM* and *SPIM*, it is possible to include these

two variables instead of *TSS*. On the other hand, some variables that did not appear significant into PCA analysis were included in the formulation. These are: *TDS*, *Re* and the *SRP* ambient concentration. *TDS* and *Re* can affect water column SRP uptake. As in sediment SRP uptake, flow turbulence can facilitate or difficult SRP uptake in water column. High turbulence could enhance SRP-TSS contact, facilitating SRP uptake. However, this is probably not a linear effect, because a laminar flow regime usually results in a lower velocity, increasing residence time, which can also increase SRP uptake. Moreover turbulence effect, *Re* formula includes water temperature, and including water temperature in the equation means to include its effect in biotic and abiotic uptake processes, which has been demonstrated in many studies.

SRP ambient concentration was included to contemplate the nutrient injection effect in the uptake process. Increasing nutrient concentration through nutrient addition can transform the nutrient equilibrium system, causing a distortion of the ambient nutrient uptake (Mulholland et al. (133)).

Total dissolved solids corresponds to the sum of Na^{+}, K^{+}, Ca^{2+}, Mg^{2+}, H_4SiO_4, $HCO3^{-}$, CO_32^{-}, $SO42^{-}$, Cl^{-}, and $NO_3{}^{-}$. The middle Ebro river water is a typical carbonate water, where the principal elements are calcium and bicarbonate, and providing that irrigation canal waters comes from the middle Ebro river, it has a high calcium and bicarbonate content (see Table 5.2). Inorganic phosphorus reacts easily with calcium and co-precipitation is an important abiotic uptake process. Therefore, *TDS* content would also

affects SRP uptake in the water column.

Hence, a non-linear regression among the quasi steady SRP uptake coefficients and *SPOM*, *SPIM*, *TDS* and *Re* was established as follows:

$$k = \frac{C_1(\frac{\frac{C_{SRP}}{C_{SRP,amb}}}{\frac{C_{SRP}}{C_{SRP,amb}}+9})C_{SRP}C_{SPOM}C_{TDS}C_{SPIM}(1+\frac{1}{Re})}{C_{SRP}+C_2(\frac{\frac{C_{SRP}}{C_{SRP,amb}}}{\frac{C_{SRP}}{C_{SRP,amb}}+9})C_{SPOM}C_{TDS}C_{SPIM}(1+\frac{1}{Re})} \tag{5.17}$$

where k is the SRP uptake coefficient (s^{-1}), C_{SPOM} is the suspended particulate organic matter (g/m^3), C_{TDS} corresponds to total dissolved solids (g/m^3), C_{SPIM} represents the suspended particulate inorganic matter (g/m^3), $C_{SRP,amb}$ is the SRP ambient concentration (g/m^3), Re is the Reynolds number, and C_1 and C_2 are constants values of $9.32E-09$ and $1.51E-07$ respectively.

5.8 Validation of a predictive model combining water column and benthic uptake

To evaluate the accuracy of the new approach, experiments 1 to 12 were simulated using the new predictive formulation (see Figure 5.19). Then, linear regressions were carried out comparing measured and calculated SRP concentrations (Table 5.12). The new approach has no influence in the transport equations, only in the reactive term. Since the chemical tracer bromide is biologically and chemically stable and not undergo microbial transformations

and gaseous losses, it is not necessary to redevelop the linear regressions with measured and calculated bromide concentrations.

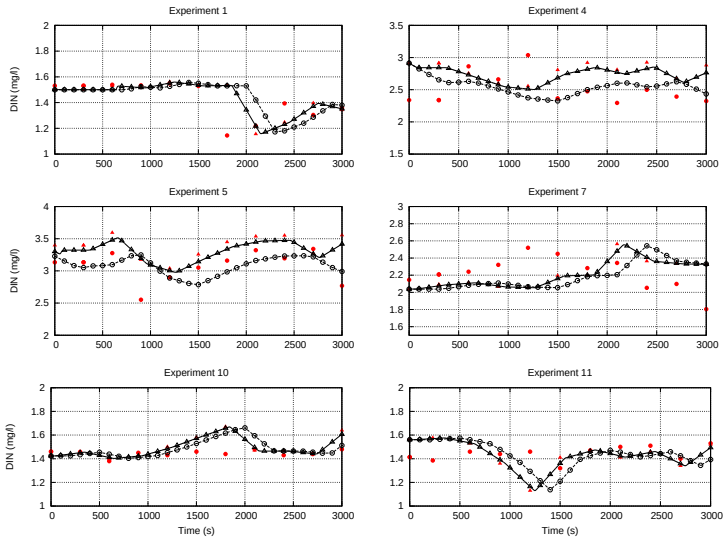

Figure 5.17: Measured and calculated DIN concentration at the irrigation canal experiments.

Comparison of the DIN concentrations during the nutrient addition experiments as computed with the 2D unsteady model and measured using the uniform uptake coefficient at the second sampling section (average of the three measurement points). Red triangles: measured input DIN concentration, black triangles: DIN computational input. Red dots: DIN measured output and black dots: DIN computed output.

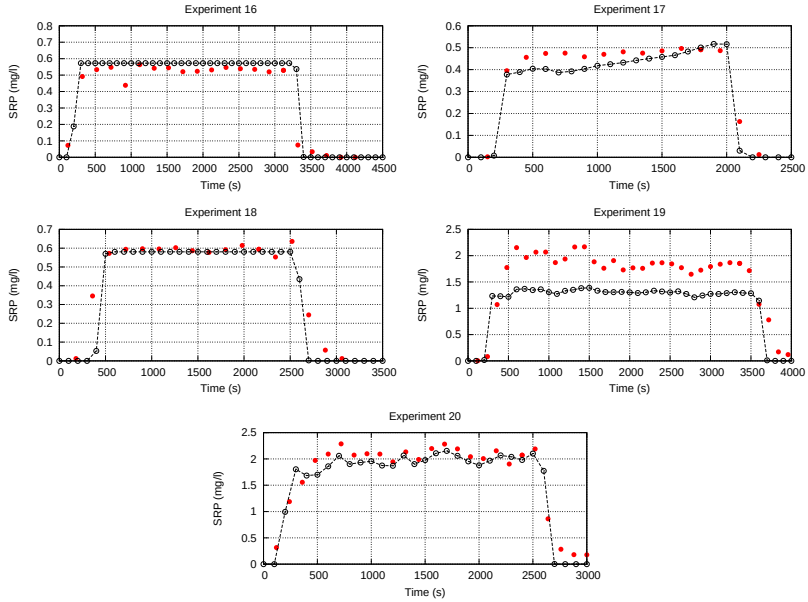

Figure 5.18: Comparison of the measured and calculated SRP concentration using the sediment SRP uptake predictive formulation for experiments 16-20.

Red dots: measured SRP concentration at the sampling section (the average of three points). Black dots: estimated SRP concentration using the sediment SRP uptake predictive formulation.

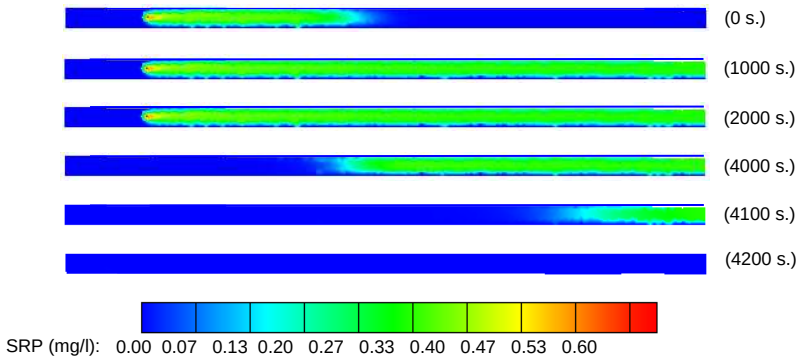

Figure 5.19: Irrigation canal SRP model validation.
Simulated SRP time evolution at the irrigation canal during experiment 3.

Table 5.12: Comparison between measured and calculated SRP concentrations using the predictive SRP uptake formulation for experiments 1-12.

Presented are- r^2, the slope, the intercept, and p values of t-test comparing the slope with 1 and the intercept with zero. Slopes differ significantly from 1 at $p \leq 0.05$ and are printed in bold. Intercepts differ significantly from 0 at $p \leq 0.05$ and are printed in bold.

Experiment	df	r^2	Slope±SE	p_{slope}	Intercept±SE	$p_{intercept}$
1	10	0.92	0.71±0.04	≤**0.01**	0.01±0.02	0.5
2	14	0.85	1.59±0.17	≤**0.01**	-0.04±0.06	0.5
3	14	0.96	0.97±0.05	0.5	0.00±0.01	1
4	14	0.69	-1.87±0.31	≤**0.01**	1.05±0.15	≤**0.01**
5	12	0.88	0.91±0.09	0.3	0.01±0.05	1
6	12	0.97	0.92±0.05	0.1	-0.04±0.03	0.5
7	10	0.88	0.91±0.01	0.3	0.03±0.04	0.5
8	11	0.98	1.19±0.04	≤**0.01**	-0.06±0.04	0.2
9	12	0.98	0.95±0.04	0.2	0.01±0.01	0.5
10	12	0.94	0.96±0.07	0.5	0.00±0.01	1
11	14	0.83	1.25±0.19	0.2	-0.11±0.07	0.2
12	8	0.83	1.18±0.18	0.2	-0.08±0.07	0.3

Results showed a good agreement between measured and calculated data ($R^2 \geq 0.69$), where linear regressions were always significant (p = 0.01). Eight experiments (3, 5, 6, 7, 9, 10, 11 and 12) provided excellent SRP concentration predictions, with slope and intercept not significantly different from 1 and 0 respectively. The rest of the experiments (1, 2, 4 and 8) showed a systematic discrepancy (slopes $p \leq 0.05$) between measured and calculated data. Experiments 1 and 4 showed the highest SRP uptake (37 ± 2 % and 39 ± 48 % respectively), and the new formulation underestimated this greatly.

On the contrary, experiments 2 and 8 showed a low SRP uptake (6.4 ± 3.0 % and 3.6 ± 1.1 % respectively), and the results provided a systematically overestimated SRP uptake. Posibly, the high dissolved phosphorus uptake at experiments 1 and 4, is an indicator of presence of other uptake agents, or a much higher biotic uptake. Providing that abiotic uptake is the main SRP uptake process considered in the new formulation, this could be one of the reasons of the systematic error. However, the low uptake level observed at experiments 2 and 8 does not suggest an important biotic uptake presence. Hence, the systematic discrepancy may be adressed by other factors such as the water variables characterization.

Equations 5.16 and 5.17 consider SPIM, SPOM and TDS. These variables are characterized using three background water samples taken before starting the nutrient addition. Hence, its variations during the experiment are not contemplated. Irrigation canal water flow was very stable, but variations of water quality parameters are possible within experiments, and those variations can affect SRP uptake. The lack of a continuous water parameters characterization could be another cause of the systematic error presence.

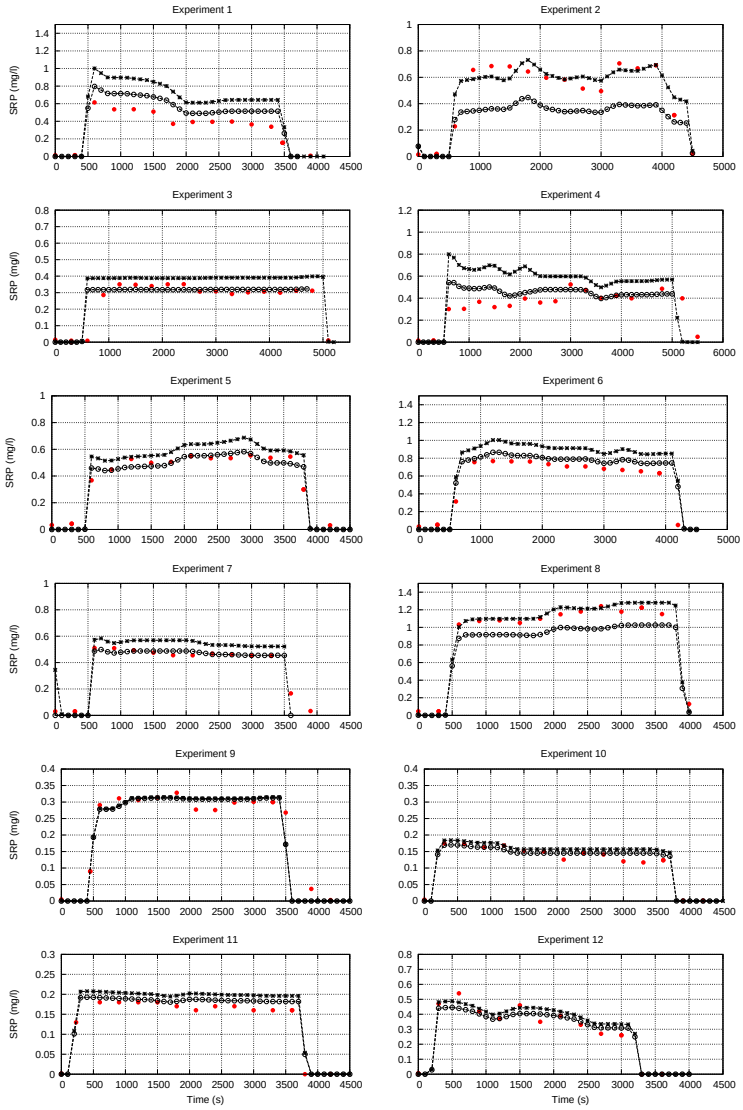

Figure 5.20: Comparison of measured and estimated SRP concentration using the predictive formulation.

Red dots: measured SRP at the second sampling site. Black dots: estimated SRP. $*$: inlet SRP.

In general, the new model provides a good agreement between measured and calculated data (Figure 5.20), where in spite of the systematic discrepancy, SRP calculations were always within the same order of magnitude as measured data. Hence, the model showed a good predictive capacity, but it should be tested in other system conditions as well as in other aquatic systems.

5.8.1 Changing temporal and spatial scale

In order to validate the predictive uptake model under different conditions, a new set of 3 nutrient addition experiments was carried out (experiments 13-15, see Subsection Experimentation number 2). The experiments were performed at a higher spatial-temporal scale, where the uptake model variables were characterized continuously during the whole experiment.

5.8.1.1 Results

New nutrient addition experiments resulted in a null mass balance, which did not significantly differ from 0, indicating the absence of SRP system uptake. In agreement with this, the estimated first order SRP uptake coefficients were not significantly different from 0 ($k = 9.34E-6 \pm 3.38E-4 s^{-1}$; $t = 0.14$, $p = 0.5$). In the same way, the average of consumed SRP was $-1.24 \pm 2.28\%$, and did not significantly differ from 0 ($t = -0.54$, $p = 0.59$). Under these results, we can not affirm that there is an SRP uptake process.

Provided that SRP uptake process is regulated by biotic and abiotic mechanisms (Reddy et al. (167)), a change in some of these mechanisms can result

in an SRP uptake variation. Therefore, a variation in physical and chemical irrigation canal water characteristics can alter the SRP uptake. Previous sections suggested that main SRP uptake process was adsorption, and it was addressed by TSS (SPIM + SPOM). If so, a significant change in TSS may result in SRP uptake alteration. In agreement with this, Table 5.13 shows physical and chemical irrigation canal water parameters and its comparison with previous experimentation (Table 5.2, where TSS, SRP and TDS significantly differ from previous values (Table 5.2). However, against expectations, TSS, TDS and SRP were higher in this new experiments, and these higher concentrations should induce an higher SRP uptake instead of a non significant SRP uptake.

Estimating nutrient uptake by means of nutrient addition can produce luxury uptake and overestimate the ambient system uptake (Mulholland et al. (133)). If the nutrient is limiting, its addition can stimulate the system, and therefore its uptake. Mulholland et al. (133) stated that this stimulation should be related to the level of nutrient addition above ambient concentrations and the degree of nutrient limitation. Phosphorus addition experiments of Mulholland et al. (133), increased the ambient SRP concentration $10-100$ times. In our own SRP addition experiments, the concentration increasing was $2-3$ times only. Hence, probably, there was an SRP uptake, but it was under our detection limits.

Although non significant SRP uptake was found, the predictive formulation should reproduce this situation. Each experiment was simulated using the new model. Then, in order to evaluate its accuracy, linear regressions were carried out between the measured and calculated SRP concentrations (Table

5.8 Validation of a predictive model combining water column and benthic uptake

Table 5.13: Physical and chemical characteristics of the irrigation canal during the experiments 13, 14 and 15.

Concentration (arithmetic mean $\pm$ SD) variables are expressed in mg/l except SRP and Chl-a, which are in $\mu g/l$. Presented are p values of t-test comparing present values to previous experimentation. Values differ significantly at $p \leq 0.05$ and are printed in bold.

Variable	Arithmetic mean $\pm$ SD	$p-value$
Discharge(m^3/s)	0.07 ± 0.01	0.59
Temp.(^oC)	9.66 ± 1.47	0.59
pH	8.33 ± 0.03	0.42
Ca^+	118.55 ± 2.54	0.06
DIN	2.85 ± 0.12	0.55
TDN	3.39 ± 0.07	0.31
SRP	0.03 ± 0.02	$\leq$**0.05**
Chl-a	11.00 ± 1.00	0.18
SPOM	8.10 ± 0.75	0.13
TSS	65.95 ± 11.07	$\leq$**0.05**
TDS	801.23 ± 11.23	$\leq$**0.05**

Table 5.14: Comparison of the measured and calculated bromide concentrations using the unsteady 2D model for experiments 13, 14 and 15.

Presented are r^2, the slope, the intercept, and p values of t-test comparing the slope with 1 and the intercept with zero. Slopes differ significantly from 1 at $p \leq 0.05$ and are printed in bold. Intercepts differ significantly from 0 at $p \leq 0.05$ and are printed in bold.

Experiment	df	r^2	Slope±SE	p_{slope}	Intercept±SE	$p_{intercept}$
13	8	0.99	0.97±0.03	0.2	0.01±0.01	0.2
14	8	0.99	1.01±0.04	0.5	-0.00±0.02	0.5
15	9	0.97	0.94±0.05	0.2	0.01±0.02	0.5

5.15) as well as between measured and calculated Br^- concentration(Table 5.14) at the new irrigation canal experiments.

Table 5.15: Comparison of measured and calculated phosphorus concentrations using the new approach for experiments 13, 14 and 15.

Presented are, the degrees of freedom df, r^2, the slope, the intercept, and p values of t-test comparing the slope with 1 and the intercept with zero. Slopes differ significantly from 1 at $p \leq 0.05$ and are printed in bold. Intercepts differ significantly from 0 at $p \leq 0.05$ and are printed in bold.

Experiment	df	r^2	Slope±SE	p_{slope}	Intercept±SE	$p_{intercept}$
13	8	0.97	0.93±0.05	0.2	0.00±0.00	0.5
14	8	0.91	0.88±0.10	0.2	0.01±0.01	0.2
15	9	0.94	0.93±0.07	0.3	0.00±0.01	0.5

As stated in previous sections, the two-dimensional simulation model represents with an excellent accuracy the transport of dissolved solutes. Results from Table 5.14 showed an excellent agreement between measured and

calculated bromide concentration, where all the regressions were significant ($p \leq 0.01$) and the slopes and intercepts did not significantly differ from 1 and 0 respectively. In the same way, regressions with measured and calculated SRP using the new predictive formulation were significant ($p \leq 0.01$), and the slopes and intercepts did not significantly differ from the unit and zero respectively (see Table 5.15). Hence, although SRP uptake was not significant, the new formulation was capable of predict it it with an excellent accuracy.

5.9 Conclusions

We hypothesized that the canal bed would function as a nutrient sink, and our observations confirm this. However, this nutrient retention capability holds for SRP but not to the Nitrogen. A drainage canal would reduce SRP by about 21%, or 0.7 $mg\ m^{-2}\ h^{-1}$ at concentrations ranging from 1 to 46 $\mu g\ l^{-1}$, whilst there would be not significant change for Nitrogen concentration. Indeed, the mean molar DIN:SRP ratio (206:1) indicates a desequilibrate system where probably Nitrogen is saturated and phosphorus is limiting nutrient.

Since SRP retention appears to be related to suspended solids first, adsorption is probably the primary process, followed by sedimentation in the channels. This is probably enhanced by a developing sediment bed and vegetation. In agreement with this, the experimental analysis shows as the most influential SRP uptake parameters: pH, TSS and TDS.

5. NUTRIENT RETENTION CAPACITY OF AN AGRICULTURAL DRAINAGE CHANNEL: DEVELOPING A PREDICTIVE MODEL

Comparison between the steady and steady state approaches shows that the assumption of a uniform uptake coefficient makes the simulation tool less accurate. An alternative calculation method was necessary to cover the spatial and temporal variability of system uptake.

The new SRP uptake predictive model, based on the water column and sediment SRP uptake, has been tested at two different spatial and temporal scales under different SRP concentrations. First 12 experiments were developed at the drainage canal using 57 m length, during $60-80$ min and increasing SRP ambient concentration $10-100$ times. The last 3 experiments were carried out in the same drainage canal but using 300 m length, during $2-4$ hr and increasing SRP ambient concentration $2-3$ times. Although SRP uptake showed high variability among experiments ($0.0009 \pm 0.0004\ s^{-1}$), our new model could predict each case with an excellent accuracy all the linear regressions of measured and calculated SRP, being significant ($p \leq 0.01$). However, four predictions showed a systematic discrepancy, but in every case, predicted SRP output concentration was within the same order of magnitude as empirical observations.

Our new model formulation was able to predict the presence/absence of a noticeable SRP uptake process. Moreover, the model did quantify system SRP uptake with a great accuracy. In short, we can affirm that new formulation is well suited to predict SRP uptake in our experimental irrigation canal system.

5.10 Management proposal

Nutrient addition experiments showed the SRP uptake capacity of the drainage canal. Hence, the development of natural sediment and vegetation in drainage canals could be a good strategy to reduce some of the SRP agricultural pollutant load to the river. Nevertheless, for nitrogen reduction, other approaches must be considered, such as those enhancing denitrification possibly in riparian wetlands (Verhoeven et al. (204)).

On the other hand, the unsteady two-dimensional model with predictive formulation as a decay expression, can be used as a tool to predict and manage the canal SRP uptake process. Since most of the canal SRP uptake capacity depends on: turbulence, SPIM, SPOM, SDT, SRP and water temperature, with an easy physical and chemical water control, it is possible to apply the simulation model and predict the system SRP load reduction in time and space.

Phosphorus is a common agricultural fertilizer, and it causes eutrophication in many agricultural catchments (Carpenter et al. (42); Zalidis et al. (220)). Possibility to determine the best drainage canal conditions to apply phosphorus as a fertilizer can reduce its load to the river. In this way, the model can be useful to select the best moment to apply the fertilizer, or to modify the drainage canal conditions in order to increase its SRP uptake capacity. However, since the main uptake process is adsorption, phosphorus accumulates in the sediment. Accumulations of sediment my clog the chan-

nel and necessitate a periodic removal. It may be possible to take advantage of this renewal and use it as a fertilizer.

6

MODELING NUTRIENT AND SEDIMENT DYNAMICS IN THE MIDDLE EBRO RIVER FLOODPLAIN (NE SPAIN): A VALIDATION

6.1 Introduction

Riparian systems have an important role in regulating longitudinal or downstream transfer of sediment and associated pollutants during overbank flooding (Steiger and Gurnell (190)). Sediment transported by flood water is deposited within riparian zones, allowing them to function as a buffer between upstream and downstream river reaches (Mitsch and Dorge (131); Hupp and

Morris (90); Fennessy et al. (55); Kleiss (106)). This interaction between land and river constitutes an essential process to the riparian ecosystems maintenance, and affects fundamental ecological characteristics such as biodiversity, water quality and viability of many riverine species (Bunn and Arthington (29)).

The hydrological interaction between land and river has been reduced in time and space because of human activities such as agriculture, ship traffic, town planning and recreational water use. This reduction allows sediment, associated nutrients and other pollutants to escape through the river system without being captured in floodplains (e.g. Walling (209)). Degradation of rivers and floodplains is increasingly being recognized as a crucial political issue with socio-economic repercussions, particularly in North America and Europe (Naiman et al. (140)). In Europe, the target of a 'good ecological status' in all water bodies and aquatic ecosystems by 2015 was accepted as the main objective of the European Community Water Framework Directive (WFD: EU, 2000). However, most of the riparian restoration efforts are based on empirical experience (Richards and Hughes. (170)) and applied using trial and error procedure. In most cases, this approach forms an expensive, inefficient and difficult extrapolation.

During the 1980s and 1990s, increasing interest in such interaction led to direct measurements of sediment deposition during individual flood events using a variety of sediment trap devices, initially emphasizing floodplain locations (e.g. Mansikkaniemi (117);Gretener and Strmquist (66); Lambert

and Walling (112); Walling and Bradley (210); Asselman and Middelkoop (6); Simm (186)), but more recently focusing on riparian zones and hardwood bottom-land forests (e.g. Kleiss (105); Kleiss (106); Brunet et al. (28); Wardrop and Brooks (216); Heimann and Roell (75); Steiger et al. (191); Steiger et al. (192)). In the same way, during the last decade, attention has also focused on the fluxes of suspended sediment and particulate phosphorus through freshwater drainage systems because of severe eutrophication effects in rivers, lakes, reservoirs and coastal waters observed throughout the world (e.g. Meybeck et al. (126), Carignan and Vaithiyanathan (40), Bowes and House (23), Olde Venterink et al. (149), Braskerud et al. (26)). Several studies based on field measurements confirm the largely influence of the sedimentation process on phosphorus uptake (Johnston (101), Alexander et al. (4), Bowes and House (23), Olde Venterink et al. (149)).

Direct measurements of riparian zone sedimentation and sediment associated pollutants within different geomorphological settings and climatic regions are still rare (Steiger and Gurnell (190)). Hence, the question of the degree to which these zones may buffer the downstream transfer of sediment remains largely unanswered (Steiger and Gurnell (190)), and other approaches are necessaries. The hydraulic approach that analyzes the interaction between main channel and floodplain flow might be suitable in this point. Sellin (185) and Rajaratnam and Ahmadi (162) investigated this interaction through experimental flume studies, and revealed boundary shear stress distributions and resulting flow structures in compound channel sections with floodplains. Floodplains can be roughened so that the influence of differential roughness

on flow structures between floodplain and main channel and the lateral and vertical momentum transfer processes can be studied (e.g. Pasche and Rouvee (157)). The results of such studies have shown that the interaction between the main channel and floodplain flows is extremely complex with the formation of various three-dimensional flow structures, such as large interrelated vortices (cf. Knight and Shiono (108)). Hence, floodplain topography and flow patterns are the key controlling parameters for both the conveyance loss and sedimentation patterns (Walling (209)).

Numerical modeling might be a useful tool for the hydraulic approach. Nicholas and Walling (143) combined numerical modeling with field observations and illustrated how both approaches indicate the dominant role played by small-scale topographic features in controlling suspended sediment transport and deposition processes on floodplain surfaces. In the past decade, several workers have developed 1D and 2D models to simulate patterns of sediment deposition on floodplains. Some of these models are based on a finite-element approach (e.g. Stewart et al. (193); Hardy et al. (69)) and other models on a finite-difference approach (e.g. (143), Nicholas and Walling (144); Middelkoop and Van der Perk (130)). Particle-tracking method is also a used methodology that avoids the numerical dispersion produced by the conventional Eulerian models Thonon et al. (197). However, these simplified methods that in most cases uncouple the hydrodynamics and the solute transport, might be not enough when dealing with real cases. Ignoring unsteady hydrodynamical effects means that only a quasi-steady process over very slowly varying bed level can be reasonably modeled, so that, the correct

simulation of solute transport in rapidly varying flows containing shocks or discontinuities remain excluded. When solving real problems one is likely to encounter all sorts of situations, with a high probability that naive methods will compromise the quality and reliability of the solution. In that sense, complex models, based on a finite volume method, that make use of the Navier-Stokes equations seems to be the best option to represent the hydrodynamic interaction between water and land.

In this context, the complete simulation model that includes dissolved and suspended solute transport, flow erosive potential estimation and SRP uptake, is proposed as a floodplain analysis tool, capable of predicting the hydrological and sediment interactions between land and river in different spatial-temporal scales. These predictions will also be used as a basis information to choose the best restoration strategy. For that purpose, the flow simulation model calibrated and validated in Chapter 4 and the predictive SRP uptake model developed in Chapter 5 will be applied in the Middle Ebro River floodplain.

The present chapter will analyze the sedimentation pattern and the SRP uptake potential of the middle Ebro river floodplain by means of experimental and numerical analysis. First, the field data are analyzed, the SRP uptake and sedimentation models validated using field data. Then, the results are used to analyze the current sedimentation, dissolved phosphorus uptake and floodplain river nutrient contribution of the study site. Finally, different scenarios, based on changes in the hydraulic river-floodplain connectivity, are gener-

ated in order to analyze their potentially beneficial effect in the ecological floodplain evolution.

6.2 Objectives

The aim of the study is to validate the predictive simulation model developed in Chapter 5, that integrates flow dynamics, sediment transport and phosphorus uptake on different spatial-temporal scales and suitable for floodplain ecological restoration. The specific objectives of the study are:

1. Validation of the predictive dissolved phosphorus uptake model in a real riparian system.
2. Validation of the sedimentation model in a real riparian system.
3. Analysis of the current sediment and dissolved nutrient floodplain dynamics through the simulation tool.
4. Generation of possible restoration scenarios using the simulation tool.

6.3 Description of the study area

The study area is a reach in the Middle Ebro River in northeast Spain, included in the Natural Reserve "Los Galachos" (see Figure 5.2). The Ebro River, 910 *km* long, is the largest river in Spain. It has an annual discharge into the Mediterranean Sea of $1.8E07\ m^3/y$ and is regulated by the presence of 170 dams and reservoirs on the river basin. The study area forms a meander (3.70 Km^2, river width: 110 *m* with one island and an oxbow lake)

located downstream Zaragoza city (NE Spain). The discharge, averaged over the years 1927 to 2003, within this reach is 230 m^3/s and the surface elevation ranges from 175 m a.s.l. at the river channel to 185 m a.s.l. at the base of the old river terrace. The flooded area by the 19 yr return period flood (3000 m^3/s, $1927-2003$) is 3.7 Km,whereas only about 40 % of the area is flooded by a river discharge of 1000 m^3/s (0.37 yr return period, $1927-2003$), and only 10 % is flooded by a river discharge of 600 m^3/s (0.14 yr return period, $1927-2003$). The oxbow lake is connected with the river when the discharge reaches 1100 m^3/s, and this occurs 1-3 times per year.

The study site receives the effluent of a Waste Water Treatment Plant (WWTP) located 1 Km upstream from the reach, with a maximum discharge of 3 m^3/s. This WWTP treats 1200000 inhabitant-equivalents, where 1 inhabitant-equivalent is the biodegradable organic matter load equivalent to a BOD5 (i.e., biochemical oxygen demand) of 60 g/day of O_2. The plant has activated sludge biological treatment as well as the technology to actively remove nitrogen (N) and phosphorus (P), where its legal effluent N and P concentrations limit is 10 mg-N$/l$ and 1 $mg-$P$/l$, respectively.

6.4 Methods

The predictive SRP uptake model (equations 5.16 and 5.17 in Chapter 5) was validated by comparing the numerical results obtained from the complete model with the experimental field data by means of a linear regression analysis. Then, validation of the sedimentation model was performed by com-

paring the numerical results with the experimental field data obtained from Cabezas and Comín. (33) and Cabezas et al. (38).

After validation, the coupled models were applied in the study site. An analysis of the current floodplain sedimentation, SRP uptake and river nutrient contribution was carried out using the complete model. Then, based on this previous analysis, some restoration scenarios are proposed and simulated.

6.4.1 Field experimentation: experiments 21, 22 and 23

Three sampling campaigns were developed at the study site, where both the inlet and outlet river phosphorus concentration were characterized during $24h$. Two sampling stations, SS 1 and SS 2, were established at the river: SS 1 was located $750m$ downstream the beginning of the domain, and SS 2 was located $1100m$ downstream SS 1 (see figure 6.1). Samples were collected using two automatic samplers (Sigma® SD900) and acid-washed (HCl 50 %) PP bottles (1 l) located at SS 1 and SS 2 respectively. The sampling interval was established in order to sample the same mass water at SS 1 and SS 2, and was calculated by means of hydraulic simulation using the model calibrated and validated at Chapter 4. Samples were collected every $20-25min$, depending on the river discharge, during $24h$. River discharge values were given by a gauging station belonging to the Ebro River Basin Administration (www.chebro.es) located approximately 12 km upstream the study site.

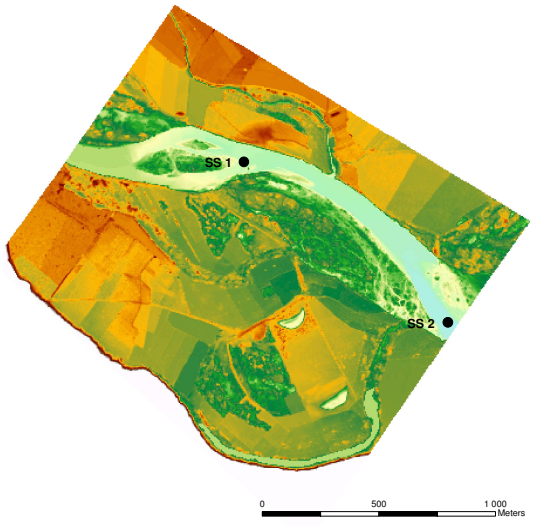

Figure 6.1: Location of the two sampling stations at the study site. Black dots represents the sampling stations: SS 1 and SS 2 respectively.

Experiment 23 showed the highest river discharge, and was developed two days after a flooding event of 1554 m^3/s peak discharge. The other experiments, 21 and 22, were developed under low and steady discharge.

Water samples were used to determine Soluble Reactive Phosphorus (SRP), total nitrogen, alkalinity, pH, conductivity, anions and cations, Total Sus-

pended Solids (TSS), Suspended Particulate Inorganic Matter (SPIM), Suspended Particulate Inorganic Matter (SPIM), Total Dissolved Solids (TDS) and suspended chlorophyll.

6.4.1.1 Water samples analysis

Water samples were transported to the chemical laboratory in dark coolboxes and filtered through 0.45 μm-pore size Whatman® GF/F glass-fiber filters. Soluble reactive phosphorus, total nitrogen and alkalinity were analyzed within 24h. The remaining samples were preserved frozen at -20^o C. SRP was analyzed using Murphy and Riley (139) molybdenum blue colorimetric method. Total nitrogen was analyzed by catalytic combustion at high temperature (850^{o}C) using a Multi-N/C 3100 analyzer (AnalytikKjena®). Anions and cations were analyzed using ionic chromatograph (Metrhom 861 Advanced compact IC) fitted with 100μl sampling loop. Alkalinity of unfiltered water was estimated within 4 h of collection by a potentiometric automatic titration with H_2SO_4 0.04 N APHA (5). TSS were determined by filtering samples through pre-combusted (450^o C, 2 h) 0.45 μm-pore size Whatman® GF/F glass-fiber filters, followed by drying filters at 60^o C until a constant weight was reached. This filter was used then to determine the SPIM by means of combustion (450^o C, 4 h) followed by weighing. SPOM was calculated as the difference between TSS and SPIM. TDS were determined by weighing the residue after evaporating 25 ml of filtered water at 100^{o}C APHA (5). Suspended Chlorophyll (a, b, c and d) was determined by filtering samples through 0.45 μm-pore size Whatman® GF/F glass-fiber

filters, followed by 23 h of filter digestion in acetone 90 %, adsorption measurements in a spectrophotometer equiped with a 1 *cm* quartz cuvette and using the mixed phytoplankton extinction coefficients (Jeffrey and Humphrey (97)).

6.4.2 Simulation model

The complete two-dimensional simulation model, calibrated and validated at Chapter 4, with the sediment transport and dissolved phosphorus uptake equations added at Chapter 5 was used in the present study.

6.4.2.1 Quantification of the groundwater contribution

Infiltration and exfiltration phenomena can be detected by means of the natural chemical tracers. Natural chemical tracers are water compounds naturally present in rivers, biologically and chemically stable and do not undergo microbial transformations and gaseous losses. There are several natural tracers, such as stable isotopes, chloride, bromide, etc., where the most widely used are chloride and bromide. Both of them are present in the Ebro river waters, both surface and groundwater, but with very different concentrations, where chloride is much higher than bromide (mean molar ratio at surface water Cl:Br 3151 : 1). To identify and quantify the groundwater contribution using a tracer present in both surface and groundwater, the natural tracer concentration should be higher in groundwater than in surface water, where a significant impact in surface water concentration is possible. At the Ebro river, chloride groundwater concentration is higher than the surface chloride water concentration (Cabezas et al. (35)), while bromide concentration is very

similar in both surface and groundwater (unpublished data). Therefore, the chloride will be used as a natural tracer of the exfiltration phenomenon, and it can be calculated as follows:

$$\frac{Q_{in}}{Q_{out}} = \frac{Cl_{in}}{Cl_{out}} \Rightarrow Q_{out} = Q_{in} + Q_{gw} \tag{6.1}$$

where Q_{in} and Q_{out} are the water discharge at the inlet and the outlet of the domain respectively, Cl_{in} and Cl_{out} are the chloride concentration at the inlet and the outlet of the domain respectively, and Q_{gw} is the groundwater discharge contribution.

The accuracy of the groundwater contribution estimation is evaluated using the field data from the three sampling campaigns.

6.4.3 Validation of the SRP uptake model

The predictive SRP uptake model was validated by comparing the numerical results obtained from the complete model with the experimental field data by means of a linear regression analysis. This validation, assumes as validated the dissolved solute transport model in previous Chapter 5.

6.4.4 Validation of the sedimentation model

Validation was performed using the field data obtained by Cabezas and Comín. (33) and Cabezas et al. (38), where the sedimentation was registered in two zones within the study area (see figure 6.2). The registered flooding events whose peak discharge and duration were very different were simulated. The

first study, Cabezas and Comín. (33), was carried out under a single flooding event of 8 days duration and 754.44 m^3/s of peak discharge. The second study, Cabezas et al. (38), reached 2250 m^3/s and lasted 27 days. Inlet TSS was also registered during both flooding events, and therefore used as a boundary condition.

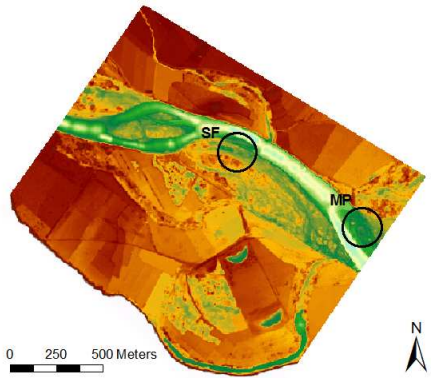

Figure 6.2: Location of the two sediment sampling areas at the study site. Circles point the sediment sampling areas SF and MP, established by Cabezas and Comín. (33) and Cabezas et al. (38) during two flooding events.

6.4.5 Model application

6.4.5.1 Evaluation of the floodplain SRP uptake potential

The total SRP uptake potential of the floodplain is analyzed by means of the nutrient addition technique. However, since the floodplain is included into a natural reserve, it was not possible to add any nutrient to the river. Hence, we use the 2D numerical model to simulate the nutrient addition experiments.

The addition of four SRP concentration: 1, 3, 5 and 10 ppm, was simulated using an steady state injection of 3 m^3/s. The river discharge was also under steady state and the evaluated discharges were: 500, 1000, 1500 and 2000 m^3/s.

The SRP addition impact into the different floodplain habitats was also analyzed. For that purpose, the floodplain was characterized according to the different habitats of interest, which are: Crops/pasture, adjacent riparian forest, remote riparian forest, paleochannel, oxbow lake, constructed wetlands distant riparian forest and main river channel (see Figure 6.3).

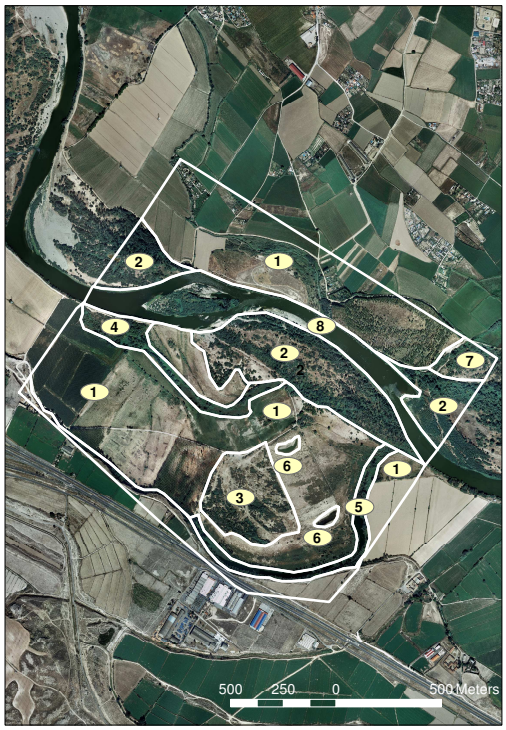

Figure 6.3: Habitats within the study site
1: Crops/pasture. 2: Adjacent riparian forest. 3: Remote riparian forest. 4: Paleochannel. 5: Oxbow lake. 6: Constructed wetlands. 7: Distant riparian forest. 8: Main river channel.

Table 6.1: Simulated hydrographs. The return period is calculated within the period: 1927-2010.

Hydrograph	Peak discharge (m^3/s)	T ($yr.$)	Duration (days)
2	800	0.21	7
3	900	0.25	8
4	1169	0.40	6
5	2250	3.4	27

6.4.5.2 Analysis of the current floodplain nutrient and sediment dynamics

The same four flooding events as simulated in Chapter 4 were simulated. All of them occurred in 2007, and peak discharges were: 800, 900, 1100 and 2250 m^3/s, at the gauging station of Zaragoza city (see Table 6.1). Discharge data were provided by the Ebro River Basin Administration (www.chebro.es). The highest flooding event was greatly regulated by the Ebro River Basin Administration, and its duration reached 27 days. Due to this regulation, three peak discharges could be differentiated within the same flooding event: 1378, 1880 and 2250 m^3/s. To reduce the simulation time consuming, this flooding event was considered as a three different flooding events, whose peak discharges reached: 1378, 1880 and 2250 m^3/s.

Water samples from the four flooding events were collected twice a day in each flooding event. Samples were collected using acid-washed (HCl 50 %) PP bottles (1.5 l) located at SS 1 and SS 2 respectively (see figure 6.1). Water samples were used to determine the inlet discharge of: SRP, total nitrogen, alkalinity, pH, conductivity, anions and cations, TSS, SPIM, SPIM and TDS.

To analyze the simulation results we used the floodplain habitats classification shown in Fig. 6.3.

6.4.5.3 Restoration scenarios

Finally, the complete validated model was used to propose two possible restoration scenarios. To analyze the simulation results we used the floodplain habitats classification showed in Fig. 6.3.

6.5 Soluble Reactive Phosphorus retention at the Ebro River

6.5.1 Physical, chemical, and biological river parameters

Experiments were developed within the winter season, in November-January on 2009-2010. During our observations, the discharge ranged between $119 - 577\ m^3/s$ (Table 6.2).

Ambient SRP concentrations were steady among and within the experiments, ranging from 0.031 to 0.050 mg/l^{-1}. The mean molar DIN:SRP ratio was 206 : 1. Ambient nutrient concentrations were higher than in most of the reported studies on streams (Hoellein et al. (79), Melody et al. (125), Newbold et al. (142), Mulholland (134), (120), House et al. (84)), but nutrient concentration in fresh water ecosystems with high agricultural activity can be orders of magnitude higher than in undisturbed systems Melody et al. (125). Moreover, the WWTP located $1Km$ upstream the domain could be increasing the nutrient river concentrations.

Table 6.2: Physical and chemical characteristics of the Ebro river (arithmetic mean $\pm$ SD). Concentration variables are expressed in mg/l except SRP and Chl-a, which are in $\mu g/l$.

Variable	Experiment 21	Experiment 22	Experiment 23
Discharge(m^3/s)	127.3 ± 1.38	323.85 ± 8.78	546.66 ± 4.0
Temp.(^oC)	18.23 ± 3.61	18.33 ± 3.93	11.95 ± 4.95
pH	7.94 ± 0.01	8.12 ± 0.01	8.35 ± 0.05
Ca^+	141.44 ± 1.01	140.00 ± 3.14	116.33 ± 3.82
Cl^-	117.65 ± 6.13	96.36 ± 3.60	65.30 ± 0.54
DIN	2.23 ± 0.08	2.36 ± 0.13	2.52 ± 0.01
TDN	3.79 ± 0.02	3.20 ± 0.05	3.09 ± 0.02
SRP	0.04 ± 0.01	0.04 ± 0.01	0.04 ± 0.00
Chl-a	3.59 ± 0.31	3.24 ± 0.41	2.38 ± 0.18
SPOM	7.20 ± 0.60	7.14 ± 0.74	5.14 ± 0.32
TSS	36.68 ± 0.87	32.98 ± 11.70	30.14 ± 0.80
TDS	733.60 ± 9.66	648.00 ± 7.03	477.14 ± 4.77

6.5.2 Soluble Reactive Phosphorus retention

The general net mass balance of SRP, using the three experiments, did not significantly differ from 0 ($4.0E-5 \pm 3.2E-5$ mg/l; $sig.0.20$), indicating neither SRP uptake or release. However, Experiment 15 showed a significant positive difference on the SRP mass balance ($1.4E-3 \pm 1.7E-3$ mg/l; $p(t-test) \leq 0.001$), while mass balances of Experiments 21 and 22 were non significant (see Table 6.3). It suggests the presence of an SRP uptake process at Experiment 23.

Experiment 23 showed a significant release of Cl^-, Br^- and TDS (see Table 6.3) into the flowing water. This could be due to a groundwater contribution. In naturals fresh water systems, such as the Ebro river, it is possible

Table 6.3: Mass balances as the difference between outflow and inflow concentration of the chemical water parameters at each experiment. Presented are $\Delta variable \pm SD$ where negative values indicates consume, and positive values indicates release. Values significantly different from 0 at $p \leq 0.05$ resultant from the *t*-test are printed in bold.

Variable	Experiment 21	Experiment 22	Experiment 23
pH	-5.6E-03±5.0E-02	**-0.03±0.04**	-4.30E-03±2.10E-02
Ca^{+}	-3.2±5.8	**-15.4±14.9**	3.1±10.2
Cl^{-}	8.4±23.8;	3.2±8.1	**0.9±2.2**
Br^{-}	5.6E-03±2.0E-02	2.0E-03±9.0E-03	**-3.4E-03±5.0E-03**
DIN	0.2±0.5	0.1±0.4	-0.2±0.5
TDN	-1.6E-03±5.2E-02	-5.1E-02±0.13	**-0.1±0.1**
SRP	1.5E-03±4.1E-03	-0.6±3.1	**-1.3±1.7**
SPOM	**-0.7±1.4**	-0.9±3.3	0.05±1.6
TSS	**-0.9±2.0**	**-2.3±3.8**	**-4.8±6.9**
TDS	1.8±38.6	7.6±22.1	**-7.6±12.8**

to find the infiltration or the groundwater exfiltration phenomenons, where surface water discharge and its chemical composition can be altered. Infiltration reduces the water discharge at the same rate as TDS, anions and cations, while TSS concentration increases. On the contrary, groundwater contribution decreases TSS and TDS concentrations, and increases water discharge, and concentration of the anions and cations whose groundwater concentration are higher than at the surface water. Experiment 23 also showed a significant decrease of suspended and dissolved solids concentration (see Table 6.3), suggesting groundwater exfiltration as well.

In experiments 21 and 22 we observed no change in chloride and bromide concentrations, but decreased and increased TSS, respectively. Variation of TSS concentration could be due to sedimentation/erosion processes. During Experiment 21, the water discharge decreased from 136.2 to 118.5 m^3/s. This probably induced sediment deposition, and therefore, a reduction in TSS concentration. During experiment 22 flow increased instead, from 270 to 390 m^3/s, which probably generated an erosive process that increased the water column TSS content.

6.5.3 Quantification of the groundwater contribution

Equation 6.1 was applied in Experiment 23 to quantify the groundwater contribution. The estimated groundwater contribution is 3.4 ± 0.3 m^3/s, and it increases the surface water discharge from 552.5 ± 3.0 to 555.8 ± 3.1 m^3/s. A new mass balance calculation correcting the outlet discharge is required,

although the proportional contribution of groundwater is limited (0.6%).

The 2D simulation model was applied to simulate Experiment 23, where the groundwater contribution was included. To evaluate the accuracy of equation 6.1, measured and calculated Cl^- concentrations were compared with linear regression (Table 6.5). Results showed an excellent agreement between measured and predicted data ($r^2 \geq 0.9$; $p \leq 0.05$), whose slope and intercept did not significantly differ from the unit and zero, respectively ($p \geq 0.5$).

New SRP mass balance was calculated in Experiment 23 using the groundwater contribution to correct the outlet river discharge. The new mass balance was still significant ($1E-03$; $p \leq 0.01\ mg/l$), suggesting the occurrence of SRP retention. The fact that we only observed significant SRP retention in experiment 23 is probably related to the size of the flood, inundating a long area with a corresponding reduction in flow velocity. Indeed, this is paralleled by a reduction in TSS.

6.6 Validation of the complete two-dimensional model

6.6.1 Validation of the sedimentation model

Validation of the sedimentation model is performed by comparing the simulated and the experimental sedimentation rate registered by Cabezas and Comín. (33) and Cabezas et al. (38) (see Table 6.4 and figures 6.2 and 6.4). Table 6.4 shows the comparison between simulated and observed sedimentation rate. Simulation results did not significantly differ from the experimental

data ($p \leq 0.09$). A general linear regression between calculated and registered sedimentation rate shows the significant agreement between both sedimentation rates ($r^2 = 0.97$; $p \leq 0.05$ and $slope = 1.20$; $p \leq 0.05$), where the slope was not significantly different from unity. Nevertheless, the intercept did significantly differ from zero, suggesting a systematic sediment deposition underestimation.

Table 6.4: Comparison of measured and calculated deposited sediment at sampling points (g/m^2). Presented are the $p-value$ from the $t-student$ comparison. SF and MP are the sampling locations.

Study	Location	Measured	Calculated	$p-value$	Calculated average
Cabezas and Comín. (33)	SF	2330.7±771.1	2970.1±545	0.05	1282
Cabezas and Comín. (33)	MP	5987.4±776.7	4607.1±670.5	0.05	5853
Cabezas et al. (38)	SF	4180±270	3202±599	0.09	3878
Cabezas et al. (38)	MP	13490±2190	11527±2750	0.05	8995

Simulated sedimentation corresponds sufficiently with observed quantities, justifying further use of the model

6.6.2 SRP uptake model validation

Validation of the reactive SRP uptake model is performed by comparing the numerical results obtained from the complete model with the experimental

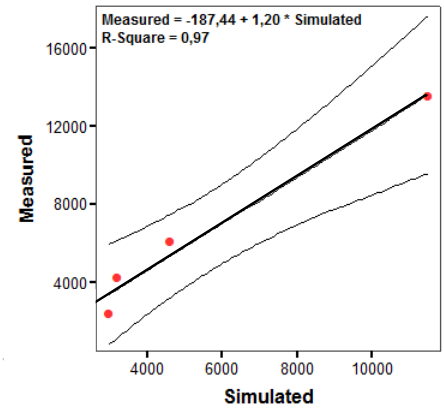

Figure 6.4: Validation of the sedimentation model.
Linear regression between measured and simulated sediment deposition. Presented are the regression equation and the confidence interval. Measured sediment deposition data are from Cabezas and Comín. (33) and Cabezas et al. (38).

field data. The 2D unsteady complete simulation model was applied to simulate the three field assessments in the (see Figures 6.5 and 6.5). Results were compared with the observed data using the linear regression.

Model predictions where quite acceptable, where the linear regressions between measured and calculated SRP concentration of the three experiments were significant ($r^2 \geq 0.6$; $p \leq 0.05$) (see Table 6.5). Model predictions did not introduce a systematic error, slopes and intercepts did not significantly differ from unity and zero respectively ($p \geq 0.1$).

6. MODELING NUTRIENT AND SEDIMENT DYNAMICS IN THE MIDDLE EBRO RIVER FLOODPLAIN (NE SPAIN): A VALIDATION

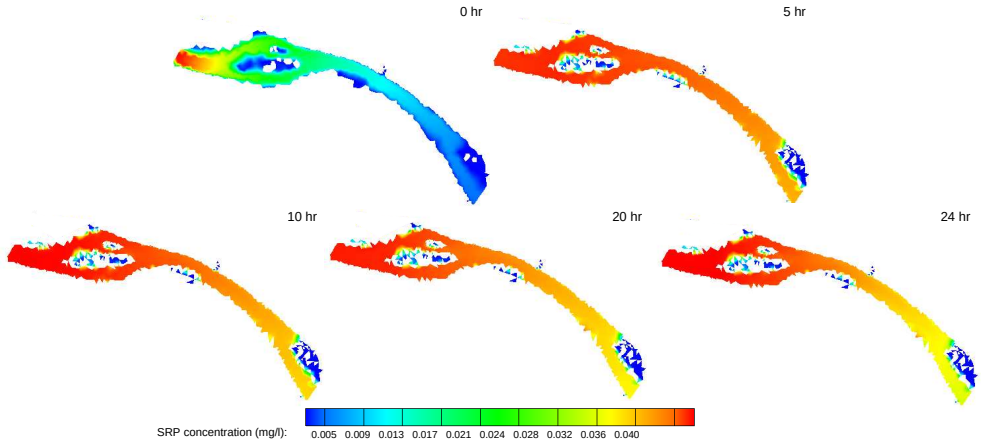

Figure 6.5: SRP model validation.
Simulated SRP time evolution at the study site during experiment 21.

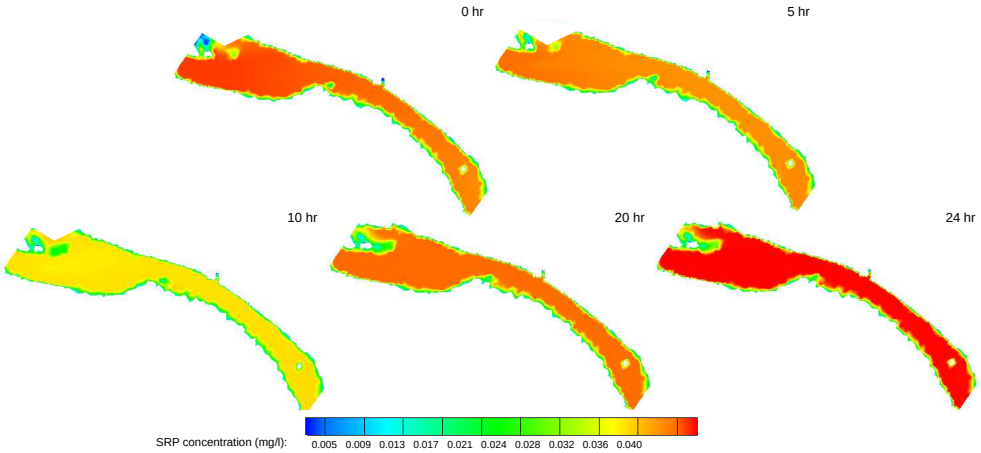

Figure 6.6: SRP simulation.
Simulated SRP at the study site during the course of experiment 23.

Table 6.5: Comparison of measured and calculated phosphorus concentrations in successive experiments using the new reactive formulation. Last row presents the comparison between measured and calculated Chloride concentration in experiment 23.

Experiment	df	R^2	Slope±SE	p_{slope}	Intercept±SE	$p_{intercept}$
21	21	0.62	0.84±0.14	0.2	0.01±0.01	0.2
22	21	0.67	1.05±0.15	1	0.00±0.01	1.0
23	20	0.76	0.85±0.10	0.1	0.01±0.00	0.1
23-Cl^-	20	0.94	1.01±0.05	0.5	-0.94±3.55	0.5

The 2D unsteady reactive simulation model was capable of reproducing the ambient SRP evolution at the middle Ebro river under three different river discharges. Hence, although river flow was unsteady, the model predicted the SRP uptake with an acceptable accuracy.

6.7 Model application

The complete 2D unsteady simulation model includes passive and reactive dissolved solute transport, suspended solute transport, erosive potential and suspended solute sedimentation. Using the complete model it is possible to reproduce erosion/sedimentation processes, hydrological connectivity, nutrient floodplain river contribution and SRP uptake, which are the main processes involved in floodplain evolution. Therefore, the model can interpret and predict the floodplain development, and it can be a useful tool in ecological restoration.

Proposing ecological restoration possibilities needs a previous analysis of

the current situation. Hence, in this section, the current floodplain SRP uptake potential, erosion and sedimentation processes, hydrological connectivity and the river nutrient contribution to the floodplain are analyzed. Then, once the ecological restoration need is known, two restoration scenarios are proposed.

6.7.1 Analysis of the current scenario

Four flooding events registered during 2007, with peak discharges of 800, 900, 1169, and 2250 m^3/s were simulated. All of them are ordinary flooding events with a recurrence period of: 0.21, 0.25, 0.4 and 3.4 *yr* respectively. The discharge of SPOM, SPIM, SRP and TDS registered at each flooding event was included into the simulations.

Floodplain hydrological connectivity was studied in Chapter 4. Results established that the study area is almost completely flooded with a return period of 3.4 yr, while 40 % of the study area is flooded every year. Almost all the yearly flooded area corresponds to the first 200 *m* from the river bank to the floodplain, where the right riverside is flooded more intensively than the left riverside.

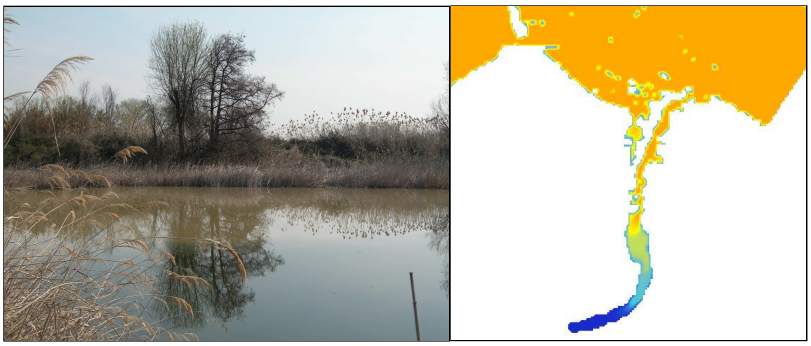

Figure 6.7: Comparison of simulated and observed River-oxbow lake connection.
Left: Oxbow lake at 1164 m^3/s river discharge. Right: Simulated oxbow-lake at 1164 m^3/s river discharge.

The oxbow lake is superficially connected to the river at least once a year, when river discharge raises to 1100 m^3/s (see Fig. 6.7). The yearly river-oxbow lake surface connection is restricted to on point located 2.2 Km downstream from the inlet domain, whose connexion discharge is 0.05 m^3/s. However, when the river discharge reaches 1100 m^3/s, the whole oxbow lake gets superficially connected to the river.

6.7.1.1 Sedimentation

Simulation results show a spatially variable sediment deposition across the flood plain, where the greater sediment quantities were deposited on those surfaces within close proximity to the river channel. Most of the sediment (80 %) is deposited in the 30 % of the yearly flooded area, which corresponds to the first 200 m from the river to the floodplain (see Figs. 6.8, 6.9, 6.10 and

6.11). In contrast, only 6 % of the sediment is deposited in the remote parts of the floodplain, which are flooded with 3.4 *yr* of recurrence period (1927-2010). The estimated yearly sediment floodplain deposition is 0.08 Kg/m^2yr, corresponding to 252.7E03 *Kg* over the full floodplain area.

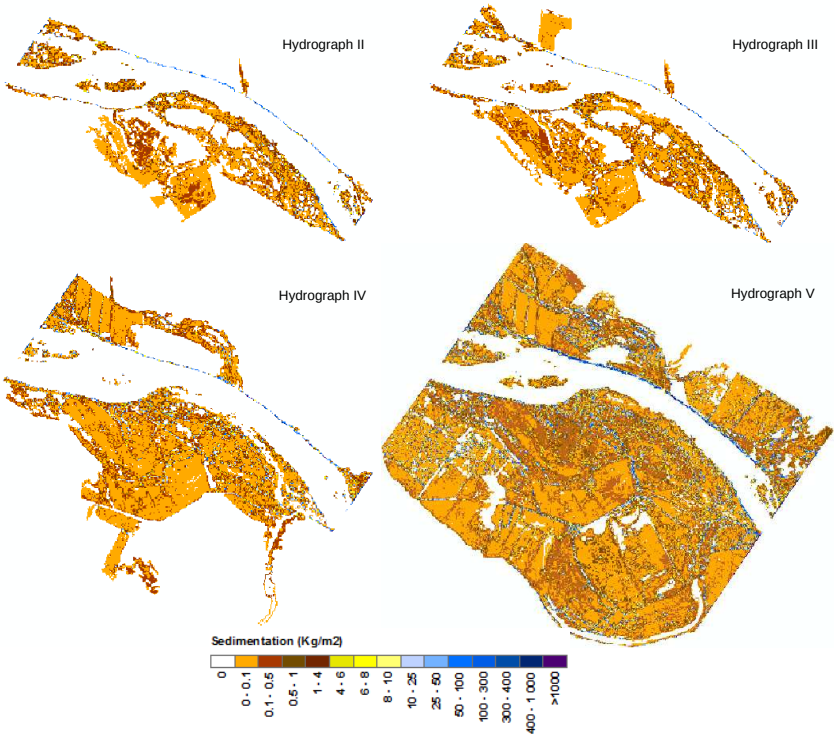

Figure 6.8: Current sediment deposition.
Simulated sedimentation at hydrographs II, III, IV and V.

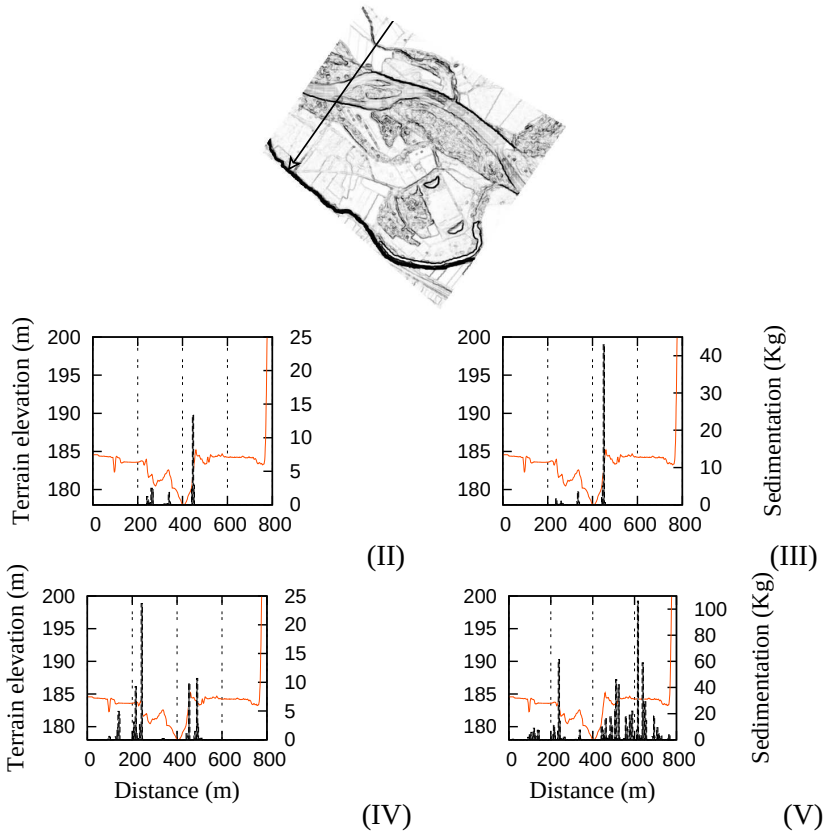

Figure 6.9: Current sediment deposition profile 1.
Upper: profile location. The arrow indicates the profile direction. Lower: sedimentation profile at hydrographs II, III, IV and V. Brown line indicates the profile of the terrain. Bars represent the sediment accumulation.

The estimated floodplain deposition ranged from 0.02 to 0.27 Kg/m^2 (see Table 6.6). This amounted 48.8E03-818.3E03 Kg of sediment and constitutes 0.08-0.15 % of the total sediment input during the considered flooding events. In general, the accumulation of sediment decreased with distance from the river channel. The adjacent riparian forest receives in almost all cases more than 50 % of the deposited sediment whilst remote riparian forest areas, located in the old floodplain terrace, receive less than 10 % of the total rate (see Table 6.6 and Table 11.1). Agricultural fields and pasture areas also show an important sedimentation rate, and it increases with river discharge. When the corridor is almost completely flooded (2250 m^3/s), sedimentation rate at crops and pasture is higher than at the riparian forest (see Table 11.1 in Appendix 11).

Table 6.6: Total simulated sediment and SRP retention during each hydrograph.

	Sediment deposition			SRP uptake		
Hydrograph	%	Tn	Kg/m^2	%	Tn	Kg/m^2
II	0.12	57.3	0.02	77	182.7	0.06
III	0.08	48.4	0.02	70	179.4	0.06
IV	0.15	147.0	0.05	56	280.6	0.07
V	0.02	818.3	0.27	83	765.5	0.25

The estimated yearly sedimentation rate within the oxbow lake is 0.7 Tn/yr (see Table 11.1 in Appendix 11). This sedimentation occurs mainly within the channel that connects the river and the oxbow lake, which is located in the downstream part of the oxbow lake. However, higher flooding events increases the connection between the river and the oxbow lake, and therefore, its sedimentation area.

6.7.1.2 Ambient SRP uptake

Simulation results estimated a high SRP uptake capacity, which ranged from 0.06 to 0.25 Kg/m^2 (see Table 6.6 and Figure 6.12). This amounts 179.4-76.5 Tn, and corresponds to 56-83 % of the total SRP input. Similar to sediment deposition, SRP uptake decreased with distance from the river channel. The main SRP uptake is realised within the main river channel and its adjacent areas whilst remote zones such as remote riparian forest, the oxbow lake and the constructed wetlands hardly received SRP load (see Table 11.2).

A significant linear regression ($r^2 = 0.59$; $p \leq 0.05$) between total sediment deposition and SRP load in the selected habitats (see Figure 6.3) after the four flooding events show the positive correlation between both processes. Hence, the main sedimentation areas correspond to the highest SRP concentration zones, and therefore, to the highest SRP uptake zones. However, the river channel is an exception, and its sedimentation and SRP concentration show a different pattern. Since main channel register the highest flow velocity, its sediment deposition is restricted to the river bank areas. Hence, if the main channel habitat is removed from the linear regression, the correlation coefficient improves from $r^2 = 0.59$ to $r^2 = 0.94$ ($p \geq 0.95$), and confirms the correlation between sedimentation and SRP uptake.

6.7.1.3 Floodplain SRP buffering potential

We have analyzed the ambient SRP uptake of the floodplain, which was carried out under low river discharge and without an additional SRP input. However, to evaluate the SRP uptake potential it is necessary to add SRP to the

system and study its buffer capability. Nutrient addition experiments may increase the natural nutrient uptake potential of the system Mulholland et al. (133), but it also gives a valuable information about the maximum buffer capability of the system. However, since the study site is included into a natural reserve, the nutrient addition experiments to the river are not possible. Therefore, four SRP addition experiments under four river discharges have been simulated (see Table 6.7).

Table 6.7: Simulated floodplain SRP buffering potential.

The SRP uptake potential (%) is calculated as consumed SRP divided by SRP input concentration and multiplied by 100. Last column represents the correlation coefficient of the linear regression between the results obtained in each discharge under the five SRP added concentration. Last row is the correlation coefficient of the linear regression between the results obtained from each SRP added concentration under the four river discharges. Bold values represents the non-significant linear regressions at $p \leq 0.05$.

Discharge (m^3/s)	0 *ppm*	1 *ppm*	3 *ppm*	5 *ppm*	10 *ppm*	r^2
500	94.2	95.3	95.9	85.2	84.7	0.78
1000	93.5	92.7	92.0	90.4	88.1	0.99
1500	94.6	95.1	95.0	92.6	91.1	0.91
2000	94.6	96.3	94.2	93.7	92.7	**0.59**
r^2	**-0.02**	**-0.22**	**-0.46**	0.96	0.96	

According to the results, the floodplain show a high SRP uptake potential that ranges from 85.2 to 96.3 % and variates negatively with the SRP concentration (see Table 6.7). The significant linear regressions between the results obtained from each river discharge suggest that the SRP uptake is more affected by the inlet SRP concentration than by the river discharge (see Table

6.7), and the effect is negative. Hence, for the same river discharge, the SRP uptake would be higher under a low SRP load. The highest SRP concentrations, 5 and 10 ppm, appears to be affected by the river discharge as well, where the highest discharge value correspond to the highest SRP uptake (see Table 6.7).

The SRP addition resulted in an increasing of the SRP concentration in almost all habitats, where the highest increasing is produced in the river and its adjacent riparian forest (see Figs. 11.7 11.8, 11.9 and 11.10 in appendix 11). The river SRP concentration increases from 4.0E-03±5.0E-02 to 0.042±0.032 ppm under 500 m^3/s river discharge, whilst the adjacent riparian forest changes from 0.009±0.005 to 0.02±0.009 ppm under 2000 m^3/s river discharge (see Fig. 6.13). Hence, the most affected habitats are the river and its adjacent riparian forest.

The paleochannel appears to be an important SRP uptake habitat as well, where during the 1500 m^3/s river discharge and 10 ppm of SRP simulation, the SRP concentration changes from 0.001±0.003 to 0.006±0.005 ppm (see Figs. 11.7 11.8, 11.9 and 11.10 in appendix 11). On the contrary, the distant and remote riparian forests showed the lowest SRP increasing (see Figs. 11.7 11.8, 11.9 and 11.10 in appendix 11). Both habitats are the furthest from the main river channel, and the low SRP increasing suggest that most of the SRP content have previously been uptaken before the water floods both areas.

The main concentration increasing as a result of the SRP addition is produced in the river and its adjacent riparian forest (see Figs. 11.7 11.8, 11.9

and 11.10 in appendix 11). The highest SRP increasing reaches 0.032 *ppm*, occurred under 500 m^3/s river discharge and 10 *ppm* of added SRP and leads to 0.042$\pm$0.032 *ppm* of SRP into the river.

In general, the estimated buffering potential of the floodplain is higher than that reported in other studies based on nutrient addition experiments. James and Larson (94) analyzed the SRP retention efficiency of the Minnesota River using the WWTP effluent as an external nutrient source and obtained a retention efficiency that ranged from 3-96.8 %. Macrae et al. (115) added SRP into an agricultural stream and found a maxium SRP retention of 23 %. Triska et al. (200) observed an SRP uptake of 2-68 % from an SRP addition experiment in Costa Rica. Jarvie et al. (95) reported an SRP retention of 72 % in a lowland eutrophic river in UK, downstream of a sewage effluent. Hence, our model is probably overestimating the floodplain buffering SRP potential. The simulation model does not include phosphorus nor sediment resuspension, and since it is an important source of phosphorus (Reddy et al. (167)), the net SRP uptake could be overestimated.

Despite the high SPR buffering potential of the floodplain, most of the SRP is just deposited into the sediment as particulate phosphorus. The phosphorus accumulation into the soil could induce eutrophication processes once it is resuspended. Furthermore, accumulating this phosphorus mainly in two habitats, the adjacent riparian forest and the paleochannel, could produce an excess of this nutrient in both habitats and a lack of phosphorus in the rest of habitats. Hence, despite the floodplain has a high SRP uptake potential, the

current morphology induces the phosphorus accumulation in a few habitats, whilst the rest hardly receive phosphorus.

6.7.1.4 River dissolved nutrient contribution to the floodplain

Dissolved nutrient was included in the simulation model as TDS, where no reaction term has been included. Therefore, floodplain dissolved nutrient contribution shows exactly the same pattern as hydrological connectivity. The calculated yearly dissolved nutrient contribution to the adjacent riparian forest is 37% of the total river load, while the remote riparian forest appears not to receive any dissolved nutrient load during an ordinary flooding event.

The calculated yearly TDS river contribution to the oxbow lake is 0.7% of the total river load, but it increases to 3% when the river discharge reaches 2250 m^3/s. In the same way, TDS contribution to remote riparian forest increases from 0 to 6% of the total load when the river discharege reaches 2000 m^3/s (see Figure 6.14).

6.7.2 Current scenario

Estimated sedimentation rate is comparable to the measured sediment deposition in other studies such as Thoms et al. (196), who reported a sedimentation rate of 0.001-1.94 Kg/m^2 in the floodplain River-Murray. Steiger and Gurnell (190), observed a similar sedimentation rate in the riparian zones of the Garonne river that ranged from 0.1 to 160.1 Kg/m^2. Kronvan et al. (110) registered an average sedimentation rate of 3.6, 6.6, 3.2 and 3.0 Kg/m^2 for the rivers Gjern, Brede, Odense and Skjern, respectively. In the same way,

the spatially variable estimated distribution of the deposited sediment is consistent with those reported in other studies (Asselman and Middelkoop (6); Walling et al. (211); Middelkoop and Asselman (129); Thoms et al. (196); Steiger and Gurnell (190)). Flood-plain topography, surface roughness, often related to vegetation, and the magnitude and frequency of flooding event are thought to have an important influence on flood-plain sedimentation processes (Thoms et al. (196)).

Estimated SRP uptake is slightly higher than those reported in other studies such as Bowes and House (23), who observed a dissolved inorganic phosphorus retention of 58-74 % during an overbank flooding, or Van der Lee et al. (202), whose phosphorus adsortion observations ranged from 50 to 70 % of the total phosphorus. Gelbrecht et al. (61) reported an SRP net retention during an overbank flooding that ranged from 64 to 76 %. The higher SRP uptake estimation is probably due to an overestimation of the net SRP uptake. Since the model does not consider the SRP remobilisation, net SRP uptake could be overestimated.

The strong correlation between SRP uptake and sediment deposition is consistent with the results of Olde Venterink et al. (149), who found that phosphorus uptake is largely influenced by the process of sedimentation. In the same way, Bowes and House (23) found that the highest dissolved inorganic phosphorus retention occurred under the highest suspended solids concentration. Alexander et al. (4) found that nutrient retention increased with decreasing water depth streams and rivers of the Mississippi catchment.

Hence, combining water flow, sediment, SRP and dissolved nutrient simulation results, there is a correlation between hydrological connectivity and the redistribution of organic matter, inorganic matter and SRP. Frequently, flooded habitats also receive more sediment and phosphorus, and the flooding gradient also creates a gradient or mosaic in nutrient availability, as in Gonzalez et al. (64). We found a lateral sediment and dissolved nutrient gradient from the river to the floodplain (see Figs 6.9, 6.10 and 6.11 for sedimentation lateral gradient). These results are consistent with those obtained by Kronvan et al. (110), who stated that approximately half of the total calculated amount of retained sediment was deposited in the near-channel area. In the same way, Brunet et al. (28) found that deposition of sediment was 50 times higher in the riparian zone (1050 m away from the river channel) than further away from the river channel.

On the other hand, sedimentation process dominates the floodplain hydromorphological activity. Hydromorphological activity is based on the cut-avulsion phenomena governed by the flow regime, where an equilibrium between both processes produces and maintains the floodplain ecosystem (Bayley (14)). However, simulation results show an important sedimentation rate within the first 200 m of the floodplain, while results from Chapter 4 showed a lack of important erosive processes. Therefore, according to the simulation results, there is non equilibrium between the erosion and sedimentation processes, and the floodplain is under accretion phenomenon that produces a gradual loss in river-floodplain connectivity.

6. MODELING NUTRIENT AND SEDIMENT DYNAMICS IN THE MIDDLE EBRO RIVER FLOODPLAIN (NE SPAIN): A VALIDATION

The exchange of nutrients, organic matter, inorganic sediments, organisms, seeds and vegetative material as well as the flow velocities and scouring during floods shapes the structure and functionality of a floodplain (Junk et al. (102), Asselman and Middelkoop (6), Heiler et al. (73), Ward et al. (214)). In that sense, the lateral gradient, restricted to the first 200 m of the floodplain, and the lack of important erosive processes would lead to an static ecosystem with most of the habitats disconnected from the river, an old riparian forest and a limited renovation rate (Junk et al. (102), Hughes and S.B. (88)). Hence, the floodplain will loose part of its functions such as flooding events mitigation, water quality improvement, wild live refuge and recreational use (Junk et al. (102), Ward et al. (215), K. and Standford (103)).

Under these results, it can be stated that the floodplain needs to restore the shifting mosaic of habitats to guarantee its functionality. It can be restored through an increase of the hydromorphological dynamism and the hydrological connectivity between the river and the floodplain (Richards and Hughes. (170)). The hydromorphological restoration should guarantee a complete and recurrent floodplain flooding that produces and maintain the dynamic equilibrium between the new and old creation habitats. Hence, a different topographic scenario that facilitate morphological changes and provide a different the nutrient and sediment distribution is needed. The most efficient scenarios in erosive potential increasing from Chapter 4, but including sedimentation, dissolved nutrient transport and SRP uptake were simulated.

6.8 Scenario 1: 2 *m* dike height

A terrain modification based on a height reduction of the river defenses may increase flooding, its erosive potential and sediment spreading to the remote riparian forest areas. As stated Chapter 4, the restoration scenario number 4, based on the 2 *m* height reduction of the river defense and abandoned crop, increases the flow erosive capability in some of the riparian forest zones. At the same time, this restoration strategy increases the flooded area, where the remote riparian forest is flooded under lower river discharge, $\cong$1200 m^3/s. Hence, it might also change the sedimentation pattern and reduce part of the vertical accretion.

Table 6.8: Total simulated sediment and SRP retention for each experimental hydrograph under Scenario 1.

	Sediment deposition			SRP uptake		
Hydrograph	%	Tn	Kg/m^2	%	Tn	Kg/m^2
II	0.06	29.1	0.01	68	161.6	0.05
III	0.09	52.0	0.02	79	202.3	0.07
IV	0.1	98.7	0.03	88	443.0	0.12
V	0.03	910.0	0.3	89	820.9	0.27

6.8.1 Sedimentation

Simulation results show a decrease of the total sediment deposition except for hydrograph V, whose sedimentation increases compared to the reference situation (see Table 11.3 and Figs. 6.15, 6.16, and 6.17 6.18). Sediment distribution among the habitats is different from the reference situation except for Hydrograph V, whose main sedimentation area remains the same although

its sedimentation rate is considerably higher (see Table 11.3). Hydrograph II changes its main deposition area from the adjacent riparian forest to the main channel, whilst at hydrographs III and IV, this changes from the crops/pasture to the adjacent riparian forest (see Table 11.3).

Although total sedimentation decreases compared to the initial situation, the difference in spatial sedimentation pattern increases sediment deposition in some of the habitats. Hydrograph II increases its sedimentation in the crops/pasture and paleochannel, whilst hydrograph III increases sedimentation in the adjacent riparian forest and the paleochannel. In the same way, hydrograph IV increases the sediment deposition at the adjacent riparian forest, remote riparian forest and oxbow lake, whilst hydrograph V increases its sedimentation in all habitats except for the main channel and its adjacent riparian forest (see Table 11.3).

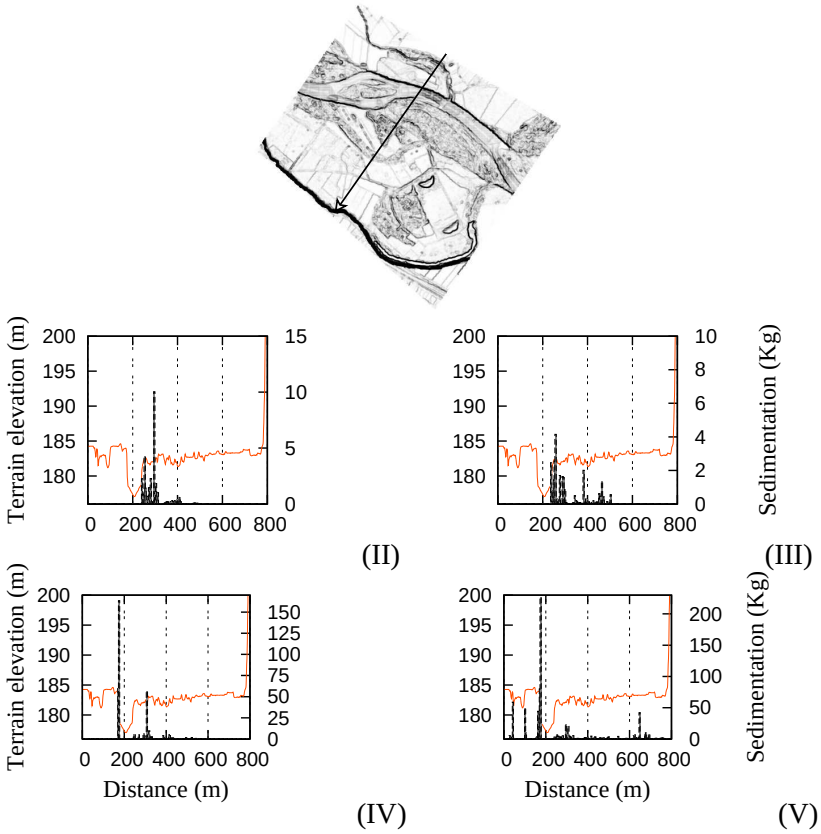

Figure 6.10: Current sediment deposition profile 2.
Upper: profile location. The arrow indicates the profile direction. Lower: sedimentation profile at hydrographs II, III, IV and V. Brown line indicates the profile of the terrain. Bars represent the sediment accumulation.

6. MODELING NUTRIENT AND SEDIMENT DYNAMICS IN THE MIDDLE EBRO RIVER FLOODPLAIN (NE SPAIN): A VALIDATION

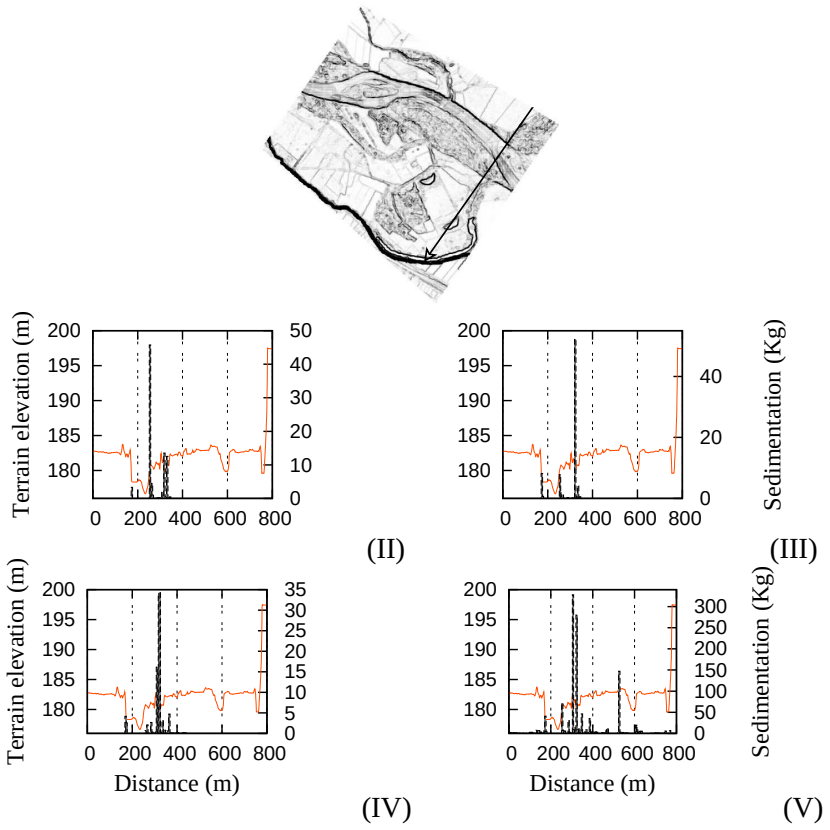

Figure 6.11: Current sediment deposition profile 3.
Upper: profile location. The arrow indicates the profile direction. Lower sedimentation profile at hydrographs II, III, IV and V. Brown line indicates the profile of the terrain. Bars represent the sediment accumulation.

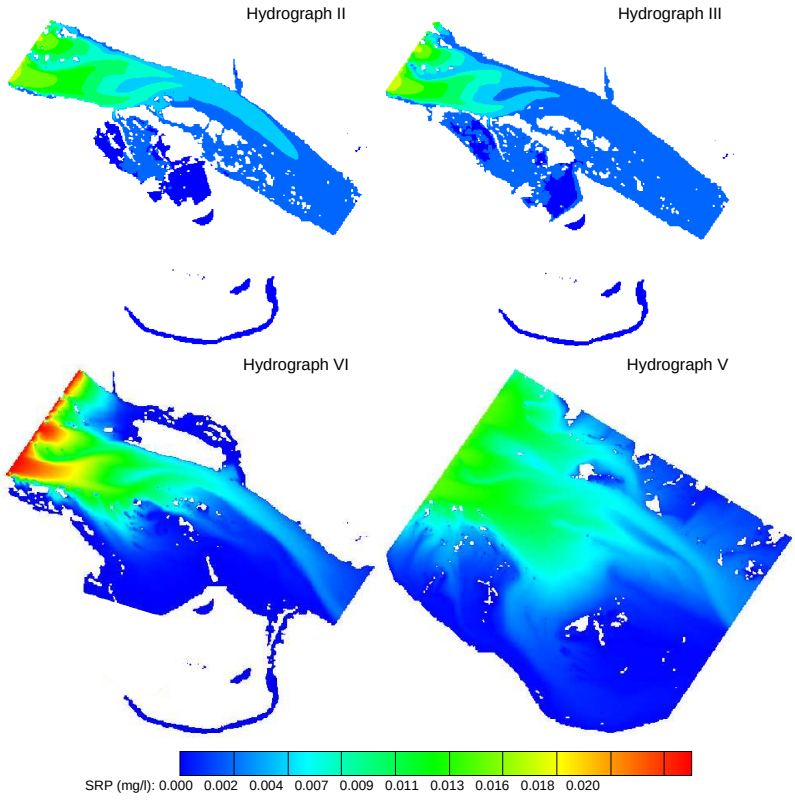

Figure 6.12: Simulated SRP concentration
SRP concentration during the peaks discharges of hydrographs II, III, IV and V.

6. MODELING NUTRIENT AND SEDIMENT DYNAMICS IN THE MIDDLE EBRO RIVER FLOODPLAIN (NE SPAIN): A VALIDATION

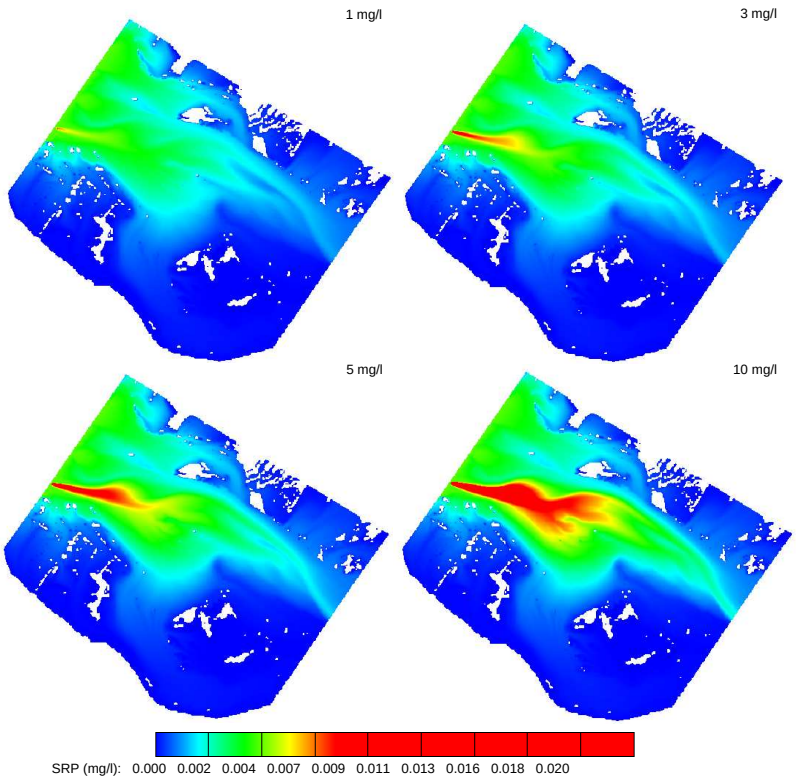

Figure 6.13: Floodplain SRP uptake potential: 2000 m^3/s
Simulated SRP concentration under 1, 3, 5 and 10 mg/l SRP added concentration

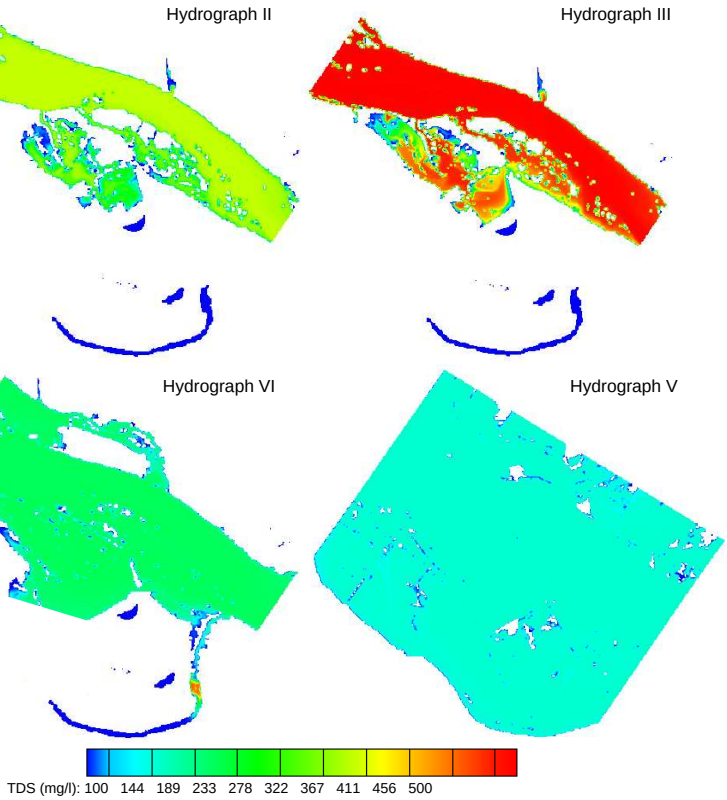

Figure 6.14: Simulated TDS concentration
TDS concentration during the peak discharges of hydrographs II, III, IV and V.

6. MODELING NUTRIENT AND SEDIMENT DYNAMICS IN THE MIDDLE EBRO RIVER FLOODPLAIN (NE SPAIN): A VALIDATION

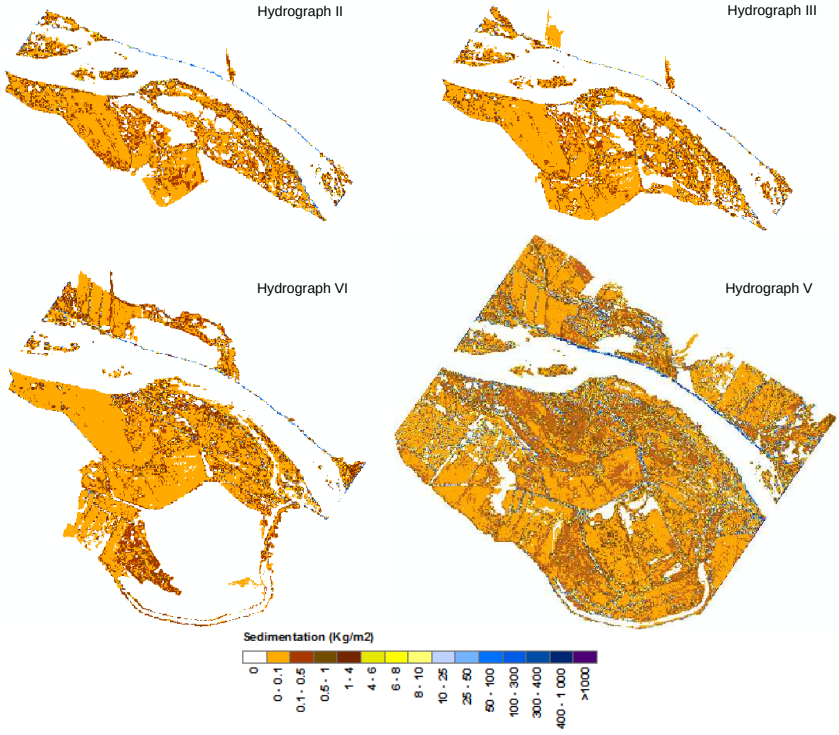

Figure 6.15: Sediment deposition under scenario 1
Simulated sediment deposited during the hydrographs II, III, IV and V.

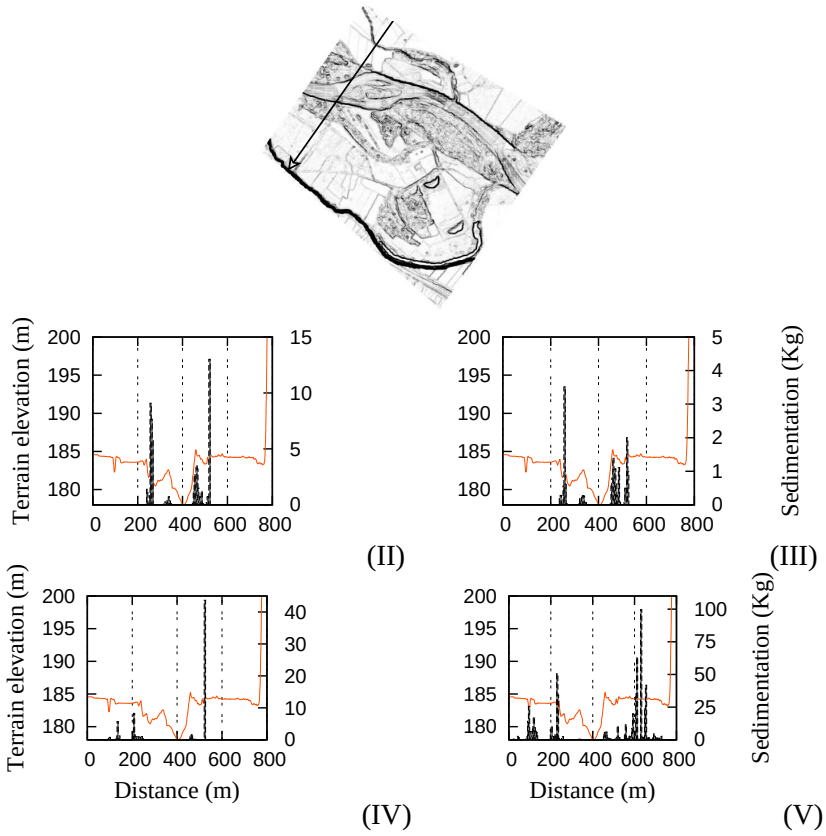

Figure 6.16: Sediment deposition profile 1 at scenario 1.
Upper: profile location. The arrow indicates the profile direction. Lower: sedimentation profile at hydrographs II, III, IV and V. Brown line indicates the profile of the terrain. Bars represent the sediment accumulation.

This strategy appears to be efficient to redistribute the sediment deposition and to decrease the vertical accretion. The terrain modification alters the water course and facilitates flooding and sediment deposition in the remote riparian forest. At the same time, it induces an increased flow velocity for hydrographs II, III and IV, which would lead to a reduced overall sediment deposition. Nevertheless, the sediment deposition increasing under hydrograph V could increase the vertical accretion phenomenon, although since this sedimentation increasing is restricted to the crops/pasture habitat (see Table 11.3 and Figure 6.15), there is no vertical accretion increasing into the natural floodplain system. Indeed, sedimentation rate into the natural floodplain system changes from 338.1 to 174.1 Tn/m^2 compared to the reference situation.

6.8.2 SRP uptake

The water course alteration increases the total SRP uptake for hydrographs III, IV and V, but not for hydrograph II, whose total SRP uptake is reduced respect to the reference situation (see Table 11.3 and Figure 6.19).

SRP concentration is higher compared to the reference situation in almost all habitats except for the main channel, whose SRP concentration decreases for hydrographs II, III and V (see Table 11.4). Since the terrain modification deviates part of the flow into the floodplain, the floodplain SRP input increases, and therefore, the main channel SRP concentration decreases. Moreover, providing that the floodplain suspended solids concentration is

also higher, the water column SRP uptake process increases, and probably, there is an increase of the floodplain SRP sediment attached contribution.

Hydrograph V show an SRP concentration increasing into the remote riparian forest, whose SRP concentration increases one magnitude of order (see 11.3 in appendix 11). Hence, simulation results shows this restoration strategy as an efficient scenario that increases the floodplain SRP uptake potential, the sediment and SRP contribution into the remote riparian forest, reduces the floodplain vertical accretion, and restore in some way the floodplain morphological dynamism (see Chapter 4).

6.9 Scenario 2: hydrological connectivity increase

A terrain modification based on hydrological connectivity restoration of the paleochannel, the secondary channel and the oxbow lake was the most efficient solution for the hydromorphological restoration purpose (see Chapter 4). This restoration strategy does not increase the flooded area but it does increase the flow erosive potential, inducing significant morphological changes (see Chapter 4).

6.9.1 Sedimentation

Simulation results show a sediment deposition increase during hydrographs II, III and IV, and a sedimentation decrease during hydrograph V (see Table 6.9). Sediment deposition increases mainly into the adjacent riparian forest and the paleochannel, whilst agricultural crops and pasture reduces its sedimentation in almost all the cases (see Table 11.5).

Table 6.9: Total simulated sediment and SRP retention during each hydrograph at Scenario 2.

	Sediment deposition			SRP uptake		
Hydrograph	%	Tn	Kg/m^2	%	Tn	Kg/m^2
II	0.26	128	0.03	88.7	210.9	0.06
III	0.23	133.3	0.04	80.4	206.1	0.05
IV	0.15	153.3	0.04	88.5	446.3	0.12
V	0.01	517.1	0.14	74.2	684.6	0.18

Sedimentation pattern reduces its heterogeneity compared to the reference situation. Main sedimentation areas are those whose topography has been modified, whilst the rest of the floodplain hardly receives sediment (see Table 11.5 and Figs. 6.21, 6.22 and 6.23). Left riverside show the lowest sediment deposition, and only under hydrograph V sedimentation is extended to the whole floodplain (see Figs. 6.21, and 6.22 6.23).

Sediment deposition increasing under low river discharges (T$\leq$1 yr) could increase the floodplain vertical accretion. Nevertheless, main sedimentation areas are also those with the highest probability of being eroded under a flooding event of 2000 or 3000 m^3/s peak discharge (see Chapter 4). Hence, although sediment could be accumulated in these areas every 0.1-0.4 yr, the sediment accumulation could also be eroded every 3.4 yr and decelerate the floodplain vertical accretion.

Hydrological connectivity between the river and the oxbow lake increases, and the threshold river discharge changes from 1100 to 800 m^3/s. Hence, it is possible to find sediment deposition within the oxbow lake under river dis-

charges close to the new threshold value, increasing from 0.0 to 0.2 Tn (see Table 11.5 in appendix 11). The higher sediment accumulation in the oxbow lake under low river discharge could increase the nutrient accumulation and probably generate eutrophication. However, the terrain modification favors the flow velocity increasing under high river discharge such as 1100, 2250 or 3000 m^3/s (see Chapter 4). The higher flow velocity reduces the oxbow lake sediment deposition and probably erodes part of the deposited sediment (see Table 11.5 in appendix 11). Hence, although certain sediment accumulation is produced under low river discharge, it could also be eroded when the river discharge rises 1100 m^3/s, reducing the possible eutrophication problems.

On the contrary, sediment contribution to the remote riparian forest decreases from 0.2 to 0.007 Tn/yr. Thus, the nutrient availability for the remote riparian forest will be even lower than in the reference situation, being possible to accelerate its aging process. Nevertheless, since this scenario induces geomorphological activity, there would be a large number of new creation habitats to compensate the system aging process.

6. MODELING NUTRIENT AND SEDIMENT DYNAMICS IN THE MIDDLE EBRO RIVER FLOODPLAIN (NE SPAIN): A VALIDATION

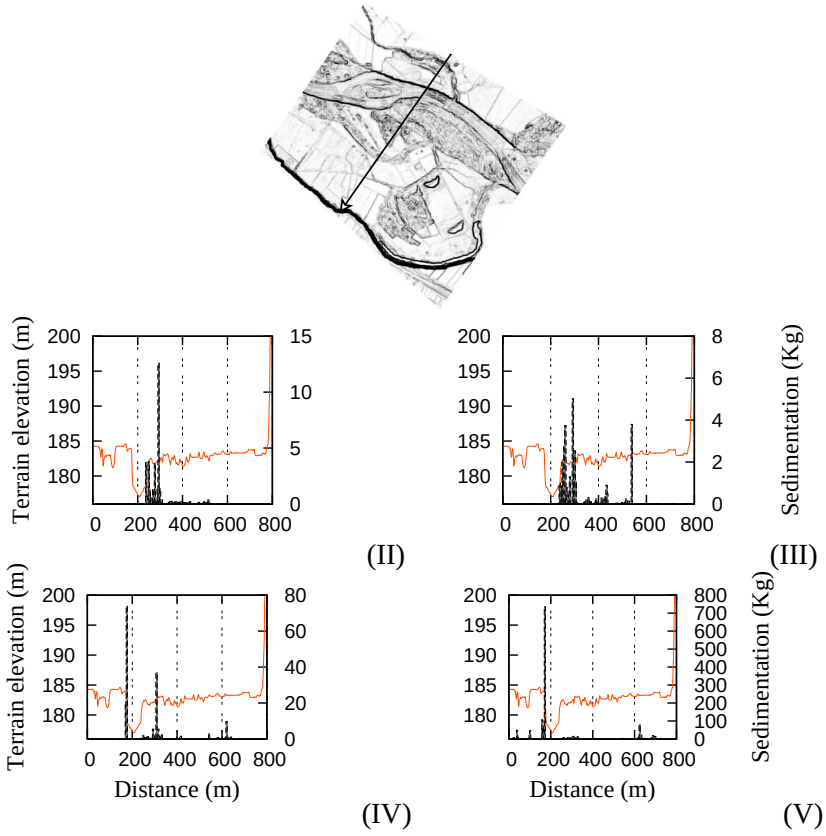

Figure 6.17: Sediment deposition profile 2 at scenario 1.
Upper: profile location. The arrow indicates the profile direction. Lower: sedimentation profile at hydrographs II, III, IV and V. Brown line represent the profile of the terrain. Bars represent the sediment accumulation.

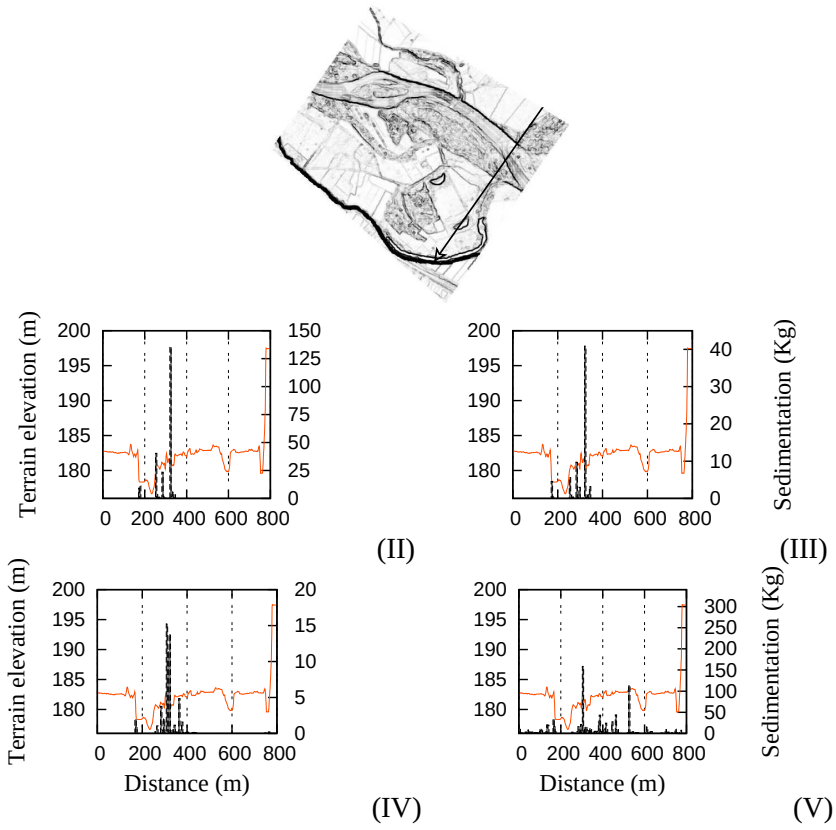

Figure 6.18: Sediment deposition profile 3 at scenario 1.
Upper: profile location. The arrow indicates the profile direction. Lower: sedimentation profile at hydrographs II, III, IV and V. Brown line represent the profile of the terrain. Bars represent the sediment accumulation.

6. MODELING NUTRIENT AND SEDIMENT DYNAMICS IN THE MIDDLE EBRO RIVER FLOODPLAIN (NE SPAIN): A VALIDATION

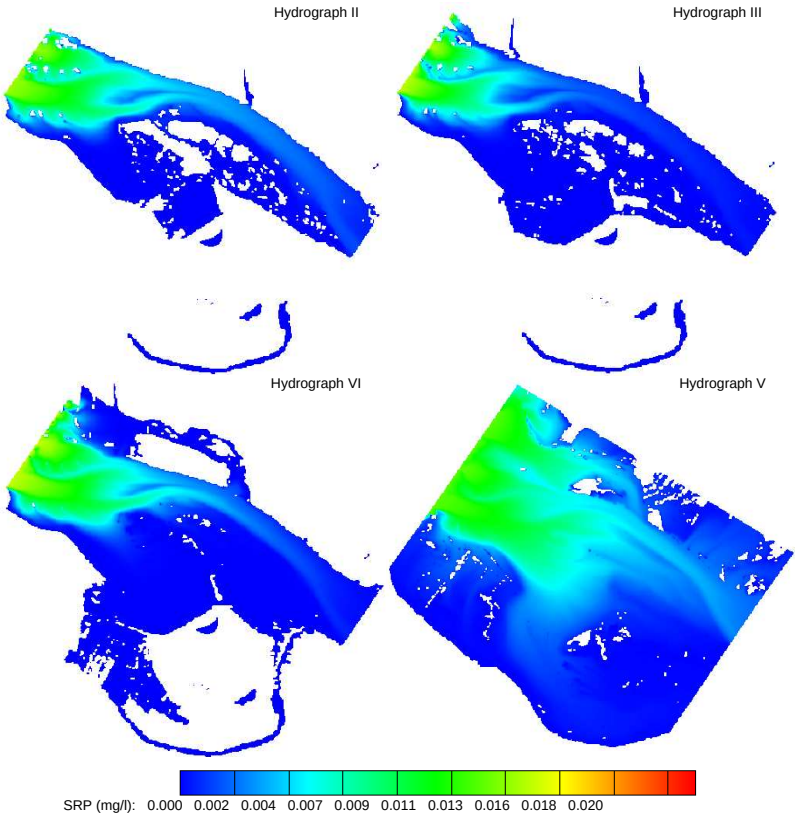

Figure 6.19: Simulated SRP concentration at scenario 3 during the peaks discharges of hydrographs II, III, IV and V.

6.9 Scenario 2: hydrological connectivity increase

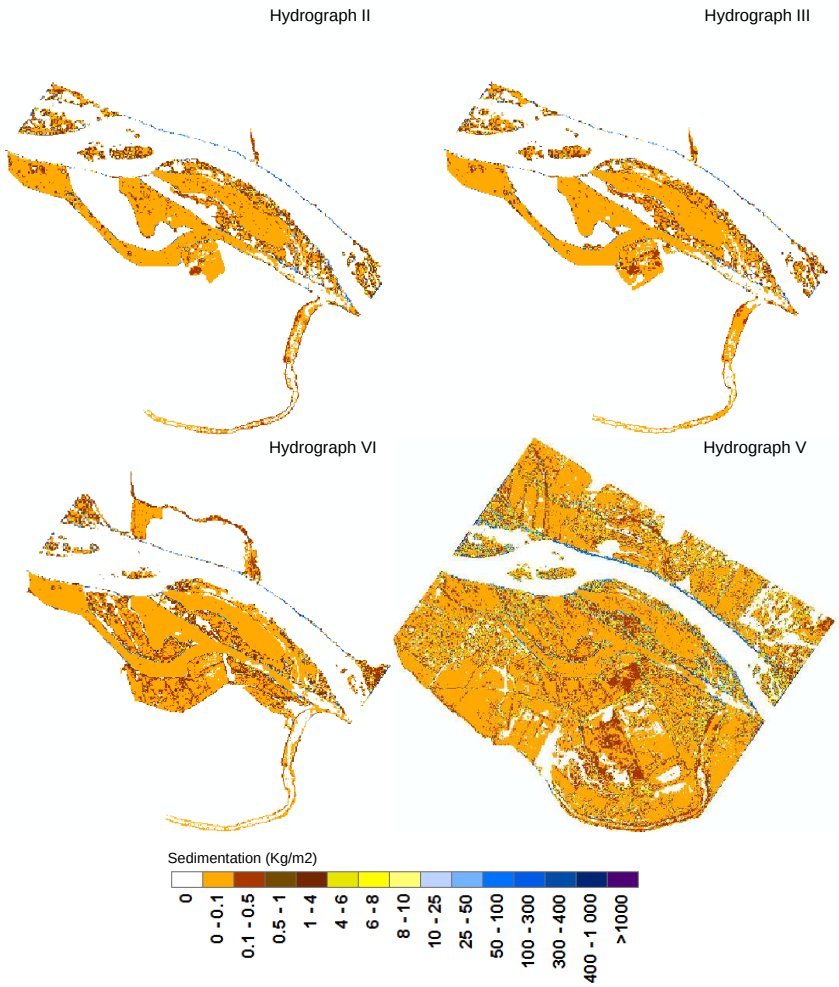

Figure 6.20: Sediment deposition at scenario 2
Simulated sediment deposition during the hydrographs II, III, IV and V.

6. MODELING NUTRIENT AND SEDIMENT DYNAMICS IN THE MIDDLE EBRO RIVER FLOODPLAIN (NE SPAIN): A VALIDATION

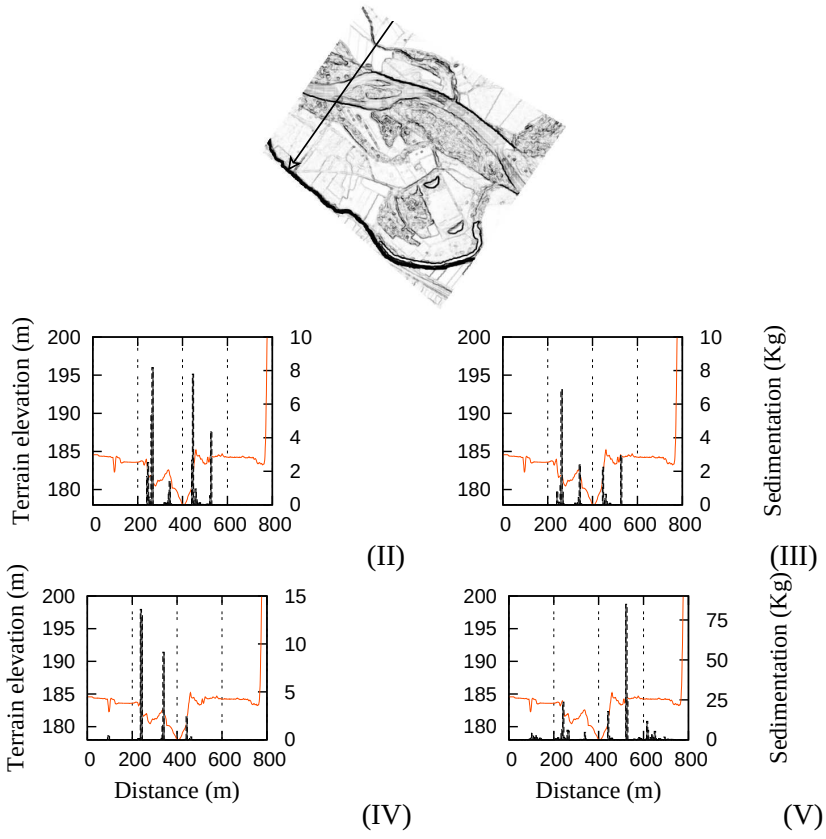

Figure 6.21: Sediment deposition profile 1 at scenario 2.
Upper: profile location. The arrow indicates the profile direction. Lower: sedimentation profile at hydrographs II, III, IV and V. Brown line indicates the profile of the terrain. Bars represent the sediment accumulation.

Under this results, we can affirm that this strategy establish certain equilibrium between erosion and sedimentation processes that provides an improved relationship between the new creation and old habitats. Erosion and sedimentation may, occur at particular locations in different events (Hughes (87)). Scenario 2 provides to certain habitats erosion or sedimentation depending on the river discharge. Low river discharge induces sedimentation at the modified habitats, and high river discharge generate erosion at the same zones.

6.9.2 SRP uptake

Estimated SRP uptake increases and ranges from 74 to 87 % of the total inlet SRP (see Table 6.9). Furthermore, this terrain modification induces an increasing of the phosphorus load whithin the modified habitats (see Table 11.6 in appendix 11), where the paleochannel, adjacent riparian forest and the oxbow lake increases its phosphorus load, whilst it decrease in the rest of the floodplain.

The paleochannel and the adjacent riparian forest appears to be the main floodplain SRP uptake habitats. Since these areas also show a high sedimentation rate, probably, most of the SRP is just deposited in the soil attached to the sediment. Hence, the rest of the habitats, such as the agricultural crops or the remote riparian forest, do not receive neither SRP or sediment, and its river nutrient contribution is reduced.

6.10 Restoration strategies

In general, scenarios 1 and 2 increase the flooded area and the potentially eroded area (see Figs. 6.24 and 6.25), improving the morphological dynamism of the floodplain respect to the current situation. However, scenario 2 generates morphological activity with a lower recurrence period, accelerating the morphological restoration. There is often a close interdependence between the channel dynamics that renew habitat and succession processes (Richards and Hughes. (170)), hence, the application of scenario 2 would generate new set of habitats whose extension increases with the river discharge. The paleochannel, oxbow lake and constructed wetlands would be eroded and partially substituted by gravel and sediment deposition. It would generate a new substrate available for the riparian vegetation recruitment and a new set of channels and gravel bars that would increase the floodplain hydrological connectivity. As a result, the floodplain structure would provide a better equilibrium between the new creation and old habitats, and therefore, biodiversity, water quality and recreation use would improve.

On the other hand, scenario 1 appears to be more efficient in sediment and SRP load retention (see Figs. 6.24 and 6.25). Thus, scenario 1 would induce the river nutrient contribution into the floodplain and probably would reduce the nutrient plant availability problems into the remote riparian forest area (see Table 11.3 in appendix 11)). Hence, if the restoration objective were to increase the floodplain nutrient plant availability, scenario 1 would be an efficient alternative. However, since the restoration objective is to increase the morphological dynamism and restore the floodplain dynamic equilibrium, scenario 2 appears to be the most efficient strategy.

6.11 Conclusions

The aim of the study was to develop a predictive simulation model that integrates flow dynamics, sediment transport and phosphorus uptake in different spatial-temporal scales and suitable for floodplain ecological restoration. In this point, SRP uptake predictions were always significant ($p \leq 0.05$) with an r^2 that ranges from 0.6 to 0.8. In the same way, sedimentation predictions were also significant ($p \leq 0.05$) and with an $r^2 = 0.99$. Hence, the validation shows the model as an excellent tool capable of predicting flooding, sedimentation and SRP uptake.

The analysis of the current floodplain sedimentation and SRP uptake shows a positive correlation between both processes, and indicates the SRP sediment adsorption as the main SRP uptake process during flooding events. The model estimates a high floodplain ambient SRP uptake, that ranged from 85.2 to 96.3 %.

The simulation estimates a sediment deposition rate that ranges from 0.02 to 0.27 Kg/m^2. Most of this sediment is deposited within the river adjacent areas, whilst the remote floodplain zones hardly receives sediment. The estimated SRP uptake ranges from 0.06 to 0.25 Kg/m^2, where most of it is uptaken within the river adjacent areas as well as within the river itself.

According to the simulation results, the remote floodplain areas shows a lack of river nutrient contribution that could affect to the nutrient plant availability. On the other hand, the concentration of sedimentation within the river

adjacent areas, might accelerate the vertical accretion phenomenon in those areas. Therefore, to guarantee the floodplain functionality, a restoration that increases the hydromorphological activity and recovers the shifting mosaic of habitats is necessary.

Restoring the natural superficial water pathways appears to be the most efficient restoration strategy to increase the floodplain morphological dynamism. It would produce a new floodplain structure with a better equilibrium between the new creation and old habitats.

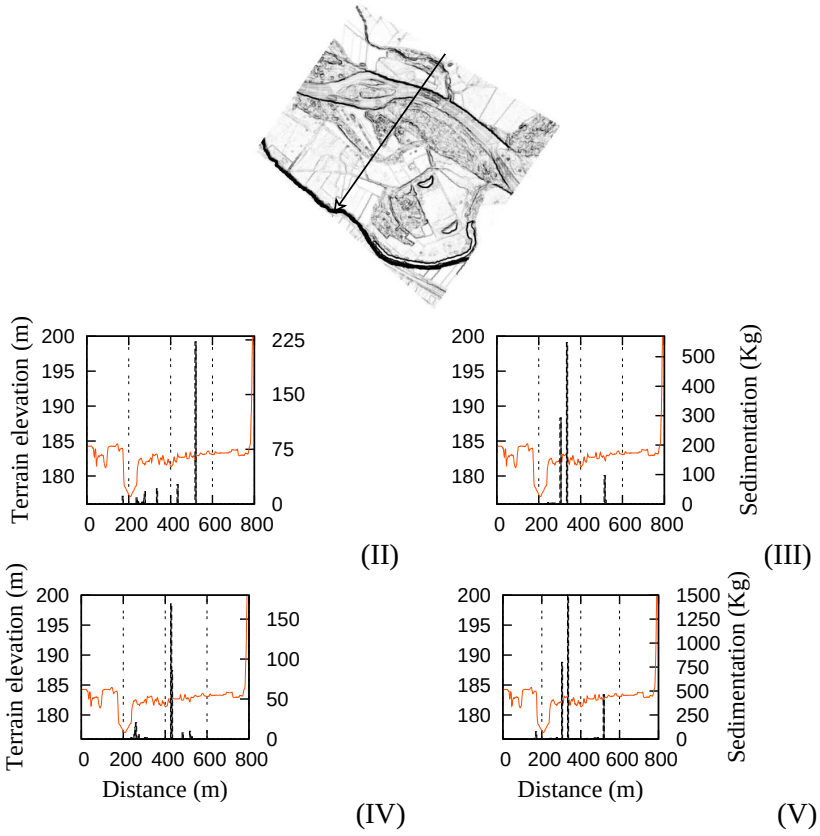

Figure 6.22: Sediment deposition profile 2 at scenario 2.
Upper: profile location. The arrow indicates the profile direction. Lower: sedimentation profile at hydrographs II, III, IV and V. Brown line indicates the profile of the terrain. Bars represent the sediment accumulation.

6. MODELING NUTRIENT AND SEDIMENT DYNAMICS IN THE MIDDLE EBRO RIVER FLOODPLAIN (NE SPAIN): A VALIDATION

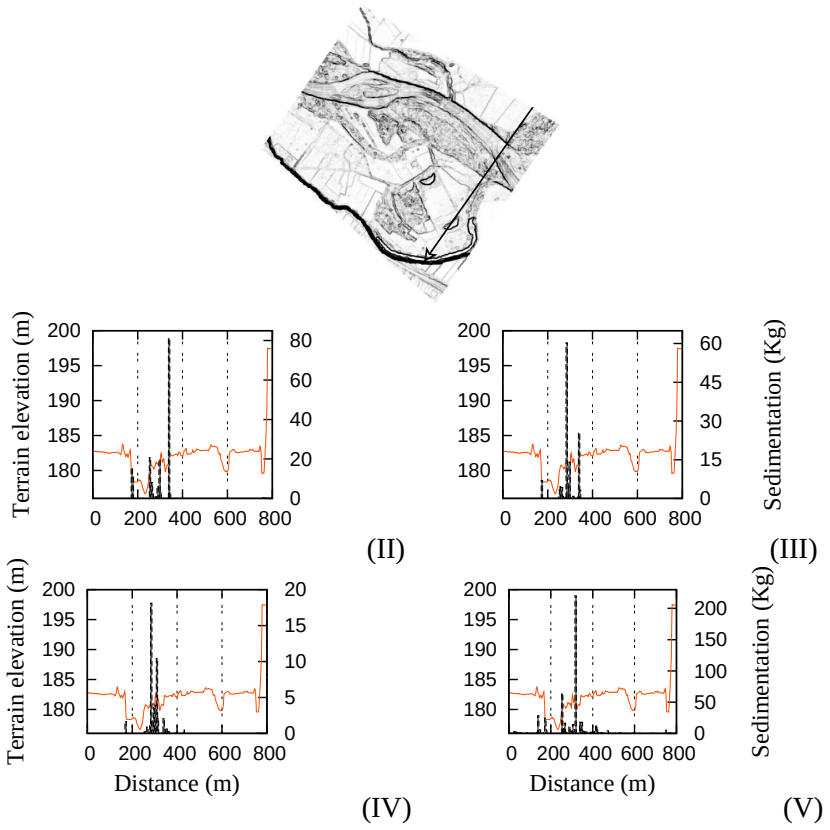

Figure 6.23: Sediment deposition profile 3 at scenario 2.
Upper: profile location. The arrow indicates the profile direction. Lower: sedimentation profile at hydrographs II, III, IV and V. Brown line indicates the profile of the terrain. Bars represent the sediment accumulation.

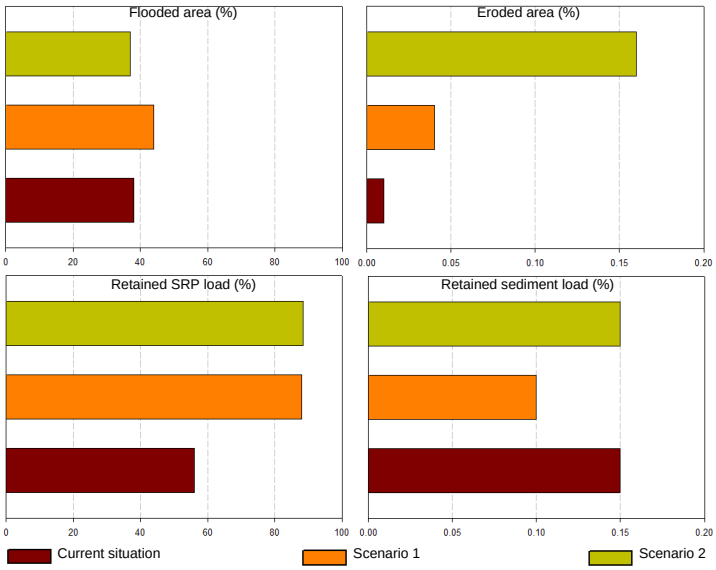

Figure 6.24: Comparison of current situation, scenario 1 and 2 at hydrograph IV.

Comparison of flooded area, eroded area, retained SRP load and retained sediment load.

6. MODELING NUTRIENT AND SEDIMENT DYNAMICS IN THE MIDDLE EBRO RIVER FLOODPLAIN (NE SPAIN): A VALIDATION

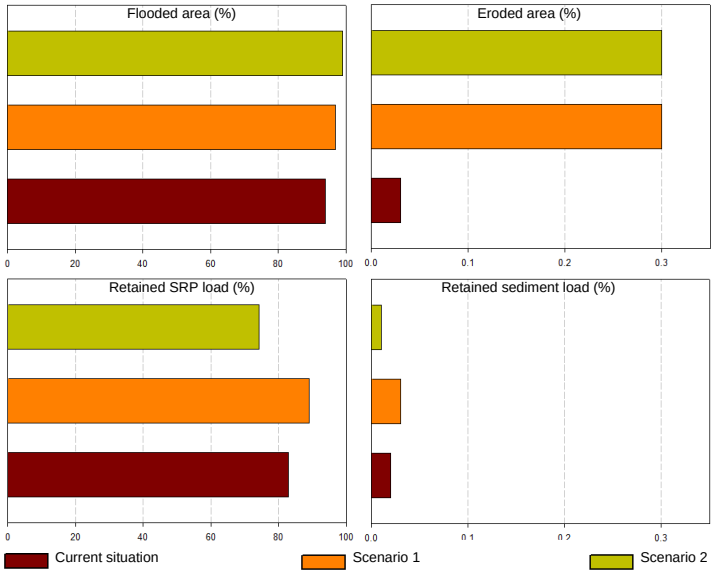

Figure 6.25: Comparison of current situation, scenario 1 and 2 at hydrograph V.

Comparison of flooded area, eroded area, retained SRP load and retained sediment load.

7

General Discussion

7.1 The hydraulic model

The hydraulic 2D model SFS2D has been validated using accurate data such as a differential GPS information for the flooding area measurements and pressure and temperature sensors for the water depth data. The accuracy of flooded area extension predictions (Fit_A) ranged from 66 to 90 %, and the average and Standart Deviation was $79 \pm 13\%$. In the same way, the accuracy of the water depht predictions ranged from 0.19 to 0.49 m with an average and Standart Deviation of 0.32 ± 0.10 m. Part of this disagreement between measured and calculated water surface level is due to the surface-groundwater interaction, which despite of it is significant at the study site (Cabezas et al. (35)), it was not considered in the hydraulic model. The disagreement is almost restricted to the initial and final stages of the flooding event (see Figures 4.15, 4.17 and 4.19), and excluding both stages from the accuracy analysis, the average of the difference between measured and predicted water level de-

creases from 0.32 ± 0.10 to 0.25 ± 0.06 *m*, making the model predictions even more accurate.

The validation results are comparable to those reported by Horritt and Bates (82), who registered a $Fit_A = 0.84\%$ using the TELEMAC-2D hydraulic model and satellite imaginary data for the validation step. The comparison should be carefully interpreted because the satellite imaginary data has not the same accuracy as our validation data, and Horritt and Bates (82) concluded that the model requires a more accurate validation. Tayefi et al. (194) reported a Fit_A that ranged from 51 to 65 % uging a 2D diffusion wave hydraulic model and surveyed wrack lines measured on the day after the flood event as a validation data.

The water depth validation results are also similar to other studies such as Connell et al. (51), who reported ± 0.26 *m* Standard Error in water depth using HYDRO-2D model and resident-supplied information and photographs for the validation purpose. Erpicum et al. (54) obtained a difference between measured and calculated water depth that ranged from 0.01 to 0.25 *m* using a 2D hydraulic model based on the shallow water equations and discretized in space with a finite volume scheme. The simulations were restricted to the steady-state peak flows considered instead of the whole flooding event simulation that we carried out. In the same way, Buttner et al. (32) simulated a steady-state flow peak discharge using the hydraulic model RMA-2 and reported a difference between measured and calculated water depth that ranged from 0.1 to 0.40 *m*. The validation data were obtained from the shoreline of

the flooded area using a differential GPS.

Comparing the validation results to other floodplain modeling studies, SFS2D accuracy does not stand out from the other 2D models. However, simulating the whole flooding event instead of steady-state flow peaks discharge such as Horritt and Bates (82), Buttner et al. (32) or Erpicum et al. (54), introduces more uncertainty in the the model predictions. Furthermore, the validation data used in the present work are more accurate than these used in most of the floodplain flooding studies (i.e. Connell et al. (51); Horritt and Bates (82); Wagner (208); Tayefi et al. (194)). A floodplain hydraulic model validation using real and accurate field spatial-temporal evolution data makes the validation step more precise.

Even though assuming that the accuracy of the SFS2D model is not significantly different from other models, since it is based on the full shallow water equations (Murillo et al. (138)), it provides a more reliable information. Most of the 2D models used in eco-hydraulics problems such as MIKE-21, RMA-2, TELEMAC-2D, TUFLOW or Tayefi et al. (194) model, are simplified models that neglect the inertial terms and assume important simplifications of the dynamics. Thus, in terms of the physical-chemical floodplain processes, the simplifications reduces significantly the meaning of the calculated velocity. For instance, simplified models based on the kinematic wave assumption are limited by the impossibility to hold backwater effects, of great importance in floodplain processes (102). Hence, the SFS2D hydraulic model provides an accurate information of the spatial and temporal evolution of the

flooded area, water depth and flow velocity, which are of paramount importance when dealing with eco-hydraulic problems.

Furthermore, the SFS2D hydraulic model couples the solute transport to the hydrodynamics, where a more realistic solute transport can be represented. The conventional methods for performing environmental simulations in rivers such as the used in HYDRO-2D, MIKE-21 or IBER hydraulic models, decouple the hydrodynamics and the transport of chemical agents. Ignoring unsteady hydrodynamical effects means that only a quasi-steady process over very slowly varying bed level can be reasonably modeled, so that, the correct simulation of solute transport in rapidly varying flows containing shocks or discontinuities remain excluded. When solving real problems one is likely to encounter all sorts of situations, with a high probability that naive methods will compromise the quality and reliability of the solution.

Nevertheless, the SFS2D model has a non negligible disadvantage compared to the simplified models, which is the computational cost. The hydraulic simulations of a real flooding events show the same computational time as the real flooding event does. Furthermore, if the simulation includes solute transport/reaction, the simulation time increases considerably. In the same way, the need of accurate information could also be considered as a disadvantage, although it is a subjective question. When the problem solution needs to be accurate, the input information has to be as accurate as the desirable solution, independently of the selected simulation model.

7.1.1 Flow erosive potential

A simple formulation to estimate the flow erosive potential based on the bottom shear stress, has been included in the SFS2D model. This formulation allows to estimate the floodplain hydromorphological activity, which is usually based on the equilibrium between concave bank erosion and the convex bank sedimentation.

The model predicts that the main erosive processes are restricted to the river adjacent areas, where the point gravel bar located in the right river margin receives most of the flow erosive potential. These results are consistent to those obtained by Gonzalez-Sanchis et al. (65), Cabezas et al. (37) and González et al. (63). Gonzalez-Sanchis et al. (65) pointed out as the only significant geomorphic change occurred after flooding event of a 2250 m^3/s peak discharge, a gravel deposition at one of the predicted eroding points. In the same way, González et al. (63) and Cabezas et al. (37) stated that the cut-avulsion phenomenon is almost restricted to the river adjacent floodplain, whilst at the rest of the floodplain prevail sedimentation process over erosion.

Although the model predictions are consistent to previous studies, there are not available real data to validate i or to compare to other formulations. Therefore, a real model validation would be desirable.

7.1.2 Solute transport

The solutes considered in the present work are dissolved as well as particulate, and their calculation need two different formulations.

7.1.2.1 Dissolved solute transport

In surface water, the dissolved solute transport can be calculated using the full shallow water equations (Murillo et al. (138)), simplifying it or using an alternative formulation such as the transient storage model (TSM) (see Chapter 5). Most of the water quality models uses a simplification of the shallow water model, decoupling the dissolved solute transport from the hydrodynamics (i.e. QUAL-W2, MIKE11, MIKE21, WASP6, IWA River Quality Model No. 1, QUASAR). Since most of these water quality models are 1D, quasi-2D or simplified 2D, its use to simulate the floodplain dissolved solute transport during a real flooding event is not correct. On the other hand, most the streams nutrient uptake studies use the transient storage model (i.e. House et al. (84), Martí and Sabater (120), Scott et al. (184), Payn et al. (158), Melody et al. (125), Michael N. Gooseff et al. (128), OConnor et al. (146)), which is implemented in common simplified 1D models such as the USGS One-dimensional Transport with Inflow and Storage (OTIS) numerical model OTIS-P.

SFS2D model uses the full shallow water model to calculate the dissolved solute transport, without decoupling it from the hydrodynamics. It has also been validated in the present by means of 20 nutrient addition experiments using the bromide as a conservative tracer. As a result, 19 out of 20 comparisons between measured and calculated data resulted in a significant linear regression ($p \geq 0.5$) whose $r^2 \geq 0.91$, and the slope and intercept did not significantly differ from the unit and zero, respectively ($p \geq 0.5$). Hence, the SFS2D model is capable of reproducing the dissolved solute transport with

an excellent accuracy.

The validation results are comparable to those obtained using the TSM, such as House et al. (84), Martí and Sabater (120), Scott et al. (184), Payn et al. (158), Melody et al. (125), Michael N. Gooseff et al. (128) or OConnor et al. (146) obtained similar or even better results. However, it is important to mention that the TSM has non predictive character, where the final tracer results are obtained by using the inverse method. The model adjust a curve that represents the tracer load in one point using the experimental tracer data in the same point. Hence, despite the model always obtain a nutrient load curve with the minimum error, it can not be applied without previous experimentation. Furthermore, this model assumes steady state flow conditions and uniform velocity and cross sectional area, being incorrect its application in a floodplain under transient flow regime such as the produced during a real flooding event.

7.1.2.2 Particulate solute transport: sedimentation model

The particulate solute transport and decay (sedimentation model) is also coupled to the model hydrodynamics using formulation to represent the sediment deposition. It has been validated using field data collected by Cabezas and Comín. (33) and Cabezas et al. (38) during 2 real flooding events (see Chapter 6). The comparison between calculated and measured sediment deposition showed a significant ($p \leq 0.05$) linear regression, whose $r^2 = 0.97$ with an slope not significantly different from the unit ($p \leq 0.05$).

7. GENERAL DISCUSSION

The sediment deposition calculation is more accurate than the one reported by Buttner et al. (32) using RMA-2 model with a decoupled sedimentation model, SED2D-WES. Buttner et al. (32) measured the floodplain sedimentation in 10 points, and the model predictions did differ one magnitude of order in 8 out the 10 points. In the same way, comparing our results to those obtained by R.W.H. Carroll et al. (176), the SFS2D model also appears to be best sediment deposition predictor. R.W.H. Carroll et al. (176) used a decoupled 1D model where the hydraulics where attended by the RIVMOD model, and the sediment transport was calculated using the WASP5 model modified by Heim and Warwick (74) and Carroll and Warwick (43). The simulated sediment deposition was drastically overestimated in 5 out of 10 sampling points.

The validation results are also more accurate than those obtained from Thonon et al. (197) using the 2D suspended sediment transport, MoCSED. Thonon et al. (197) obtained a significant linear regression between measured and calculated sediment deposition whose $r^2 = 0.52$.

Hence, looking at the validation results and its comparisons to other models, coupling the solute transport to the hydrodynamics and solving them using the full shallow water equations appears to be an accurate methodology to calculate them. However, the sedimentation model does not include erosion, and it could be an inconvenient to calculate the yearly floodplain sediment accumulation. At the beginning of the flooding event, until the peak discharge is reached, the flow has its highest erosive potential, and probably, it erodes

more than sediment deposits. Subsequently, as water discharge decreases, the sedimentation process increases, and most of the flooding event sediment is deposited. Therefore, if this first erosive process is not considered, the yearly sediment accumulation might be overestimated.

7.1.3 Nutrient uptake

Nutrient uptake in streams or rivers is usually calculated by means of a simplified 1D model such as the OTIS model (i.e.Martí and Sabater (120)), the kinetic approach (e.g. Bowie et al. (24), Mcintire and Colby (124), Mulholland et al. (133), Payn et al. (158)) and the TSM model (House et al. (84), Martí and Sabater (120), Scott et al. (184), Payn et al. (158), Melody et al. (125), Michael N. Gooseff et al. (128), OConnor et al. (146)). All of them have in common the need of a previous experimentation to estimate some coefficients. Furthermore, the 1D simplified and the TSM assumes steady-state flow conditions, uniform velocity and cross sectional area. The kinetic approach is independent to the hydraulics.

A comparison between the steady and unsteady state approaches shows that both formulations produced a satisfying simulations of SRP retention (Table 5.10), but the unsteady approach was more accurate than the steady model, mainly with variable flow. The agreement between both formulations under steady flow conditions is probably due to the uniform laboratory channel and irrigation canal characteristics, where the uniform cross sectional area assumption was also accomplished. However, full steady-state assumptions

may well be unrealistic in natural floodplain systems, where it is very difficult to find a river or stream with a uniform cross sectional area or flow velocity. The unsteady approach, in contrast, accommodates variable flow velocity, cross sectional area and discharge. Therefore, this model would reproduce the nutrient transport and uptake processes more realistically than the steady-state simplification, but it still requires a sound estimate for the uptake coefficient.

In order to avoid the need of a previous experimentation and to assume uniform velocity and cross sectional area, a new SRP uptake formulation, for both the water column and the sediment, was developed. It was formulated as a function of the main SRP uptake agents, which were determined thorough field and laboratory experimentation. Both experimentations pointed out the adsorption as the main SRP uptake process, where most of the SRP is attached to the water column suspended matter and subsequently deposited on to the bed. These results are in agreement with many studies that indicates the SRP adsorption as the main uptake process in rivers with high suspended solids concentration (i.e. M. Stone et al. (114), Reddy et al. (167), House et al. (85), Bowes and House (23), Olde Venterink et al. (149), Schulz and Herzog (182), Jarvie et al. (96), James and Larson (94), etc.). As a result, no constants or inlet-outlet SRP concentration are needed to predict the SRP river uptake, where the only required model input data are: water discharge, inlet of the suspended organic matter, suspended inorganic matter and the total dissolved solids, ambient SRP concentration, water temperature, and sediment density and porosity.

The new formulation was included in the SFS2D hydraulic model, and resulted to be an excellent predictor of the SRP uptake in both, the sediment and the water column. The comparison between measured and simulated data provided always a significant linear regression ($p \leq 0.05$) whose $r^2 \geq 0.83$ in 19 out of 20 experiments, where 3 of them were carried out using a different spatial-temporal scale. The linear regression slopes did significantly differ from the unit at $p \leq 0.05$ in 6 out of 20 experiments.

Some of the predictive nutrient uptake formulation are only applicable within the system where it was developed (Schulz et al. (183)). The same inconvenient is produced when using the simplified 1D model, the TSM or the kinetic approach, where the experimental parameters are only valid for the systems where they have been estimated. On the contrary, the model presented in this work was formulated to make possible its application in a floodplain-river system. The model validation in the river showed the model applicability in a real riparian system. The model predictions showed a great accuracy, where the linear regressions between measured and calculated SRP concentration of the three experiments were significant ($r^2 \geq 0.62$; $p \leq 0.05$) (see Table 6.5). Model predictions did not introduce a systematic error, slopes and intercepts did not significantly differ from the unit and zero respectively ($p \geq 0.1$).

The validation results are more accurate than those obtained by Schulz et al. (183), who developed an empirical predictive SRP uptake formula-

tion for small pristine streams. Schulz et al. (183) obtained a significant ($p \leq 0.05$) linear regression between measured and calculated SRP data, whose $r^2 = 0.43$ is noticeably lower than our approximation. In the same way, Rajendra Paudel et al. (163) simulated a wetland phosphorus uptake using the volumetric first order reaction rate, and the model predictions where not always of the same order of magnitude as them measured data.

The model has proved to be a good predictor of the SRP uptake in a laboratory channel, irrigation canal and in the river, but since the formulation considers the adsorption as the main SRP uptake process, it would be not applicable to systems where the biotic SRP uptake is significantly higher than the abiotic. In this way, probably the model is not applicable in small pristine streams or general river basin headwaters, where the suspended solid concentration is very low, and the SRP uptake is more biotic than abiotic (Reddy et al. (167)). Therefore, this model appears to be a good SRP uptake predictor for middle and low river basin reaches.

Furthermore, since the model does not include the SRP remobilization process, the net SRP uptake results must be carefully interpreted because they could be overestimated.

7.2 The floodplain analysis across numerical simulation

Using the complete simulation model, where the erosive potential, the solute transport and SRP uptake are included, it is possible to simulate and analyze the main process that produces and maintains the floodplain ecosystem such as hydrodynamics, sediment deposition, river nutrient contribution and SRP uptake.

The simulation results showed that the study area is almost completely flooded with a return period of 3.4 yr (from 1927-2010), while 40 % of the study area is flooded every year. Almost all the yearly flooded area corresponds to the first 200 *m* from the river bank to the floodplain, where the right riverside is flooded more intensively than the left riverside. The simulation results showed a disequilibrium between the erosion and sedimentation processes where despite the sedimentation rate estimation is within the literature values, (e.g Thoms et al. (196) and Steiger and Gurnell (190)), the flow erosive potential is almost restricted to the river channel adjacent areas. Hence, as Cabezas et al. (37) stated, sedimentation process prevails over erosion, where the vertical accretion process gains relevance.

The simulation of different topographic scenarios based on the hydromorphological activity recovering showed that the disequilibrium is probably due to the river constructed defenses, which decrease the floodplain eroding capability and the hydraulic connectivity between the river and its floodplain (Ollero (152) and González et al. (63)). These results are consistent with

those obtained by Ollero (152), Cabezas et al. (34) and Cabezas et al. (37), who stated that the study site is notably affected by embankment structures, where limited morphodynamic activity has been observed since the last half of the twentieth century.

On the other hand, the sediment deposition showed an irregular pattern, similar to those reported in other studies (e.g. Asselman and Middelkoop (6); Walling et al. (211); Middelkoop and Asselman (129); Thoms et al. (196); Steiger and Gurnell (190)). Flood-plain topography, surface roughness, often related to vegetation, and the magnitude/frequency of the flood event are thought to have an important influence on flood-plain sedimentation processes Thoms et al. (196). Furthermore, the simulation suggest the presence of a lateral sedimentation gradient that in general decreases as distance to the river increases. According to this gradient, the remote floodplain zones would receive a very low or null river sediment contribution, whilst the adjacent riparian forest would receive the highest sediment concentration.

The same lateral gradient is observed at the river dissolved nutrient contribution, and it is more significant in the case of SRP. Since the main SRP uptake process is the solute adsorption, most of the inlet floodplain SRP concentration is uptaken within the first 200 m and subsequently deposited as a particulate phosphorus. Hence, there are zones where despite they are flooded under an ordinary flooding event, the river sediment and dissolved nutrient contribution is low. In the same way, the remote floodplain zones that are only flooded from 2000 m^3/s river discharge, receive a very low or

null sediment and dissolved nutrient concentration, and it might be affecting negatively the riparian vegetation. In agreement with these results, Gonzalez et al. (64) found at a remote floodplain zone, a lower nutrient plant availability where phosphorus seems to be more limiting than nitrogen.

On the other hand, the simulation estimates a high floodplain SRP uptake capability, and highlights its SRP buffer capability under normal or altered conditions. Under normal conditions, the mean molar DIN:SRP ratio (206:1) indicates that probably the phosphorus is a floodplain limiting nutrient Under altered conditions, such as a high SRP effluent concentration, the model enhance the high floodplain buffering potential and its important role for the water quality improvement.

7.2.1 Floodplain restoration need

River regulation (by channelization or flood control) results in terrestrialisation of the vegetation, associated with a reduced rate of turnover of the fluvial landscape, reduced rates of ecosystem change, reductions of channel and ecosystem dynamics and of mosaic detail, reduced flood frequency, and loss of habitat and age diversity (Richards and Hughes. (170)). Hence, floodplain regulation lead to a degradation of the floodplain functionality that affects biodiversity, water quality improvement and recreational use (Ward and Standford (212), Ward et al. (214), K. and Standford (103)).

Results from the analysis of the floodplain current dynamics are consistent with this statement. The current erosion-sedimentation disequilibrium and the lateral gradient in the river nutrient contribution is accelerating the

floodplain vertical accretion and the general ecosystem aging process. The lack of geomorphological activity is decreasing the shifting mosaic of habitats and its change capability. The vertical accretion decrease the hydrological connectivity between the river and its floodplain, and induces the terrestrialisation of the vegetation.

Under these results, we can affirm that the floodplain needs to restore the shifting mosaic of habitats to guarantee its functionality. It can be restored through an increasing of the hydromorphological dynamism and the hydrological connectivity between the river and the floodplain Richards and Hughes. (170).

Critically, the channel dynamics lead to new surfaces for colonization and regeneration, and modeling tools are required to enhance understanding of the ecological consequences of reach-scale channel dynamics, and of their alteration by river management practices (Richards and Hughes. (170)). In this context, five restoration scenarios based on discharge management or terrain modification were generated in order to increase the floodplain geomorphological dynamism. However, only two of them, reduction of the dike height and restoration of the old superficial water pathways, demonstrated to be effective inducing morphological changes into the floodplain.

In general both scenarios increases flooded and potentially eroded areas, improving the morphological dynamism of the floodplain respect to the current situation. However, the second scenario, restoration of the old superficial

water pathways, generates the morphological activity with a lower recurrence period, inducing a higher morphodynamism into the floodplain. Fluvial disturbance processes create a mosaic of alluvial surfaces with vegetation stands in different successional stages (Richards and Hughes. (170)). Hence, the application of the second scenario would generate new set of habitats whose extension would increase with the river discharge. The combination of erosion and sedimentation at certain habitats would generate a fine sediment patches on gravel bar surfaces important for the recruitment of individuals and the renewal of plant succession, as seeds germinate and seedlings survive in the patches of finer sediment that retain moisture and provide an accessible nutrient store (Richards and Hughes. (170)). As a result, the floodplain structure would provide a better equilibrium between the new creation and old habitats, and therefore, biodiversity, water quality and recreation use would improve.

7. GENERAL DISCUSSION

8

General Conclusions

The final aim of the study was the development of a simulation tool to analyze the main process that produces and maintains floodplain ecosystem. For this purpose, a complete simulation model based on a roughness and topographic model, a main channel characterization and a finite volume hydraulic model that couples dissolved and particulate solute transport, sedimentation and SRP uptake has been calibrated and validated using experimental and field data. Then, an analysis of the current floodplain status has been carried out using the new simulation tool. Finally, some restoration scenarios based on the floodplain analysis results have been proposed and simulated.

The specific conclusions of the present work are described below.

8.1 The hydraulic model

The validation of a finite volume hydraulic model of the surface water flow has demonstrated to be an suitable tool to predict the hydrological connectivity between river and floodplain, provided that the correct topographical information is supplied. At the same time, the model supplies detailed information on the flow characteristics over the irregular floodplain. These flow characteristics determine important ecological properties such as the ecosystem morphodynamism, the particulate organic matter contribution, the dissolved oxygen content or the type of macroinvertebrate community at certain habitats.

- The full model is based on a finite volume hydraulic model of the surface water flow, a roughness model and a topographic model from the available DTM obtained by means of the LIDAR technology. The method provides information of the time and space variation of the water depth, the depth-averaged velocities and the friction bottom stress, indicative of the erosive capacity of the flow.

- The calibration of the model has been based on available field information on water level elevations for two discharges. The calibration phase has revealed the extreme sensitivity of the hydraulic model to the river bed shape. As standard LIDAR techniques do not supply information on the part of the river covered by water, this can be considered an important issue.

- The interpolation methods based on statistical treatment of the overall information, such as the GIS tools, provide incorrect results when reconstructing the river bed and are therefore unable to recover with accuracy the measured field data. In consequence, the numerical results for flood modeling based on the GIS model reconstruction alone are inaccurate. In this work, a simple procedure to recover the river bed shape from both geometric and hydraulic information has been proposed leading to a correct model performance in almost all the measured situations.

- There is a systematic discrepancy during the rising limb of the flood at one of the measured probes. The explanation for this discrepancy comes from the groundwater-surface flow interaction, at that particular location, that is not considered in our model. The field observations concerning water temperature indicate important mixing of water from different sources near that point. The extension of the model to include this flow interaction is part of the immediate future work but is out of the scope of the present work.

- The hydraulic model has also an important weakness relative to the computational cost, which can be not assumable when dealing with certain eco-hydraulics problems.

- The need of accurate input information such as the DTM, boundary conditions or the roughness map could also be considered as a disadvantage. However, it is a subjective question, an accurate problem

solution requires also an accurate terrain, roughness and boundary conditions characterization.

8.2 Nutrient uptake modeling

A predictive unsteady SRP uptake model has been developed and validated, for both the sediment and the water column. The model has been was formulated as a function of the main SRP uptake agents, which were determined through field and laboratory experimentation. As a result, no constant or inlet-outlet SRP concentrations are needed to predict the SRP river uptake, where the only required model input data are: water discharge, inlet of the suspended organic matter, suspended inorganic matter and the total dissolved solids, ambient SRP concentration, water temperature, and sediment density and porosity.

8.2.1 Laboratory and irrigation canal experimentations

- The channel bed functions as a nutrient sink, but only in the case of phosphorus. A drainage channel would reduce SRP by about 21%, or 0.7 $mg\ m^{-2}\ h^{-1}$ at concentrations ranging 1 to 46 $\mu g\ l^{-1}$, whilst there would be not significant change for nitrogen concentration. Indeed, the mean molar DIN:SRP ratio (206:1) indicates a desequilibrate system whereas probably nitrogen is saturated and the phosphorus is a limit nutrient.

- The development of natural sediment and vegetation in drainage channels could be a good strategy to reduce some of the SRP agricultural

pollutant load to the river.

- Other approaches must be considered for nitrogen reduction, such as those enhancing denitrification possibly in riparian wetlands (Verhoeven et al. (204)).

- Comparison between the steady and steady nutrient uptake approaches shows that the assumption of a uniform uptake coefficient makes the simulation tool less accurate. An alternative calculation method is necessary in order to provide the spatial and temporal variability of system uptake.

- It was not possible to apply the kinetic formulation and the Elovich equation because of the high SRP concentration.

- The experimental analysis pointed out the SRP suspended solute adsorption as the main SRP uptake process. In agreement with this, the experimental analysis show as the most influential SRP uptake parameters: pH, TSS, TDS, and SRP concentrations.

- The new SRP uptake predictive model, based on the water column and sediment SRP uptake, has been tested in two different spatial and temporal scales under different SRP concentrations. First 12 experiments were developed at the drainage canal using 60 m length, during $60 - 80$ min and increasing SRP ambient concentration $10 - 100$ times. The Last 3 experiments were carried out at the same drainage canal but using 300 m length, during $2 - 4$ hr and increasing SRP ambient

concentration $2-3$ times. Although SRP uptake showed high variability among experiments ($0.0009 \pm 0.0004\ s^{-1}$), the new model was able to predict each case with an excellent accuracy, being significant ($p \leq 0.01$) for all the linear regressions between measured and calculated SRP. However, four predictions showed a systematic discrepancy, but at every case, predicted SRP output concentration was within the same order of magnitude as empirical observations.

- The new formulation was able to predict the presence/absence of a noticeable SRP uptake process under both, unsteady and steady flow conditions. Furthermore, the model did quantify system SRP uptake with a great accuracy. Under these results, we can affirm that new formulation is an excellent tool to predict SRP uptake, at least at the irrigation canal system.

8.2.2 The river model validation

- The new predictive formulation has been validated in the river by means of three experimentations. The validation of the new SRP uptake model has proved to be an excellent simulation tool to predict the SRP uptake in a river under both, steady and unsteady flow conditions. The model predictions were always significant ($p \leq 0.05$) with an r^2 that ranges from 0.6 to 0.8.

- Since the formulation assumes that the SRP adsorption is the main SRP uptake process, the model might not be applicable to those systems where the biotic SRP uptake prevails over abiotic. Hence, it is probably

not applicable to pristine streams and headwaters in general. On the contrary, the model might predict accurately the SRP uptake of middle and low river basin reaches.

- The SRP uptake model does not considers phosphorus remobilization, so it could overestimate the predicted SRP uptake rate.

- The validation process highlighted again the need to include the groundwater-surface flow interaction, which is considered as a future work.

8.3 Sediment deposition modeling

A sediment deposition model has been coupled to the hydrodynamic model. The sediment deposition velocity is based on Jimenez and Madsen (98) formulation. The model has been validated using the field data obtained by Cabezas and Comín. (33) and Cabezas et al. (38), and it resulted to be an excellent sedimentation predictor.

- Comparison between measured and predicted sediment deposition resulted in a significant linear regression ($p \leq 0.05$) with an $r^2 = 0.97$. Hence, the validation shows the model as a suitable tool capable of predict flooding, sedimentation and SRP uptake.

- Since the sedimentation model does not include the erosion process, the yearly sedimentation rate could be overestimated. Hence, it would be desirable to include the erosive process in the hydraulic model.

8.4 The floodplain analysis through numerical simulation

The application of the complete simulation model has proved to be very useful in the floodplain eco-hydraulic analysis. It is capable of reproducing and predict with an excellent accuracy the main process that create and maintain the floodplain ecosystems. The final application highlighted the need of a floodplain restoration and conservation efforts.

- There is a disequilibrium between erosion and sedimentation where sedimentation prevails noticeably over erosion. As a consequence, the floodplain has lost most of its hydromorphological activity, being it restricted to the main river channel adjacent areas.
- The river defenses play a key role in the current lack of hydromorphological activity. Increasing the flow regime without a previous river defense modification does not improves the hydromorphological activity. The simulation model is an efficient tool to design this restoration strategy.
- The floodplain SRP uptake process takes place mainly by the suspended solute adsorption. Therefore, most of the phosphorous river contribution would be particulate phosphorus.
- The floodplain shows a high SRP uptake potential under both, normal and altered conditions. The high suspended solute concentration increases the floodplain SRP buffering capability, reducing SRP concentration downstream. However, as the SRP is uptaken, it could easily be

deposited into the floodplain, being an important source of particulate phosphorus.

- There is lateral gradient that dominates the river nutrient contribution. According to this gradient, adjacent riparian zones receives most of the dissolved and particulate nutrient whilst, remote floodplain areas hardly receive nutrients. This nutrient distribution could be affecting negatively the riparian vegetation and accelerating its aging process.

8.5 Floodplain restoration proposal through numerical simulation

- Five restoration scenarios based on discharge management or terrain modification were generated in order to increase the floodplain geomorphological dynamism. Only two of them, reduction of the dike height and restoration of the old superficial water pathways, demonstrated to be effective inducing morphological changes into the floodplain.

- The restoration scenario based on increasing the water discharge indicates that probably, the lack of geomorphic activity is actually influenced more by the constructed river defenses and the floodplain land use than by the Ebro river basin discharge regulation.

- The reduction of the dike height increases the river nutrient contribution into the floodplain but the morphodynamism is restricted to the river adjacent areas.

8. GENERAL CONCLUSIONS

- The restoration of the old superficial water pathways has demonstrated to be the most efficient alternative to restore the shifting mosaic of habitats of the floodplain and increasing its morphological activity. It would produce a new floodplain structure with a better equilibrium between the new creation and old habitats.

9

Conclusiones generales

El objetivo final del estudio era el desarrollo de una herramienta de simulación para analizar los principales procesos responsables de la creación y mantenimiento de los ecosistemas de llanuras de inundación. Para ello, se ha calibrado y validado un modelo de simulación completo basado en los modelos de rozamiento y topografía, la caracterización del cauce y el modelo hidráulico de volúmenes finitos que acopla el transporte de sólidos disueltos y en suspensión, la sedimentación y la retención de fósforo inorgánico disuelto (SRP). A continuación, se ha analizado el estado actual de la llanura de inundación a través de la herramienta de simulación. Finalmente, en base a dicho análisis, se han propuesto, simulado y analizado distintos escenarios de restauración. Las conclusiones específicas del presente trabajo se describen a continuación.

9.1 El modelo hidráulico

La validación del modelo hidráulico de flujo superficial ha demostrado que éste puede ser una herramienta de gran utilidad en la predicción de la conectividad hidrológica entre el río y la llanura de inundación, siempre y cuando se disponga de una correcta información topográfica. El modelo proporciona una información detallada de las características hidráulicas del flujo a través de una topografía irregular. Dichas características son las que determinan importantes propiedades ecológicas del sistema, tales como el morfodinamismo, el aporte de materia orgánica del río a la llanura, el contenido de oxígeno disuelto o el tipo de comunidad de macroinvertebrados en cada hábitat.

- El modelo completo se basa en el modelo hidráulico, calculado según el método de los volúmenes finitos, el de rozamiento y el topográfico, derivado del modelo digital disponible a partir de un vuelo LIDAR. El método proporciona información de la variación espacio-temporal del calado, velocidades promediadas en la vertical, y de la fricción estrés del fondo como indicativo de la capacidad erosiva del flujo.

- La calibración del modelo se basa en la información disponible del nivel de agua bajo dos caudales diferentes. La fase de calibración revela la extrema sensibilidad del modelo hidráulico a la forma del cauce. Dado que las técnicas estándares de LIDAR no proporcionan información del terreno cubierto por el agua, éste ha sido considerado como un punto clave en la fase de calibración del modelo.

- Los métodos de interpolación basados en el tratamiento estadístico de la información, tales como las herramientas GIS, proporcionan resultados incorrectos en la reconstrucción del cauce. En consecuencia, los resultados numéricos de la simulación empleando la reconstrucción del cauce mediante los GIS son muy poco precisos. En el presente trabajo, se propone un método sencillo de reconstrucción del cauce del río que emplea la información tanto de la forma del cauce como de sus características hidráulicas. Las simulaciones numéricas desarrolladas con dicha reconstrucción del cauce dieron como resultado una mayor precisión en la predicción tanto del calado como en el área inundada de la llanura de inundación.

- Existe un error sistemático en la predicción del nivel de agua en una de las sondas. Ello puede ser debido a la interacción entre el agua subterránea y superficial que se produce que se produce en esa zona particular y que no es considerada en el modelo. Las medidas registradas de temperatura del agua indican la presencia de una importante mezcla de aguas procedentes de dos fuentes diferentes. La extensión del modelo para incluir la interacción del agua subterránea y superficial se abordará con la mayor celeridad posible en el futuro.

- El gran inconveniente de este modelo es el elevado coste computacional, el cual puede resultar inasumible a la hora de enfrentarse con ciertos problemas en el campo de la eco-hidráulica

- La necesidad de proporcionar una información precisa de la topografía, el rozamiento y las condiciones de contorno puede ser considerada

también como un inconveniente. Sin embargo, esto es una cuestión subjetiva ya que el modelo tan sólo necesita como mínimo la misma resolución de datos de entrada que se va a demandar en los datos de salida.

9.2 Modelización de la retención de nutrientes

Se ha desarrollado y validado un modelo predictivo de retención de SRP tanto para el sedimento como para la columna de agua. El modelo ha sido formulado en función de los principales agentes relacionados con la captación de SRP, los cuales han sido determinados mediante experimentación en campo y en laboratorio. Como resultado, un modelo transitorio de retención de SRP en el que no es necesaria la concentración de salida del SRP ha sido desarrollado. Los datos de entrada del modelo son por tanto: caudal, entrada de materia orgánica en suspensión, materia inorgánica en suspensión, los sólidos disueltos totales, la concentración de entrada y ambiental de SRP, la temperatura del agua y la densidad y porosidad del sedimento.

9.2.1 Experimentación en laboratorio y canal de riego

- El lecho del canal de riego funciona como sumidero de nutrientes, pero tan sólo en el caso del fósforo. La acequia es capaz de reducir la concentración de fósforo alrededor de un 21%, o 0.7 $mg\ m^{-2}\ h^{-1}$ cuando la concentración de entrada se encuentra entre 1 y 46 $\mu g\ l^{-1}$. Sin embargo, no se detectó cambio significativo alguno entre la concentración de entrada y salida del nitrógeno. De hecho, el ratio molar medio de

DIN:SRP ratio (206:1) indica la presencia de un desequilibrio en el sistema donde probablemente el nitrógeno se encuentra saturado y el fósforo en condiciones limitantes.

- La sedimentación y el desarrollo natural de la vegetación en la acequia podría ser una buena estrategia para reducir parte del aporte de fósforo al río por parte de la agricultura.

- Se deben de considerar otras metodologías relativas a la reducción del nitrógeno agrícola en los canales de riego y drenaje, como por ejemplo que incrementen la desnitrificación en humedales (Verhoeven et al. (204)).

- La comparación entre los planteamientos estacionario y transitorio ene l cálculo de la retención de SRP muestra que la asunción de velocidad y coeficientes de captación uniformes da como resultado una herramienta mucho menos precisa que la transitoria. Por tanto, se requiere una metodología alternativa que contemple la variación espacial y temporal tanto de la velocidad como del coeficiente de captación de SRP.

- No se ha podido aplicar ni la ecuación de Elovich ni la formulación cinética debido a la elevada concentración final de.

- El análisis experimental ha puesto de manifiesto que el principal proceso implicado en la retención de SRP es la adsorción de éste por parte de los sólidos en suspensión. De acuerdo con esto, el análisis estadístico mostró como principales agentes relacionados con la retención de SRP a: pH, TSS, TDS y la concentración existente de SRP.

9. CONCLUSIONES GENERALES

- El nuevo modelo predictivo de retención de SRP tanto de la columna de agua como del sedimento ha sido desarrollado y validado en dos escalas espacio-temporales diferentes así como bajo distintas concentraciones de SRP. Los primeros 12 experimentos fueron desarrollados en el canal de riego utilizando para ello 60 m de longitud del mismo, durante $60-80$ min e incrementando la concentración ambiental de SRP $10-100$ veces. Los últimos 3 experimentos (13-15) se llevaron a cabo dentro del mismo canal de riego pero empleando 300 m de longitud, durante $2-4$ hr e incrementando la concentración de base de SRP $2-3$ veces. A pesar de que la retención de SRP mostró una elevada variabilidad entre experimentos ($0.0009 \pm 0.0004\ s^{-1}$), el nuevo modelo de retención de SRP fue capaz de reproducir dicha captura con una excelente precisión, resultando significativas ($p \leq 0.01$) todas las regresiones lineales entre la concentración de SRP calculada y la. Sin embargo, cuatro de las predicciones mostraron un error sistemático, aunque en en cualquier caso, la concentración calculada de SRP fue siempre del mismo orden de magnitud que la observada.

- La nueva formulación fue capaz de reproducir la presencia/ausencia de retención apreciable de SRP tanto bajo condiciones de flujo estacionario como transitorio. Bajo estos resutados, podemos afirmar que la nueva formulación es una herramienta excelente para predecir la retención de SROP al menos en el sistema del canal de riego.

-

9.2.2 La validación del modelo completo en el río

- La nueva formulación predictiva de retención de SRP ha sido validada en el río mediante tres experimentos de campo. Dicha validación ha demostrado la elevada capacidad predictiva del modelo, tanto bajo flujo transitorio como estacionario. Las predicciones del modelo resultaron siempre significativas ($p \leq 0.05$) y cuyos coeficientes de regresión r^2 varían entre 0.6 y 0.8.

- Dado que la formulación asume como principal proceso de retención de SRP su adsorción, éste no será aplicable a quellos sistemas en los que la retención biótica prevalezca sobre la abiótica. Por tanto, el modelo probablemente no será aplicable a tramos de cabecera. Por el contrario, el modelo presenta una gran capacidad predictiva en tramos de ríos medios y bajos.

- El modelo de retención de SRP no contempla la resuspensión del mismo, pudiendo por tanto sobreestimar la retención real del sistema.

- El proceso de validación del modelo puso de manifiesto de nuevo la necesidad de incluir la interacción entre el agua subterránea y la superficial en el modelo hidráulico.

9.3 Modelo de sedimentación

Se ha acoplado un modelo de sedimentación al modelo hidráulica. La velocidad de sedimentaicón se basa en la formulación de Jimenez and Madsen (98). Tel modelo se ha validado utilizando los datos experimentales de Cabezas and

Común. (33) y Cabezas et al. (38), y ha resultado ser una buena herramienta de cálculo de la seimentación.

- La comparación entre la sedimentación calculada y la observada dio como resultado una regresión lineal significativa ($p \leq 0.05$) cuya $r^2 = 0.97$. Por tanto, la validación constata la capacidad predictiva del modelo completo de flujo, sedimentación y retención de SRP.

- Dado que el modelo de sedimentación no incluye erosión, el cálculo de la tasa anual de sedimentación podría resultar sobreestimado. Por tanto, sería deseable incluir dicho proceso en el modelo hidráulico.

9.4 Análisis de la llanura de inundación a través de la simulación numérica

La aplicación del modelo completo de simulación ha demostrado ser una herramienta útil en el campo de la eco-hidráulica. Dicha herramienta es capaz de reproducir y predecir con una excelente precisión los principales procesos que generan y mantienen los ecosistemas de llanura de inundación. La aplicación final de la misma ha puesto de manifiesto la necesidad de restaurar y conservar dicho ecosistema.

- Existe un desequilibrio entre erosión y sedimentación a favor de este último. Como consecuencia, la llanura de inundación ha perdido gran parte de su actividad geomórfológica viéndose restringida casi por completo a las zonas adyacentes al cauce principal.

- Las defensas construidas del río juegan un papel clave en la actual falta de actividad geomorfológica. De esta forma, ni siquiera el incremento del régimen de caudales ni del caudal en si aumentaría significativamente la actividad geomorfológica si no se realiza una modificación previa de las defensas del río existentes.

- El proceso de retención de SRP en la llanura de inundación responde principalmente a la adsorción de SRP por parte de los sólidos en suspensión. Por tanto, la mayor parte del fósforo que el río aporta a la llanura de inundación es en su forma particulada.

- La llanura de inundación muestra una elevada capacidad de retención de SRP tanto bajo condiciones alteradas como naturales. La elevada concentración de sólidos en suspensión del río incrementa la capacidad de retención de SRP de la llanura de inundación, reduciendo su concentración aguas abajo del mismo. Sin embargo, a medida que el SRP es retenido, es también fácilmente sedimentado en la llanura, siendo por tanto el río una importante fuente de fósforo particulado.

- Existe un gradiente lateral que domina el aporte de nutrientes del río a la llanura de inundación. Según dicho gradiente, las zonas riparias adyacentes al río, reciben la mayor parte de sólidos tanto disueltos como particulados, mientras que las zonas remotas a penas reciben nutrientes. Esta distribución de los nutrientes podría estar afectando de forma negativa a la vegetación riparia de dichas zonas remotas, acelerando su proceso de envejecimiento.

9.5 Propuesta de restauración de la llanura de inundación a través de la simulación numérica

- Se han propuesto, simulado y analizado cinco escenarios de restauración con el objetivo de incrementar el morfodinamismo y basados en el manejo del caudal o de la modificación del terreno. Sin embargo, sólo dos de ellos, el basado en la reducción de la altura de las defensas del río y el basado en la recuperación de la conectividad hidrológica de ciertos hábitats, han demostrado ser efectivos en la inducción de cambios geomorfológicos en la llanura de inundación.

- La alternativa de restauración basada en el incremento del caudal indica que probablemente, la falta de actividad geomorfológica se encuentra actualmente más influida por las defensas del río y el uso del territorio que por el régimen de caudales del Ebro.

- El recrecimiento de las defensas del río incrementa el aporte de nutrientes del río a la llanura de inundación. Sin embargo, el morfodinamismo que genera dicha estrategia de restauración se restringe a las zonas adyacentes al cauce principal.

- La restauración de los antiguos canales de agua superficial ha demostrado ser la alternativa más eficaz en la restauración del mosaico cambiante de hábitats y el incremento del morfodinamismo de la llanura de inundación. Dicha estrategia generaría una nueva estructura en la llanura con un mejor equilibrio entre los hábitats de nueva formación y los viejos.

10

Further Research

- Reducing the model computational cost would be desirable in order to improve the model applicability. To reduce the simulation time, an optimization of the method could be the implementation of a parallel strategy reaching acceptable computational cost.

- Groundwater-surface flow interaction constitutes an important part of nutrient cycling. Hence, including the exfiltration and infiltration phenomenon is the next step to increase the model representativity. Then, a development of a complete 3D model would be desirable.

- Erosion process is fundamental to establish the real equilibrium between erosion and sedimentation. In the same way, to calculate the yearly sediment deposition, it is necessary to consider the erosive phenomenon. In that sense, we consider as a further work, to include the erosion process in the model.

10. FURTHER RESEARCH

- The SRP resuspension could constitute an important SRP source. To include it in the SRP uptake model more experimentation should be carried out.
- In order to develop a complete floodplain modeling, more nutrient species should be considered. Considering the relevance of the nitrogen in agricultural catchments, it would be the next nutrient to include in the model.

11

Appendix A: Tables

Table 11.1: Simulated sediment deposition at the current situation

Calculated sediment deposition (Tn) at each considered habitat during hydrographs (Hydr.) II, III, IV and V. RF: Riparian Forest

Hydr.	Crop/pasture	Adjacent RF	Distant RF	Paleochannel	Oxbow lake	Constructed wetlands	River channel	Remote RF
II	3.1	33.2	0.0	0.7	0.0	0.0	20.3	0.0
III	4.4	29.4	0.0	1.3	0.0	0.0	13.2	0.0
IV	39.9	76.9	0.0	5.6	0.7	0.0	23.8	0.2
V	480.2	206.1	11.8	24.8	18.7	0.3	60.7	15.6

Table 11.2: Simulated SRP at the current situation

Calculated average SRP concentration ± standard deviation at each considered habitat during the peak discharge of hydrographs (Hydr.) II, III, IV and V. SRP is expressed in $\frac{\mu g}{ls}$. RF: Riparian Forest

Hydr.	Crop/ pasture	Adjacent RF	Distant RF	Paleochannel	Oxbow lake	Constructed wetlands	River channel	Remote RF
II	5.0E-02±0.1	1.0±3.0	0.0±0.0	0.2±1.2	0.0±0.0	0.0±0.0	5.0±3.0	0.0±0.0
III	1.0E-02±0.2	1.0±3.0	0.0±0.0	0.2±1.0	0.0±0.0	0.0±0.0	4.0±3.0	0.0±0.0
IV	0.2±1.0	2.1±4.0	0.0±0.0	0.7±2.4	1.0E-02±2.0E-02	0.0±0.0	5.1±5.0	0.0±0.0
V	4.1±5.0	1.0E-02±5.0	1.4±1.0	9.0±5.0	0.2±2.0E-04	6.0E-02±0.2	1.2E-02±5.1	0.9±0.7

Table 11.3: Simulated sediment deposition at scenario 1

Calculated sediment deposition (Tn) at each considered habitat during the hydrographs (Hydr.) II, III, IV and V. Bold: higher sedimentation respect to the reference situation. Italics: lower sedimentation respect to the reference situation. RF: Riparian Forest

Hydr.	Crop/pasture	Adjacent RF	Distant RF	Paleochannel	Oxbow lake	Constructed wetlands	River channel	Remote RF
II	**3.7**	*3.5*	0.0	**2.5**	0.0	0.0	*19.4*	0.0
III	*4.6*	**3.2**	0.0	**2.6**	0.0	0.0	*12.5*	0.0
IV	*28.6*	**52.6**	0.0	*2.8*	**1.2**	0.0	*12.9*	**0.6**
V	**735.6**	*25.1*	**15.8**	**25.7**	**33.5**	**0.345**	*5.1*	**23.0**

Table 11.4: Simulated SRP at scenario 1

Calculated average SRP concentration ± standard deviation at each considered habitat during the peak discharge of hydrographs (Hydr.) II, III, IV and V. SRP is expressed in $\frac{\mu g}{ls}$. Bold: averages that significant differ with a $p \geq 0.95$ from the current situation as a result of a paired $T - test$. RF: Riparian Forest

Hydr.	Crop/ pasture	Adjacent RF	Distant RF	Paleochannel	Oxbow lake	Constructed wetlands	River channel	Remote RF
II	**5.9E-02±0.5**	**1.3±3.0**	0.0±0.0	**1.9±2.8**	0.0±0.0	0.0±0.0	**4.9±3.3**	0.0±0.0
III	**3.4E-02±0.3**	**1.0±2.8**	0.0±0.0	**1.3±2.2**	0.0±0.0	0.0±0.0	**3.4±3.4**	0.0±0.0
IV	**9.0E-02±0.8**	**2.3±6.1**	0.0±0.0	**2.4±4.2**	0.0±0.0	0.0±0.0	**5.6±7.5**	0.0±0.0
V	**4.4±5.1**	**8.8±5.5**	**1.6±1.0**	**1.0E-02±5.0**	**0.2±0.2**	**5.1E-02±0.1**	**1.1E-02±5.1**	**1.6±0.9**

Table 11.5: Simulated sediment deposition at scenario 2

Calculated sediment deposition (Tn) at each considered habitat during the hydrographs (Hydr.) II, III, IV and V. Bold: higher sedimentation respect to the reference situation. Italics: lower sedimentation respect to the reference situation. RF: Riparian Forest.

Hydr.	Crop/pasture	Adjacent RF	Distant riparian forest	Paleochannel	Oxbow lake	Constructed wetlands	River channel	Remote RF
II	**21.2**	**72**	0.0	**12.9**	**0.21**	0.0	**21.7**	0.0
III	*26.1*	**75.2**	0.0	**16.6**	**0.20**	0.0	**15.1**	0.0
IV	*35.3*	**81.1**	0.0	**21.2**	0.7	0.0	*15.1*	*0.01*
V	*149.8*	**246.8**	*2.0*	*59.5*	*4.1*	*0.02*	*53.6*	*2.7*

Table 11.6: Simulated SRP at scenario 2

Calculated average SRP concentration ± standard deviation at each considered habitat during the peak discharge of hydrographs (Hydr.) II, III, IV and V. SRP is expressed in $\frac{\mu g}{ls}$. Bold: averages that significant differ with a $p \geq 0.95$ from the current situation as a result of a paired $T - test$. RF: Riparian Forest

Hydr.	Crop/ pasture	Adjacent RF	Distant RF	Paleochannel	Oxbow lake	Constructed wetlands	River channel	Remote RF
II	**6.0±0.1**	**1.9±2.9**	0.0±0.0	**1.3±2.3**	**4.0E-03±2.8E-02**	0.0±0.0	**5.3±3.5**	0.0±0.0
III	**3.0E-03±6.6E-02**	**1.3±2.7**	0.0±0.0	**7.7E-04±1.7**	0.0±0.0	0.0±0.0	**3.8±3.6**	0.0±0.0
IV	**0.1±0.7**	**4.8±6.2**	0.0±0.0	**3.1±4.6**	**2.2E-02±8.0E-02**	0.0±0.0	**1.0E-02±6.8**	0.0±0.0
V	**3.5±5.0**	**9.0±5.4**	**1.5±1.1**	**8.7±5.2**	**5.8E-02±0.1**	**8.7E-02±7.8E-02**	**11.5±5.4**	**0.5±0.3**

Table 11.7: Simulated SRP addition experiment: river discharge 500 m^3/s

Calculated average SRP concentration $\pm$ standard deviation at each considered habitat, under five different SRP added concentrations. Calculated SRP is expressed in $\frac{\mu g}{ls}$. Bold: averages that significant differ from the 0 $\mu g/l$ SRP with a $p \geq 0.95$. RF: Riparian Forest

SRP (mg/l)	Crop/ pasture	Adjacent RF	Distant RF	Paleochannel	Oxbow lake	Constructed wetlands	Main channel	Remote RF
0	4.0E-03±5.0E-02	1.6±4.0	0.0±0.0	8.0E-02±1.2	0.0±0.0	0.0±0.0	10.4±5.0	0.0±0.0
1	5.0E-03±0.2	**1.7±4.0**	0.0±0.0	8.0E-02±1.2	0.0±0.0	0.0±0.0	**10.3±5.0**	0.0±0.0
3	**4.0E-03±1.6E-02**	**1.6±4.0**	0.0±0.0	8.0E-02±1.2	0.0±0.0	0.0±0.0	**10.3±5.0**	0.0±0.0
5	**7.0E-03±3.0E-02**	**2.2±4.6**	0.0±0.0	8.0E-02±1.2	0.0±0.0	0.0±0.0	**26.0±17.6**	0.0±0.0
10	**1.0E-02±0.4**	**2.7±5.6**	0.0±0.0	8.0E-02±1.2	0.0±0.0	0.0±0.0	**42.0±32.0**	0.0±0.0

Table 11.8: Simulated SRP addition experiment: river discharge 1000 m^3/s

Calculated average SRP concentration $\pm$ standard deviation at each considered habitat, under five different SRP added concentrations. Calculated SRP is expressed in $\frac{\mu g}{ls}$. Bold: averages that significant differ from the 0 $\mu g/l$ SRP with a $p \geq 0.95$. RF: Riparian Forest

SRP (mg/l)	Crop/ pasture	Adjacent RF	Distant RF	Paleochannel	Oxbow lake	Constructed wetlands	Main channel	Remote RF
0	6.0E-02±0.5	1.7±3.9	0.0±0.0	0.4±1.6	0.0±0.0	0.0±0.0	4.9±4.9	0.0±0.0
1	**2.8±1.5**	**4.9±5.7**	0.0±0.0	1.0±3.1	4.0E-03±0.3	0.0±0.0	**13.5±5.8**	0.0±0.0
3	**0.3±0.2**	**5.1±6.0**	0.0±0.0	**1.0±3.2**	0.0±0.0	0.0±0.0	**17.0±9.0**	0.0±0.0
5	**0.3±1.7**	**5.7±6.2**	0.0±0.0	**1.1±3.1**	**3.0E-03±3.0E-02**	0.0±0.0	**21.0±12.0**	0.0±0.0
10	**0.4±1.9**	**6.9±6.9**	0.0±0.0	**1.1±3.2**	**4.0E-03±3.0E-02**	0.0±0.0	**31.0±21.0**	0.0±0.0

Table 11.9: Simulated SRP addition experiment: river discharge 1500 m^3/s

Calculated average SRP concentration $\pm$ standard deviation at each considered habitat, under five different SRP added concentrations. Calculated SRP is expressed in $\frac{\mu g}{ls}$. Bold: averages that significant differ from the 0 $\mu g/l$ SRP with a $p \geq 0.95$. RF: Riparian Forest

SRP (mg/l)	Crop/ pasture	Adjacent RF	Distant RF	Paleochannel	Oxbow lake	Constructed wetlands	Main channel	Remote RF
0	0.5±1.9	3.0±4.5	0.0±0.0	1.4±3.0	0.0±0.0	0.0±0.0	5.0±5.0	0.0±0.0
1	**3.8±5.0**	**9.5±5.6**	1.2±1.0	9.0±4.7	0.1±0.	7.0E-03±2.4E-02	**13±5.8**	**0.7±0.7**
3	**1.7±3.9**	**8.9±6.2**	**0.4±0.5**	**5.3±4.8**	1.0E-02±0.01	0.0±0.0	**16±8.2**	**4.4E-02±0.9E-02**
5	**1.7±4.1**	**9.9±6.7**	**0.2±0.4**	**5.3±5.0**	1.0E-02±0.01	0.0±0.0	**18.0±11.0**	**4.4E-02±1.9E-02**
10	**1.9±4.5**	**12±8.4**	**0.4±0.6**	**5.8±5.0**	1.0E-02±0.01	0.0±0.0	**25.0±18.0**	**4.4E-02±0.9E-02**

Table 11.10: Simulated SRP addition experiment: river discharge 2000 m^3/s

Calculated average SRP concentration $\pm$ standard deviation at each considered habitat, under five different SRP added concentrations. Calculated SRP is expressed in $\frac{\mu g}{ls}$. Bold: averages that significant differ with from the 0 $\mu g/l$ SRP a $p \geq 0.95$. RF: Riparian Forest

SRP (mg/l)	Crop/ pasture	Adjacent RF	Distant RF	Paleochannel	Oxbow lake	Constructed wetlands	Main channel	Remote RF
0	3.7±4.9	8.7±5.5	1.2±1.0	8.8±4.7	0.1±0.2	7.0E-03±2.3E-02	12±5.1	0.7±0.7
1	**3.8±5.0**	**9.5±5.6**	1.2±1.0	**9.0±4.7**	**0.1±0.2**	7.0E-03±2.4E-02	**13±5.8**	**0.7±0.7**
3	**3.9±5.1**	**11±6.1**	1.2±1.0	**9.3±4.7**	**0.1±0.2**	7.0E-03±2.6E-02	**15±7.7**	**0.8±0.7**
5	**4.0±5.3**	**12±6.9**	1.2±1.0	**9.6±4.8**	**0.1±0.2**	8.0E-03±2.7E-02	**17±10**	**0.8±0.8**
10	**4.2E±5.7**	**16±9.3**	**1.3±1.1**	**10±5.2**	**0.2±0.2**	**2.0E-03±0.5**	**22±16**	**0.9±0.9**

11. APPENDIX A: TABLES

Bibliography

[1] G.C. Acrement and V.R Schenides. *Guide for Selecting Manning's Roughness Coefficients for Natural Channels and Flood Plains*. Water-Supply Paper No. 2339 (Department of the Interior, U.S. Geological Survey, Reston, VA), 1990. 44, 110

[2] S. Ahmad. *Comparison of One-Dimensional and Two-Dimensional Hydrodynamic Modeling Approaches For Red River Basin*. Natural Resources Institute. Facility for Intelligent Decision Support. University of Manitoba, Canada, 1999. 10

[3] A.A. Akanbi and N.D. Katopodes. Model for flood propagation on initially dry land. *J. of Hydraulic Engineering*, 114:689–706, 1987. 40

[4] R.B. Alexander, R.A. Smith, and G.E. Schwartz. Effect of stream channel size on the delivery of nitrogen to the gulf of mexico. *Naturel*, 403:758–761, 2000. 4, 175, 208

BIBLIOGRAPHY

[5] APHA. *Standard methods for the examination of water and wastewater*. 17Th ed. American Public Health Association (APHA), Washington D.C., USA., 1989. 117, 182

[6] N. E. M. Asselman and H. Middelkoop. Floodplain sedimentation: quantities, patterns and processes. *Earth Surf. Processes and Landforms*, 20:481–499, 1995. 175, 208, 210, 250

[7] E. Audusse, F. Bouchut, M. O. Bristeau, and B. Klein, R. andPerthame. A fast and stable well-balanced scheme with hydrostatic reconstruction for shallow water flows. *Journal of Sci. Comp.*, 25(6):2050–2065, 2004. 40

[8] L. A. Baker. Introduction to nonpoint source pollution in the united states and prospects for wetland use. *Ecological Engineering*, 1:1–26, 1992. 100

[9] R.J. Batalla, C.M. Gomez, and G.M. Kondolf. Reservoir-induced hydrological changes in the ebro river basin (ne spain). *Journal of Hydrology*, 290:117–136, 2004. 7

[10] P. Bates, M.S. Horrit, C.N. Smith, and D.. Mason. Integrating remote sensing observations of flood hydrology and hydraulic modelling. *Hydrological Processes*, 11:1777–1795, 2000. 53, 73

[11] P. D. Bates and A. P. J. De Roo. A simple raster-based model for flood inundation simulation. *Journal of Hydrology*, 236(1-2):54 – 77, 2000. ISSN 0022-1694. 49, 51

[12] Paul D. Bates, Richard J. Dawson, Jim W. Hall, Matthew S. Horritt, Robert J. Nicholls, Jon Wicks, and Mohamed Ahmed Ali Mohamed Hassan. Simplified two-dimensional numerical modelling of coastal flooding and example applications. *Coastal Engineering*, 52(9):793 – 810, 2005. ISSN 0378-3839. 11

[13] P.D. Bates, M.S. Horritt, and J.-M. Hervouet. Investigating twodimensional, finite element predictions of floodplain inundation using fractal generated topography. *Hydrological Processes*, 12:12571277, 1998. 11

[14] P.B. Bayley. Understanding large river-floodplain ecosystems. *BioScience*, 45:153–158, 1995. 1, 38, 77, 209

[15] P.B. Bedient and W.C. Huber. *Hydrology and floodplain analysis*. Addison-Wesley, Reading, Mass. (USA), 1988. 44

[16] C. Beffa and R.J. Connell. Two-dimensional flood plain flow. i: Model description. *Journal of Hydrologic Engineering*, 6:397–402, 2001. 10, 11

[17] S. Beguería, J. I. Lopez-Moreno, A. Gomez-Villar, V. Rubio, N. Lana-Renault, and J. M. García-Ruíz. Fluvial adjustments to soil erosion and plant cover changes in the central spanish pyrenees. *Geografiska Annaler Series a-Physical Geography*, 88A:177–186, 2003. 7

[18] S. Beguería, J. I. Lopez-Moreno, A. Lorente, M. Seeger, and J. M. García-Ruíz. Assessing the effect of climate oscillations and land-use

changes on streamflow in the central spanish pyrenees. *Ambio*, 32: 283–286, 2003. 7

[19] K. E. Bencala. Interactions of solutes and streambed sediment: 2. a dynamic analysis of coupled hydrologic and chemical processes that determine solute transport. *Water Resources Research*, 20:1804–1814, 1984. 121

[20] K. E. Bencala and R. A. Walters. Simulation of solute transport in a mountain pool-and-riffle stream: a trasnient storage model. *Water Resources Research*, 19:718–724, 1983. 101, 121

[21] D. Binkley, H. Burnham, and H.L. Allen. Water quality impacts of forest fertilization with nitrogen and phosphorous. *For. Ecol. and Manage.*, 121:121–191, 1999. 102

[22] R. Bouza-Deano, M. Ternero-Rodríguez, and A.J. Fernández-Espinosa. Trend study and assessment of surface water quality in the ebro river (spain). *Journal of Hydrology*, 361:227–239, 2008. 22

[23] M. J. Bowes and W. A. House. Phosphorus and dissolved silicon dynamics in the river swale catchment, uk: a mass-balance approach. *Hydrological Processes*, pages 261–280. 3, 4, 175, 208, 246

[24] G. L. Bowie, Mills W. B., D. P. Porcella, C. L. Campbell, J. R. Pagenkop, G. L. Rupp, K. M. Jhonson, P. W. H. Chan, S. A. Gherini, and C. E. Chamberlin. *Rates, constants, and kinetics formulations in surface water quality modelling.* U.S. Environmental Protection Agency, EPA/600/3-85/040, 1985. 123, 245

[25] S.F. Bradford and B.F. Sanders. Finite-volume model for shallow water flooding of arbitrary topography. *J. of Hydraulic Engineering*, 128: 289–298, 2002. 40

[26] B.C. Braskerud, K. S. Tonderski, B. Wedding, R. Bakke, A.-G.B. Blankenberg, B. Ulen, and J. Koshiaho. Can constructed wetlands reduce the diff use phosphorus loads to eutrophic water in cold temperate regions? *Journal of Environmental Quality*, 34:21452155, 2005. 3, 175

[27] J. D. Brown, T. Spencer, and Moeller I. Modeling storm surge flooding of an urban area with particular reference to modeling uncertainties: A case study of canvey island, united kingdom. *Water Resources Research*, 43, 2007. doi: DOI:10.1029/2005WR004597. 40, 48

[28] R. C. Brunet, G. Pinay, F. Gazelle, and Roques. Role of the floodplain and riparian zone in suspended matter and nitrogen retention in the adour river, south- west france. *Regulated Rivers: Research and Management*, page 5563. 175, 209

[29] S.E. Bunn and A.H. Arthington. Basic principles and ecological consequences of altered flow regimes for aquatic biodiversity. *Enviromental Management*, 4:492–507, 2002. 174

[30] J Burguete, P Garcia-Navarro, and J. Murillo. Preserving bounded and conservative solutions of transport in one-dimensional shallow-water flow with upwind numerical schemes: Application to fertigation and

solute transport in rivers. *International Journal of Numerical Methods in Fluids*, 56:1059–1092, 2008. 32

[31] T. P. Burt, L. S. Matchett, K. W. T. Goulding, C. P. Webster, and N. E. Haycock. Denitrifcation in riparian buffer zones: the role of foodplain hydrology. *Hydrological processes*, 13:1451–1463, 1999. 2

[32] O. Buttner, K. Otte-Witte, F. Kruger, G. Meon, and M. Roded. Numerical modelling of floodplain hydraulics and suspended sediment transport and deposition at the event scale in the middle river elbe, germany. *Acta hydrochim. hydrobiol.*, 34:265 278, 2006. 238, 239, 244

[33] A. Cabezas and F. A. Comín. Carbon and nitrogen accretion in the topsoil of the middle ebro river (ne spain): implications for their ecological restoration. *Ecological Engineering*, 36:640–652, 2010. xx, 7, 23, 180, 184, 185, 193, 194, 195, 243, 261, 272

[34] A. Cabezas, F.A. Comin, S. Begueria, and M. Trabucchi. Hydrologic and land-use change influence landscape diversity in the Ebro River (NE Spain). *Hydrology and Earth System Sciences Discussions*, 5: 2759–2789, September 2008. 7, 78, 79, 80, 81, 250

[35] A. Cabezas, M. García, B. Gallardo, E. González, M. González-Sanchis, and F. A. Comín. The effect of anthropogenic disturbance on the hydrochemical characteristics of riparian wetlands at the middle ebro river (ne spain). *Hydrobiologia*, 617:101–116, 2008. 81, 183, 237

[36] A. Cabezas, E. Gonzalez, B. Gallardo, M. García, M. González-Sanchis, J.J. Jimenez, and F. A. Comín. Effects of hydrological connectivity of riparian wetlands in the middle ebro river (ne spain): Implications for restoration and management. *Aquatic Science*, 70:361–376, 2008. 7, 73

[37] A. Cabezas, F. A. Comín, and D. E. Walling. Changing patterns of organic carbon and nitrogen accretion on the middle ebro floodplain (ne spain). *Ecological Engineering*, 35:1547–1558, 2009. 78, 79, 80, 241, 249, 250

[38] A. Cabezas, M. Angulo-Martínez, M. González-Sanchis, J.J. Jimenez, and F. A. Comín. Spatial variability in floodplain sedimentation: the use of generalized linear mixed-effects models. *Hydrol. Earth Syst. Sci. Discuss.*, 7:1589–1619, 2010. xx, 180, 184, 185, 193, 194, 195, 243, 261, 272

[39] G. Cao, Z.and Pender and J. Meng. Explicit formulation of the shields diagram for incipient motion of sediment. *Journal of Hydraulic Engineering*, 132:1097–1099, 2006. 30

[40] R. Carignan and P. Vaithiyanathan. Phosphorus availability in the parana floodplain lakes (argentina): Influence of ph and phosphate buffering by fluvial sediments. *Limnol. Oceanogr.*, 44:15401548, 1999. 3, 175

[41] R. Carignan and P. Vaithiyanathan. Modeling sediment transport dynamics in thompson island pool, upper hudson river. *Water environmental Research*, 30:193–222, 2000. 4

[42] S. R. Carpenter, N. F. Caraco, D. L. Correl, R. W. Howarth, A. N. Sharpley, and V. H. Smith. Nonpoint pollution of surface waters with phosphorus and nitrogen. *Ecological Applications*, 8(3):559–568, 1998. 100, 171

[43] R.W.H. Carroll and J. J. Warwick. Uncertainty analysis of the carson river mercury transport model. *Ecological modeling*, 137:211–224, 2001. 244

[44] A.R. Castaneda and S.I. Bhuiyan. Sediment pollution in a gravity irrigation system and its effects on rice production. *Agriculture, Ecosystems and Environment*, 45:195–202, 1993. 101

[45] P. Castro, J. Guerrero, and M.A. Muoz. *Restauracion del Bosque de rivera en la Reserva Natural de los galachos (Zaragoza)*. Consejo de Proteccion de la Naturaleza de Aragon, 2001. 7

[46] J. Causape, Qulez D., and Aragues R. Irrigation efficiency and quality of irrigation return flows in the Ebro river basin: an overview. *Environmental Monitoring and Assessment*, 117:451–461, 2006. 101

[47] Centro de Estudios y Experimentación de Obras Pblicas. CEDEX. *Modelización bidimensional del flujo en lmina libre en aguas poco profundas. Manual bsico de usuario*. Environmental Spanish Ministry, Spain, 2010. 10

[48] V.T. Chow. *Open-Channel Hydraulics*. 1959. 44

[49] C.P. Cirmo and J.J. McDonnell. Linking the hydrologic and biogeochemical controls of nitrogen transport in near-stream zones of temperate- forested catchments: A review. *Journal of Hydrology*, 199: 88–120, 1997. 4

[50] David M. Cobby, David C. Mason, Matthew S. Horritt, and Paul D. Bates. Two-dimensional hydraulic flood modelling using a finite-element mesh decomposed according to vegetation and topographic features derived from airborne scanning laser altimetry. *Hydrological Processes*, 17(10):1979–2000, 2003. ISSN 1099-1085. doi: 10.1002/hyp.1201. URL http://dx.doi.org/10.1002/hyp.1201. 11

[51] R. J. Connell, D. J. Painter, and C. Beffa. Two-dimensional flood plain flow.i i: Model validation. *Journal of Hydrologic Engineering*, 6:406–415, 2001. 10, 49, 238, 239

[52] A. Cook and V. Merwade. Effect of topographic data, geometric configuration and modelling approach on flood inundation mapping. *Journal of Hydrology*, 377:131–142, 2009. 38, 51

[53] W. Marshall Darley. *Algal biology: A physiological approach*. Blackwell Scientific Publications (Oxford and Boston and St. Louis, Mo.)., 1982. 102

[54] S. Erpicum, B. Dewals, P. Archambeau, S. Detrembleur, and Pirotton M. Detailed inundation modelling using high resolution dems. *En-*

gineering Applications of Computational Fluid Mechanics, 4(2):196–208, 2010. 238, 239

[55] M.S. Fennessy, C.C. Brueske, and W.J. Mitsch. Sediment deposition patterns in restored freshwater wetlands using sediment traps. *Ecological Engineering*, 3:409–428, 1994. 174

[56] J.L. Florsheim and J.F. Mount. Restoration of floodplain topography by sand-splay complex formation in response to intentional levee breaches, lower cosumnes river, california. *Geomorphology*, 44:67–94, 2002. 38

[57] P.N. Froelich. Kinetic control of dissolved phosphste in natural rivers and estuaries: a primer on the phosphate buffer mechanism. *Limnology and Oceanography*, 33(4):649–668, 1988. 113, 137

[58] L.M. Frutos, A. Ollero, and M. Sanchez Fabre. *Caracterizacion del Ebro y su cuenca y variaciones en su comportamiento hidrologico.* in A. Gil Oncina (ed.), Alteracion de los regímenes fluviales peninsulares. Fundacion Caja Murcia, 2004. 7

[59] D.L. Galat, J.F. Kubisiak, J.B. Hooker, and L.M. Sowa. Geomorphology, distribution and connectivity of lower missouri river floodplain waterbodies scoured by the flood of 1993. *Verhandlungen der Internationalen Vereinigung fu r Theoretische und Angewandte Limnologie.*, 26:869–878, 1997. 1

[60] J. M. García-Ruíz, Ortigosa L. Lasanta, T., P. Ruizflano, C. Martí, and C. Gonzalez. Sediment yield under different land uses in the spanish pyrenees. *Mountain Research and Development*, 15:229–240, 1995. 7

[61] J. Gelbrecht, H. Lengsfeld, R. Pothig, and D. Opitz. Temporal and spatial variation of phosphorus input, retention and loss in a small catchment of ne germany. *Journal of Hydrology*, 304:151–165, 2005. 208

[62] Ps S. Giller. River restoration: seeking ecological standards. editor's introduction. *Journal of Applied Ecology*, 42:201–207, 2005. 5

[63] E. González, M. González-Sanchis, A. Cabezas, F.A. Comín, and E. Muller. Recent changes in the riparian forest of a large regulated mediterranean river: Implications for management. *Environmental Management*, 45:669–681, 2010. 7, 23, 78, 79, 80, 81, 241, 249

[64] E. Gonzalez, E. Muller, F. A. Comín, and M. Gonazlez-Sanchis. Leaf nutrient content as an indicator of populus and tamarix response to flooding. *Perspectives in Plant Ecology, Evolution and Systematics*, 20:257–266, 2010. 209, 251

[65] M. Gonzalez-Sanchis, J. Murillo, A. Cabezas, F. Comín, and P. García-Navarro. *Analysis of floodplain dynamics using numerical simulation at the middle Ebro river.* 4th Annual Meeting of the European Chapter of the Society of Wetlands Scientists (SWS). 20-24 May Erkner (Germany)., 2009. 79, 241

[66] B. Gretener and L. Strmquist. Overbank sedimentation rates of fine grained sediments. a study of the recent deposition in the lower river fyrisan. *Geografiska Annaler 69A*, 1:139–146, 1987. 174

[67] B. E. Haggard, D. E. Storm, R. D. Tejral, Y. A. Popova, V. G. Keyworth, and E. H. Stanley. Stream nutrient retention and limitation in three northeastern oklahoma agricultural catchments. *Trans.*, 44:597–605, 1999. 137

[68] B.E. Haggard, D.E. Storm, R.D. Tejral, Y.A. Popova, V.G. Keyworth, and E.H. Stanley. Stream nutrient retention in three northeastern Oklahoma agricultural catchments. *American Society of Agricultural Engineers*, 3:597–605, 2001. 101, 133

[69] R.J. Hardy, P.D. Bates, and M.G. Anderson. Modelling suspended sediment deposition on a fluvial floodplain using a two-dimensional dynamic finite element model. *Journal of Hydrology*, 229:202–218, 2000. 176

[70] F.F. Hattermann, V. Krysanova, A. Habeck, and A. Bronstert. Integrating wetlands and riparian zones in river basin modelling. *Ecological Modelling*, 199:379–392, 2006. 4

[71] F. R. Hauer and M. S. Lorang. River regulation, decline of ecological resources, and potential for restoration in a semi-arid lands river in the western usa. *Aquat. Sci.*, 66:388401, 2004. 1, 37, 38

[72] G. Heiler, T. Hein, F. Schiemer, and G. Bornette. Hydrological connectivity and flood pulses as the central aspects for the integrity of a

riverfloodplain system. *Regulated Rivers: Research and Management*, 11:8194, 1995. 5

[73] G. Heiler, T. Hein, F. Schiemer, and G Bornette. Hydrological connectivity and flood pulses as the central aspects for the integrity of a river-floodplain system. *Regulated Rivers: Research and Management*, 11: 351–361, 1995. 1, 210

[74] J. K. Heim and J. J. Warwick. Simulating sediment transport in the carson river and lahontan reservoir, nevada. *Journal of the American Water Resources Association*, 33:171–197, 1997. 244

[75] D.C. Heimann and M.J. Roell. Sediment loads and accumulation in a small riparian wetland system in northern missouri. *Wetlands*, 20: 219231, 2000. 175

[76] J.-M. Hervouet. *Comparison of experimental data and laser measurements with the computational results of the TELEMAC-2D code (shallow water equations)*. C. Maksimovic, M. Radojkovic, Editors Elsevier, Amsterdam. Computational and Experimental Methods in Hydraulics (HYDROCOMP '89), 1989. 10, 11

[77] J.-M. Hervouet. Validating the numerical simulation of dam-breaks and floods. *Advances in Hydroscience and Engineering Volume*, 1: 754761, 1993. 10, 11

[78] A. R. Hill. Phosphorus and major cation mass balances for two rivers during low summer flows. *Freshwater Biology*, 12:293304, 1982. 137

[79] T.J. Hoellein, J.L. Tank, E. J. Rosi-Marshall, S.A. Entrekin, and G.A. Lamberti. Controls on spatial and temporal variation of nutrient in three Michigan headwater streams. *Limnology and Oceanograohy.*, 5: 1964–1977, 2007. 101, 129, 189

[80] M.S. Horrit and P. D. Bates. Evaluation of 1d and 2d numerical models for predicting river flood inundation. *Journal of Hydrology*, 268:87–99, 2002. 49

[81] M.S. Horritt. Calibration of a two-dimensional finite element flood flow model using satellite radar imagery. *Water Resources Research*, 36:3279–3291, 2000. 11

[82] M.S. Horritt and P. D. Bates. Predicting floodplain inundation: raster-based modelling versus the finite-element approach. *Hydrological Processes*, 15:825–842, 2001. 10, 238, 239

[83] W.A. House and F.H. Denison. Factors influencing the measurement of equilibrium phosphate concentrations in river sediments. *Water Research*, 34(4):1187–2000, 2000. 113

[84] W.A. House, F.H. Denison, and P.D. Armitage. Comparison of the uptake of inorganic phosphorus to a suspended and stream bed-sediment. *Water Research*, 29(3):767–779, 1995. 129, 137, 189, 242, 243, 245

[85] W.A. House, F.H. Denison, and P.D. Armitage. Comparison of the uptake of inorganic phosphorus to a suspended and stream bed-sediment. *Water Research*, 29(3):767–779, 2000. 246

[86] M.E. Hubbard and P. García-Navarro. Flux difference splitting and the balancing of source terms and flux gradients. *Journal of Comp. Physics*, 165:89–125, 2000. 40

[87] F.M.R. Hughes. Floodplain biogeomorphology. *Progress in Physical Geography*, 21:501–529, 1997. 229

[88] F.M.R. Hughes and Rood S.B. Allocation of river flows for restoration of floodplain forest ecosystems: A review of approaches and their applicability in europe. *Environmental Management*, 32:1233, 2003. 210

[89] N.M. Hunter, P.D. Bates, S. Neelz, G. Pender, I. Villanueva, N.G. Wright, D. Liang, R.A. Falconer, B Lin, S. Waller, A. J. Crossley, and D.C. Mason. Benchmarking 2d hydraulic models for urban flooding. *Water Management*, 36:13–30, 2008. 39

[90] C.R. Hupp and E.E. Morris. A dendrogeomorphic approach to measurement of sedimentation in a forested wetland, black swamp, arkansas. *Wetlands*, 10:107–124, 1990. 174

[91] H. B. N. Hynes. *The biology of polluted waters.* Liverpool University Press, Liverpool., 1960. 100

[92] C. Ibanez, N. Prat, and A. Canicio. Changes in the hydrology and sediment transport produced by large dams on the lower ebro river and its estuary. *Regulated Rivers-Research and Management*, 12:51–62, 1996. 7

[93] Danish Hydraulic Institute. *Mike 21 User guide and reference manual*. 1998. 10

[94] W.F James and C.E. Larson. Phosphorus dynamics and loading in the turbid minnesota river (usa): controls and recycling potential. *Biogeochemistry*, 90:75–92, 2008. 206, 246

[95] H.P. Jarvie, Neal C., R. J. RWilliams, M. Neal, H. D Wickham, L. K Hill, A. Wade, A. Warwick, and J. White. Phosphorus sources, speciation and dynamics in the lowland eutrophic river kennet, uk. *Science of The Total Environment*, 23:175–203, 2002. 206

[96] H.P. Jarvie, Neal C., M. D. Jurgens, E. J. Sutton, M. Neal, H. D. Wickham, L. K. Hill, S. A. Harman, J. J. L. Davies, A. Warwick, C. Barrett, J. Griffiths, A. Binley, N. Swannack, and N. McIntyre. Within-river nutrient processing in chalk streams: The pang and lambourn, uk. *Journal of Hydrology*, 330:101–125, 2006. 246

[97] S.W. Jeffrey and G.F. Humphrey. New spectrophotometric equations for determining chlorophylls a, b, c_1 and c_2 in higher plants, algae and natural phytoplankton. *Biochem. Physiol. Planzen.*, 53:191–194, 1975. 118, 183

[98] J. A. Jimenez and O. S. Madsen. A simple formula to estimate settling velocity of natural sediments. *Journal of Waterway, Port, Coastal and Ocean Engineering*, 129:70–78, 2008. 29, 261, 271

[99] A. H. Johnson, D.R. Bouldin, E.A. Goyette, and A.M. Hedges. Phosphorus loss by stream transport from a rural watershed: quantities,

processes and sources. *Journal of Environmental Quality*, 5:148–157, 1978. 137

[100] L. B. Johnson, C. Richards, G. E. Host, and Arthur J. W. Landscape influences on water chemistry in midwestern stream ecosystems. *Freshwater Biology*, 37:193208, 1997. 100

[101] C.A. Johnston. Sediment and nutrient retention by freshwater wetlands: Effects on surface water quality. *Crit. Rev. Environ. Control*, 21:491565, 1991. 3, 4, 175

[102] W. J. Junk, P. B. Bayley, and R. E. Sparks. The flood pulse concept in river-floodplain systems. *Canadian Special Publication in Fisheries and Aquatic Sciences*, 106:110–127, 1989. 1, 2, 38, 210, 239

[103] Tockner K. and J. A. Standford. Riverine flood plains: present state and future trendsy. *Environmental Conservation*, 29:308330, 2002. 4, 210, 251

[104] I. King. *Users Guide to RMA2 Version 4.3*. 1996. 10, 11

[105] B.A. Kleiss. *Methods for measuring sedimentation rates in bottomland hardwood (BLH) wetlands*. Wetlands Research Program Technical Note SD-CP-4.1. U.S. Army Engineer Waterways Experiment Station, Vicksburg, MS, USA., 1993. 175

[106] B.A. Kleiss. Sediment retention in a bottomland hardwood wetland in eastern arkansas. *Wetlands*, 16:321–333, 1996. 174, 175

[107] R.L. Klotz. Controlling phosphorus limitation in stream sediments. *Limnology and Oceanography*, 30:543–553, 1985. 100

[108] D.W. Knight and K. Shiono. *River channel and floodplain hydraulics.* In: Anderson, M.G., Walling, D.E., Bates, P.D. (Eds.), Floodplain Processes. Wiley, Chichester, pp. 139 181., 1996. 176

[109] W. Koerselmanb and J.T.A. Verhoeven. *Eutrophication of fen ecosystems: external and internal nutrient sources and restoration strategies*. In Wheeler, B. D., S. C. Shaw, W. J. Fojt and R. A. Robertson (eds), Restoration of Temperate Wetlands. JohnWiley and Sons Ltd, Chichester: 91112., 1995. 3

[110] B. Kronvan, C.C. Hoffmann, L.M. Svendsen, J. Windolf, J.P. Lars, M. Svendsen, J. Windolf, and P. Jens. Retention of nutrients in river basins. *Aquatic Ecology*, 33:29–40, 1999. 207, 209

[111] J. S. Kuwabara and P. Helliker. Copper transport along sierra nevada stream. *Journal of Enviromental Engineering*, 110:646–655, 1984. 101

[112] C.P. Lambert and D.E. Walling. Floodplain sedimentation: a preliminary investigation of contemporary deposition within the lower reaches of the river culm, devon, uk. *Geografiska Annaler 69A*, 3-4:393–404, 1987. 175

[113] J. I. Lopez-Moreno, S Beguería, and J. M. García-Ruíz. Trends in high flows in the central spanish pyrenees: resopnse to climatic factors

or to land-use change?. *Hydrological Sciences Journal-Journal Des Sciences Hydrologiques*, 51:1039–1050, 2006. 7

[114] M. M. Stone, G. Mulamoottil, and L. Logan. Grain size distribution effects on phosphate sorption by fluvial sediment: implications for modelling sediment- phosphate transport. *Hydrological Sciences Journal*, 40:67–81, 1995. 246

[115] M. L. Macrae, M. C. English, S. L. Schiff, and M. A. Stone. Phosphate retention in an agricultural stream using experimental additions of phosphate. *Hydrological Processes*, 17:36493663, 2003. 206

[116] F Magdaleno and J. A. Fernandez-Yuste. Meander dynamics in a changing river corridor. *Geomorphology*, 15:197–207, 2011. 79, 81

[117] H. Mansikkaniemi. Sedimentation and water quality in the flood basin of the river kyronjoki in finland. *River Research and Applications*, 1: 155–194, 1985. 174

[118] M. (Ed.) Marchand. *Floodplain Rehabilitation*. Gemenc: Main Report. Delft Hydraulics, RIZA/Vituki, Delft, Lelystad, The Netherlands/Budapest, Hungary., 1993. 5

[119] K. Marks and P. Bates. Integration of high-resolution topographic data with floodplain flow models. *Hydrological Processes*, 14:2109–2122, 2000. 48, 49

[120] E. Martí and F. Sabater. High variability in temporal and spatial nutrient retention in mediterranean streams. *Ecology*, 77(3):854–869, 1996. 101, 129, 189, 242, 243, 245

[121] J.F. Martin and K. Reddy. Interaction and spatial distribution of wetland nitrogen process. *Ecological Modelling*, 105:1–21, 1997. 4

[122] J.P Martin Vide. *Ingeniería de los ríos*. Ediciones UPC, Barcelona, 2002. 44

[123] D. L. McCallister and T.J. Logan. Phosphate adsorptiondesorption characteristics of soils and bottom sediments in the maumee river basin of ohio. *Journal of Environmental Quality*, 7:87–92, 1978. 137

[124] D. C. Mcintire and J. A. Colby. A hierarchical model of lotic ecosystems. *Ecological Monographs*, 48:167–190, 1978. 123, 245

[125] J. B. Melody, J. L. Tank, V. R. Todd, and B. D. Mark. Nutrient uptake in streams draining agricultural catchments of the midwestern united states. *Freshwater Biology*, 51:499–509, 2006. 100, 101, 129, 189, 242, 243, 245

[126] M. Meybeck, D. Chapman, and R. Helme. *Global Fresh Water Quality: A First Assessment.* Basil Blackwell, Oxford, 1989. 3, 175

[127] J. L. Meyer. The role of sediments and bryophytes in phosphorus dynamics in a headwater stream ecosystem. *Limnology and Oceanography*, 24:365–375, 1979. 100, 137

[128] M. N. Michael N. Gooseff, R. O. Hall, and J. L. Tank. Relating transient storage to channel complexity in streams of varying land use in jackson hole, wyoming. *Water Resources Research*, 43:174–182, 2007. doi: 10.1029/2005WR004626. 242, 243, 245

[129] H. Middelkoop and N. E. M. Asselman. Spatial variability of floodplain sedimentation at the event scale in the rhine-meuse delta, the netherlands. *Earth Surf. Processes and Landforms*, 23:561–573, 1998a. 208, 250

[130] H. Middelkoop and M. Van der Perk. Modelling spatial patterns of overbank sedimentation on embanked floodplains. *Geografiska Annaler Series A: Physical Geography*, 80:95–109, 1998b. 176

[131] W.J. Mitsch and J.R. Dorge, C.L .and Wiemhoff. Ecosystem dynamics and phosphorus budget of an alluvial cypress swamp in southern ilinois. *Ecology*, 60:11161124, 1979. 3, 173

[132] J. Monod. The growth of bacterial cultures. *Ann. Rev. Microbiol*, 3: 371394, 1949. 123

[133] P. J. Mulholland, J. L. Tank, J. R. Webster, W. B. Bowden, W. K. Dodds, S. V. Gregory, N. B. Grimm, S. K. Hamilton, S. L. Jonhson, E. Martí, W.H. MCdowell, J. L. Merriam, J. L. Meyer, B. J. Peterson, H.M. Valett, and W. M. Wollheim. Can uptake length in streams be determined by nutrient addition experiments? results from an interbiome comparison study. *Journal of the North American Benthological Society*, 21:544–560, 2002. 123, 156, 166, 204, 245

[134] P.J. Mulholland. Can uptake length in streams be determined by nutrient addition experiments? Results from an interbiome comparison study. *North American Benthological Society*, 21(4):544–560, 2002. 129, 189

[135] P.J. Mulholland, J.W. Elwood, J.D. Newbold, J.R. Webster, L.A. Ferren, and R.E. Perkins. Phosphorus uptake by decomposing leaf detritus: effect of microbial biomass and activity. *Internationales Vereinigung fr theoretische und angewandte Limnologie, Verhandlungen*, 22: 1899–1905, 1984. 101

[136] J. Murillo, P. Garcia-Navarro, J. Burguete, and P. Brufau. A conservative 2d model of inundation flow with solute transport over dry bed. *International Journal of Numerical Methods in Fluids*, 52:1059–1092, 2005. 10, 12, 26, 40, 125

[137] J. Murillo, P. García-Navarro, J. Burguete, and P. Brufau. The influence of source terms on stability, accuracy and conservation in two-dimensional shallow flow simulation using triangular finite volumes. *International Journal of Numerical Methods in Fluids*, 54:543–590, 2007. 40

[138] J. Murillo, P. Garcia-Navarro, and J. Burguete. Conservative numerical simulation of multi-component transport in two-dimensional unsteady shallow water flow. *Journal of Computational Physics*, 228(15):5539–5573, 2009. 10, 11, 12, 26, 31, 32, 38, 125, 239, 242

[139] J. Murphy and J.P. Riley. A modified single solution method for determination of phosphate in natural waters. *Analytica Chimica Acta*, 27: 31–36, 1962. 113, 117, 182

[140] R.J.a nd J.J. Magnunson Naiman, D.M. McKnight, and J.A. Standford. *The freswater Imperative - A research Agenda.* Island Press, Alstone, Washingtong, D.C., 2001. 174

[141] J.D. Newbold, J. W. Elwood, R. V. O'Neill, and A. L. Sheldon. Phosphorus dynamics in a woodland stream ecosystem: a study of nutrient spiralling. *Ecology*, 64:1249–1265, 1983a. 101

[142] J.D. Newbold, T.L. Bott, and L.A. Kaplan. Uptake of nutrients and organic C in streams in New York City. *J. N. Am. Benthol. Soc.*, 25(4): 998–1017, 2006. 121, 129, 189

[143] A.P. Nicholas and D. E. Walling. Modelling flood hydrailics and overbank deposition on river floodplains. *Earth Surf. Processes and Landforms*, 22:59–77, 1997. 176

[144] A.P. Nicholas and D.E. Walling. Numerical modelling of floodplain hydraulics and suspended sediment transport and deposition. *Hydrological Processes*, 12:1339–1355, 1998. 176

[145] C. Nilsson, C.A. Reidy, M. Dynesius, and C. Revenga. Fragmentationand flow regulation of the worlds large river systems. *Science*, 308: 405–408, 2005. 5

[146] B. L. OConnor, M. Hondzoy, and J. W. Harvey. Predictive modeling of transient storage and nutrient uptake: Implications for stream restoration. *Journal of Hydraulic Engineering*, 136:1018–1033, 2010. 122, 242, 243, 245

[147] W. E. Odum. *Internal Processes Influencing the Maintenance of Ecotones: Do They Exist*. In: The Ecology and Management of Aquatic-Terrestrial Ecotones. The Parthenon Publishing Group, Carnforth, England., 1990. 2

[148] H. Olde Venterink, N.M. Pieterse, J.D.M. Belgers, M.J. Wassen, and P.C. de Ruiter. N, p and k budgets along nutrient availability and productivity gradients in wetlands. *Ecological applications*, 12:1010–1026, 2002. 3

[149] H. Olde Venterink, F. Wiegman, G. E. M. Van Der Lee, and J.E. Vermaat. Role of active floodplains for nutrient retention in the river rhine. *Journal of Environmental Quality*, 32:14301435, 2003. 3, 4, 175, 208, 246

[150] H. Olde Venterink, J.E. Vermaat, M. Pronk, F. Wiegman, G. E. M. Van Der Lee, M. W. van den Hoorn, L.W.G. Hilger, and J.T.A. Verhoeven. Importance on sediment deposition and denitrification for nutrient retention in floodplain wetlands. *Applied Vegetation Science*, 9:163–174, 2006. 3

[151] A. Ollero. Dinamica reciente del cauce del ebro en la reserva natural

de los galachos (zaragoza). *Cuaternario y Geomorfologia*, 9:85–93, 1995. 7, 79, 80

[152] A. Ollero. Channel adjustments, floodplain changes and riparian ecosystems of the middle ebro river: assessment and management. *International Journal of Water Resources Development*, 18:73–90, 2007. 22, 78, 79, 80, 81, 84, 249, 250

[153] A. Ollero. Channel changes and floodplain management in the meandering middle ebro river, spain. *Geomorphology*, 117(3-4):247 – 260, 2010. ISSN 0169-555X. Introduction to Management of Large Rivers. 22, 79

[154] M.A. Palmer, E.S. Bernhardt, J. D. Allan, P.S. Lake, G. Alexander, S. Brooks, J. Carr, S. Clayton, C. N. Dahm, J. Follstand SHAH, D. L. Galat, S. G. Loss, P. Goodwin, D.D. Hart, B. Hassett, R. Jekinson, G.M. Kondolf, R. Lave, J.L. Meyer, T.K. O'Donell, L. Pagano, and E. Sudduth. Standards for ecologically successful river restoration. *Journal of Applied Ecology*, 42(2):208–217, 2005. ISSN 1365-2664. 5

[155] F. Palmeri, Silvn F., Prieto I., Balboni M., and Garcia-Mijangos I. *Manual de técnicas de ingenieréa naturaléstica en ambito fluvial*. Basque Government, Spain, 2002. 44, 110

[156] J. T. C. Parker, K. D. Fossum, and T. L. Ingersoll. Chemical characteristics of urban stormwater sediments and implications for environ-

mental management, maricopa county, arizona. *Environmental Management*, 26:99–115, 2002. 100

[157] E. Pasche and G. Rouvee. Overbank flow with vegetatively roughened floodplains. *Journal of Hydraulic Engineering*, 111:1262–1278, 1985. 176

[158] R.A. Payn, J. R.Webster, P.J. Mulholland, H.M. Valett, and W. K. Dodds. Estimation of stream nutrient uptake from nutrient addition experiments. *Limnology and Oceanography: Methods*, 3:174–182, 2005. 123, 242, 243, 245

[159] C. G. Peterson, H. Maurice, and N. D. Clifford. Shifts in habitat templates for lotic microalgae linked to interannual variation in snowmelt intensity. *Limnology and oceanography*, 6:858–870, 2001. 152

[160] V. Pinilla. The development of irrigated agriculture in twentieth-century spain: a case study of the ebro basin. *Agr. Hist. Rev*, 54: 122141, 2006. 7, 22

[161] G.C. Poole, J.A. Stanfor, S.W. Running, C.A. Frissell, W.W. Woessner, and B.K. Ellis. A patch hierarchy approach to modeling surface and subsurface hydrology in complex flood-plain environments. *Earth Surface Processes and Landforms*, 10:1259–1274, 2004. 44

[162] N. Rajaratnam and R.M. Ahmadi. Hydraulics of channels with floodplainss. *Journal of Hydraulic Research*, 3:43–60, 1981. 175

[163] R. Rajendra Paudel, J-H. Min, and J. W. Jawitz. Management scenario evaluation for a large treatment wetland using a spatio-temporal phosphorus transport and cycling model. *Ecological Engineering*, 36: 1627–1638, 2010. 248

[164] A.K. Rastogi and W. Rodi. Predictions of heat and mass transfer in open channels. *Journal of the Hydraulic Division, ASCE*, pages 397–420, 1978. 28

[165] W. Reckendorfer, R. Schamalfuss, C. Baumgartner, H. Habersack, S. Hohensinner, M. Jungwirth, and F. Scheimer. The integrated river engineering project for the free-flowing danube in the austrian alluvial zone national park: contradictory goals and mutual solutions. *Arch. Hydrobiol. Suppl.*, 155:613–630, 2005. 5

[166] K. Reddy, O.A. Diaz, L.J. Scinto, and M. Agami. Phosphorus dynamics in selected wetlands and streams of the lake okeechobee basin. *Ecologica Engineering*, 5:183–207, 1995. 3

[167] K. Reddy, R. Kadlec, R.H. Flaig, and P. M. Gale. Phosphorus retention in streams and wetlands: a review. *Critical Reviews in Envairomental Science and Technology*, 1:83–146, 1999. 100, 103, 104, 137, 165, 206, 246, 248

[168] P. Regato. *Contribucion al estudio de la flora y la vegetacion del galacho de la Alfranca en relacion con la evolucion del sistema fluvial.* Diputacion General de Aragon, Zaragoza, 1988. 7

[169] D.S. Rhee, H. Woo, B.A. Kwon, and H.K. Ahn. Hydraulic resistance of some selected vegetation in open channel flows. *River Research and Applications*, 24:673–687, 2008. 44

[170] J. Brasington Richards, K. and and F. M. R. Hughes. Geomorphic dynamics of floodplains: ecological implications and a potential modelling strategy. *Freshwater Biology*, 47:559579, 2002. 5, 174, 210, 230, 251, 252, 253

[171] C.J. Richardson. Mechanisms controlling phosphorus retention capacity in freshwater wetlands. *Science*, 228:1424–1427, 1985. 3, 100

[172] C.J. Richardson and P. E. Marshall. Processes controlling movement, storage and export of phosphorus in a fen peatland. *Ecological Monographs*, 56:279–320, 1986. 3

[173] P.L. Roe. *A basis for Upwind Differencing of the Two-Dimensional Unsteady Euler Equations*. Numerical Methods in Fluid Dynamics, Vol II. Oxford University Press, Oxford., 1986. 32

[174] L. C. Roig. *Mathematical theory and numerical methods for the modeling of wetland hydraulics. Water Resources Engineering*. Mathematical theory and numerical methods for the modeling of wetland hydraulics. Water Resources Engineering, 1995. 10, 11

[175] G Rosatti, J. Murillo, and L. Fraccarollo. Generalized roe schemes for 1d two-phase, free-surface flows over a mobile bed. *Journal of Computational Physics*, 54:543–590, 2007. 32

[176] R. W. H R.W.H. Carroll, J. J. Warwicka, A. I. James, and J. R. Miller. Modeling erosion and overbank deposition during extreme flood conditions on the carson river, nevada. *Journal of Hydrology*, 297:1–21, 2004. 244

[177] C.J. Sande van Der, S.M. Jong, and A.P.J. Roo. A segmentation and classification approach of ikonos-2 imagery for land cover mapping to assist flood risk and flood damage assessment. *International Journal of Applied Earth Observation and Geoinformation*, 4:217–229, 2003. 44

[178] P.L. Santos. Modernization of irrigation systems: A case of research, oriented to improve management. *Irrigation and Drainage Systems*, 2: 63–77, 1988. 101

[179] D.L. Saunders and J. Kalff. Nitrogen retention in wetlands, lakes and rivers. *Hydrobiologia*, 443:205–212, 2001. 3

[180] F. Schiemer, C. Baumgartner, and K. Tockner. Restoration of floodplain rivers: The danube restoration project. *Regul. Rivers Res. Mgmt.*, 115:231244, 1999. 5, 77

[181] J. E. Schubert, B. F. Sanders, M. J. Smith, and Wright N. G. Unstructured mesh generation and landcover-based resistance for hydrodynamic modeling of urban flooding. *Advances in Water Resources*, 131:1603–1621, 2008. 39, 48

[182] M. Schulz and C. Herzog. The influence of sorption processes on the phosphorus mass balance in a eutrophic german lowland river. *Water, Air, and Soil Pollution*, 155:291–301, 2004. 246

[183] M. Schulz, M. Bischoff, J. Klasmeier, J. Berlekamp, and M. Matthies. An empirical regression model of soluble phosphorus retention for small pristine streams evaluating tracer experiments. *Aquat. Sci.*, 70: 115–122, 2008. 247, 248

[184] D. T. Scott, M. N. Gooseff, K. E. Bencala, and R. L. Runkel. Automated calibration of a stream solute transport model: implications for interpretation of biogeochemical parameters. *J. N. Am. Benthol.*, 22 (4):492510, 2003. 242, 243, 245

[185] R.H.J. Sellin. A laboratory investigation into the interaction between the flow in the channel of river and that over its floodplain. *La Houille Blanche*, 7:793–802, 1964. 175

[186] D.J. Simm. *The rates and patterns of overbank deposition on a lowland floodplain.* In: Foster, I., Gurnell, A., Webb, B. (Eds.), Sediment and Water Quality in River Catchments. Wiley, Chichester, pp. 247 264., 1995. 175

[187] Nicholas L. G. Somes, Warwick A. Bishop, and Tony H. F. Wong. Numerical simulation of wetland hydrodynamics. *Environment International*, 25:773 – 779, 1999. 11

[188] J.A. Standford. Rivers in the landscape: Introduction to the special issue on riparian and groundwater ecology. *Freshwater Biology*, 40: 217–229, 1998. 38

[189] J.A. Standford, Ward J. V., W. J. Liss, C. A. Frissell, R. N. Williams, J. A. Lichatowich, and C. C. Coutant. A general protocol for restoration of regulated rivers. *Regulated Rivers: Research and Management*, 12:391–413, 1996. 100

[190] J. Steiger and A. M. Gurnell. Spatial hydrogeomorphological influences on sediment and nutrient deposition in riparian zones: observations from the garonne river, france. *Geomorphology*, 49:1–23, 2002. 77, 173, 175, 207, 208, 249, 250

[191] J. Steiger, A.M. Gurnell, P. Ergenzinger, and D. Snelder. Sedimentation in the riparian zone of an incising river. *Earth Surface Processes and Landforms*, 26:91–108, 2001a. 175

[192] J. Steiger, A.M. Gurnell, and G.E. Petts. Sediment deposition along the channel margins of a reach of the middle river severn, uk. *Regulated Rivers: Research and Management*, 17:441–458, 2001b. 175

[193] M.D. Stewart, P.D. Bates, D.A. Price, and T.P. Burt. Modelling the spatial variability in floodplain soil contamination during flood events to improve chemical mass balance estimates. *Hydrological Processes*, 12:1233–1255, 1998. 176

[194] V. Tayefi, S. N. Lane, R. J. Hardy, and D. Yu. A comparison of one- and two-dimensional approaches to modelling flood inundation over

complex upland floodplains. *Hydrological Processes*, 21:3190–3202, 2007. 238, 239

[195] M. Terrado, r M. Kuste, D. Ralda, M. López de Alda, D. Barceló, and R. Tauler. Use of chemometric and geostatistical methods to evaluate pesticide pollution in the irrigation and drainage channels of the Ebro river delta during the rice-growing season. *Anal Bioanal Chem*, 387: 1479–1488, 2007. 101

[196] M. C. Thoms, J. M. Foster, and B. Gawne. Flood-plain sedimentation in a dryland river: the river murray, australia. *The Role of Erosion and Sediment Transport in Nutrient and Contaminant Transfer (Proceedings of a symposium held at Waterloo, Canada, July*, pages 227–236. 207, 208, 249, 250

[197] I. Thonon, K. Jong, M. Van der Perk, and H. Middelkoop. Modelling floodplain sedimentation using particle tracking. *Hydrological Processes*, 21:14021412, 2007. 176, 244

[198] Néstor J. Torrecilla, Jorge P. Galve, Lidia G. Zaera, Javier F. Retamar, and Alejandro N.A. álvarez. Nutrient sources and dynamics in a mediterranean fluvial regime (ebro river, ne spain) and their implications for water management. *Journal of Hydrology*, 304(1-4):166 – 182, 2005. ISSN 0022-1694. Nutirent Mobility within River Basins: A European Perspective. 22, 108

[199] C. R. Townsend, C. J. Arbuckle, T. A. Crowl, and M. R. Scarsbrook. The relationship between land use and physicochemistry, food re-

sources and macroinvertebrate communities in tributaries of the taieri river, new zealand: A heirarchically scaled approach. *Freshwater Biology*, 37:177–191, 1997. 100

[200] F. Triska, C. M. Pringle, J. H. Duff, R. J. Avanzino, and G. Zellweger. Soluble reactive phosphorus (srp) transport and retention in tropical, rain forest streams draining a volcanic landscape in costa rica: in situ srp amendment to streams and aboratory studies. *Biogeochemistry*, 81: 145157, 2006. 206

[201] T. Uchida, Y. Kawahara, and Y. Ito. *Modeling of inundation flow in urbanized area using a high-resolution method with Cartesian mesh*. 2002. 39, 48

[202] G. E. M. Van der Lee, H. O. Venterink, and N. E. M Asselman. Nutrient retention in floodplains of the rhine distributaries in the netherlands. *River Research and Applications*, 20:315325, 2004. 208

[203] M.E. Vazquez-Cendon. Improved treatment of source terms in upwind schemes for the shallow water equations in channels with irregular geometry. *Journal of Computational Physics*, 148(2):497–526, 1999. 40

[204] J.T.A. Verhoeven, W. Koerselmanb, and A.F.M. Meulemanb. Nitrogen- or phosphorus-limited growth in herbaceous, wet vegetation: relations with atmospheric inputs and management regimes. *Trends in Ecology and Evolution*, 11:494–497, 1996. 171, 259, 269

[205] D. Vericat and R.J. Batalla. Sediment transport in a large impounded river: The lower ebro, ne iberian peninsula. *Geomorfology*, 79:72–79, 2006. 7

[206] L.B.M. Vought, J. Dahl, C. Lauge Pedersen, and J.O. Lacousire. Nutrient retention in riparian ecotones. *Ambio*, 23:342–348, 1994. 3

[207] C.B. Vreugdenhil. *Numerical methods for shallow-water flow*. 1994. 9, 38

[208] C. R. Wagner. *Results of a Two-Dimensional Hydrodynamic and Sediment-Transport Model to Predict the Effects of the Phased Construction and Operation of the Olmsted Locks and Dam on the Ohio River near Olmsted, Illinois*. U.S. Department of the Interior, Louisville, Kentucky., 2004. 10, 239

[209] D.E. Walling. Linking land use, erosion and sediment yields in river basins. *Hydrobiologia*, 410:223–240, 1999. 174, 176

[210] D.E. Walling and S.B. Bradley. Rates and patterns of contemporary floodplain sedimentation: a case study of the river culm, devon, uk. *GeoJournal*, 19:53–62, 1993. 175

[211] D.E. Walling, P. N. Owens, and G. J. L. Leeks. The characteristics of overbank deposits associated with a major flood event in the catchment of the river ouse, yorkshire, uk. *Catena*, 31:53–75, 1997. 208, 250

[212] J.V. Ward and J.A. Standford. The serial discontinuity concept: extending the model to floodplain rivers. *Regulated Rivers: Research and Management.*, 10:159–168, 1995. 1, 251

[213] J.V. Ward, G. Bretschko, M. Brunkev, D. Danielopol, Gibert J., T. Gonser, and A.G. Hildrew. The boundaries of river systems: the metazoan perspective. *Freshwater Biology*, 40:531–569, 1998. 1

[214] J.V. Ward, K. Tockner, and F. Schiemer. Biodiversity of floodplain river ecosystems: ecotones and connectivity. *Regulated Rivers-research and Management*, 15:125–139, 1999. 38, 210, 251

[215] J.V. Ward, K. Tockner, U. Uehlinger, and F. Malard. Understanding natural patterns and processes in river corridors as the basis for effective river restoration. *Regulated Rivers-research and Management*, 17: 311–324, 2001. 5, 210

[216] D.H. Wardrop and R.P. Brooks. The occurrence and impact of sedimentation in central pennsylvania wetlands. *Environmental Monitoring and Assessment*, 51:119–130, 1996. 175

[217] R. C. Wissmar and R. L. Beschta. Restoration and management of riparian ecosystems: A catchment perspective. *Freshwater Biology*, 40:571–585, 1998. 100

[218] Stream Solute Workshop. Concepts and methods for assessing solute dynamics in stream ecosystems. *J. N. Am. Benthol. Soc.*, 9(2):95–119, 1990. 101, 120, 123

BIBLIOGRAPHY

[219] W. Wu. *Computational River Dynamics*. 2007. 9, 30, 38

[220] G. Zalidis, V. Stamatiadis, S. andTakavakolglou, K. Eskridge, and N. Misopolinos. Impacts of agricultural practices on soil and water quality in the mediterranean region and proposed assessment methodology. *Agricultural, Ecosystem and Enviroment*, 88:137–146, 2002. 171

[221] Ji Zhen-Gang. *Hydrodinamics and Water Quality*. 2008. 25, 131, 132

[222] J. G. Zhou, D. M. Causon, C. G. Mingham, and D. M Ingram. Principles and conditions of the movements of groundwater. *US Geol. Survey 19th Ann. Rep. Part 2*, pages 59–294, 1988. 74

[223] J. G. Zhou, D. M. Causon, C. G. Mingham, and D. M Ingram. The surface gradient method for the treatment of source terms in the shallow-water equations. *Journal of Computational Physics*, 168(1):1–25, 2001. 40

Declaration

I herewith declare that I have produced this paper without the prohibited assistance of third parties and without making use of aids other than those specified; notions taken over directly or indirectly from other sources have been identified as such. This paper has not previously been presented in identical or similar form to any other Spanish or foreign examination board.

Valencia, March 2012.